Numerical Investigation & Modelling of Modern Container Ship Squat

by

Zhen Kok
B.Eng. (Hons)
Australian Maritime College

Submitted in fulfilment of the requirements for the degree of Doctor of Philosophy

University of Tasmania

July 2021

Declaration of Originality

This thesis contains no material which has been accepted for a degree or diploma by the University or any other institution, except by way of background information and duly acknowledged in the thesis, and to the best of my knowledge and belief, no material previously published or written by another person, except where due acknowledgement is made in the text of the thesis, nor does the thesis contain any material that infringes copyrights.

Statement of Authority of Access

This thesis may be made available for loan and limited copying in accordance with the *Copyright Act 1968*.

Zhen Kok

1st April 2021

Declaration of Published Work Contained in Thesis

The publishers of the papers comprising Chapters 3 to/and 5 hold the copyright for that content and access to the material should be sought from the respective journals. The remaining non-published content of the thesis may be made available for loan and limited copying and communication in accordance with the Copyright Act 1968.

Statement of Co-Authorship

The following people and institutions contributed to the publication of work undertaken as part of this thesis:

Candidate	--	Mr. Zhen Kok, University of Tasmania
Author 1	--	Dr. Jonathan Duffy, University of Tasmania
Author 2	--	Prof. Shuhong Chai, University of Tasmania
Author 3	--	Dr. Yuting Jin, Technology Centre for Offshore & Marine Singapore
Author 4	--	Dr. Mohammadreza Javanmardi, OMC International

Contribution of work by co-authors for each paper:

Paper 1: Located in Chapter 3

Kok, Z., Duffy, J., Chai, S. & Jin, Y. 2020, "Comparison of Unsteady Reynolds-Averaged Navier-Stokes Prediction of Self-Propelled Container Ship Squat against Empirical Methods and Benchmark Data", ***Transactions of the Royal Institution of Naval Architects, Part A: International Journal of Maritime Engineering*****, 162 (Part A), pp. 193-206.**

Author Contributions:

Conceived and designed the investigation: Candidate, Author 1, Author 2, Author 3

Performed the investigation: Candidate

Analysed the data: Candidate

Wrote the manuscript: Candidate

Revised the manuscript: Candidate, Author 1, Author 2, Author 3

Paper 2: Located in Chapter 3

Kok, Z., Duffy, J., Chai, S. & Jin, Y. 2020, "Multiple Approaches to Numerical Modelling of Container Ship Squat in Confined Water", ***Journal of Waterway, Port, Coastal, and Ocean Engineering*****, 146 (4), p.04020017.**

Author Contributions:

Conceived and designed the investigation: Candidate, Author 1, Author 2, Author 3

Performed the investigation: Candidate

Analysed the data: Candidate

Wrote the manuscript: Candidate

Revised the manuscript: Candidate, Author 1, Author 2, Author 3

Paper 3: Located in Chapter 4

Kok, Z., Duffy, J., Chai, S. & Jin, Y. 2020, "Benchmark Case Study of Scale Effect in Self-propelled Container Ship Squat", ***ASME 2020 39th International Conference on Ocean, Offshore and Arctic Engineering*****, Virtual, Online.**

Author Contributions:

Conceived and designed the investigation: Candidate, Author 1, Author 2, Author 3

Performed the investigation: Candidate

Analysed the data: Candidate

Wrote the manuscript: Candidate

Revised the manuscript: Candidate, Author 1, Author 2, Author 3

Paper 4: Located in Chapter 4

Kok, Z., Duffy, J., Chai, S., Jin, Y. & Javanmardi, M. 2020, "Numerical Investigation of Scale Effect in Self-propelled Container Ship Squat", ***Applied Ocean Research*****, 99, p.102143.**

Author Contributions:

Conceived and designed the investigation: Candidate, Author 1, Author 2, Author 3

Contributed data for analysis: Author 4

Performed the investigation: Candidate

Analysed the data: Candidate

Wrote the manuscript: Candidate

Revised the manuscript: Candidate, Author 1, Author 2, Author 3, Author 4

Paper 5: Located in Chapter 5

Kok, Z., Duffy, J., Chai, S., Jin, Y. & Javanmardi, M. 2021, "Numerical Parametric Study of Medium Sized Container Ship Squat", ***Applied Ocean Research*****, 109, p.102563.**

Author Contributions:

Conceived and designed the investigation: Candidate, Author 1, Author 2, Author 3

Contributed data for analysis: Author 4

Performed the investigation: Candidate

Analysed the data: Candidate

Wrote the manuscript: Candidate

Revised the manuscript: Candidate, Author 1, Author 2, Author 3, Author 4

We, the undersigned, endorse the above stated contribution of work undertaken for each of the published (or submitted) peer-reviewed manuscripts contributing to this thesis:

Signed:

Zhen Kok Candidate Australian Maritime College University of Tasmania	Dr. Jonathan Duffy Primary Supervisor Australian Maritime College University of Tasmania	Dr. Vikram Garaniya Head of School Australian Maritime College University of Tasmania

Date: 1st April 2021

Acknowledgements

All the work produced in this project could not have been possible without the guidance, help and support from my superiors, colleagues, technicians, friends and loved ones. I cannot understate the appreciation I have for my primary supervisor Dr. Jonathan Duffy, for sharing his valuable technical wisdom, enthusiasm, inspiration and readiness to provide guidance despite his often-busy schedule. I would also like to thank my co-supervisor Professor Shuhong Chai, for her significant administrative and academic support of which made my doctoral study possible in the first place. My sincerest thanks to co-supervisor Dr. Yuting Jin, who has supervised me since my undergraduate research days and honed my numerical simulation skills as well as research skills.

I would like to extend my thanks to the towing tank staff for their indispensable assistance in helping me conduct my experiment. Thanks, to Dr. Nick Johnson, Liam Honeychurch and Toby Davis. Special thanks to Jock Ferguson for his assistance in 3D-printing propellers for the experiment, Dane Colman for his significant contributions to the experiment, and Kynan Maley for troubleshooting my simulations. Acknowledgement to the Underwater Collision Research Facility and DST for allowing access to the 3D laser scanner used in the generation of the numerical hull model.

During my studies, I have had a wonderful opportunity to cooperate with expert consultants OMC International thanks to Chris Hens. Many thanks to Jack Bucher for organising the full scale squat measurement activity and Dr. Mohammadreza Javanmardi for providing valuable feedback regarding my simulations. The full scale squat data generously provided to me have been very impactful to my research.

Most importantly, my sincerest gratitude to my parents; Kok Nyuk Fah and Cheng Mee Sing for their unyielding care and support in all my endeavours as well as my partner Chen Shu Han for always being there for me.

Table of Contents

Declaration of Originality ii

Statement of Authority of Access ii

Declaration of Published Work Contained in Thesis iii

Statement of Co-Authorship iii

Acknowledgements vi

List of Figures xi

List of Tables xvi

Nomenclature xix

Abbreviations xxi

Abstract xxii

Chapter 1 – Introduction 1

1.1. Background 1

1.2 Theory & Past Literature 2

1.2.1 Key Variables & Terminologies 3

1.2.2 History of Ship Squat Prediction 5

1.2.3 Problem Statement 13

1.3 Objectives 16

1.4 Methodology 17

1.5 Research Novelty 18

1.6 Thesis Structure Overview 19

Chapter 2 – Computational Method & Regression Analysis 21

2.1 Computational Method (CFD) 21

2.1.1 Governing Equations 21

2.1.2 Turbulence Modelling 22

2.1.3 Verification and Validation Procedure 23

2.2 Regression Analysis 26

2.2.1 Multiple Linear Regression Model 26

Chapter 3 – Benchmarking Study 28
3.1 Benchmark Cases 28
3.1.1 Model Test Case 1 28
3.1.2 Model Test Case 2 30
3.1.3 Model Test Case 3 31
3.2 First Numerical Modelling Iteration & Benchmarking Exercise 31
3.2.1 Propeller Modelling 32
3.2.2 Squat Simulation Modelling 34
3.2.3 Verification and Validation 37
3.2.4 Numerical Results Comparison 38
3.2.5 Self-propulsion Effect 41
3.3 Second Numerical Modelling Iteration & Benchmarking Exercise 44
3.3.1 Initial Benchmarking Process & Results 44
3.3.2 Morphing Mesh Method 46
3.3.3 Verification and Validation 46
3.3.4 Results 47
3.4 Third Benchmarking Exercise 49
3.4.1 Modelling Set-up 49
3.4.2 Results 49
3.5 Empirical Methods 50
3.5.1 Overview of Readily Available Methods 51
3.5.1 Comparison of Empirical Predictions 52
3.7 Concluding Remarks 54
Chapter 4 – Scale Effect Investigation 57
4.1 Full Scale Resistance Investigation in Deep Water Condition 58
4.2 Full Scale Resistance Validation in Confined Water Condition 60
4.3 Scale Effect in Squat Predictions 63
4.3.1 Results for *Model Test Case 1* 63
4.3.2 Results for *Model Test Case 3* 67

4.4 Full Scale Case Studies 69
4.5 Concluding Remarks 71
Chapter 5 – Effect of Hull Principal Particulars 73
5.1 Statistics of Container Ship Principal Particulars 73
5.2 Systematic Hull Parametric Investigation 74
5.3 Results 76
5.3.1 Effect of *L/B* & *B/T* 76
5.3.2 Effect of Block Coefficient 79
5.3.3 Changes in Trim Direction 82
5.3.4 Comparison Against Existing Empirical Predictions 83
5.4 Concluding Remarks 84
Chapter 6 – Regression Analysis and Empirical Formulae Modelling 87
6.1 Regression Analysis 87
6.1.1 Additional Cases for Regression 87
6.1.2 Regression Process & Correction Factor Development 88
6.1.3 Performance of the Empirical Formulae 91
6.2 Lateral Restriction Effect 92
6.2.1 Blockage Ratio Calculation 93
6.2.2 Results 95
6.3 Initial Trim Effect 99
6.3.1 Cases Investigated 99
6.3.2 Results 100
6.4 Evaluation of the New Formulae 103
6.4.1 Evaluation for Laterally Unrestricted Cases 103
6.4.2 Evaluation for Laterally Restricted Cases 108
6.4.3 Evaluation for Full Scale Trials 113
6.5 Concluding Remarks 115
Chapter 7 – Conclusions and Future Work Recommendations 117
7.1 Conclusions 117

7.2 Future Work Recommendations 119
References 121
Appendix A – Model Test Study (*Model Test Case 2*) 128
Test Description 128
Test Results 129
Conclusions 130
Appendix B – List of Currently Available Empirical Formulae Investigated. 131
Appendix C – Particulars of the Sister KCS Hulls Developed from Parametric Transformations. 134
Appendix D – Equations of the New Empirical Formulae 135
Appendix E – Publications 142

List of Figures

Figure 1: Container ship cargo capacity trend over a span of five decades. 1

Figure 2: The squat phenomenon occurs when a ship travels through water. The ship sinks and trims due to changes in flow and this effect is accentuated in shallow water conditions. 2

Figure 3: Wave patterns generated during the three different regimes. Figure adapted from Macfarlane (2012). 3

Figure 4: The three main types of waterway configurations. 4

Figure 5: Profile view of the DTC hull (top) and cross section of the asymmetrical canal (bottom). .. 29

Figure 6: Profile view of the S175 hull. 30

Figure 7: Profile view of the KCS hull. 31

Figure 8: The open water propeller simulation domain design and boundary conditions (Kok et. al., 2020c). 32

Figure 9: Side view of the open water propeller simulation set-up (left) and perspective view of the propeller mesh (right). 33

Figure 10: Comparison of open water propeller curve results from CFD and EFD (Barnitsas et al., 1981). 34

Figure 11: The domain dimensions and boundary conditions for *Model Test Case 1* (Kok et. al., 2020c). 35

Figure 12: Perspective view of the mesh generated for the computation domain. 36

Figure 13: Profile view of the hull mesh for (a) QS-T and QS-VD methods, (b) the QS-DP method where overset mesh is applied to the discretised propeller, (c) the OV-T and OV-VD methods where overset mesh is applied to the entire hull (Kok et al., 2020b). 37

Figure 14: Comparison of various CFD predictions for AP & FP sinkage at *h/T* = 1.23. 40

Figure 15: Comparison of various CFD predictions for AP & FP sinkage at *h/T* = 1.14. 40

Figure 16: Comparison of various CFD predictions for AP & FP sinkage at *h/T* = 1.10. 41

Figure 17: Comparison of the stern region flow velocity (right) and the wake pattern at 0.49*L* aft of midships (left) predicted by QS-T (a), QS-VD (b) and QS-DP (c) for *h/T*=1.23 at 0.56Fr_h. 43

Figure 18: The computation domain dimensions and boundary conditions for the S175 case study. .. 44

Figure 19: Top view of the Kelvin wake pattern mesh refinement at the free surface (top left), cross-sectional view of the mesh (top right) and profile view of the hull mesh (bottom). 45

Figure 20: Comparison of midship sinkage and trim results from the experiment against the QS-VD predictions for *h/T* = 1.20. 45

Figure 21: Comparison of morphing mesh method predictions against experiment data and QS-VD method for *Model Test Case* 2 at *h/T* = 1.20. 48

Figure 22: Comparison of morphing mesh method predictions against experiment data for *Model Test Case* 2 at *h/T* = 1.10. 48

Figure 23: Comparison of morphing mesh method predictions against experiment data for *Model Test Case 3* at *h/T* = 1.30. 49

Figure 24: Comparison of morphing mesh method predictions against experiment data for *Model Test Case 3* at *h/T* = 1.20. 50

Figure 25: Comparison of the maximum sinkage predictions by the empirical formulae and CFD model (morphing mesh method) against benchmark data for *Model Test Case 2* (a) in *h/T* = 1.2, (b) in *h/T* = 1.1 (Kok et al., 2021) 53

Figure 26: Comparison of the maximum sinkage predictions by the empirical formulae and CFD model (morphing mesh method) against benchmark data for *Model Test Case 3* (a) in *h/T* = 1.3 and (b) in *h/T* = 1.2 (Gronarz et al., 2009). 53

Figure 27: The computation domain for deep water resistance prediction (similar for both model scale and full scale cases). 58

Figure 28: The mesh generated for the computation domain viewing from (left to right) the symmetry plane, the front end and the free surface plane. 59

Figure 29: Free surface elevation comparison between full scale and model scale deep water CFD computations for *Fr* = 0.218 (25 knots in full scale). 59

Figure 30: Experimental data depicting the relationship between V_h/V_I and $\sqrt{A_X}/R_h$ presented by Landweber (1939). 62

Figure 31: Confined water resistance comparison between Landweber (1939) estimation of the extrapolated benchmark resistance data against full scale CFD prediction. 63

Figure 32: Comparison of model scale and full scale CFD AP and FP sinkage against that of the *Model Test Case 1* results (Mucha et. al., 2014) at h/T = 1.23 (top) and at h/T =1.10 (bottom). 65

Figure 33: Plan view of free surface elevation comparison between full scale (top) and model scale (bottom) conditions in confined water for h/T = 1.23 at Fr_h = 0.53. 66

Figure 34: The dynamic pressure distribution on the bottom of the full scale and model scale hulls in confined water for h/T = 1.23 at Fr_h = 0.53. 66

Figure 35: Comparison of model scale and full scale CFD AP and FP sinkage against that of the *Model Test Case 3* results (Gronarz et al., 2009) for h/T = 1.3 (top) and h/T = 1.2 (bottom). 68

Figure 36: Plot of Case A squat measurement (OMC International, 2003) in comparison to the CFD prediction. 70

Figure 37: Plot of Case B squat measurement (OMC International, 2003) in comparison to the CFD prediction. 71

Figure 38: Parametric variation of 85 unique container ships visiting/departing an Australian port (OMC International, 2018). The mean of each parameter is shown with standard deviation bounds (B/T or C_B for vertical bound and L/B for horizontal bound). 74

Figure 39: Profile view of the KCS hull appended with a rudder. 74

Figure 40: Computation domain for the systematic study of effect of KCS hull parametric variations on squat (Kok et al., 2021). 75

Figure 41: Surface plot of the changes in (a) midship sinkage/T, (b) trim (positive by the bow), (c) FP sinkage/T, and (d) AP sinkage/T with respect to B/T and L/B for h/T =1.3 at 0.683 Fr_h and fixed C_B of 0.648. 77

Figure 42: Comparison of the velocity profile between hulls of varying L/B but equal B/T of 2.50 at 0.683 Fr_h in 1.3 h/T. The slender hull of L/B = 8.60 (top) has relatively lower flow velocity magnitude in the underkeel and wake region in comparison to the stubby hull of L/B = 6.50 (bottom). 78

Figure 43: Comparison of the pressure coefficient contours between the hull of *L/B* = 8.60 (top) against hull of *L/B* = 6.50 (bottom) at 0.683 Fr_h in 1.3 *h/T*. The pressure distribution on the keel of the hull *L/B* = 6.50 is significantly lower which results in greater sinkage and trim. 78

Figure 44: Comparison of the velocity profile between hulls of varying *B/T* but equal *L/B* of 6.50 at 0.683 Fr_h in 1.3 *h/T*. The wider hull of *B/T* = 3.90 (top) has relatively similar underkeel flow velocity magnitude in comparison to the deeper hull of *L/B* = 2.50 (bottom). 79

Figure 45: Comparison of the pressure coefficient contours between the hull of *B/T* = 3.90 (top) against hull of *B/T* = 2.50 (bottom) at 0.683 Fr_h in 1.3 *h/T*. The pressure distribution on the keel of both hulls are fairly similar which effectively yields comparable proportion of sinkage. 79

Figure 46: Comparison of the curve of areas about the LCF among the hulls of varying C_B. The increase in aft section area is greater than that of the fore section for this hull form using the Maxsurf Modeler Advanced parametric transformation tool. 80

Figure 47: Plot of midship sinkage/*T* and trim (positive by the bow) as a function of C_B. The change in midship sinkage/*T* is negligible while trim increases linearly with C_B. 80

Figure 48: Comparison of the pressure coefficient contours among the hulls of varying C_B at 0.683 Fr_h in 1.3 *h/T*. The maximum suction pressure gradually shifts aftward as the C_B increases for this particular hull form using the Maxsurf Modeler Advanced parametric transformation tool. 81

Figure 49: Plot of midship sinkage/*T* and trim with respect to L_{BF}. The change in midship sinkage/*T* is negligible while trim varies linearly with C_B and eventually changes direction. 82

Figure 50: Sample case comparison between empirical predictions against CFD results for varying *L/B*, *B/T* and C_B for the KCS hull. All maximum sinkage occurs by the bow except for CFD results for C_B = 0.689. 83

Figure 51: Effect of L_{BF} on midship sinkage (left) and trim (right) for varying Fr_h and *h/T* conditions. There is no significant relationship between sinkage and L_{BF} but trim is directly proportional to L_{BF} and the rate of change is dependent on Fr_h. 90

Figure 52: Comparison of the empirical formulae against the original data points for regression. 92

Figure 53: Illustration of some of the restricted channel geometries investigated (from top to bottom): *W/B* = 10 with h_m/T = 0.4 at *h/T* = 1.3, *W/B* = 5 with h_m/T = 0.7 at *h/T* = 1.3, and *W*/B = 2.5 with h_m/T = 0.4 at *h/T* = 1.3. 93

Figure 54: Comparison between cases with fixed h_m/T but varying W/B against cases of fixed W/B but varying h_m/T at h/T = 1.3. Midship sinkage results are shown on the left and trim on the right. For the same speed, sinkage increases collinearly for both fixed h_m and fixed W cases when normalised m_{eq} increases whereas there is no significant change in trim with respect to normalised m_{eq}. 96

Figure 55: Comparison of the sinkage (left) and trim (right) results for fixed h_m/T cases at varying speeds for h/T = 1.3. The sinkage result trendlines show that the gradient increases with speed. The change in trim for each speed are relatively small when normalised m_{eq} increases. 97

Figure 56: Comparison of the sinkage (left) and trim (right) results for fixed W cases at varying h/T for Fr_h = 0.47. The sinkage result trendlines show that the gradient increases with h/T. Trim only appears to increase with normalised m_{eq} for h/T = 1.1. 97

Figure 57: Comparison of the sinkage (left) and trim (right) results of various systematic hull form variations at Fr_h = 0.57 and h/T = 1.3. The gradient for sinkage is similar across all the different hull forms. Changes for trim is generally unnoticeable except for one of the hull forms. 98

Figure 58: Plot of midship sinkage and running trim against initial trim for the three hull forms. The change in midship sinkage varies with hull form but are all still within uncertainty limits whereas changes in running trim are linear. 100

Figure 59: Hydrodynamic pressure distribution on the hulls for different initial trim conditions. 101

Figure 60: Plot of net changes in trim against initial trim (left) and comparison of the actual resultant maximum sinkage against the approximated resultant maximum sinkage (right). It is shown that the approximated maximum sinkage is a reasonable approximation to the actual results. 101

Figure 61: Comparison of the new empirical formulae predictions against CFD and existing empirical formulae for various laterally unrestricted cases. Cases (a) to (d) are used in the regression but cases (e) and (f) are not. 107

Figure 62: Comparison of the new empirical formulae predictions against CFD and existing empirical formulae for various laterally restricted cases. All cases shown are not used in the derivation of the correction factor. 112

Figure 63: Comparison of Full scale squat predictions from the new formulae and actual measurements for Case FS1 114

Figure 64: Full scale squat predictions from the new formulae in comparison to actual measurements for Case FS2 115

List of Tables

Table 1: Principal particulars of the DTC hull and propeller. 29

Table 2: Test conditions investigated for DTC benchmark exercise. 29

Table 3: Principal particulars of the S175 hull and propeller. 30

Table 4: Test conditions investigated for S175 benchmark exercise. 30

Table 5: Principal particulars of the KCS hull. 31

Table 6: Test conditions investigated for KCS benchmark exercise. 31

Table 7: Summary of key differences between the different CFD techniques to be compared. 35

Table 8: Mesh count details for the grid spacing uncertainty study (1st modelling iteration). 37

Table 9: Results of the grid spacing and time step uncertainty study (1st modelling iteration). 38

Table 10: Validation of the simulation results by comparing the comparison error, E, against the validation uncertainty, U_V, which is computed from the simulation uncertainty, U_{SN}, and experimental uncertainty, U_D (1st modelling iteration). 38

Table 11: Mesh count for each modelling technique at varying *h/T* for *Model Test Case 1*. 38

Table 12: Summary of the computation requirements and limitations of each modelling technique. 39

Table 13: Mesh count details for the grid spacing uncertainty study (2nd modelling iteration). 46

Table 14: Results of the grid spacing and time step uncertainty study (2nd modelling iteration). 47

Table 15: Validation results for the 2nd modelling iteration. 47

Table 16: Overview of the range of applicability and properties of the formulae used where the symbols U, R and C refer to unrestricted channel, restricted channel and canal respectively. 51

Table 17: Comparison of the average difference and standard deviation in results between CFD (morphing mesh) and empirical predictions against benchmark data. 54

Table 18: Comparison of resistance results from CFD and benchmark EFD (El Moctar et. al., 2012). 60

Table 19: Details of the original DTC hull in comparison to the transit cases to be replicated. 69

Table 20: Statistics of different ships visiting/departing a busy Australian port (OMC International, 2018). Here, length L refers to length between perpendiculars and draft T refers to the operating draft during measurement. 74

Table 21: Principal particulars of the SVA-VP1193 propeller 75

Table 22: Range of cases investigated. 76

Table 23: Additional cases conducted for regression analysis and correction factor derivation. Positive L_{BF} implies the LCB is forwards of LCF. The range presented here will also be the recommended range of applicability for the formulae to be derived. 88

Table 24: Independent variables (IV) selected for each dependent variable (DV) in the regression analysis. 88

Table 25: Regression results obtained for the initial default procedure and revised condition where number of terms are reduced. 89

Table 26: Values of each coefficient for the derived regression formulae. 90

Table 27: Cases examined to assess the performance of the empirical formulae against the original data. 91

Table 28: Test matrix for investigation of lateral restriction effects. Refer to Figure 53 for visual definition of some of the symbols. 92

Table 29: Sample calculated blockage ratio, m, in comparison to the m_{eq} and normalised m_{eq} for a subset of the cases to be investigated. The value of m is indifferent to bank height and ship speed whereas both m_{eq} and $m_{eq\text{-}norm}$ varies with bank height and ship speed. 95

Table 30: Suggested limits of applicability for the lateral restriction correction factors after consideration of trans-critical cases that were omitted from the derivation. 99

Table 31: Cases investigated for the study of initial trim effect. 100

Table 32: Comparison of the empirical predictions against CFD results for various cases not used to develop the regression (no lateral restrictions). Fr_h values in orange signify it is beyond the recommended range of applicability. 105

Table 33: Comparison of the empirical predictions against CFD/EFD results for various laterally restricted cases that were not used in the derivation of the laterally unrestricted formulae and the lateral restriction correction factor. Lateral restriction with orange values signifies it is beyond the limits of applicability by ±15% while red values are well beyond the limits of applicability (> ±15%). 109

Table 34: Principal particulars of the container ships in the full scale trials. 113

Nomenclature

Symbol	Description
A_C	Cross sectional area of canal or channel (m^2)
A_E	Propeller expanded area (m^2)
A_O	Propeller disc area (m^2)
A_S	Immersed midship cross sectional area (m^2)
B	Ship beam (m)
$c_{0.7}$	Propeller chord length at 0.7 radius (m)
C_B	Block coefficient
C_P	Pressure Coefficient $(p-p_0)/(0.5\rho V^2)$
D_P	Propeller diameter (m)
Fr	Froude length number ($Fr = V/\sqrt{gL}$)
Fr_h	Froude depth number ($Fr_h = V/\sqrt{gh}$)
GM_L	Longitudinal metacentric height (m)
g	Gravitational constant (m/s^2)
h	Water depth (m)
h_m	Bank height (m)
L	Ship length between perpendiculars (m)
M_{TC}	Moment to change trim by 1cm (tonne.m/cm)
m	Blockage ratio (A_S/A_C)
m_{eq}	Equivalent blockage ratio
$m_{eq\text{-}norm}$	Normalised equivalent blockage ratio
p	Pressure at the point of interest (N/m^2)
p_0	Ambient pressure in undisturbed flow (N/m^2)
$P_{0.7}$	Propeller blade pitch at 0.7 radius (m)
S_{pred}	Predicted midship sinkage using new formulae (in terms of T)
$S_{pred\text{-}LR}$	Predicted midship sinkage using new formulae with consideration of lateral restrictions (in terms of T)
T	Ship draft (m)
T_{PC}	Tonnes per centimetre immersion (tonne/cm)
Tr_{pred}	Predicted trim using new formulae (°)
$Tr_{pred\text{-}LR}$	Predicted trim using new formulae with consideration of lateral restrictions (°)
V	Ship speed (m/s)
W	Width of channel or canal (m)

Δ	Ship displacement (tonne)
λ	Scale
ρ	Fluid density (kg/m^3)
χ	"Weight" of a cross-section
χ_{ocean}	"Weight" of an infinitely deep and wide cross-section
χ_{p}	"Weight" of the port side cross-section
χ_{s}	"Weight" of the starboard side cross-section
χ_{ship}	"Weight" of the ship cross-section
∇	Ship volumetric displacement (m^3)
∇_S	Rate of change of midship sinkage with respect to normalised m_{eq} (m)
∇_{Tr}	Rate of change of trim with respect to normalised m_{eq} (°)

Abbreviations

Symbol	Description
AMC	Australian Maritime College
AP	Aft perpendicular
CFD	Computational fluid dynamics
CoG	Centre of gravity
DOF	Degree of freedom
DTC	Duisburg Test Case (Container ship)
EFD	Experimental fluid dynamics
FP	Forward perpendicular
FS	Full scale
KCS	KRISO Container Ship
KVLCC2	KRISO Very Large Crude Carrier 2
LNG	Liquefied natural gas
LCB	Longitudinal centre of buoyancy
LCF	Longitudinal centre of flotation
LCG	Longitudinal centre of gravity
MS	Model scale
OV	Over-set mesh modelling technique
OV-T	Over-set hull model without propeller (towed)
OV-VD	Over-set hull model with body-force propulsion virtual disc
QS	Quasi-static modelling technique
QS-DP	Quasi-static hull model with discretised propeller model
QS-T	Quasi-static hull model without propeller (towed)
QS-VD	Quasi-static hull model with body-force propulsion virtual disc
RANS	Reynolds-Averaged Navier-Stokes
UKC	Underkeel clearance
URANS	Unsteady Reynolds-Averaged Navier-Stokes
VCG	Vertical centre of gravity
VLCC	Very large crude carrier

Abstract

The size of container ships has increased significantly over the past decades as shipping companies merge and adopt tactics of economies of scale to meet increasing demands. Such practice has incessantly caused complications to operate larger container ships in relatively shallow approach channels and ports. This is because when ships move in water, changes in the flow around the hull causes the hull to sink vertically and trim either by the bow or stern. This hydrodynamic phenomenon is known as “ship squat”. In shallow water conditions, the squat effect is accentuated. Given that ever larger container ships are being introduced and the fact that the rate of ship size growth outpaces dredging and port expansion projects, the likelihood of grounding is increased.

Various studies have been conducted to provide empirical methods for squat prediction but most methods are based on outdated hull forms and some do not include self-propulsion effect. It is known that there are large deviations between different prediction methods and this is especially true for high speed conditions where accurate prediction of container ship squat is important. Furthermore, unlike bulk carriers, the trim direction of container ships is not well understood. There are also other unaddressed concerns regarding squat such as significance of scale effect and initial trim. The accuracy of using the typical blockage ratio to quantify the effect of lateral restriction for channels with submerged banks is also doubtful. Consequently, the reliability of readily available empirical methods for accurate rapid assessment of squat is questionable, particularly for newer and larger container ships.

Therefore, this thesis presents a systematic investigation into the hydrodynamic squat phenomenon on modern container ships when underway in shallow water conditions using Computational Fluid Dynamics (CFD) simulations. Model tests are also undertaken to validate the CFD model. The ultimate goal of this investigation is to produce a new set of improved empirical formulae suitable for more accurate prediction of container ship squat by using regression analysis on the CFD predicted results.

Firstly, various CFD modelling techniques are benchmarked against model scale experiments conducted in this study and readily available experimental results in literature. The modelling of self-propulsion effect is also studied. Having determined the most suitable CFD modelling approach, the scale effect on squat is then investigated with account of self-propulsion effect. Upon investigating the possible influence of scale effect, systematic investigations to quantify the influence of hull principal particulars on squat are conducted. The quantified influence of principal particulars is then used to understand the trim behaviour of container ships as well as to develop a new set of regression formulae. Finally, investigations to quantify the effect of lateral restriction and initial trim effect are conducted to develop correction factors for the new empirical formulae. The final form of the formulae is tested against various cases and found to provide accurate predictions for cases that are within the recommended range. The new formulae is also shown to be consistently more accurate than existing

empirical methods for the cases tested. Reasonable correlations are also observed for comparisons against actual full scale squat measurements. The empirical formulae developed is an improved tool to perform rapid assessment of container ship squat that is well suited to time domain mathematical models. Hence, all the research objectives have been addressed satisfactorily.

Chapter 1 – Introduction

1.1. Background

The container shipping industry is highly competitive where an economy of scale is a fundamental tactic required to reap substantial profits as well as to meet increasing demands. Tactics of economies of scale involves the merging of shipping companies where funds are pooled to finance and introduce larger container ships. These large container ships have lower unit costs and the substantial savings contribute to considerable decrease in maritime transport cost. The decrease in transport cost in turn facilitates trade (Merk, 2018). Consequently, the increase in container ship size has accelerated and this potential growth trend over the years can also be seen in Figure 1.

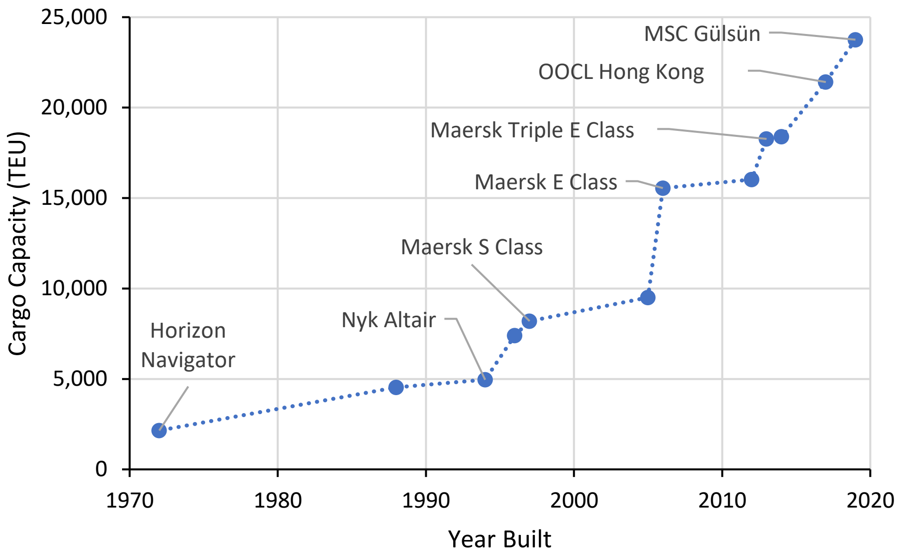

Figure 1: Container ship cargo capacity trend over a span of five decades.

This trend has continuously brought challenges to operate larger container ships in relatively shallow water regions such as approach channels and ports. This is because the flow around the hull changes as the ship moves, which causes the hull to sink vertically and trim either by the bow or stern. This is a common hydrodynamic phenomenon known as "ship squat". However, when vessels move in shallow water conditions, the squat effect is accentuated (refer to Figure 2). Therefore, the risk of grounding imposed by ever larger container ships squatting in shallow waterways has been a severe threat to the operational safety of undersized ports. Consequently, it is critical to understand the influence of ship design and operation parameters as well as channel restrictions on squat so that transits can be optimised. In essence, the ultimate goal is to maximise cargo throughput whilst avoiding grounding by having a reliable and accurate method for squat prediction.

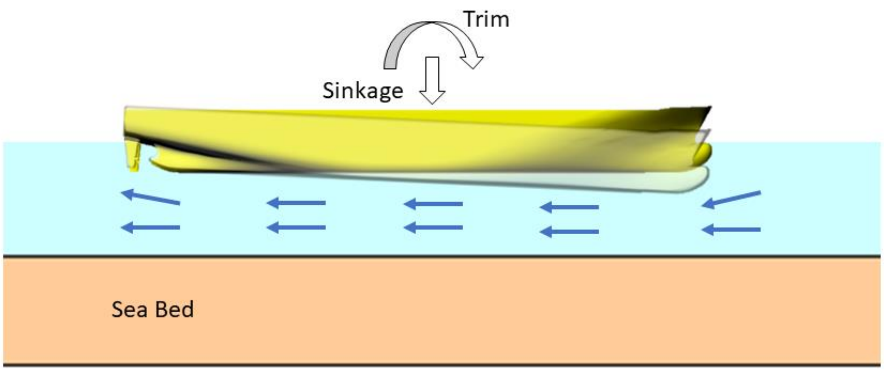

Figure 2: Squat occurs when a ship travels through water. This phenomenon can be considered a Bernoulli wave system where the water level around the ship decreases because of an increased relative speed between the ship and the surrounding water. The decrease in water level causes the ship to sink and trim. This effect is accentuated in shallow water conditions.

The focus of this investigation is on container ships because the accurate prediction of squat for these relatively slender hull forms is neither well understood nor has it received adequate attention. Unlike fuller hull forms, such as bulk carriers that are generally known to consistently trim by the bow, the trim direction of different container ships can be either by the bow or stern (Gourlay et al., 2015). Further complications arise as most existing empirical techniques are very dated and the spread between these predictions is often wide (Elsherbiny et al., 2020; Terziev et al., 2018; Collinson, 1994). There are various reasons for the spread in predictions, such as use of outdated hull forms, use of different predictor variables, possible inaccurate quantification, neglect of self-propulsion effect and possible scale effect. In addition, to the author's knowledge, there is no empirical technique dedicated for container ships. Instead, empirical techniques that claim to be valid for container ship hull forms are derived from a variety of starkly different hull forms. This may have also affected the reliability of the predictions.

Hence, this research aims to develop accurate modelling of squat using modern computational fluid dynamics (CFD) simulations and then investigate the various factors affecting squat systematically with exclusive focus on container ships. Data derived from the simulations will then be used to produce a more updated and reliable empirical tool for accurate prediction of container ship squat. This empirical tool will be helpful for quick assessment of container ship squat, and it will also be useful in dynamic underkeel clearance (DUKC) models.

1.2 Theory & Past Literature

This section firstly discusses the basic variables and terminologies often used in the study of ship squat. This is followed by a review of the various methods employed in the study of squat and key findings. Gaps in the literature and existing problems are then discussed at the end of this section.

1.2.1 Key Variables & Terminologies

In the discussion of shallow water investigations and ship squat, it is useful to define the key variables and terminologies often used. Pioneering studies into shallow water physics were focused on changes in a ship's wave pattern. Havelock (1908) studied wave pattern changes for a point pressure impulse travelling over a free surface in shallow water with respect to ship speed and water depth. The investigation led to the development of the non-dimensional relationship between ship speed and water depth known as the depth Froude number, Fr_{h}. The Fr_{h} is the defining parameter used for squat and shallow water related studies and the equation for this non-dimensional term is given as:

$$Fr_{\mathrm{h}} = \frac{V}{\sqrt{gh}} \qquad 1.$$

According to Constantine (1960), there are three distinct flow regimes for ships operating in shallow water; sub-critical ($Fr_{\mathrm{h}} < 1$) , critical ($Fr_{\mathrm{h}} = 1$) and super-critical ($Fr_{\mathrm{h}} > 1$) regimes. In the sub-critical range, flow is steady and squat can be considered to be governed by simple Bernoulli effect. During trans-critical flow, the flow becomes unsteady and a body of water accumulates by the bow until a solitary wave is produced forward of the ship. During the super-critical regime, the equations of Bernoulli and continuity apply but there is a reduced velocity alongside the ship and hence an increase in the depth of water causing the ship to rise above its original static position. The changes in the wave pattern during the three regimes are shown in Figure 3. For very shallow and laterally restricted water conditions, the critical or super-critical regime can be achieved with lower speeds (this is discussed further later). However, it should be noted that this study (and most existing literature) is only concerned with squat in the sub-critical regime because in practice, container ships do not have sufficient power to reach the critical or super-critical regime.

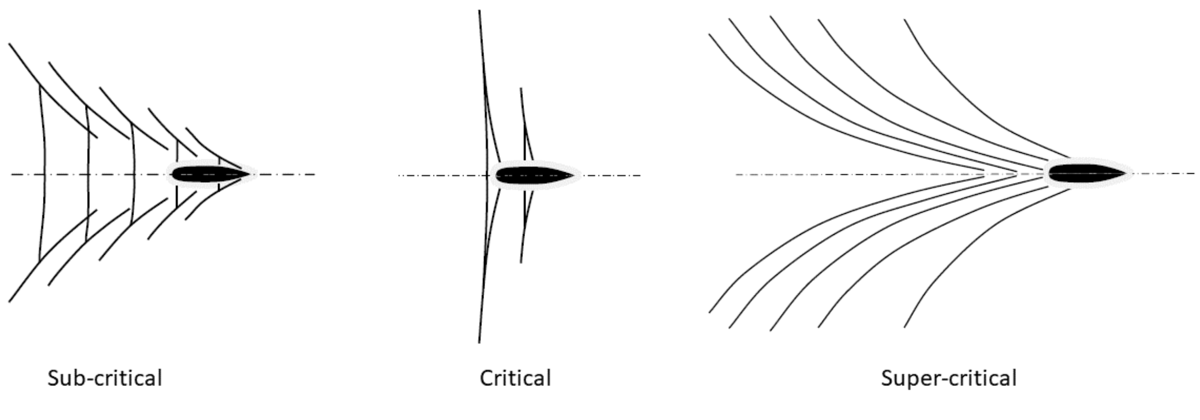

Figure 3: Wave patterns generated during the three different regimes. Figure adapted from Macfarlane (2012).

As mentioned earlier, water depth is an important factor in squat studies and it is usually non-dimensionalised simply as water depth to draft ratio (h/T).

Besides ship speed and water depth, the waterway configuration is also crucial and studied in detail. Generally, there are three main types of waterway configurations; unrestricted channel, restricted channel and canal configuration (refer to Figure 4). An unrestricted channel is simply a shallow channel without lateral boundaries such as the offshore end of entrance channels. An unrestricted channel is often referred interchangeably as "shallow open water". A restricted channel is representative of a dredged shallow channel and thus, have submerged banks/trenches whose height is denoted as h_m. Canal-type channels have lateral bounds from the channel floor up to the free surface such as in the case of rivers. Canals are also referred interchangeably as "confined waters". For laterally restricted configurations, the blockage ratio, m, is used to quantify the degree of restriction and is expressed as the ratio between the cross-sectional area of the ship, A_S, to that of the channel, A_C:

$$m = \frac{A_S}{A_C} \qquad 2.$$

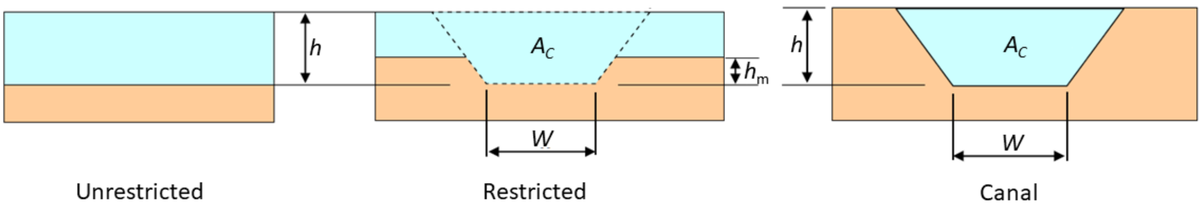

Figure 4: The three main types of waterway configurations.

In unrestricted channels, only the undulatory effect occurs. The undulatory effect is characterised as changes to wave pattern which in turn changes the wavemaking resistance. In restricted channels and canals, hydraulic effect appears in addition to the undulatory effect. The hydraulic effect here is an increase in viscous resistance due to return current or backflow. The magnitude of sinkage and trim in these laterally restricted conditions also becomes greater due to the backflow (Pompée, 2015). Therefore, the critical speed for laterally restricted conditions is no longer calculated using Equation 1. Instead, the below equation introduced by Schijf (1949) is used for laterally restricted conditions:

$$Fr_{\mathrm{h,Crit}} = \frac{V_{\mathrm{Cr}}}{\sqrt{gh}} = \left(2\sin\left(\frac{\mathrm{Arcsin}(1-m)}{3}\right)\right)^{3/2} \qquad 3.$$

The particulars of the ship such as length (typically the length between perpendiculars), beam, draft and block coefficient are also commonly used variables in existing empirical prediction methods. The choices of ship parameters however can vary significantly from method to method. A discussion of the relevant empirical methods is disclosed later in Section 3.5.1 and the formulae for these methods can be referred in Appendix B.

1.2.2 History of Ship Squat Prediction

Numerous studies have been conducted regarding ship squat and there are various methods developed to predict squat. Generally, the different categories of prediction methods can be classified as theoretical, semi-empirical and empirical. It should be noted that model testing covers a significant portion of past and ongoing studies but the improvement of computation power has also allowed for the use of numerical methods. Relevant summaries for each of the prediction methods, and findings from model tests as well as numerical methods are disclosed below.

Theoretical Methods

Theoretical methods are one of the pioneering methods developed and a common theoretical technique employed is prediction of water-level depression to predict the resulting squat. The basis of this theory is that the uniform water-level depression during squat can be calculated via use of the continuity equation, in conjunction with the conservation of energy (Bernoulli's equation) or conservation of momentum. In such methods, the ship is simplified as a fixed obstacle, whose cross-section is uniform across the entire length i.e. end effects are ignored. The ship sinkage is assumed to be equal to the water-level depression and trim is ignored. In addition, the flow is assumed to be one-dimensional and the water particle velocities in any cross-section of the channel are constant over that cross-section. The effects of the secondary wave system are ignored as well. Calculations using this method are effective when near the ship where the lengthwise-averaged water-level depression and ship sinkage are similar. However, when the channel width becomes wider, the assumptions tend to break down and accuracy of the predictions decreases.

There are many sinkage prediction methods based on the prediction of water-level depression coupled with conservation of energy (these are sometimes referred simply as "energy methods"). Examples of such energy methods are those presented by Constantine (1960), Balanin and Bykov (1965), Tothill (1967), McNown (1976) and Gates and Herbich (1977). Predictions from these methods are mostly similar and demonstrated reasonable correlation with measured sinkage values. Nonetheless, when the channel width to ship beam ratio is greater than 5, these methods tend to underpredict the sinkage (Blaauw & Knaap 1983).

Examples of the prediction of water-level depression via the conservation of momentum variant are works presented by Sharp and Fenton (1968) and Bouwmeester (1977). Their methods calculate both water-level depression and backflow velocity. The method of Sharp and Fenton (1968) is based on a channel with a rectangular cross-section whereas that of Bouwmeester (1977) is based on a trapezoidal cross-section and accounts for upstream water-level changes. Predictions using the method of Bouwmeester (1977) were found to yield reasonable correlations with model test results for a certain range of channel width. It was also noted that the sinkage predictions from Sharp and Fenton (1968) were significantly underestimated relative to that of Bouwmeester (1977) (Blaauw & Knaap 1983).

Another prominent theoretical method for squat prediction is the slender-body theory developed by Tuck (1966). The slender-body theory is used to calculate the vertical force and trim moment acting on slender ships in shallow water at both sub-critical and super-critical speeds. The calculated force and moment can then be used along with the ship hydrostatic particulars to predict the sinkage and trim. The assumptions in this theory are that the flow is incompressible, inviscid and irrotational. It is also assumed that the ships operate at high Reynolds number (order of 10^9) and are slender streamlined objects. Therefore, the viscous effects are confined to a thin boundary layer close to the hull and have negligible effect on the pressure distribution around the hull except at the stern (Gourlay, 2011). Tuck's results showed that sinkage is dominant in sub-critical speeds while trim is dominant in super-critical speeds. Predictions from the slender-body theory were observed to have reasonable correlations with model test results but correlations deteriorated for deeper water depths and when approaching critical speed (Blaauw & Knaap 1983). Tuck (1967) then extended his work to channels of finite width for sub-critical cases. It was found that the effect of finite width is more significant on sinkage than trim.

Tuck's formula became the foundation for the development of many other methods, some of which can be considered semi-empirical methods. For example, Tuck's formula was modified by Hooft (1974) to estimate bow squat. Huuska (1976) then conducted experiments in restricted shallow water conditions to derive a correction factor for blockage effect. Similarly, Vermeer (1977) modified Tuck's formulae to account for narrow canals. A three-dimensional squat theory for water of finite depth and width was later developed by Tuck and Taylor (1970). Pettersen (1982) introduced a numerical method to compute the three-dimensional, steady state potential flow past an arbitrary body moving horizontally in shallow water where the free surface is replaced by a rigid wall. In this method, the flow around midships is treated as two-dimensional whereas that at the ends are treated as three-dimensional. An iterative scheme is implemented to calculate the velocity potential in the two-dimensional region based on values from the three-dimensional region. Results using this method were found to have good agreement with model test results. Naghdi and Rubin (1984) used non-linear steady-state solution of the differential equation of the slender-body theory to predict squat in shallow water. Predictions from this method generally agrees well with model test results but accuracy deteriorates for shallower conditions. Cong and Hsiung (1991) then consolidated the slender-body theory and flat ship theory to predict squat for transom stern ships.

Semi-empirical Methods

There are also several semi-empirical methods for the prediction of squat. These methods combine theoretical methods with empirical corrections. For instance, Dand and Ferguson (1973) developed a semi-empirical formula for full form ships based on their model scale squat measurements in conjunction with a one-dimensional theory based on the continuity equation and conservation of energy. Dand and Ferguson (1973) also utilised Tuck's effective width parameter and developed propulsion correction factors for their semi-empirical method. Comparisons between their predictions and full scale measurements were encouraging considering the practical limitations relating to the accuracy of the full scale measurements. Similarly, Fuehrer and Römisch (1977) developed a semi-empirical method based on the energy approach and model test investigations. Their method evaluates the squat at critical speed as a function of the draft and then elaborates a speed dependent coefficient which enables squat to be predicted for any speed. Blaauw and Knaap (1983) found that predictions from the method of Fuehrer and Römisch (1977) generally overpredict squat whereas investigations by Millward (1990) reported that the bow sinkage was underestimated by up to 50% but midship sinkage prediction was more accurate.

Empirical Methods

Empirical formulae derived from model scale experiments are aplenty. Examples of such methods are those of Eryuzlu and Hausser (1978), Barrass (1979) and Millward (1992). The method of Eryuzlu and Hausser (1978) was derived from tests on three self-propelled VLCC models in an unrestricted channel of various depths. Barrass (1979) developed a formula based on 300 squat results where some are measurements from ships and others are from model tests. Millward (1992) derived an empirical formula based on experiments which account for ship speed and various hull forms (different C_B). Comparisons conducted showed that predictions using the method of Eryuzlu and Hausser (1978) correlated satisfactorily with model test results for a range of channel widths (Blaauw & Knaap 1983). The method of Barrass (1979) correlated well for VLCCs but poor correlations were observed for LNG carriers. Predictions from Millward's formulae agreed well with published data for a ferry but it was noted to have a tendency to overestimate squat at high Fr_h (Millward, 1992). A more recent empirical method derived from model tests is that of Ankudinov (2009). This method is one of the most thorough as well as complicated methods which has undergone considerable revision as new data were collected and compared. Comparisons demonstrated that the bow and stern squat predictions using this method tend to be overpredicted by factors of two or larger relative to most of the other empirical formulae (Briggs, 2009).

Comparisons between prediction formulae have been made by several authors and the general consensus is that a large divergence of results amongst the different formulae is often observed. Investigations by Collinson (1994) concluded that no single prediction method provided the best correlation for all cases. The wide scatter in results is also acknowledged in recent comparisons by Terziev et al. (2018), Elsherbiny et al. (2020) and Kok et al. (2020c). In fact, the Permanent International Association of Navigation Congress (PIANC) recommends model tests be conducted for specific ship and channel conditions, especially if the conditions are novel so that better estimates of squat are possible (Briggs, 2006).

Contemporary Model Testing

Different kinds of model tests have been and are still being carried out to improve the understanding on squat and the fidelity of predictions. The impact of propeller action on squat is one of the effects that has been investigated in detail by many researchers. It is known that an operating propeller increases the sinkage force and also the trim moment by the stern depending on ship speed and water depth. This is because a rotating propeller accelerates the flow near the stern. The reduced pressure due to accelerated flow at the stern results in an increased sinkage and trim by the stern. The greater the thrust, the greater the sinkage and trim by the stern but the effect upon trim tends to be more significant than on sinkage (Duffy & Renilson, 2000). Dand and Ferguson (1973) are among the earliest to investigate the effect of self-propulsion on sinkage and trim via model testing which they then incorporated into their semi-empirical formulae. Similarly, Duffy and Renilson (2000) conducted model scale experiments to derive empirical corrections for the propulsion effect for bulk carriers at a range of thrust settings. Lataire et al. (2012) also conducted model tests that demonstrated the increase in aft perpendicular (AP) sinkage with respect to propeller rate. They developed a correction factor based on propeller thrust and propeller diameter to be applied to their variation of the Dand & Ferguson (1973) formulation.

Duffy (2008) also conducted extensive model testing to develop a novel set of empirical formulae with emphasis on unsteady squat predictions and dynamic acceleration effects for a ship travelling in water of non-uniform depth. His investigations showed that ships can "detect" abrupt changes in water depth ahead and there will be instantaneous changes to the squat before the ship reaches the point of abrupt change in water depth. Generally, the unsteady sinkage trend predicted by the formulae developed is reasonable when compared against unsteady sinkage measurement of a model ship travelling over a simplified ramp bank. Changes in bow sinkage due to abrupt changes in water depth was also modelled satisfactorily by including the dynamic acceleration effects. Nonetheless, the maximum unsteady sinkage was not always predicted accurately which may be due to the limitations and assumptions of the technique applied.

Bank effects on squat are also widely studied. It should be noted however that most studies regarding bank effects are concerned with the induced yaw moment and sway force. The current discussion will only discuss recent findings regarding bank effects on squat. Lataire and Vantorre (2008) studied the forces and moments induced by irregular bank geometries via model testing. Through their investigations, they proposed a parameter for horizontal reach of a bank known as the "influence width". A ship travelling at a distance further than the influence width does not encounter significant bank effects. They also introduced a parameter known as "equivalent blockage" which is a more sophisticated method of quantifying blockage based on the concept of "weight distribution" described by Norrbin (1976). Similarly, a sophisticated method to quantify the distance of a bank to the ship based on the “weight distribution” was also introduced as the “distance to bank” or “d2b”. Lataire et al. (2016) also quantified the change in bow and stern sinkage with respect to canal width, lateral position, bank slope and water depth.

There are many more variables that are being investigated experimentally and taken into account to improve the fidelity of squat predictions. The mathematical model developed by Eloot et al. (2008) is among the relatively newer empirical formulae developed which accounts for a significant amount of variables. Their formulae accounts for the ship speed, ship geometry, loading condition, drift and yaw rate, propeller action, the fairway restrictions, bank geometry and ship-ship interaction. Their Tuck parameter based formulae have been compared against full scale measurements, where the absolute maximum sinkage was noted to have good correlations but the direction of trim was wrongly predicted for certain cases.

Other model testing aimed to improve the fidelity of squat predictions include the study of muddy bottom effects. The presence of a soft fluid mud layer on the bottom of a channel is not uncommon but its effects are mostly assumed to be negligible in the prediction of squat. Literature regarding muddy bottom effects is scarce and findings are sometimes in contradiction. The latest relevant experimental study was conducted by Delefortrie et al. (2010) where it was concluded that the presence of a mud layer tends to decrease sinkage but trim changes are not always consistent. Based on the model test data, they developed a mathematical model of reasonable accuracy which accounts for the bottom conditions, propeller action and the principle of a hydrodynamically equivalent water depth.

Numerical Methods – Potential Flow

The advancement of computation power has enabled the implementation of numerical methods in the study of ship squat. In fact, an increasing portion of recent literature report numerically based research. The potential flow method also sometimes referred as panel method, is the earliest form of numerical method introduced and still actively used today.

Potential flow methods come in many variants but generally, these methods (as evident in their namesake) solve potential flow problems, where arbitrary flow geometry is mathematically generated by distributing singularities over planes (panels) in the field. Sources are used and distributed in a manner such that a closed streamline is formed. Closed streamlines can be thought of as boundaries of a solid body since no flow can travel over these streamlines. However, the limitation of such an approach is that these “streamline bodies” have no boundary layers. Thus, typical panel methods cannot account for viscous effects and “no-slip” conditions on solid surfaces. Generally, potential flow solutions are also only valid for conditions where the flow is inviscid, incompressible, irrotational and steady (Larsson, 1993).

Modelling of the free surface in potential flow methods is achieved either by panelling the free surface or for low speed conditions; by adopting the double body approach. The double body approach assumes that the free surface is nominally flat such that the resulting flow field can be modelled without panelling the free surface. Instead, a mirror image of the hull sources is reflected about the free surface. Consequently, there is no need for large numbers of panels to model the free surface. For low ship speeds, the free surface wavelengths are sufficiently small such that the double body approach can yield good and robust results (Garrison, 1978).

One of the earliest implementations of the potential flow method was conducted by Dawson (1977). Dawson (1977) presented the wave resistance and wave elevation predictions obtained through potential flow for a Wigley hull and Series 60 hull in deep, laterally-unrestricted water. The predictions were found to have good correlation with model test data especially when more panels were used for the numerical predictions. Yasukawa (1993) then developed a Rankine source panel method which is able to compute the steady wave-making resistance of a ship including the effects from sinkage and trim. The wave-making resistance, sinkage and trim measured from model testing of a Wigley hull were found to compare well with that of Yasukawa's method.

Eventually, potential flow methods were adapted for shallow water investigations. Jiang (1998) applied the Boussinesq type shallow water equations in his numerical investigations on the waves generated by a ship at three different speed regimes.The numerical problem was represented by a finite-difference equation system and solved iteratively. Satisfactory agreement was found when the wave resistance, sinkage and trim of a Series 60 hull measured from experiments were compared against the numerical predictions. Gourlay (2008b) presented a review of linear slender-body theories for the prediction of squat in shallow open water, a rectangular canal, a dredged channel, a stepped canal and a channel of arbitrary cross-section. Then, Gourlay (2008a) introduced a slender-body based numerical method to predict sinkage and trim of fast displacement catamarans in shallow open water. He demonstrated that the demihull centreline spacing does not significantly impact sinkage and trim at sub-critical speeds but trim significantly decreases at higher super-critical speeds.

Yao and Zou (2010) used a first order, three-dimensional panel method to study the sinkage and trim of a hull advancing in a restricted channel. They discretised the hull surface, channel walls and free surface into panels on which Rankine sources of constant strength are distributed upon. An iterative scheme was implemented to deal with the non-linear boundary conditions of the free surface. Raised panels above the free surface were also used to satisfy the radiation condition and the channel bottom boundary condition was modelled via the method of images. The wave pattern, wave-making resistance, sinkage and trim predicted by their numerical method correlated well with that of model test data for a Series 60 hull.

Alderf et al. (2011) developed a finite element method for numerical modelling of dynamic squat. Their model allows interaction between a two-dimensional potential flow in highly restricted channels having non-uniform depths with stationary free surface. Their method implemented a mesh update model known as the “moving submesh approach”, which is computationally economical. It was demonstrated that their model could provide accurate steady squat predictions as well as output dynamic responses of a ship in highly restricted channels with arbitrarily shaped bottoms.

Gourlay et al. (2016) presented a comparison of various potential flow methods against model test results for a KVLCC2 model for a range of canal widths ($1.05 \leq W/B \leq 9.05$) and water depths ($1.1 \leq h/T \leq 1.5$). The methods compared are the linear two-dimensional, non-linear one-dimensional, double body and Rankine source methods. Comparisons of the predictions with model test data suggest that the accuracy of each method varies with the cases. The linear two-dimensional method yielded good results for wider canals particularly with shallower water depths. The non-linear one-dimensional method was the most accurate for the narrowest canals. The Rankine source method was preferable for wider canals at high speeds. Across all conditions investigated, the double body method tended to be the most consistent.

McTaggart (2018) used a boundary element method for different hull forms and compared four different types of free surface modelling; fully-nonlinear, double body linearised, uniform linearised and double body approaches. The fully-nonlinear approach was found to give the best sinkage and trim predictions for the DTMB 5515 destroyer and series 60 hull. However, all four approaches underestimated the sinkage for the KVLCC2 in much shallower water ($1.1 \leq h/T \leq 1.5$).

Numerical Methods – CFD

In recent years, more powerful numerical methods, such as Computational Fluid Dynamics (CFD) have become feasible for hydrodynamic predictions. CFD has been used extensively for ship hydrodynamics and even became first generation simulation-based design tools. This is because CFD accounts for important features of the actual flow such as viscous effects and turbulence, in addition to the development of various enabling technologies. Some of these enabling technologies include free surface tracking/capturing, turbulence modelling, six degree of freedom (6-DOF) motion prediction, dynamic overset grids, local/adaptive grid refinement, high performance computing, environmental modelling and optimisation methods. CFD methods can be further categorised based on the turbulence modelling method applied; Direct Numerical Simulation (DNS), Large Eddy Simulations (LES), Reynolds-Averaged Navier-Stokes (RANS) approach and hybrid RANS-LES.

The DNS approach directly resolves the Navier-Stokes equations and thus, all the spatial scales of the turbulence are resolved. However, this approach requires significantly large numbers of grids such that it is not practical to conduct with current computation power. LES is similar to DNS except that the smallest spatial scales of turbulence are ignored via low-pass filtering of the Navier-Stokes equations and so, reducing most of the computational cost. Nonetheless, the grid requirements for LES is still large such that it has limited practical use. RANS approach is the most used method where the large scales of motion are resolved while the entire turbulence scale is modelled. A hybrid RANS-LES applies RANS approach to the boundary layer and LES in the inviscid flow region (Stern et al. 2013).

It should be noted that the RANS approach is the most practical CFD method for hydrodynamic investigations such that the mention of CFD in most literature on squat studies is generally referring to the RANS approach. One of the earliest uses of CFD in the study of ship squat was conducted by Jachowski (2008). Fluent, a commercial RANS solver, was used to predict the squat of a model KCS in open water of different water depths ($1.2 \leq h/T \leq 22.4$) and varying ship speeds. Comparison of the numerical results correlate well with the mean of several empirical formulae. Prakash and Chandra (2013) used a similar RANS solver to study the effect of confined waters on wave pattern and ship resistance at various speeds. The wave pattern generated by the CFD method showed general agreement and the predicted resistance compared well with the approximated resistance using the method of Schlichting (1939).

Linde et al. (2015) investigated the effect of waterway restrictions on resistance and sinkage by using a quasi-Newton approach that bypasses the transient state, effectively speeding up the convergence. The importance of accounting for the change in sinkage in the prediction of resistance in confined waters was highlighted. Tezdogan et al. (2016) used a commercial RANS solver, STAR-CCM+ to investigate the resistance and sinkage of the KCS hull advancing through a canal. It was concluded that the resistance increases with both speed and vessel draft. The sinkage predictions compared well with experiment data where sinkage is greater for deeper vessel draft. Trim was not analysed in the study. Shevchuk et al. (2016) compared the flow field under a ship's keel in finite water depth predicted from both unsteady RANS (URANS) and hybrid URANS-LES simulations. It was noted that the boundary layer grew on both the hull and the channel bottom which led to significant viscous effects. The costly hybrid URANS-LES simulations exhibited the existence of flow separation structures at very shallow water depths but the mean dynamic sinkage and trim was still similar to that of the pure URANS simulations.

The findings discussed thus far are all based on model scale conditions. However, full scale investigations are also possible and has been conducted with the use of CFD. Castro et al. (2011) presented results of full scale self-propulsion computations using a fully discretised propeller for a KCS hull in deep open water. The propeller open water curves from both model scale simulation and benchmark data were shown to have excellent correlation. Comparisons between the model scale and full scale self-propelled simulations concluded that the mean thrust output for both scales are similar but the smaller load fluctuations for the full scale condition suggest that propeller operation is more efficient in full scale. Deng et al. (2014) conducted shallow water simulations that compared the bow and stern sinkage predictions for a DTC hull at both model scale and full scale conditions. The results show that the trim for model scale condition changes from bow down to stern down as speed increases while the trim for full scale becomes increasingly bow down when speed increases. Overall, the bow sinkage for full scale condition is consistently greater than that at model scale whereas the stern sinkage for full scale condition is consistently smaller than that at model scale. Tezdogan et al. (2015) also conducted full scale simulations to study the motion and added resistance of the KCS hull at different speeds. The predicted heave and pitch transfer functions, total resistance coefficients and added resistance coefficients were all within 10% of the benchmark data. This study also demonstrated the superiority of the CFD predictions over that of a linear potential flow method, especially for high speed conditions.

More published literature relating to squat in shallow water using CFD methods soon became available in the midst of the execution of this dissertation. Yuan et al. (2019) studied the change in sinkage, trim and total resistance of the DTC hull in calm water using the morphing mesh approach. They also studied the change in sinkage, trim, wave forces and added resistance in head wave conditions. Their results suggest that waves with longer wavelengths tend to increase the overall response amplitude operator (RAO) of both heave and pitch which ultimately reduces the underkeel clearance. Bechthold and Kastens (2020) also implemented the morphing mesh method to predict the sinkage and trim of three container ships in different channel configurations. Reasonable correlation between the CFD predictions and experiment data for sinkage and trim was noted for very low water depth to draft ratios. The change in sinkage and trim patterns due to change in channel configurations and blockage ratio were discussed.

Other unique CFD studies conducted in recent years include the study of the muddy layer effect. Kaidi et al. (2020) was able to model and study the muddy layer effect on ship resistance, sinkage and trim. Their results were validated against model test data. They found that the internal wave patterns depend strongly on the mud properties. It was shown that the ship's sinkage was only influenced by the mud layer when the underkeel clearance was negative but the ship's resistance was affected even when the underkeel clearance is positive.

1.2.3 Problem Statement

From the review above, there are several issues and unresolved matters in relation to accurate prediction of ship squat. Firstly, most of the readily available prediction methods are at least two to four decades old. Most of these methods are semi-empirical or empirical methods such as that of Dand and Ferguson (1973), Fuehrer and Römisch (1977), Eryuzlu and Hausser (1978), Barrass (1979) and Millward (1992). As pointed out by Gourlay et al. (2015), the design of modern container ships has changed significantly over the years. Modern designs represented by the KCS and DTC hulls have noticeably higher bulbous bows, pronounced stern bulbs and transom sterns in comparison to the dated designs represented by the

S175 model. This raises concerns regarding the validity of many readily available prediction methods for application to modern container ships.

To the author's knowledge, the method of Ankudinov (2009) is the most updated method that is readily available for public use. Nonetheless, the method of Ankudinov (2009), like many other existing methods share a common feature which the author believes may not be favourable in practice. This unfavourable feature is that the methods that are valid for fine hull forms (container ships) are usually based on data for vessels with a wide range of block coefficients. This brings complications to the prediction of trim and thus, the overall accuracy of squat predictions. It may be generally agreed that fuller hull forms such as bulk carriers will consistently trim by the bow but this is not the case for container ships. Initial suggestions that the block coefficient determines the trim (Barrass 1979) proved otherwise as Uliczka and Wezel (2005) pointed out that the trim depends on hull form details and vessels with the same block coefficient but a subtly different hull form may exhibit different trim direction. To make matters worse, most of the existing formulae just assumes maximum sinkage occurs by the bow and do not output trim predictions. Therefore, the author believes that a formulae developed exclusively based on container ship hull forms would be more suitable for container ship squat predictions and further investigation into the trim direction of container ships needs to be undertaken.

In order to ensure accurate trim predictions (as well as sinkage), self-propulsion effects must be accounted for, especially at higher speeds as highlighted by Lataire et al. (2012), and Duffy and Renilson (2000). Nonetheless, most of the CFD investigations on ship squat conducted thus far are in bare hull conditions or with a stationary propeller. There is a need to investigate whether self-propulsion effects in shallow water can be modelled adequately via a body-force propulsion virtual disc or otherwise, a fully discretised propeller model.

In conjunction to the above, the accuracy of existing methods for high speed ($Fr_h > 0.5$) squat predictions are also a concern. Although *slow steaming* is gradually becoming a widely adopted practice to combat rising fuel cost and stringent emission policies, there are still occasions where compromise is necessary. High speed sailing is sometimes required to avoid delays and port congestion (Lee at al., 2015). Unfortunately, as mentioned previously, the predictions of existing methods can differ significantly especially at higher speeds. Therefore, it is beneficial to be able to accurately predict the squat for high speed conditions so that port throughput can be maximised whilst avoiding grounding.

In addition, there is the issue of scale effect. There is limited literature available regarding full scale investigations and scale effect in ship squat. Ha and Gourlay (2017) demonstrated that the slender-body theory can predict squat with reasonable accuracy for container ships at full scale in open dredged channels. However, scale effect in ship squat was investigated by Eryuzlu et al. (1994) where it was noted that the boundary layer thickness and viscous effects on the model scale ship hull cannot be extrapolated linearly as the model scale experiments are conducted at a smaller Reynolds number than the full scale scenario. In addition, model and full scale CFD simulation comparisons conducted by Deng et al. (2014) and Gilligan (2015) have shown for isolated simplified cases that scale effect is indeed significant. In summary, the available findings regarding scale effect on squat are contradictory and remain unclear. Further complications arise as most of the full scale CFD simulations do not include self-propulsion effect.

Moreover, there is a lack of understanding regarding the effect of changes in principal particulars of a modern container ship on squat. Given that subtle changes to hull form can cause substantial difference in squat (Uliczka & Wezel 2005) and that the container ship hull designs are ever changing to increase payload, it is necessary to understand the effect of manipulating certain design variables on squat. Currently, there are no literature discussing the sensitivity of squat to ship design parameters. It should be borne in mind that currently existing squat prediction methods can yield starkly different results for the same case studies (Collison, 1994) and this is particularly true at high speeds (Kok et. al., 2020c).

Another issue to consider is the method of quantifying the blockage of a restricted channel or canal. Most existing methods share the same method for calculating the blockage ratio, which is simply the ratio of midship cross-sectional area to channel/canal cross-sectional area. In the author's opinion, this is not an adequate method especially for channels with submerged banks (restricted channels). This is because the method for calculating the channel cross-sectional area does not account for the height of the submerged bank since the channel cross-sectional area is taken simply as the area bounded by the channel bottom and extrapolation of the bank slopes to the water surface (refer to Figure 4). This would imply that two restricted channels of the same widths but significantly different bank heights would have the same cross-sectional area and thus, same blockage ratio. Evidently, this is not an accurate method to quantify the cross-sectional area and blockage ratio. Instead, the author proposes the use of the concept of "equivalent blockage" and "weight factor" introduced by Lataire and Vantorre (2008). Lataire and Vantorre (2008) have utilised these methods to quantify bank induced yaw and sway effectively. The author believes that these methods will be similarly effective in the quantification of squat change due to lateral restrictions.

Finally, there needs to be consideration of the effect of initial trim on squat. In practice, ships will often operate with an uneven static trim. This is because various investigations have found that trim optimisation can help sailing ships save 2-5% on fuel costs and this also corresponds to reduction in greenhouse gas emissions (ABS, 2014; IMO, 2016). It should also be stressed that trim optimisation is important for the management of underkeel clearance in shallow water conditions (Harting & Reinking 2002). However, literature regarding the impact of initial trim is mostly concerned with resistance whereas results on the impact of initial trim on squat is scarce. It is not known whether changes to the initial trim of a container ship will change the hydrodynamic features such that the squat behaviour of the ship is altered significantly. An investigation is necessary to determine whether initial trim is worth consideration in the prediction of container ship squat.

Hence, there are clear gaps in the literature which this study seeks to address. Nevertheless, all these issues highlighted are interrelated and should be tackled individually in an order that is strategic. The first problem to be addressed is to develop a CFD model for squat prediction which includes self-propulsion effect and is reliable at relatively high speeds ($Fr_h > 0.5$). The next step would be to investigate the scale effect in squat. Then, the effect of hull principal particulars on squat of a relatively modern container ship is to be quantified to study the nature of sinkage and especially trim direction. This is followed by development of an improved empirical prediction method based on the derived CFD data to address the issue of conflicting predictions from currently existing methods. Lateral restriction and initial trim effects are also to be quantified to be developed as correction factors for the formulae. Successful modelling of the self-propulsion effect will provide more accurate quantification of scale effect. The quantified scale effect can then be applied in the quantification of the effect of hull principal particulars, which in turn can be used for modelling an improved empirical formulae-based rapid squat assessment technique. Such a technique will be ideal to include in dynamic underkeel clearance (DUKC) models.

1.3 Objectives

As highlighted in the previous section, there remains some uncertainty regarding the study and accurate prediction of container ship squat which this study aims to investigate. The objectives of the present study are:

- Develop a reliable CFD modelling technique that accounts for self-propulsion effect to predict midship sinkage and trim accurately at relatively high speeds ($Fr_h > 0.5$)
- Investigate scale effect in container ship squat. Self-propulsion effect is to be accounted for where possible.
- Quantify the influence of principal particulars (hull parametric variations) on both midship sinkage and trim of a relatively modern container ship. Self-propulsion effect is to be accounted for. The nature of a container ship's trim direction is to be determined as well.
- Produce an empirical formulae-based rapid assessment technique for high speed modern container ship squat which outputs both midship sinkage and trim. Consideration of lateral restriction and initial trim effects are to be included.

Therefore, the significance of this study is to provide a rapid assessment technique for better container ship squat predictions that are valid for high speed conditions. This will enable container ship operators to maximise operational efficiencies whilst avoiding grounding. From another perspective, the empirical formulae produced can also be thought of as an aid for ship or approach channel designers to understand the implication of certain design changes on squat.

1.4 Methodology

In order to achieve the objectives of this research, the work is broken down into four chronological phases as listed below. Phase 1 of the research aims to develop a reliable CFD model for accurate prediction of midship sinkage and trim at high speeds with consideration of self-propulsion effect. Various CFD modelling techniques are benchmarked against published experimental results and the most suitable modelling technique is determined. Data from model tests conducted as part of this study as well as published model test data are used to validate the CFD models. The accuracy of the chosen CFD model in comparison to existing empirical methods are also compared. In Phase 2, scale effect investigations are performed using the chosen CFD model to determine the credibility of extrapolating model scale results to provide a full scale prediction. Actual full scale cases are replicated to assess the validity of the scale effect finding. This is followed by Phase 3 where an extensive systematic study is conducted to quantify the effect of hull parametric variations on midship sinkage and trim. Statistics of currently operating container ships are firstly studied to quantify the range of different principal particulars. The influence of principal particulars on sinkage and trim is then investigated and analysed. The nature of container ship trim direction is also examined. The database of results from Phase 3 is extended in Phase 4 where multiple linear regression analysis is conducted on the results to develop a set of empirical formulae. Further investigations to quantify the effect of lateral restrictions and initial trim on squat are carried out to be incorporated in the new empirical formulae. The four phases are outlined below:

- Phase 1 – Benchmarking Study
    - Explore various CFD modelling techniques to determine the most suitable model
    - Benchmark the CFD models against existing and also locally conducted model test data
    - Investigate whether the developed CFD model is more accurate than existing empirical methods

- Phase 2 – Scale Effect Investigation
    - Develop and validate full scale CFD model for squat prediction
    - Replicate full scale squat cases provided by OMC International

- Phase 3 – Effect of Hull Principal Particulars on Squat
    - Investigate statistics of the principal particulars of currently operating container ships
    - Systematically vary hull principal particulars and investigate the effect on squat

    - Investigate the nature of a container ship's trim direction

- Phase 4 – Modelling of Container Ship Squat
    - Develop empirical formulae using regression analysis techniques on CFD results for laterally unrestricted and evenly trimmed cases
    - Quantify and incorporate lateral restriction effect and initial trim effect to the formulae
    - Evaluate developed formulae against further simulation results and real-world cases

1.5 Research Novelty

The novel components of the work and contributions to the research field of container ship squat can be summarised as follows:

- Published studies regarding CFD simulations of ship squat is relatively scarce in comparison to model tests. In addition, there are a variety of approaches to model the ship squat phenomenon in CFD. Most of the past literature on CFD simulations of squat also do not account for self-propulsion effect. Therefore, in this study, a comprehensive benchmarking study of various CFD modelling techniques to determine the most suitable modelling technique is presented. The performance of set-ups based on quasi-static, overset mesh and morphing mesh techniques are reviewed. The performance of a body-force propulsion virtual disc and a fully discretised propeller for modelling self-propulsion effect in squat is also compared. The subsequent incorporation of the body-force propulsion virtual disc with the chosen quasi-static and morphing mesh methods are novel techniques for squat simulation.
- A handful of past studies have investigated scale effect in container ship squat but the self-propulsion effect was not considered in these studies. Hence, this study adopts a more comprehensive CFD modelling technique which incorporates self-propulsion effect to study the scale effect in container ship squat where possible. This helps determine the validity of full scale squat predictions extrapolated from model scale predictions more accurately.
- The influence of principal particulars on container ship squat is not explicitly investigated in existing literature. Given that current container ship designs can vary significantly and new designs are changing to maximise cargo-carrying capacity, it is useful to understand changes in squat due to changes in principal particulars of a container ship. The influence of length-to-beam ratio, beam-to-draft ratio and block coefficient on midship sinkage and trim has been investigated and discussed in this study.
- Previous studies have identified that the direction of trim for container ships can either be by the bow or stern unlike bulk carriers that tend to trim by the bow (Gourlay et al., 2015). The nature of the trim direction is not well understood. Some studies attempted to use the block coefficient as a parameter to determine the trim direction but this was proven ineffective

(Uliczka and Wezel, 2005). In this study, a systematic investigation has been undertaken which successfully demonstrates the gradual change of trim direction with respect to a new parameter. This new parameter uses the LCB and LCF to quantify the hull volume distribution which is more reliable than the block coefficient for determining the trim direction and magnitude.

- Most existing empirical techniques are designed to be applied for full form hulls only or a range of hull forms which affects the accuracy of predictions for container ships. Furthermore, most existing methods do not output trim predictions or just erroneously assume that the maximum sinkage occurs by the bow. Hence, a new set of empirical formulae based on CFD computations dedicated to predicting modern container ship squat is presented. Trim direction and magnitude are accounted for explicitly in this new set of formulae. The effect of initial trim on squat is also considered in the development of the formulae.
- The accuracy of most existing empirical methods is inconsistent and differ significantly from one another especially at high speeds ($Fr_h > 0.5$). The new set of formulae developed is based on CFD that is validated for high speed conditions up to $Fr_h = 0.683$. Therefore, the developed set of formulae is specially designed to consider high speed conditions and has been shown to consistently produce accurate predictions at high speeds for various cases that are within the recommended range of applicability.
- Most existing empirical methods utilise the blockage ratio to account for the effect lateral restrictions and finite depth on squat. In the author's opinion, the blockage ratio is not sufficiently adequate to quantify the said effect. On the contrary, the concept of "equivalent blockage" and "weight factor" introduced by Lataire and Vantorre (2008) have been shown to be able to quantify the effect of bank-induced yaw and sway accurately. Hence, the formulae produced in this study adapts the concept of "equivalent blockage" and "weight factor" for squat predictions in laterally restricted cases.

1.6 Thesis Structure Overview

The content of this thesis is distributed into 7 chapters. Chapter 1 serves as an introduction to the work of the thesis. Chapter 2 provides an in-depth discussion about the technical methodologies implemented in the research including the nature of the CFD method applied and the subsequent regression analysis technique to develop a set of empirical formulae. Chapter 3 discusses the various modelling techniques as well as empirical predictions that were benchmarked and compared in the study. Results of experimental validation are also demonstrated in this chapter. The possible influence of scale effect is then discussed in Chapter 4. Chapter 5 addresses the investigation of the influence of principal particulars on container ship squat whereas Chapter 6 discusses the development of the new empirical formulae and incorporation of lateral restriction and initial trim effects. Performance of the developed formulae are also evaluated. Finally, Chapter 7 provides concluding remarks and recommendations for future work.

The contents of Chapters 3 to 5 have been published as journal and or conference articles. The specific publications for each chapter are mentioned in the opening of the respective chapters. All of these publications can be viewed in Appendix E.

Chapter 2 – Computational Method & Regression Analysis

This chapter provides an overview concerning the primary technical methodologies applied in the research; CFD and regression analysis. Firstly, background is given on the CFD method that is used to develop a validated model for producing a matrix of squat data. Secondly, background is provided on the regression analysis techniques used to develop empirical formulae from the matrix of squat data.

2.1 Computational Method (CFD)

An unsteady RANS solver (URANS) is adopted in this study to account for viscous effects and unsteady components such as propeller action. The commercial STAR-CCM+ URANS solver was used to conduct all the computations presented. The finite volume method of discretisation is used to resolve the incompressible RANS equation in integral form.

2.1.1 Governing Equations

The modelling of the container ship squat in this study accounts for free surface effects and hence, involves two phases; air and water. The governing equations for URANS which includes two phase incompressible flow are given as (Rusche, 2003):

$$\nabla \cdot \mathbf{u} = 0 \qquad 4.$$

$$\frac{\partial \rho \mathbf{u}}{\partial t} + \nabla \cdot \left[\rho \mathbf{u}\mathbf{u}\right] = -\nabla p^{*} - \mathbf{g} \cdot \mathbf{x} \nabla \rho + \nabla \cdot \left[\mu \nabla \mathbf{u} + \rho \boldsymbol{\tau}\right] + \sigma_T \kappa_\gamma \nabla_\gamma \qquad 5.$$

In the above equations, $\mathbf{u}$ = (u,v,w) or in other words, the velocity field in cartesian coordinates. ∇ is the gradient operator (∂/∂x, ∂/∂y, ∂/∂z), p* is the pressure including hydrostatic pressure, ρ is the fluid density which varies with the content of air/water in the computational cells, **g** is the gravitational acceleration, μ is the dynamic molecular viscosity, σ_T is the surface tension coefficient and κ_γ is the surface curvature. The term $\boldsymbol{\tau}$ is the Reynolds stress tensor and it is given as:

$$\boldsymbol{\tau} = \frac{2}{\rho} \mu_t \mathbf{S} - \frac{2}{3} k \mathbf{I} \qquad 6.$$

where μ_t is the effective dynamic eddy viscosity, $\mathbf{S} = (1/2\ (\nabla \mathbf{u} + (\nabla \mathbf{u})^T))$ is the fluid strain rate tensor, k is the turbulent kinetic energy per unit mass and **I** is the identity matrix.

In order to solve the above equations for air and water simultaneously, the fluids are tracked using the volume of fraction, γ. γ indicates the relative proportion of fluid in each cell and its value is always between 0 and 1:

$\gamma = 0$ air

$\gamma = 1$ water

$0 < \gamma < 1$ interface/mixture of air and water

The following advection equation models the distribution of γ (also known as the Volume of Fluid (VOF) equation):

$$\frac{\partial \gamma}{\partial t} + \nabla \cdot [\mathbf{u}\gamma] + \nabla \cdot [\mathbf{u_r}\gamma(1-\gamma)] = 0 \qquad 7.$$

where $\mathbf{u_r} = \mathbf{u_{water}} - \mathbf{u_{air}}$ is the relative velocity vector. With the implementation of γ, the spatial variation in ρ and μ in the governing equations are defined as:

$$\rho = \gamma\rho_{water} + (1-\gamma)\rho_{air} \qquad 8.$$

$$\mu = \gamma\mu_{water} + (1-\gamma)\mu_{air} \qquad 9.$$

2.1.2 Turbulence Modelling

Closure of the RANS equations is achieved with the implementation of the k-epsilon (k-ε) model. The justification for the use of the k-ε model is that it is more computationally economical compared against the k-ω model (Tezdogan et al., 2016) and that the squat prediction is not influenced greatly by the type of turbulence model (Deng et al., 2014). In fact, there have been various positive results for squat studies that use the k-ε model (Bechthold and Kastens, 2020; Deng et al., 2014; Kok et al., 2020c; Tezdogan et al., 2016). The specific k-ε model implemented in the study is the Realizable k-ε Two-Layer turbulence model. According to CD-Adapco (2014), this variant is the default k-ε model as it is substantially better than the Standard k-ε model for many applications and has the added flexibility of an all y+ wall treatment. The transport equations in STAR-CCM+ are on the basis of the descriptions by Jones and Launder (1972):

$$\frac{\partial(\rho k)}{\partial t} + \nabla \cdot [\rho k \mathbf{u}] = \nabla\left[\left(\mu + \frac{\mu_t}{\sigma_k}\right)\nabla k\right] + P_k - \rho(\varepsilon - \varepsilon_0) + S_k \qquad 10.$$

$$\frac{\partial(\rho \varepsilon)}{\partial t} + \nabla \cdot [\rho \varepsilon \mathbf{u}] = \nabla\left[\left(\mu + \frac{\mu_t}{\sigma_\varepsilon}\right)\nabla \varepsilon\right] + \frac{1}{T_e}C_{\varepsilon 1}P_\varepsilon - C_{\varepsilon 2} f_2 \rho\left(\frac{\varepsilon}{T_e} - \frac{\varepsilon_0}{T_e}\right) + S_\varepsilon \qquad 11.$$

In the above equations, ε is the turbulent dissipation rate, ε_0 is the ambient turbulence value in the source terms that counteracts turbulence decay, S_k and S_ε are the user-specified source terms. T_e is the large-eddy time scale ($T_e = k/\varepsilon$). P_k and P_ε are production terms whereas f_2 is a damping function. For the case of the Realizable K-Epsilon Two-Layer turbulence model, the terms P_k, P_ε and f_2 are defined as follows:

$$P_k = f_c\left[\mu_t\mathbf{S}^2 - \frac{2}{3}\rho k\nabla\cdot\mathbf{u} - \frac{2}{3}\mu_t\left(\nabla\cdot\mathbf{u}\right)^2\right] + \beta\frac{\mu_t}{Pr_t}\left(\nabla\bar{T}\cdot\mathbf{g}\right) + \frac{2k\varepsilon}{c^2} \quad 12.$$

$$P_k = f_c\mathbf{S}k + \tanh\frac{|\mathbf{v}_b|}{|\mathbf{u}_b|}\beta\frac{\mu_t}{Pr_t}\left(\nabla\bar{T}\cdot\mathbf{g}\right) \quad 13.$$

$$f_2 = \frac{k}{k+\sqrt{\nu\varepsilon}} \quad 14.$$

where β is the thermal expansion coefficient, Pr_t is the turbulent Prandtl number, $\bar{T}$ is the mean temperature, c is the speed of sound, $\mathbf{v}_b$ is the velocity components parallel to the gravitational vector, $\mathbf{u}_b$ is the velocity components parallel to the gravitational vector, and ν is the kinematic viscosity.

Despite the availability of the all y+ wall treatment in the current turbulence model, it should be noted that only the wall function treatment is used in this research. The wall function is a wall treatment method which does not resolve the viscous sublayer but instead uses empirical equations to satisfy the physics of the flow in the near wall region. This method requires that the first cell centre at the wall to be placed in the logarithmic layer where turbulence stress dominates (y+ > 30). As a result, the number of cells and computation time required can be reduced significantly (Liu, 2016) which is beneficial when large number of cases are to be conducted such as in this research. The previously mentioned numerical studies which demonstrated the satisfactory results from k-ε model also use wall function treatment in their respective studies (Bechthold and Kastens, 2020; Deng et al., 2014; Kok et al., 2020c; Tezdogan et al., 2016).

2.1.3 Verification and Validation Procedure

Verification and validation of the numerical simulations in this investigation are conducted based on the triplets method discussed by Wilson et al. (2001) and Stern et al. (2001). The numerical uncertainty U_{SN} is approximated as the combination of iterative convergence uncertainty, U_I, grid-spacing uncertainty, U_G, and time-step uncertainty, U_T, as shown below:

$$U_{SN}^2 = U_I^2 + U_G^2 + U_T^2 \quad 15.$$

However, according to Tezdogan et al. (2015), the iterative uncertainty for ship motion response simulations in STAR-CCM+ URANS solver is less than 0.2% for seakeeping applications and hence, U_I is negligible and disregarded in the uncertainty analysis. Investigation of the grid-spacing and time-step uncertainty are of primary interest.

Triple solutions are obtained each for grid-spacing and time-step uncertainty where the grid-spacing uncertainty analysis is conducted with the smallest time-step while the time-step uncertainty analysis is conducted with the finest grid setting. A standard grid refinement ratio, r_G, of $\sqrt{2}$ is applied for the grid-spacing uncertainty study whereas the time-step uncertainty study has a time-step refinement, r_T, of 2.

The time-step is determined using the Courant number (CFL) where Δl is the mesh dimension, V is the ship speed and target CFL value of 1:

$$\Delta t = \frac{CFL \times \Delta l}{V} \tag{16.}$$

The obtained solution, S for all three grid-spacings; fine (1), medium (2) and coarse (3) as well as the three time-steps; short (1), medium (2) and long (3) are recorded. The changes in solution, ε, between each change in grid or time-step are calculated:

$$\begin{aligned} \varepsilon_{32} &= S_3 - S_2 \\ \varepsilon_{21} &= S_2 - S_1 \end{aligned} \tag{17.}$$

Next, the convergence ratio, R_i is determined based on the changes in solution. Note that the subscript i represents either grid-spacing or time-step for all ensuing formulae:

$$R_i = \frac{\varepsilon_{21}}{\varepsilon_{32}} \tag{18.}$$

The possible outcomes for the assessment of the convergence ratio, R_i, are as follows:

1) $0 < R_i < 1$, where monotonic convergence has been achieved (MC)

2) $R_i < 0$; $|R_i| < 1$, where oscillatory convergence has been achieved (OC)

3) $1 < R_i$, where monotonic divergence has been achieved (MD)

4) $R_i < 0$; $|R_i| > 1$, oscillatory divergence has been achieved (OD)

Uncertainty estimates cannot be made for divergent cases (outcomes 3 and 4) whereas the numerical uncertainty for oscillatory convergent cases (outcome 2) can be estimated by bounding the error based on the upper limit of obtained solutions, S_U, and lower limit of obtained solutions, S_L, as such:

$$U_i = \left| \frac{1}{2}\left(S_U - S_L\right) \right| \tag{19.}$$

For the case of monotonic convergence (outcome 1), the generalised Richardson extrapolation method can be used to approximate the order of convergence, p, given as:

$$p = \frac{\ln(\varepsilon_{32} / \varepsilon_{21})}{\ln(r_i)} \tag{20.}$$

The error of the finest grid or shortest time-step, δ^*_{Re}, can then be estimated as:

$$\delta^*_{\mathrm{Re}} = \frac{\varepsilon_{21}}{\mathrm{r}_i^p - 1} \qquad 21.$$

This is followed by the calculation of the correction factor, C_G:

$$\mathrm{C_G} = \frac{\mathrm{r}_i^P - 1}{\mathrm{r_i^{p_{est}}} - 1} \qquad 22.$$

where p_{est} is the limiting or theoretical accuracy of the applied numerical method. If the correction factor is close to unity, then the solutions are close to the asymptotic range, the sign of the error can be identified, the numerical error, δ_{SN}, corrected simulation results, S_C, and corrected uncertainty, U_{Ci}, can be calculated:

$$\delta^*_{\mathrm{SN}} = \mathrm{C_G}\delta^*_{\mathrm{Re}} \qquad 23.$$

$$\mathrm{S_C} = \mathrm{S} - \delta^*_{\mathrm{SN}} \qquad 24.$$

$$\mathrm{U_{Ci}} = \begin{cases} \left(2.4\left(1-\mathrm{C_G}\right)^2 + 0.1\right)\left|\delta^*_{\mathrm{Re}}\right|, & \text{when } \left|1-\mathrm{C_G}\right| < 0.125 \\ \left|1-\mathrm{C_G}\right|\left|\delta^*_{\mathrm{Re}}\right| & , \text{ when } \left|1-\mathrm{C_G}\right| \geq 0.125 \end{cases} \qquad 25.$$

When the correction factor is far from unity, then only the numerical uncertainty, U_i, can be determined:

$$\mathrm{U_i} = \begin{cases} \left(9.6\left(1-\mathrm{C_G}\right)^2 + 1.1\right)\left|\delta^*_{\mathrm{Re}}\right|, & \text{when } \left|1-\mathrm{C_G}\right| < 0.125 \\ \left(2\left|1-\mathrm{C_G}\right| + 1\right)\left|\delta^*_{\mathrm{Re}}\right| & , \text{ when } \left|1-\mathrm{C_G}\right| \geq 0.125 \end{cases} \qquad 26.$$

In order to validate the simulation results, the validation uncertainty, U_V, must first be determined using the previously derived simulation uncertainty, U_{SN}, and the experimental data uncertainty, U_D:

$$\mathrm{U_V} = \sqrt{\mathrm{U_{SN}^2} + \mathrm{U_D^2}} \qquad 27.$$

For this study, the experimental data uncertainty, U_D, is calculated based on the method suggested by Duffy (2008). Sources of uncertainty that are smaller than 1/4th or 1/5th of the largest sources are considered negligible (Longo & Stern, 2005).

Next, the comparison error, E, is computed as the difference between the experimental data, D and simulation data, S as shown below. Validation is successfully achieved if E is smaller than U_V.

$$\mathrm{E} = \mathrm{D} - \mathrm{S} \qquad 28.$$

2.2 Regression Analysis

Regression analysis is a statistical method for studying and modelling the relationship between independent variable(s) and dependent variable (Montgomery et al., 2012). A regression model is usually developed by minimising the square of the residuals, where the residuals are the differences between the predicted and observed values. A regression model involving more than one independent variable is termed a multiple regression model, and this is the model that is used for modelling the sinkage and trim empirical equations respectively in this study. The regression analysis for this study were conducted using MATLAB version R2017a.

2.2.1 Multiple Linear Regression Model

The specific multiple regression model of interest in this study is the multiple linear regression model. This particular model assumes a linear relationship between the independent variables, X_i, and the dependent variable, Y (refer to Equation 29).

$$Y = b_0 + b_1 X_1 + b_2 X_2 + b_3 X_3 + ... + b_i X_i \qquad 29.$$

where b_0, b_1, b_2, b_3, b_i are constants.

It should be noted that a multiple regression model is still considered linear even when the independent variables are non-linear (i.e. $X_2 = X_1^2$, $X_3 = X_1^3$, … $X_i = X_1^i$) since the coefficient estimates, b_i, are still linear. The coefficient estimates are obtained by minimisation of the square of the residuals whereas the maximum exponent or form of each independent variable for the multiple linear regression analysis is determined by using a non-linear regression.

In the execution of the regression, a forward stepwise method was used. Using this method, the model begins with no independent variables other than the intercept. Then, independent variables are introduced one by one based on significance testing. The variable with the greatest statistical significance is added first and followed by more variables based on the newly-adjusted significance test. Any previously added variables that become statistically insignificant due to the addition of another variable are removed from the regression. The process is repeated until no significant independent variables can be identified outside the regression model. For better fidelity in the regression modelling, interaction terms were included in the analysis such as X_1X_2 , X_1X_3 , $X_1X_2X_3$.

The statistical significance test used for the acceptance and rejection of variables is the p-value measure. The p-value is the probability of error that is involved in accepting the result (in this case, the independent variable) as representative of the population (the modelling data). The stepwise procedure was set to only contain variables with a p-value of less than 0.05 (5%). In other words, the final regression model contains variables with less than 5% probability of error.

The level of fit of the regression model to the actual data is assessed using the coefficient of determination, R^2, given in the equation below. The value of R^2 describes the variability of the residual values about the regression line with respect to the overall variability. The value of R^2 is between 0 and 1 where for instance, a value of 0.8 signifies that the model is successful in explaining 80% of the original variability but 20% is left unexplained.

$$R^2 = 1 - \frac{\text{Sum Squared Residual}}{\text{Sum Squared Total Error}} \tag{30.}$$

When multiple dependent variables are involved, the adjusted coefficient of determination, R^2_{Adjusted}, is used instead and is given in the equation below.

$$R^2_{\text{Adjusted}} = 1 - \frac{\left(1-R^2\right)\left(N-1\right)}{N-k-1} \tag{31.}$$

where N is the sample size and k is the number of independent variables.

As for the measure of dispersion of the observed values about the regression line, the root mean squared error (RMSE) is used. A small root mean squared error of estimate signifies a low dispersion of observed values about the regression line.

Chapter 3 – Benchmarking Study

This chapter presents the benchmarking study for the CFD modelling techniques based on three model scale experiment datasets. The first benchmark case involves a self-propelled Duisburg Test Case (DTC) model in a canal conducted in the Federal Waterways Engineering and Research Institute (BAW) (Mucha et al., 2014), the second benchmark case is conducted as part of the current study at AMC on a self-propelled S175 in the towing tank (Kok et al., 2021) and the final benchmark case is based on the KRISO container ship (KCS) model in a rectangular canal conducted by the Development Centre for Ship Technology and Transport Systems (DST) (Gronarz et al., 2009). Initially, a fully discretised propeller is modelled and validated against experimental data. The fully discretised propeller model is then used along with various other CFD modelling techniques to benchmark against the first benchmark case. Then, the most suitable method is selected and fine-tuned to benchmark against the second benchmark case. The fine-tuned method is then benchmarked again against the third benchmark case dataset. In addition, the CFD results are compared to existing empirical predictions to assess whether the chosen CFD model is an improvement over existing empirical methods.

The research presented in this chapter has been published in the following articles (which are provided in Appendix E):

Kok, Z., Duffy, J., Chai, S. and Jin, Y., 2020c. Comparison of unsteady Reynolds-averaged Navier-Stokes Prediction of Self-Propelled Container Ship Squat against Empirical Methods and Benchmark Data. *Transactions of the Royal Institution of Naval Architects, Part A: International Journal of Maritime Engineering*, *162*(Part A), pp.193-206.

Kok, Z., Duffy, J., Chai, S. and Jin, Y., 2020b. Multiple Approaches to Numerical Modeling of Container Ship Squat in Confined Water. *Journal of Waterway, Port, Coastal, and Ocean Engineering*, *146*(4), p.04020017.

Kok, Z., Duffy, J., Chai, S., Jin, Y. and Javanmardi, M., 2021. Numerical Parametric Study of Medium Sized Container Ship Squat. *Applied Ocean Research*, *109*, p.102563.

Chapter 3 has been removed for copyright or proprietary reasons.

The research presented in this chapter has been published in the following articles:

Kok, Z., Duffy, J., Chai, S. and Jin, Y., 2020c. Comparison of unsteady Reynolds-averaged Navier-Stokes Prediction of Self-Propelled Container Ship Squat against Empirical Methods and Benchmark Data. Transactions of the Royal Institution of Naval Architects, Part A: International Journal of Maritime Engineering, 162(Part A), pp. 193-206.

Kok, Z., Duffy, J., Chai, S. and Jin, Y., 2020b. Multiple Approaches to Numerical Modeling of Container Ship Squat in Confined Water. Journal of Waterway, Port, Coastal, and Ocean Engineering, 146(4), p. 04020017.

Kok, Z., Duffy, J., Chai, S., Jin, Y. and Javanmardi, M., 2021. Numerical Parametric Study of Medium Sized Container Ship Squat. Applied Ocean Research, 109, p. 102563.

Chapter 4 – Scale Effect Investigation

This chapter investigates the significance of scale effect in container ship squat or in other words, to determine whether it is feasible to predict full scale squat by direct extrapolation of model scale results. However, prior to the scale effect investigation, it is first necessary to validate the CFD method for full scale simulations. In the absence of acceptable full scale squat data, a series of alternative full scale investigations are conducted instead. The ITTC 1978 method for full scale extrapolation of deep water resistance is well documented and endorsed. Therefore, in the absence of other data, full scale predictions using this method are used to assess the accuracy of the full scale CFD simulations. Then the full scale resistance prediction in a confined water condition is assessed against empirical resistance estimations. Finally, the full scale squat predictions in confined water condition are compared against model scale results to quantify the scale effect. In addition, actual full scale measurements are also investigated. Case specific empirical predictions are developed based on approximated model scale hull forms of the actual cases. These case specific model scale squat predictions are extrapolated to full scale and assessed against their respective actual full scale measurements to evaluate the practicality of extrapolating model scale squat results for full scale predictions.

It should be noted that the majority of the study conducted in this chapter is based on the QS-VD / QS-T modelling technique due to convergence issues in implementing the morphing mesh method for full scale simulations. Care is taken to ensure the cases investigated using the QS methods are within its limit of applicability ($Fr_{\mathrm{h}} < 0.55$). However, there are still some results derived successfully from the morphing mesh implementation valid for higher speed conditions and are discussed towards the end of the chapter. The morphing mesh based results provide comparison for scale effect at much higher speeds where viscous effects are expected to be more pronounced.

The research presented in this chapter has been published in the following articles (which are provided in Appendix E):

Kok, Z., Duffy, J., Chai, S., Jin, Y. and Javanmardi, M., 2020a. Numerical Investigation of Scale Effect in Self-propelled Container Ship Squat. *Applied Ocean Research*, *99*, p.102143.

Kok, Z., Duffy, J., Chai, S. and Jin, Y., 2020d. Benchmark Case Study of Scale Effect in Self-propelled Container Ship Squat. *ASME 2020 39th International Conference on Ocean, Offshore and Arctic Engineering*. Virtual, Online.

Chapter 4 has been removed for copyright or proprietary reasons.

The research presented in this chapter has been published in the following articles:

Kok, Z., Duffy, J., Chai, S., Jin, Y. and Javanmardi, M., 2020a. Numerical Investigation of Scale Effect in Self-propelled Container Ship Squat. Applied Ocean Research, 99, p.102143.

Kok, Z., Duffy, J., Chai, S. and Jin, Y., 2020d. Benchmark Case Study of Scale Effect in Self-propelled Container Ship Squat. ASME 2020 39th International Conference on Ocean, Offshore and Arctic Engineering. Volume 8: CFD and FSI. Virtual, Online. August 3–7, 2020.

Chapter 5 – Effect of Hull Principal Particulars

Container ship designs are becoming larger and the principal particulars can vary significantly from one design to another. It is known that subtle changes to hull form can result in significantly different squat behaviour (Uliczka & Wezel 2005). Therefore, it is necessary to understand the impact of a container ship's hull form on the squat experienced. In this chapter, numerical investigations are undertaken to quantify the significance of various hull principal particulars on midship sinkage and trim. These quantified findings will then be used later in the development of the new empirical formulae. The systematic investigation of varying principal particulars is also important in studying the nature of the trim direction of container ships.

Initially, a statistical review of the principal particulars of commonly operating container ships is discussed and used to determine the range for length-to-beam ratio (L/B), beam-to-draft ratio (B/T) and block coefficient (C_B) to be analysed. Then, systematic hull parametric transformations are conducted and the morphing mesh method with body force propulsion virtual disc is used to study the effect of varying L/B, B/T and C_B on squat. Empirical predictions are also compared against the CFD results.

The research presented in this chapter has been published in the following article (which is provided in Appendix E):

Kok, Z., Duffy, J., Chai, S., Jin, Y. and Javanmardi, M., 2021. Numerical Parametric Study of Medium Sized Container Ship Squat. *Applied Ocean Research*, *109*, p.102563.

5.1 Statistics of Container Ship Principal Particulars

Sample data of 85 different container ships visiting/departing an Australian port courtesy of OMC International (2018) is used to study the range of parameters of currently operating container ships. Statistics of these ships are provided in Table 20. The ships sampled have an average length of 268 m with average displacement of approximately 75,000 tonnes. A plot of the parametric ratios of these ships demonstrates the vast variety of currently operating container ships (Figure 38). These large deviations in parameters are likely to result in very different squat behaviour among these container ships and hence, it is necessary to understand the effect of each parametric ratio on squat. By identifying and quantifying the impact of each parametric ratio on squat, a more accurate empirical formulae can be developed. More accurate predictions of squat will in turn allow ship operators to ship more cargo per voyage whilst avoiding grounding.

Table 20: Statistics of different ships visiting/departing a busy Australian port (OMC International, 2018). Here, length L refers to length between perpendiculars and draft T refers to the operating draft during measurement.

Data	**Δ (Tonnes)**	**L (m)**	**B (m)**	**T (m)**	**L/B**	**B/T**	**C_B**
Average	74,619	268	38.0	11.8	7.11	3.23	0.607
Std. Dev.	9,093	16.7	3.47	0.487	0.690	0.332	0.0421
Max	100,757	293	42.8	13.1	8.80	3.92	0.773
Min	55,708	225	32.2	10.7	6.04	2.47	0.544

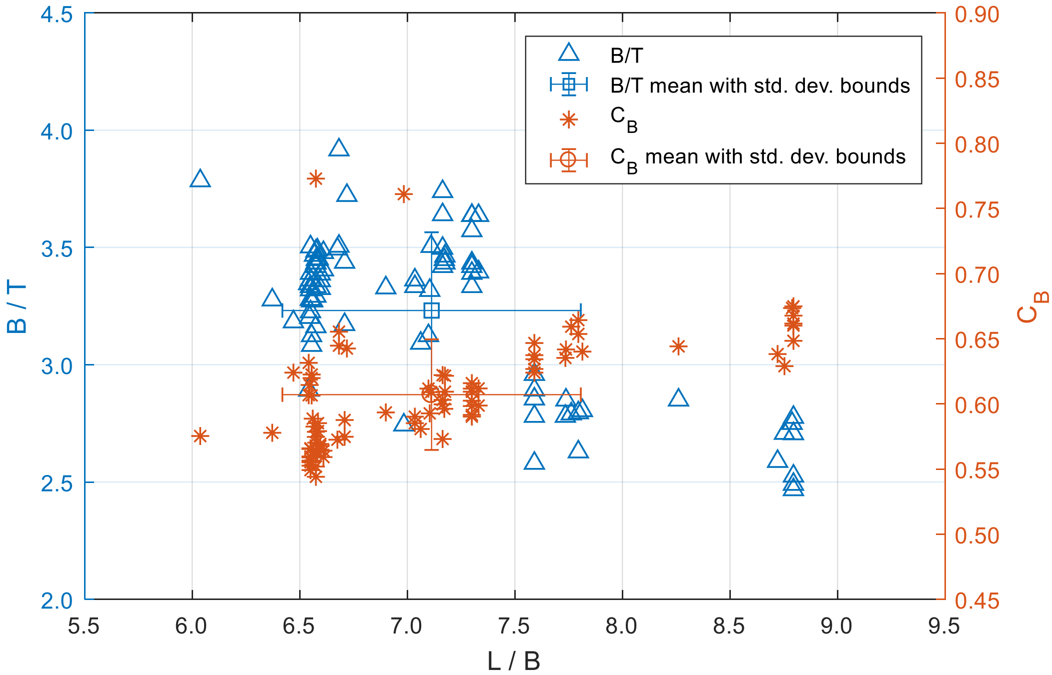

Figure 38: Parametric variation of 85 unique container ships visiting/departing an Australian port (OMC International, 2018). The mean of each parameter is shown with standard deviation bounds (B/T or C_B for vertical bound and L/B for horizontal bound).

5.2 Systematic Hull Parametric Investigation

The parent hull form used for the systematic parametric investigation is the KCS hull since the L/B and B/T ratios of 7.14 and 3.23 respectively are close to the average of currently operating container ships. In addition, the KCS hull form is still representative of modern designs as it has features which are present on recent designs; pronounced bow bulb, stern bulb and transom stern (refer to Figure 39). In this study, the KCS is appended with a SchiffbauVersuchsanstalt Potsdam (SVA)-developed VP1193 stock propeller and rudder. The principal particulars of the propeller are given in Table 21.

Figure 39: Profile view of the KCS hull appended with a rudder.

Table 21: Principal particulars of the SVA-VP1193 propeller

Propeller Particulars	**Model Scale**	**Full Scale**
D_P (m)	0.25	7.9
Blades	5	5
$P_{0.7}/D_P$	1.3	1.3
A_E/A_O	0.7	0.7

In the design of the computation domain, lateral restriction effects are avoided so that emphasis can be given to the effects of hull parametric variations. In order to ensure that the lateral boundaries are sufficiently far away from the hull, the distance of the side walls from the hull centreline are placed greater than the influence width, y_{infl}, as derived by Lataire and Vantorre (2008) in Equation 42 and slip-wall conditions are applied to these side walls (refer to Figure 40). It should be noted that all cases are conducted in model scale as scale effects have been shown to be within the numerical uncertainty limits and model scale simulations are also more computationally economical (Kok et al., 2020a). The validated morphing mesh method is used in this study to ensure accurate squat predictions for $Fr_{\mathrm{h}} > 0.6$. Self-propulsion effect has been accounted for by inclusion of the body force propulsion virtual disc.

$$y_{\mathrm{infl}} = 5B(Fr_{\mathrm{h}} + 1) \qquad 42.$$

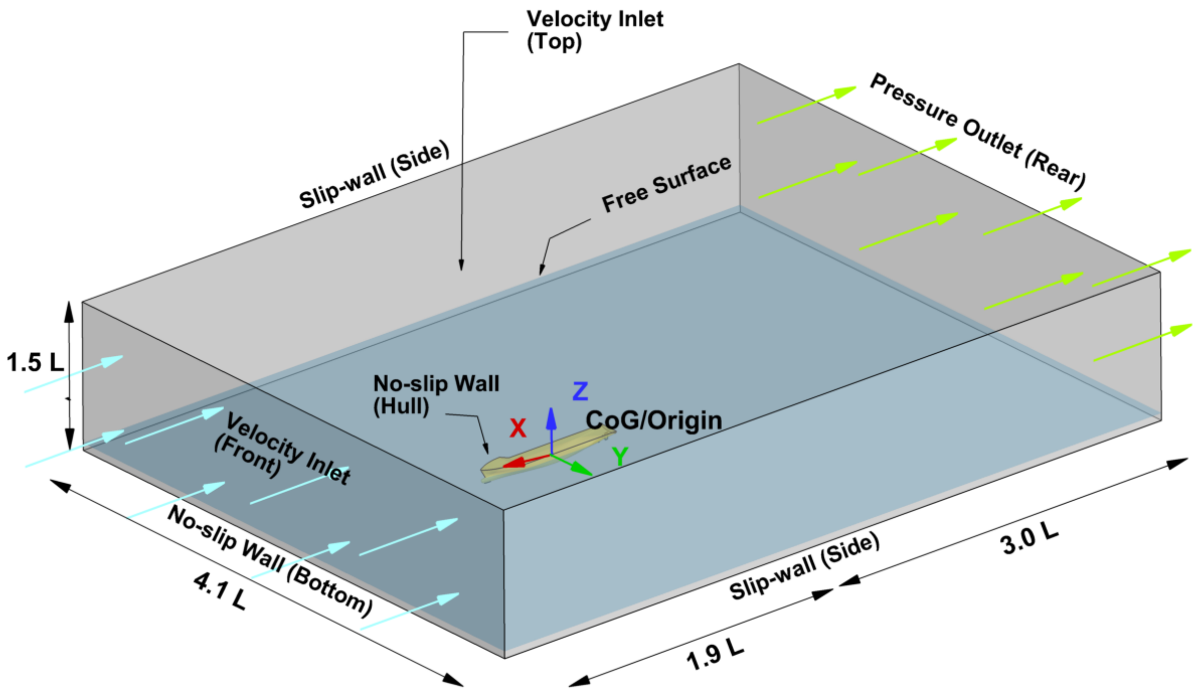

Figure 40: Computation domain for the systematic study of effect of KCS hull parametric variations on squat (Kok et al., 2021).

The parametric ratios to be investigated are the length-to-beam ratio, L/B, beam-to-draft ratio, B/T, and block coefficient, C_B, where the range of each ratio is based on the statistics presented previously in section 5.1. The range of values to be tested are summarised in Table 22. Two sets of systematic investigations are to be investigated; cases with fixed $C_{\mathbf{B}}$ and cases with varying $C_{\mathbf{B}}$. The cases with fixed $C_{\mathbf{B}}$ includes variations in *L/B* and *B/T* while the cases with varying $C_{\mathbf{B}}$ has fixed *L/B* and *B/T*. All parametric transformations are completed using the Maxsurf Modeler Advanced version 20 software. Further details of the hulls produced from the parametric transformations are tabulated in Appendix C. At this stage of the study, only the change in midship sinkage and trim at one speed that is as high as possible is of interest. This is to help identify the significance of the hull parameters and their respective general trends. Therefore, this current matrix only represents a small subset of the complete test matrix for the development of the new empirical formulae.

Table 22: Range of cases investigated.

L/B	***B/T***	$C_{\mathbf{B}}$	***h/T***	$Fr_{\mathbf{h}}$
6.50 – 8.60	2.50 – 3.90	0.648	1.3	0.683
7.14	3.22	0.589 – 0.689	1.3	0.683

5.3 Results

5.3.1 Effect of *L/B* & *B/T*

Figure 41 depicts the surface plots of the results for fixed C_B cases at h/T =1.3 and Fr_h of 0.683. When the midship sinkage is expressed as a fraction of *T*, it can be clearly observed in Figure 41(a) that the midship sinkage/*T* has an inverse relationship with *L/B* but is generally independent from the variation of *B/T*. On the contrary, trim (by the bow) has an inverse relationship with both *L/B* and *B/T* (Figure 41(b)). Consequently, the maximum sinkage occurs by the FP and Figure 41(c) demonstrates that the FP sinkage/*T* increases as *L/B* and *B/T* decreases albeit the effect of *B/T* is less dominant. Conversely, Figure 41(d) shows that the AP sinkage/*T* increases when *L/B* decreases, but increases slightly with *B/T*. It is of interest to note that the trim direction never changed which implies that the principal dimensions of the hull only affects the magnitude but not the direction of the trim in this set of results.

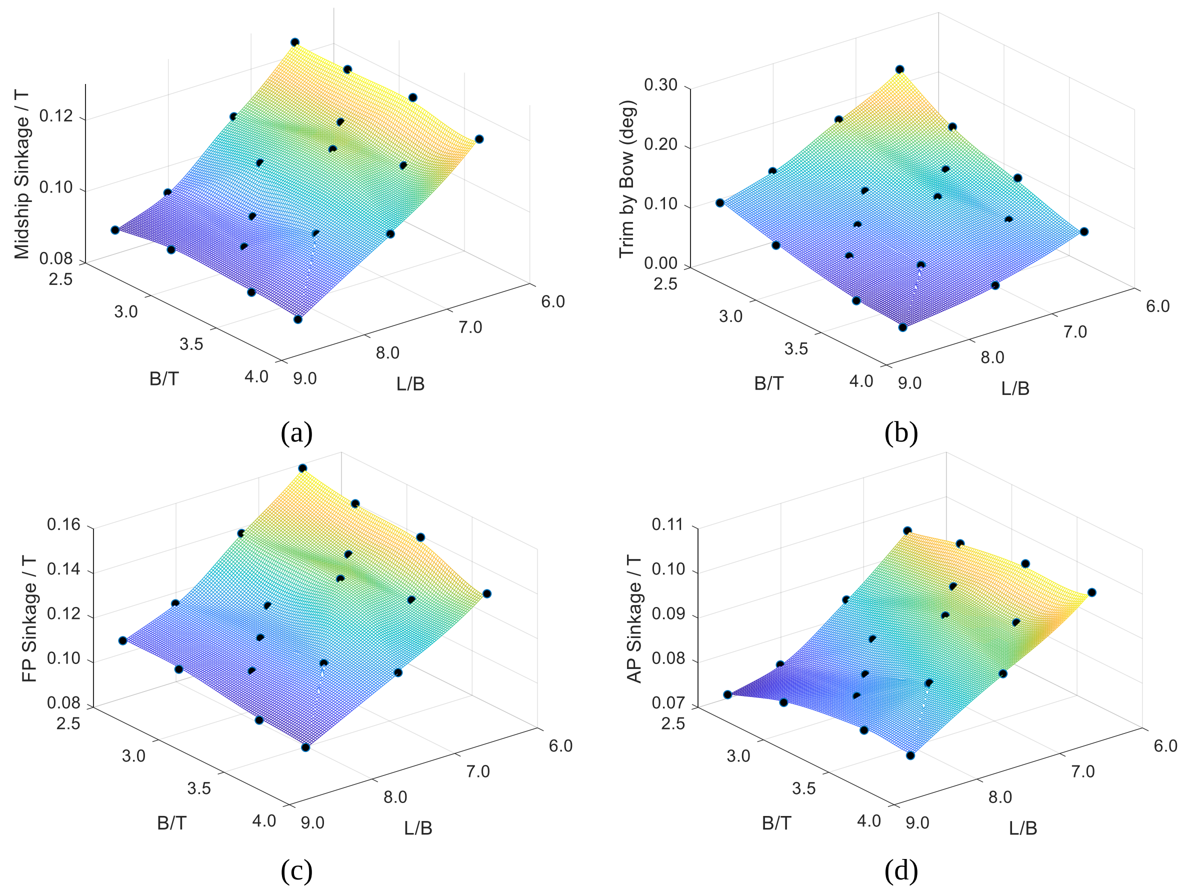

Figure 41: Surface plot of the changes in (a) midship sinkage/T, (b) trim (positive by the bow), (c) FP sinkage/T, and (d) AP sinkage/T with respect to B/T and L/B for h/T =1.3 at 0.683 Fr_h and fixed C_B of 0.648.

To gain better understanding of the observed trends relating to the effect of L/B, a comparison of two velocity profiles for two cases with a similar B/T and different L/B ratios are presented in Figure 42. The hull with the more slender profile (L/B = 8.60) can be seen to have lower flow velocity magnitude in the underkeel and wake region in comparison to that of the stubbier hull (L/B = 6.50). The relatively lower flow velocity in the underkeel region for the slender hull implies that the suction pressure and therefore sinkage, is less significant for the slender hull as presented in Figure 43. This is in agreement with the findings of Han et al. (2012) where a "longer" hull form has less wave-making resistance which results in smaller magnitude of the pressure distribution. Similarly, since there is less pressure acting on a more slender hull, then the net trimming moment, will be less for a more slender hull as well. Furthermore, trim is also expected to reduce for a relatively longer hull as longitudinal length contributes to a greater longitudinal metacentric height (refer to Appendix C). A larger moment is required to trim a hull with larger longitudinal metacentric height. These observations imply that a more slender hull form (larger L/B) is more beneficial in shallow water operation as both midship sinkage and trim is relatively lower. This also implies that the impact of L/B ratio is significant and should be accounted for in the development of the regression formulae.

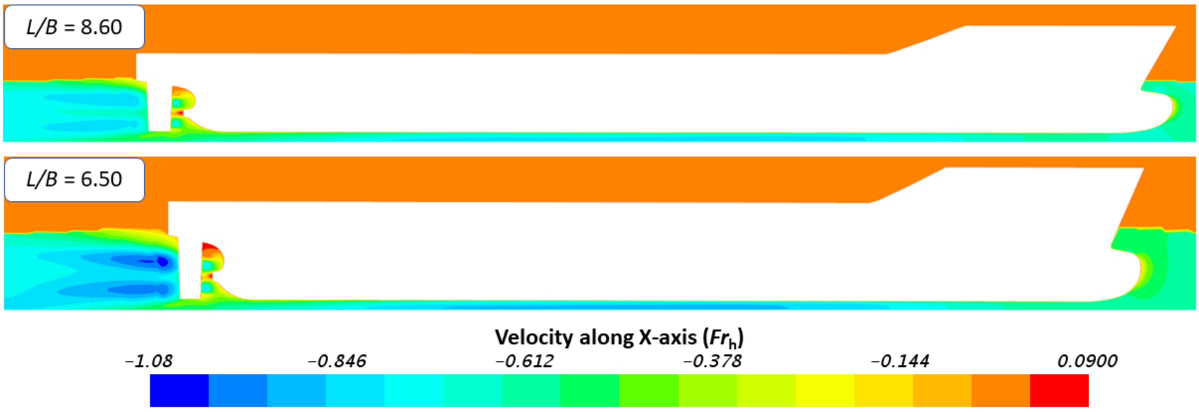

Figure 42: Comparison of the velocity profile between hulls of varying *L/B* but equal *B/T* of 2.50 at 0.683 Fr_h in 1.3 *h/T*. The slender hull of *L/B* = 8.60 (top) has relatively lower flow velocity magnitude in the underkeel and wake region in comparison to the stubby hull of *L/B* = 6.50 (bottom).

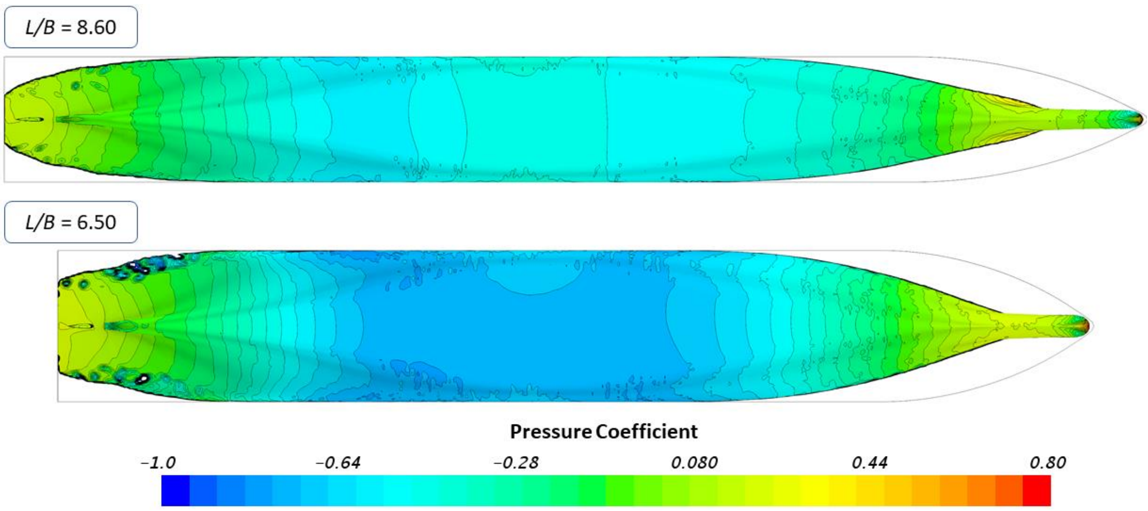

Figure 43: Comparison of the pressure coefficient contours between the hull of *L/B* = 8.60 (top) against hull of *L/B* = 6.50 (bottom) at 0.683 Fr_h in 1.3 *h/T*. The pressure distribution on the keel of the hull *L/B* = 6.50 is significantly lower which results in greater sinkage and trim.

A similar comparison between two hull forms of similar *L/B* but varying *B/T* is made to observe the effect of varying *B/T* on the velocity profile (Figure 44). The underkeel and wake region for both cases appear to be comparable in magnitude. Consequently, comparison of the pressure distribution on the hull (Figure 45) demonstrates that the magnitude of the pressure distribution on both hulls are similar. Effectively, the proportion of sinkage experienced by both hulls are similar. In regard to trim, the wider hull has a longer length for the same *L/B* ratio which implies greater longitudinal metacentric height and hence, reduced trim relative to the deeper hull. Therefore, the *B/T* ratio does not significantly impact the midship sinkage but a larger *B/T* ratio results in reduced trim. This also implies that the *B/T* ratio should be considered in the modelling of the empirical formulae for trim whereas that for midship sinkage could be neglected for the cases investigated.

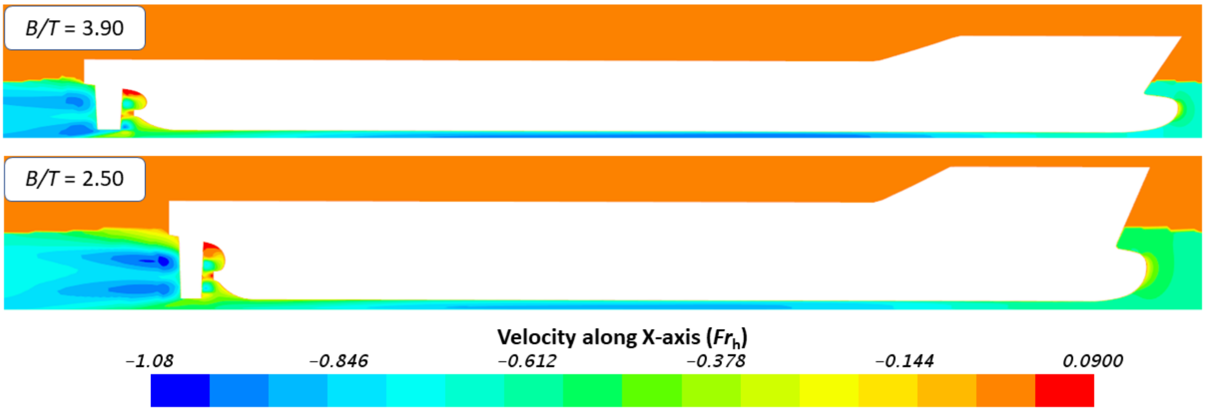

Figure 44: Comparison of the velocity profile between hulls of varying *B/T* but equal *L/B* of 6.50 at 0.683 Fr_h in 1.3 *h/T*. The wider hull of *B/T* = 3.90 (top) has relatively similar underkeel flow velocity magnitude in comparison to the deeper hull of *L/B* = 2.50 (bottom).

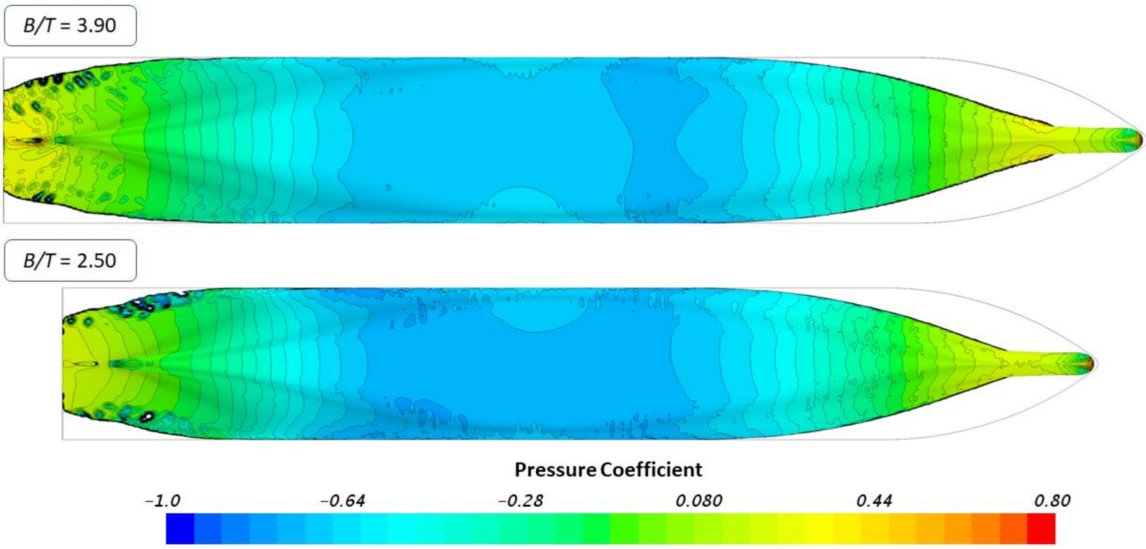

Figure 45: Comparison of the pressure coefficient contours between the hull of *B/T* = 3.90 (top) against hull of *B/T* = 2.50 (bottom) at 0.683 Fr_h in 1.3 *h/T*. The pressure distribution on the keel of both hulls are fairly similar which effectively yields comparable proportion of sinkage.

5.3.2 Effect of Block Coefficient

In the current study, the parametric transformations for altering the C_B of hulls only alters the shape of the fore and aft section of the hull while the parallel midbody is either elongated or shortened. Furthermore, it can be clearly seen from the curve of areas in Figure 46 that the parametric transformation undertaken has inevitably expanded the aft section more than the fore section (i.e. the LCB and LCF positions are altered, refer to Appendix C). Consequently, interesting impacts on midship sinkage and trim can be observed in Figure 47. The midship sinkage shows no significant changes with respect to C_B (the differences in sinkage/*T* among the datapoints are in the order of 1-4%) whereas a linear relationship is identified between trim and C_B.

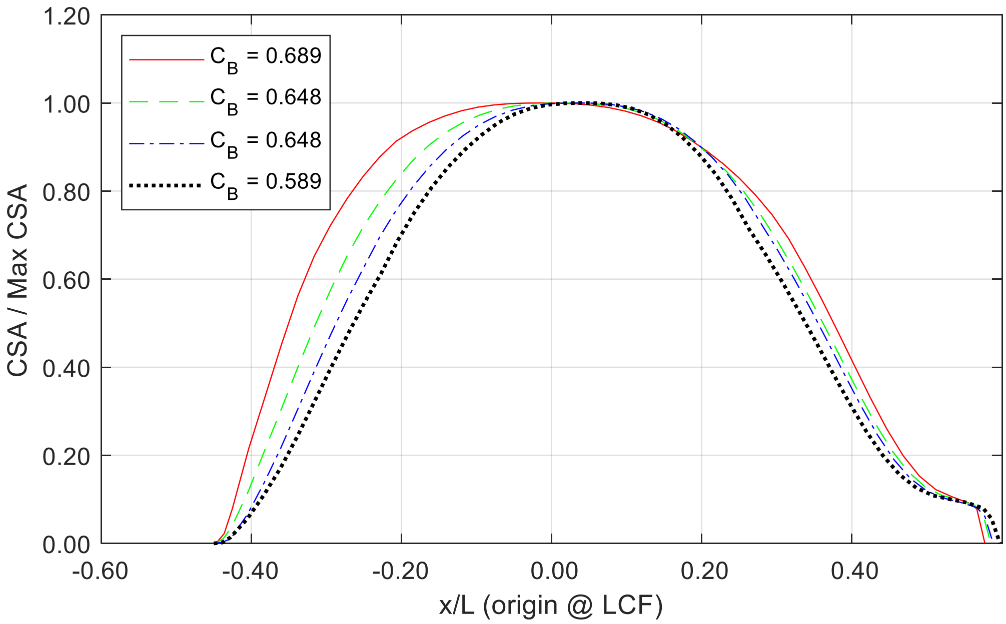

Figure 46: Comparison of the curve of areas about the LCF among the hulls of varying C_B. The increase in aft section area is greater than that of the fore section for this hull form using the Maxsurf Modeler Advanced parametric transformation tool.

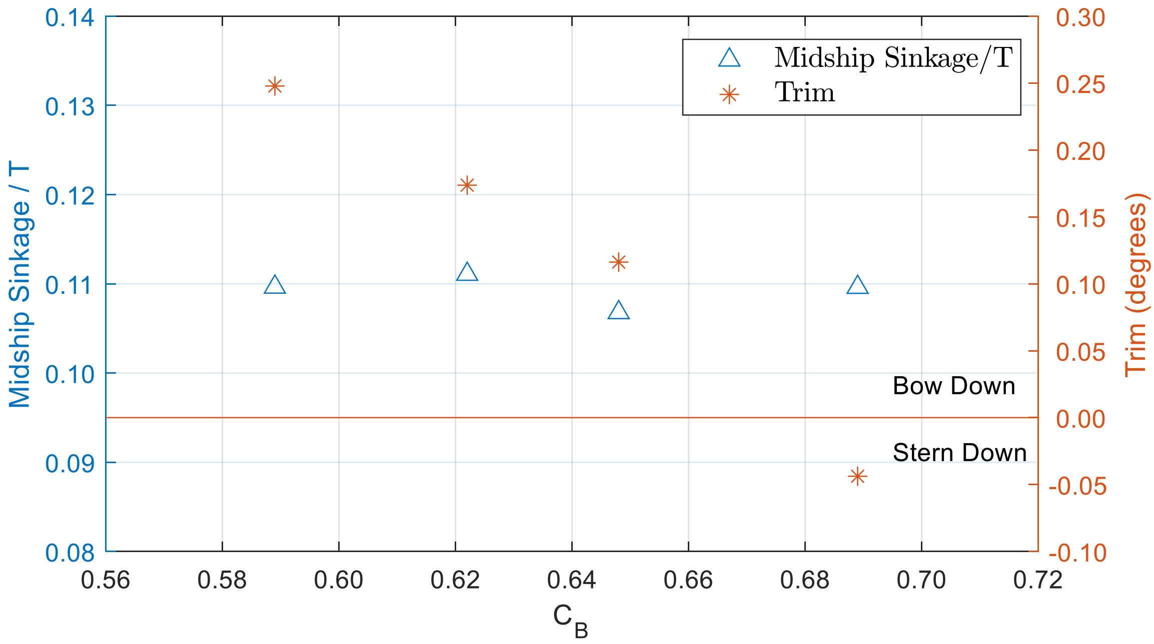

Figure 47: Plot of midship sinkage/T and trim (positive by the bow) as a function of C_B. The change in midship sinkage/T is negligible while trim increases linearly with C_B.

The independence of midship sinkage with respect to C_B is likely due to the fact that the sinkage component of squat is greatly influenced by the geometry of the midship region where the suction pressure acts. As mentioned earlier, the parametric transformations do not alter the midship region and thus, the suction pressure acting on this region is left unaltered which corresponds to similar magnitude of midship sinkage between hulls. Conversely, since the parametric transformations alter the fore and aft sections of the hull, the flow fore and aft is expected to differ accordingly. Therefore, the trimming moment and subsequent trim changes as well. In addition, the magnitude of trim which is observed to gradually change from bow down to stern down as C_B increases can be explained by the previous curve of areas (Figure 46). The hulls with larger C_B have greater aft region area which implies larger suction force acting on the aft section. This is evident in Figure 48 where the maximum suction pressure gradually shifts aftward as the C_B is increased. Therefore, the postulate by Barrass (1979) that a relatively large C_B value would imply trim direction by the bow has been disproven.

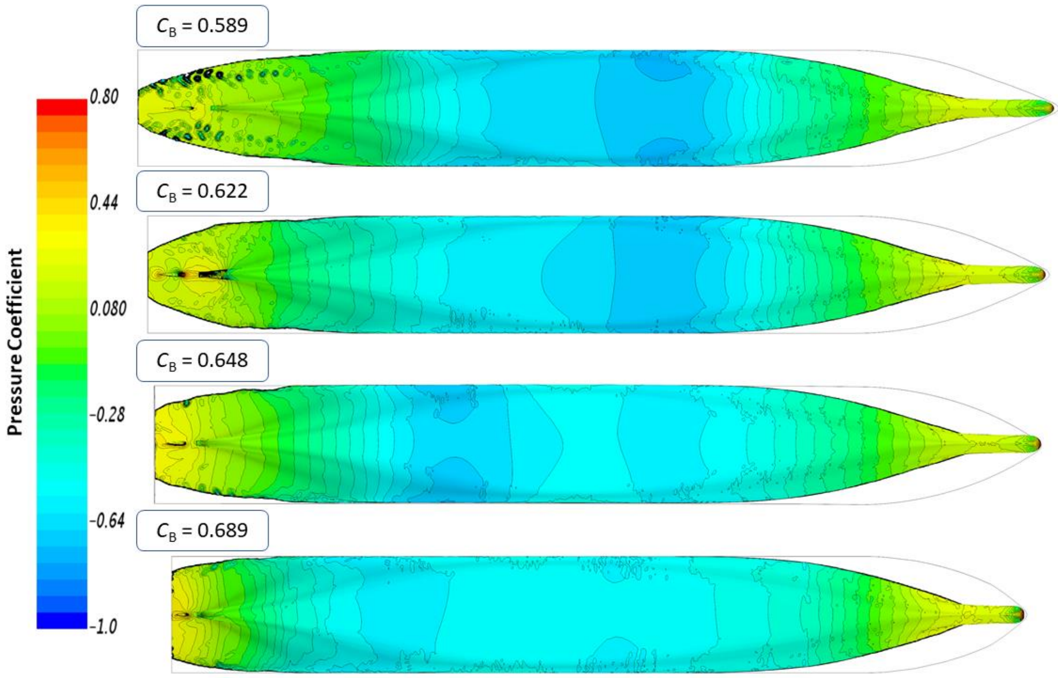

Figure 48: Comparison of the pressure coefficient contours among the hulls of varying C_B at 0.683 Fr_h in 1.3 *h/T*. The maximum suction pressure gradually shifts aftward as the C_B increases for this particular hull form using the Maxsurf Modeler Advanced parametric transformation tool.

The implications from these observations are that C_B may neither be a significant factor to sinkage nor a reliable factor for trim, or at least for the current range tested and sister hulls used. It has been demonstrated that a larger C_B value does not necessarily result in trim by the bow. Instead, the relative volume distribution across the length of the hull (curve of areas) or simply, the position of the LCB relative to the LCF plays an important role in determining the trim direction and magnitude. These are to be taken into account and investigated further in the following chapter for the new empirical formulae development.

5.3.3 Changes in Trim Direction

In the previous section, changes in C_B which inevitably result in changes to the position of the LCB relative to the LCF have been shown to cause changes in trim magnitude and eventually change in trim direction. Incidentally, changes to *L/B* and *B/T* which maintains the position of the LCB relative to the LCF do not result in changes to trim direction. Thus, it is evident that the trim direction of a container ship is affected by the relative position of the LCB to the LCF (this will now be expressed as L_{BF} and given in Equation 43). Therefore, the changes in trim should be analysed with respect to L_{BF} as illustrated in Figure 49.

$$L_{\mathrm{BF}} = \frac{(\mathrm{LCB}-\mathrm{LCF})}{L} \times 100\% \qquad 43.$$

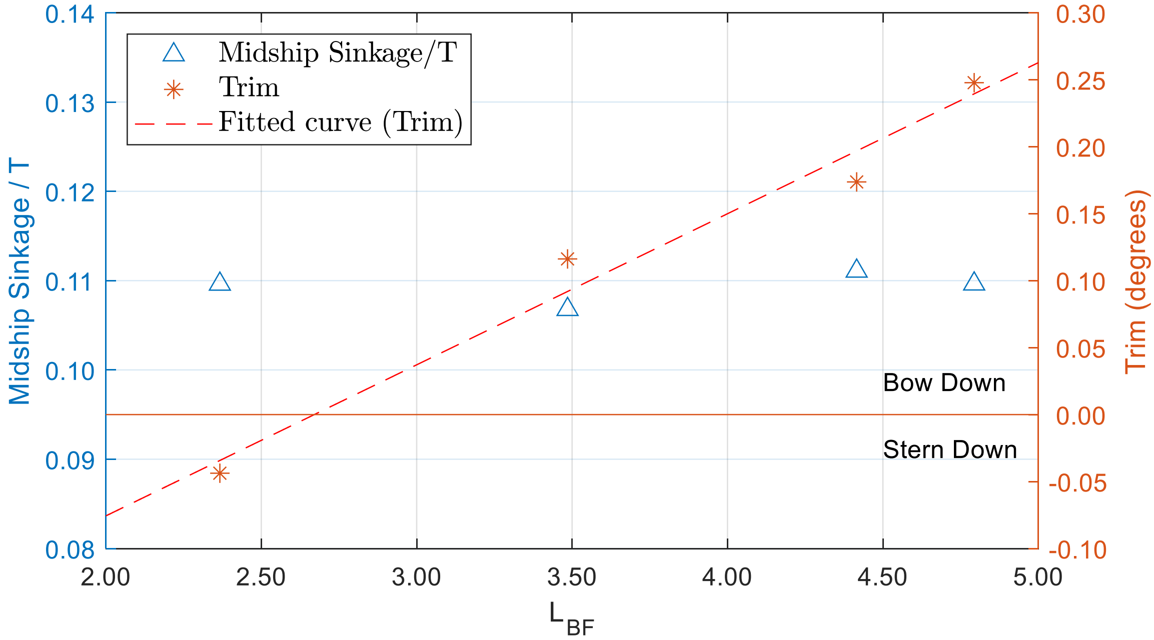

Figure 49: Plot of midship sinkage/*T* and trim with respect to L_{BF}. The change in midship sinkage/*T* is negligible while trim varies linearly with C_B and eventually changes direction.

From this study it is identified that the change in trim is still linear when analysed with respect to L_{BF} and midship sinkage remains unaffected by changes in L_{BF}. Generally, the shorter the L_{BF} is, the more stern down the trim is. It is also noted that the change in trim is very sensitive to L_{BF} considering that there are significant changes in trim between L_{BF} of 2-5%. The point of direction change for this particular case is approximately L_{BF} = 2.7%. This correlates with observations made in the work of Gourlay et al. (2015) where the JUMBO hull that has L_{BF} of 3.46% was seen to trim by the bow whereas the MEGA-JUMBO hull that has L_{BF} of 0.85% trims by the stern. Furthermore, this correlates with the general observation that bulk carriers tend to trim by the bow as these hulls are likely to have longer L_{BF} due to their fuller fore sections.

Repeating this study using a different set of parametrically transformed hull to provide further validation to the findings would be favourable. However, given the limited time available to deal with the highly problematic nature of the parametric transformations for varying L_{BF} (by varying C_B), and since there are some affirmations made already with external observations for the findings presented, the repeat of this study using a different set of hulls is suggested as future work.

Regardless, the findings here suggest that the L_{BF} should be considered as a factor in determining the direction of trim of a container ship and its effect should be investigated further for the development of the empirical formulae.

5.3.4 Comparison Against Existing Empirical Predictions

Having observed the CFD predictions for the effect of *L/B*, *B/T* and C_B on squat, it is of interest to observe whether existing empirical formulae are able to produce similar findings for this laterally unrestricted case study. Thus, the following empirical formulae are investigated: Ankudinov (2009), Barrass II (1979), Führer & Römisch (1977), Hooft (1974), ICORELS (1980), Millward (1992) and Römisch (1989). Note that the predicted squat using the method of Huuska (1976) is essentially identical to that of ICORELS (1980) for such laterally unrestricted conditions and is thus excluded. A few sample cases from the CFD results are compared against the corresponding empirical formulae predictions as shown in Figure 50.

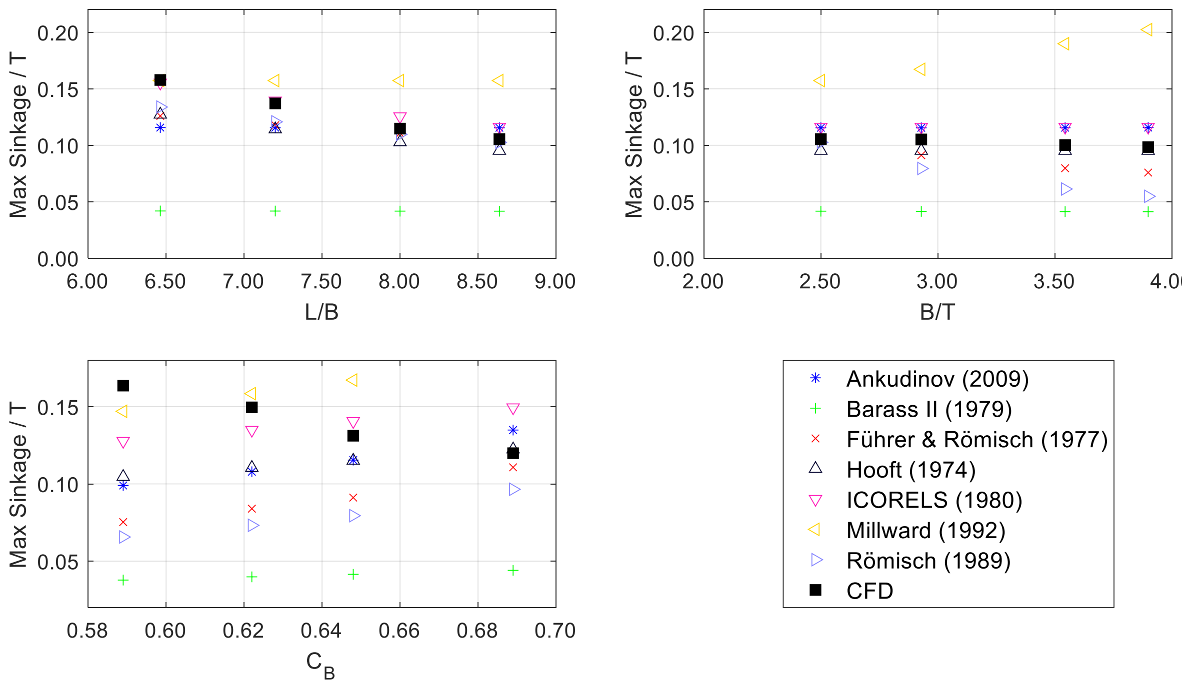

Figure 50: Sample case comparison between empirical predictions against CFD results for varying *L/B*, *B/T* and C_B for the KCS hull. All maximum sinkage occurs by the bow except for CFD results for C_B = 0.689.

For the case of varying *L/B*, most empirical formulae can be seen to demonstrate a similar trend to the CFD results where maximum sinkage (trim is accounted for) has an inverse relation to *L/B* albeit having slight differences in slope and magnitude. However, the methods of Barrass II (1979) and Millward (1992) are indifferent to *L/B*. For the case of varying *B/T*, most empirical predictions demonstrate minimal changes in maximum sinkage, which is similar to the CFD results. Nonetheless, there are more conflicting trends observed such as increasing and decreasing maximum sinkage with respect to *B/T* are both predicted by Millward (1992) and Römisch (1989) respectively. ICORELS (1980) have shown the best correlation to the CFD results in terms of trend and magnitude for varying *L/B* and *B/T* followed by that of Hooft (1974).

However, conflicting trends are observed when comparing predictions for varying C_B. All empirical predictions suggest that maximum sinkage occurs by the bow and it increases with C_B but this is not the case for CFD results. It is postulated that the empirical predictions behave as such because they are based on (or considers) bulk carrier squat predictions. Bulk carriers are at the larger end of the C_B spectrum ($C_B > 0.7$) and generally trim by the bow due to their signature fuller bow. Therefore, the empirical methods tend to predict increasing bow sinkage when C_B increases. In contrast, the parametrically transformed hulls in this particular study inevitably altered L_{BF} where there is increasingly greater aft volume which results in more sternwards trim for increasing C_B. Effectively, the CFD predictions for maximum sinkage reduces when C_B increases since the trim direction is gradually changing from bow down to stern down and this is not anticipated by the empirical methods studied. This highlights that caution should be exercised when using the presented empirical methods to predict squat for particular changes in hull design. A more accurate empirical method to determine the squat of a container ship may have to consider the hull volume distribution i.e. L_{BF}.

5.4 Concluding Remarks

A systematic numerical investigation has been undertaken to study the effect of parametric hull variations on container ship squat. Firstly, a simple statistical study on the principal particulars of currently operating container ships surveyed by OMC International (2018) is discussed. It is shown that the range of ship parameters i.e. *L/B*, *B/T* and C_B for currently operating container ships are wide and varied. This range of parameters is then used as a basis for the numerical investigation into the influence of hull form on container ship squat.

Based on the parameter statistics, the KCS is chosen as the parent hull and parametric transformations of the hull are developed. Systematic computations using these hulls are then conducted where the lateral bounds of the computation domain are placed sufficiently far away to avoid lateral restriction effects. The findings of the study follow for the range of specific cases investigated in this study:

- Sinkage and trim increase as *L/B* decreases. Sinkage increases due to increase in midship suction pressure as a result of increasing wave-making resistance. This causes the pressure distribution to become worse when *L/B* decreases. Trim increases when the suction pressure increases as well. Trim also increases because the hull length and hence, longitudinal metacentric height decreases when *L/B* decreases for the same *B/T* ratio.
- Sinkage is not significantly affected by *B/T* whereas trim increases when *B/T* decreases. The pressure distribution on the hull of varying *B/T* is relatively similar which results in comparable proportion of sinkage. Trim increases because again, the hull length and thus, longitudinal metacentric height decreases when *B/T* decreases for the same *L/B* ratio.
- The parametric transformations conducted in this study for varying C_B are found to increase the area of the aft section more than the fore section. Consequently, it is observed that sinkage is not significantly affected by the changes in C_B since the midship region remains unchanged. Trim appears to become increasingly stern-down as C_B increases due to uneven changes in the aft and fore sections by the parametric transformations. It has been demonstrated that a relatively larger C_B value does not necessarily imply trim direction by the bow. These observations suggest that C_B may neither be a significant factor to sinkage nor a reliable factor for trim. Instead, the hull volume distribution or simply, the position of LCB relative to LCF is important in determining the trim behaviour.
- Change in trim direction is shown to be linearly related to the relative position of the LCB to LCF (L_{BF}) in this study. The shorter the L_{BF} is, the more stern down the trim is. The change in trim is very sensitive to L_{BF} where changes in the range of 2-5% in L_{BF} can result in changes to direction of trim. The quantified findings here correlate with observations made in the work of Gourlay et al. (2015). Repeating the study for a different set of parametrically transformed container ship hulls would be favourable as future work.
- Comparison between existing empirical predictions against the CFD results show that most empirical methods are able to reproduce similar trends for the effect of varying *L/B* and *B/T* with only a few contradicting predictions particularly for varying *B/T* cases. On the contrary, all empirical predictions tested are found to have opposite trends to that of the CFD results for cases of varying C_B. This is thought to be due to the compromise of empirical methods to account for bulk carrier predictions instead of evaluating the hull's actual volume distribution and form. Thus, development of a more accurate empirical method should consider the hull volume distribution.

Chapter 6 – Regression Analysis and Empirical Formulae Modelling

The work in the previous chapter is extended to obtain a wider range of data in terms of h/T and Fr_h for the purpose of developing a set of regression based empirical formulae. The first section of this chapter discusses the regression analysis process, correction factor for hull volume distribution and performance of the formulae (for laterally unrestricted conditions). Further systematic studies are then conducted to develop a correction factor for lateral restriction effects and initial trim to be incorporated in the formulae. Finally, various comparison of the performance of the final set of empirical formulae against existing methods are conducted and actual full scale cases are also examined to determine whether the research objective of developing an improved empirical method has been achieved. The aim of this work is to develop a new tool for rapid assessment of container ship squat.

6.1 Regression Analysis

6.1.1 Additional Cases for Regression

In the previous chapter, the effects of parametric hull variations were investigated only for fixed h/T and Fr_h conditions. Thus, in this chapter, the same methodology was applied to conduct additional cases and extend the results for varying h/T and Fr_h conditions. The range investigated for each parameter is summarised in Table 23, which also serves as the recommended range of applicability for the formulae to be derived. It should be remembered that the parametric transformations conducted using Maxsurf Modeler Advanced for varying L/B and B/T do not alter the relative positions of LCB and LCF. Thus, the L_{BF} remains similar for these cases. Only parametric transformations of C_B alter the L_{BF}. Due to the large amount of simulation cases to be conducted (152 cases) as well as computational and time constraints, cases for varying L_{BF} are very limited (12 cases). Furthermore, it is also possible to keep cases for varying L_{BF} limited as it has been shown previously that the L_{BF} is linearly related to trim. The trend is relatively predictable with minimal data points. Hence, cases for varying L_{BF} are not included in the regression, but instead are used to derive a correction factor. It should be noted that all the simulations include self-propulsion effect so that self-propulsion effect will be inherently accounted for in the formulae development.

Table 23: Additional cases conducted for regression analysis and correction factor derivation. Positive L_{BF} implies the LCB is forwards of LCF. The range presented here will also be the recommended range of applicability for the formulae to be derived.

h/T	***Fr*h**	***L/B***	***B/T***	***C*B**	***L*BF (% of *L*)**	**Total Cases**	**Implement**
1.3	0.683 – 0.273	6.50 – 8.60	2.50 – 3.90	0.648	3.49	57	Regress.
1.2	0.570 – 0.273	6.50 – 8.60	2.50 – 3.90	0.648	3.49	38	Regress.
1.1	0.570 – 0.273	6.50 – 8.60	2.50 – 3.90	0.648	3.49	57	Regress.
1.3, 1.1	0.683 – 0.273	7.14	3.22	0.589 – 0.689	2.37 – 3.49	12	Corr.Factor

6.1.2 Regression Process & Correction Factor Development

The relevant independent variables (IV) for each dependent variable (midship sinkage and trim) are sorted to simplify the regression analysis. For instance, it was determined in the previous chapter that the midship sinkage is dependent on *L/B*, Fr_h and *h/T*. Therefore, only these three IVs are considered in the regression analysis for midship sinkage. The required form for the selected variables; *L/B*, Fr_h and *h/T* are then tested by inversing where necessary and then attempting polynomial fitting of different degrees such that a strong correlation (goodness of fit) is obtained. The degree of polynomial required is then the maximum exponent for that particular variable to be trialled in the regression. A similar process is conducted for trim and the processed variables for the respective dependent variables are shown in Table 24. Generally, trim is more sensitive to Fr_h and *h/T* and exhibits greater non-linearity which requires higher degree polynomials for Fr_h and *h/T*.

Table 24: Independent variables (IV) selected for each dependent variable (DV) in the regression analysis.

DV	**Relevant Form of IV**	**Max Polynomial**	R^2	$R^2_{Adjusted}$	**RMSE**
Midship Sinkage/*T*	Fr_h	3	1	N/A	N/A
	T/h	2	0.994	0.982	2.86e-4
	B/L	2	0.996	0.987	1.88e-3
Trim (°)	Fr_h	4	0.991	0.973	8.82e-3
	T/h	3	1	N/A	N/A
	B/L	2	0.998	0.994	4.34e-3
	T/B	2	0.997	0.991	2.45e-3

A forward stepwise multiple linear regression method with consideration of interaction terms is then conducted based on the configured variables. The criteria for the acceptance and rejection of terms is based on the *p*-value measure. Only terms with a *p*-value of less than 0.05 (5%) are included. This implies that only terms with less than 5% probability of error are included. The outcome of the regression analysis is tabulated in Table 25.

The initial regression process based on the default procedure yielded excellent correlation with the original data but the number of terms, particularly for trim, is relatively high and may not be practical. The large number of terms is due to the nature of the stepwise regression algorithm. As the regression proceeds forward, more high order terms are included (terms with higher exponents). The addition of higher order terms causes some lower order terms to become less statistically significant such that their p-values become larger than 0.05. However, most of these lower order terms that have become statistically insignificant are not removed by the algorithm. This is because the algorithm is unable to remove lower order terms that are subsets of higher order terms that remain in the model. Thus, a revision is conducted where the maximum number of terms are reduced by manual elimination of terms with the larger p-values one-by-one while closely monitoring the change in R^2 value. The elimination process is undertaken by only removing terms with p-values > 0.05. The outcome of the revised regression process yielded less terms for midship sinkage while maintaining high correlation. As for trim, the number of terms has been significantly reduced at the cost of very minor correlation loss. Any further attempt to reduce the number of terms for trim would result in considerable decrease in R^2 value.

Table 25: Regression results obtained for the initial default procedure and revised condition where number of terms are reduced.

Results	**DV**	**No. of Terms**	$\boldsymbol{R^2}$	$\boldsymbol{R^2_{\mathrm{Adjusted}}}$	**RMSE**
Initial	Midship Sinkage (T)	11	0.999	0.999	1.16e-3
	Trim (°)	22	0.981	0.979	5.51e-3
Revised	Midship Sinkage (T)	8	0.999	0.999	1.18e-3
	Trim (°)	12	0.972	0.971	6.57e-3

Based on the results of the revised regression process, the produced regression formulae are presented as follows where the values of each coefficient are in Table 26:

$$S_{\mathrm{pred}} = Fr_{\mathrm{h}}\left[z_1 Fr_{\mathrm{h}}^2 + z_2 Fr_{\mathrm{h}}\, B/L + z_3 Fr_{\mathrm{h}}\, T/h + z_4\, B^2\big/\left(L^2 Fr_{\mathrm{h}}\right) + z_5 Fr_{\mathrm{h}} + z_6\, B/L + z_7\right] + z_8 \qquad 44.$$

where S_{pred} is the predicted midship sinkage in terms of the input T.

$$Tr_{\mathrm{pred}} = -Fr_{\mathrm{h}}\begin{bmatrix} k_1 Fr_{\mathrm{h}}^3 + k_2\left(T/h\right)^3 + k_3 Fr_{\mathrm{h}}^2\, T/B + k_4 Fr_{\mathrm{h}}^2\, B/L + k_5 Fr_{\mathrm{h}}\, T/L + \\ k_6 Fr_{\mathrm{h}}\, TB/\left(hL\right) + k_7 Fr_{\mathrm{h}}^2 + k_8\left(T/h\right)^2 + k_9 Fr_{\mathrm{h}}\, T/B + k_{10} T/B + k_{11} T/h \end{bmatrix} - k_{12} \qquad 45.$$

where Tr_{pred} is the predicted trim in degrees (°) where positive values signify trim by the bow.

Table 26: Values of each coefficient for the derived regression formulae.

S_{pred}				Tr_{pred}			
Coeff.	**Value**	**Coeff.**	**Value**	**Coeff.**	**Value**	**Coeff.**	**Value**
z_1	0.7771	z_7	0.3826	k_1	1.4597	k_7	0.1865
z_2	3.4937	z_8	-0.0314	k_2	3.7578	k_8	-6.0074
z_3	0.1093	-	N/A	k_3	-6.9341	k_9	6.9351
z_4	1.0202	-	N/A	k_4	-15.5692	k_{10}	-0.7477
z_5	-1.0904	-	N/A	k_5	-17.4567	k_{11}	1.5585
z_6	-1.5493	-	N/A	k_6	15.0199	k_{12}	0.0892

As for the modelling of the L_{BF} correction factor, plots of the change in midship sinkage and trim with respect to L_{BF} for varying Fr_h and h/T are firstly compared in Figure 51. As in agreement with findings from the previous chapter, sinkage is independent of L_{BF} and further observations can be made here that this is still true for cases of varying Fr_h and h/T. However, trim is found to be linearly related to L_{BF} and the rate of change is dependent on Fr_h. It is also of interest to note that the trim tends to be bow down when L_{BF} increases i.e. LCB is further forward of LCF whereas the trim tends to become stern down when L_{BF} decreases i.e. LCB is close to LCF. Furthermore, when the speed is kept constant ($Fr_h = 0.57$) while varying h/T between 1.1 and 1.3, the rate of change in trim remains similar. This implies that the rate of change in trim is only dependent on Fr_h.

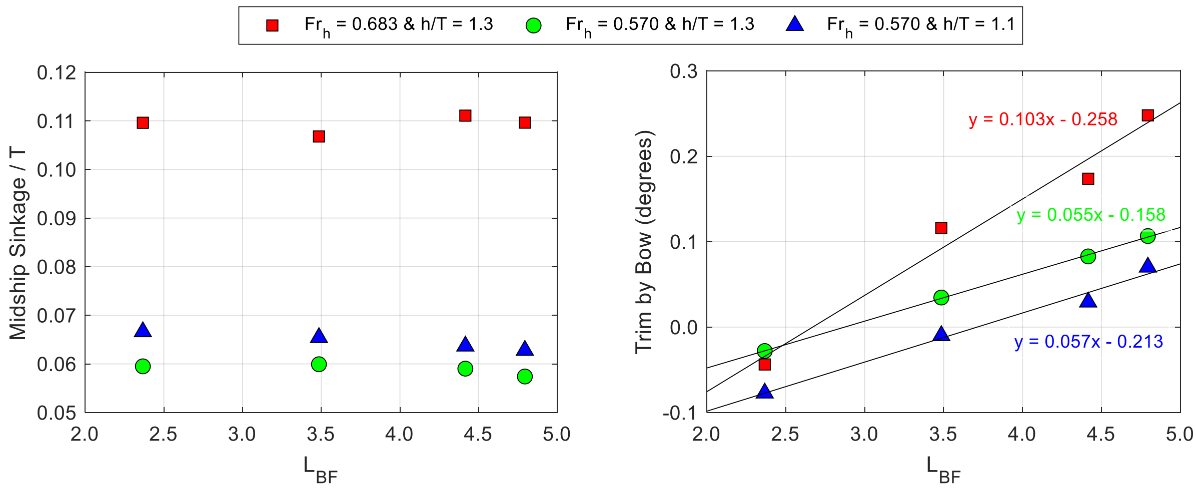

Figure 51: Effect of L_{BF} on midship sinkage (left) and trim (right) for varying Fr_h and h/T conditions. There is no significant relationship between sinkage and L_{BF} but trim is directly proportional to L_{BF} and the rate of change is dependent on Fr_h.

Having shown that the relationship between trim and L_{BF} is linear and that the gradient (rate of change in trim) is only dependent on Fr_h, it is possible to develop a simple correction factor with the data presented especially when the trendline for high speed conditions are known. This is because the impact of trim on the overall squat is only significant for high speed conditions whereas the trim for lower speeds can be extrapolated from the current range with reasonable accuracy. The performance of this correction factor based on this approach is also proven to be satisfactory later in the next section. This linear correction factor models the gradient as a function of both Fr_{h} and the initially predicted trim (Tr_{pred} for the default L_{BF} = 3.485 condition). By doing so, the change in slope with respect to Fr_{h} can be accounted for which is important at high speeds where the impact of trim magnitude is significant. Consequently, the corrected trim, $Tr_{\mathrm{pred\text{-}cor}}$, is expressed as shown below:

$$Tr_{\mathrm{pred\text{-}cor}} = \frac{(Tr_{\mathrm{pred}} - c_1)}{3.485} \times L_{\mathrm{BF}} + c_1 \qquad 46.$$
$$c_1 = 0.0055 - 0.3455 Fr_{\mathrm{h}}$$

Nevertheless, there are limitations arising from this approach which should be acknowledged. Firstly, inaccurate predictions may manifest for hull forms which have L_{BF} values significantly beyond the range tested ($2.37 \leq L_{\mathrm{BF}} \leq 3.49$; $Fr_{\mathrm{h}} \leq 0.683$; $h/T < 1.1$; $h/T > 1.3$). In addition, erroneous predictions may also arise for hull forms that are not typical of standard container ship designs such as having fuller fore sections similar to bulk carriers.

6.1.3 Performance of the Empirical Formulae

The performance of the derived empirical formulae is assessed by comparing against some of the original data used for the regression. Five sets of cases inclusive of the extremities of the range of applicability for *L/B* and *B/T* are examined (refer to Table 27). The performance of the formulae against these original cases is illustrated in Figure 52. Good correlations are achieved for all cases examined both in terms of midship sinkage and trim predictions. Although slight discrepancies in the trim trend are observed at low speeds, these are negligible. The larger trim angles at high speeds are of more importance and these are well reflected by the formulae. The performance of the formulae in predicting new cases not used in the regression will be examined and discussed later in Section 6.4.

Table 27: Cases examined to assess the performance of the empirical formulae against the original data.

Case No.	***L/B***	***B/T***	***Fr*****h**	***h/T***
1	8.60	2.50	0.273 – 0.567	1.2
2	7.14	3.22	0.273 – 0.683	1.3
3	6.50	2.50	0.361 – 0.683	1.3
4	8.60	3.90	0.3 – 0.683	1.3
5	6.50	3.90	0.287 – 0.570	1.2

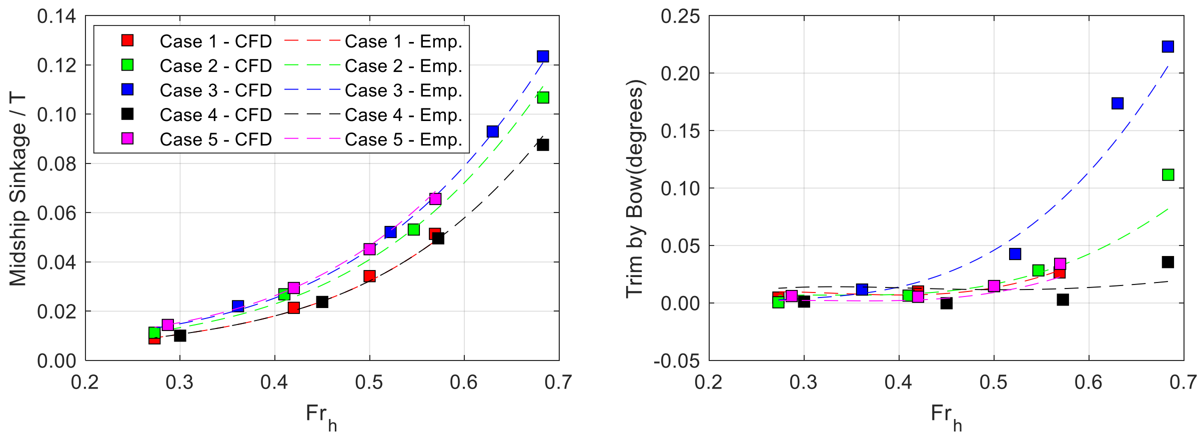

Figure 52: Comparison of the empirical formulae against the original data points for regression.

6.2 Lateral Restriction Effect

The empirical formulae developed in the previous section covered the effects of hull parametric variations on squat in shallow but laterally unrestricted water conditions. Therefore, this section of the study aims to quantify the effect of lateral restrictions to be incorporated as a correction factor in the development of the new empirical formulae. Due to time and resource constraints, the scope of this investigation is limited to cases of laterally restricted channels with symmetrical banks. Cases where the ship is not in the centre of the channel or single bank restriction cases are not considered.

In this investigation, two sets of systematic simulations are conducted; cases with fixed bank height but varying bank widths, and cases with fixed bank width but varying bank height (refer to Table 28). For all these cases, the bank slope is kept similar and illustrations of some of these channel geometries are shown in Figure 53. The CFD simulation set-up and modelling method is identical to that in Chapter 5.

Table 28: Test matrix for investigation of lateral restriction effects. Refer to Figure 53 for visual definition of some of the symbols.

Bank Width to Vessel Beam Ratio, *W/B*	**Bank Height to Water Depth Ratio, h_m/T**	**Froude Depth Number, Fr_h**	**Water Depth to Draft Ratio, *h/T***
Fixed h_m/T, Varying *W/B*			
10	0.4	0.57 – 0.37	1.3
7.5	0.4	0.57 – 0.37	1.3
5.0	0.4	0.57 – 0.37	1.3
2.5	0.4	0.57 – 0.37	1.3
Fixed Bank *W/B*, Varying h_m/T			
5.0	0.7	0.57 – 0.42	1.3 – 1.1
5.0	0.4	0.57 – 0.42	1.3 – 1.1
5.0	0.2	0.57 – 0.42	1.3 – 1.1
5.0	0.1	0.57 – 0.42	1.3 – 1.1

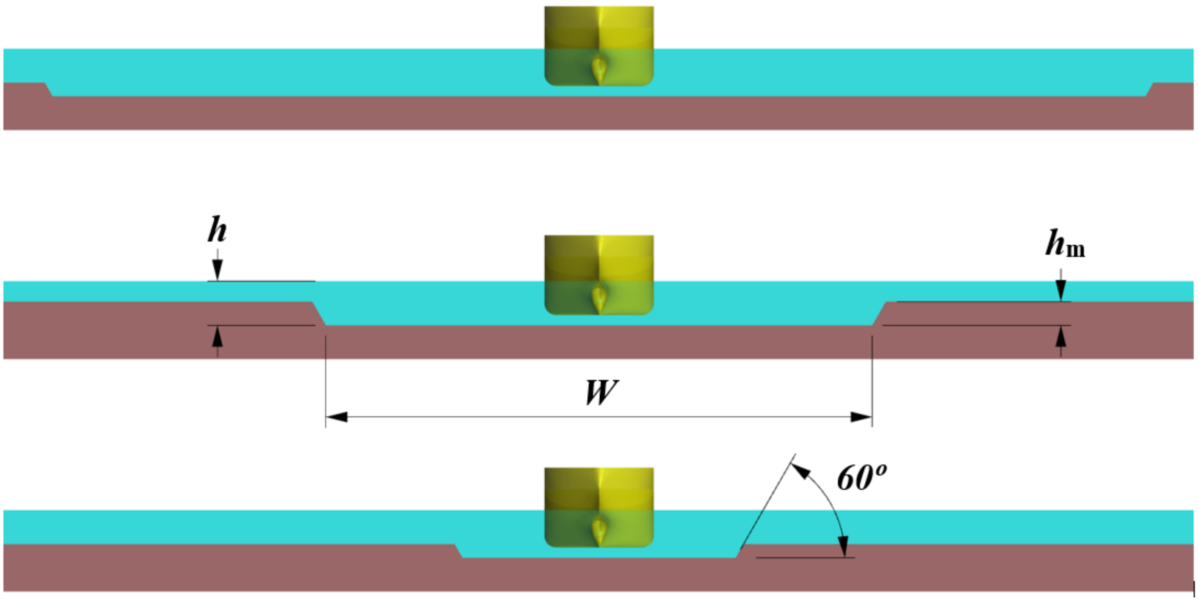

Figure 53: Illustration of some of the restricted channel geometries investigated (from top to bottom): W/B = 10 with h_m/T = 0.4 at h/T = 1.3, W/B = 5 with h_m/T = 0.7 at h/T = 1.3, and W/B = 2.5 with h_m/T = 0.4 at h/T = 1.3.

6.2.1 Blockage Ratio Calculation

Traditionally, the blockage ratio, m is calculated to quantify the relationship between blockage and squat. However, in this study, a more sophisticated and holistic approach to calculate blockage ratio is applied. This method uses the concept of equivalent blockage, m_{eq} and "weight factor" introduced by Lataire and Vantorre (2008).

The "weight factor" has a value between 0 and 1, which indicates the influence of a water particle on the manoeuvrability of a hull. A water particle close to the hull has a weight factor close to 1 whereas the weight factor tends to 0 the further the water particle is from the hull. The weight factor is 1 at the centre line of the hull and on the free surface while the area occupied by the hull has 0 weight factor (Lataire and Vantorre, 2008). The weight distribution is similar to the decreasing exponential function described by Norrbin (1976). When using the ship bound coordinate system, the weight distribution function can be expressed as:

$$e^{-a|y|-b|z|} \qquad 47.$$

The coefficient a is a function of the y_{infl} defined earlier in Equation 42 while coefficient b is a function of the ship draft as expressed below:

$$a = \frac{3}{y_{infl}} \qquad 48.$$

$$b = \frac{1}{3T} \qquad 49.$$

Therefore, the "weight", χ, of a body of water in a rectangular canal with coordinates (y_1, z_1), (y_1, z_2), (y_2, z_1) and (y_2, z_2) can be given as:

$$\chi_{\text{rect}} = \int_{z_1}^{z_2} \int_{y_1}^{y_2} e^{-(ay+bz)} dy\ dz = \frac{1}{ab}\left(e^{-ay_1} - e^{-ay_2}\right)\left(e^{-bz_1} - e^{-bz_2}\right) \qquad 50.$$

Similarly, the "weight" of the water displaced by a ship, χ_{ship}, with beam, B and draft T, can be simplified as:

$$\chi_{\text{ship}} = 2\int_0^T \int_0^{B/2} e^{-(ay+bz)} dy\ dz = \frac{2}{ab}\left(1 - e^{-aB/2}\right)\left(1 - e^{-bT}\right) \qquad 51.$$

It should be noted that the "weight" has a non-infinite solution at an infinite depth and infinite width condition i.e. when in deep open water:

$$\chi_{\text{ocean}} = 2\int_0^\infty \int_0^\infty e^{-(ay+bz)} dy\ dz = \frac{2}{ab} = 2y_{\text{infl}}T \qquad 52.$$

Similarly, the "weight" of a laterally unrestricted but shallow waterway of depth h can be simplified as:

$$\chi_{\text{unrestricted}} = 2\int_0^h \int_0^\infty e^{-(ay+bz)} dy\ dz = \frac{2\left(1 - e^{-hb}\right)}{ab} = 2y_{\text{infl}}T\left(1 - e^{-\frac{h}{3T}}\right) \qquad 53.$$

The equivalent blockage, m_{eq}, can then be expressed in the below form where χ_{p}, is the "weight" of the fairway at port side of the ship (excluding "weight" of ship) whereas χ_{s} is that of the starboard side:

$$m_{\text{eq}} = \frac{\chi_{\text{ship}}}{\chi_{\text{p}} + \chi_{\text{s}}} - \frac{\chi_{\text{ship}}}{\chi_{\text{ocean}} - \chi_{\text{ship}}} \qquad 54.$$

The above expression for m_{eq} accounts for the weight distribution, position of the ship relative to the bank(s) and speed of the ship. However, as the scope of the current study does not include off-centre/asymmetrical bank effects, the following simplification can be made: $\chi_{\text{p}} = \chi_{\text{s}}$. Regardless of the simplification, it should be noted that the m_{eq} of a fairway with width X and depth Y will still be different from a fairway with width Y and depth X (Lataire and Vantorre, 2008). Similarly, for cases with the same waterway but different ship speed will also have different m_{eq}. Thus, for the purpose of comparing between different cases, the m_{eq} for each case is normalised to their respective laterally unrestricted conditions (refer to Equation 55). Sample calculations of the traditional blockage ratio, m, in comparison to the m_{eq} and normalised m_{eq} ($m_{\text{eq-norm}}$) in Table 29 demonstrates that the value of m is indifferent to bank height and ship speed whereas both m_{eq} and $m_{\text{eq-norm}}$ varies with bank height and ship speed. Therefore, the use of the $Fr_{\text{h,Crit}}$ parameter which is a function of m is not recommended and not used for analysis for the ensuing investigations here.

$$m_{\text{eq-unrestricted}} = \frac{\chi_{\text{ship}}}{\chi_{\text{unrestricted}} + \chi_{\text{ship}}} - \frac{\chi_{\text{ship}}}{\chi_{\text{ocean}} - \chi_{\text{ship}}}$$

55.

$$m_{\text{eq-norm}} = m_{\text{eq}} / m_{\text{eq-unrestricted}}$$

Table 29: Sample calculated blockage ratio, *m*, in comparison to the m_{eq} and normalised m_{eq} for a subset of the cases to be investigated. The value of *m* is indifferent to bank height and ship speed whereas both m_{eq} and $m_{eq\text{-}norm}$ varies with bank height and ship speed.

W/B	h_m/T	Fr_h	***h/T***	**Blockage Ratio ($m = A_S/A_C$)**	**Equivalent Blockage, m_{eq}**	**Normalised m_{eq}, $m_{eq\text{-}norm}$**
∞	-	0.572	1.3	N/A	0.149	1.00
2.5	0.4	0.572	1.3	0.276	0.201	1.35
5.0	0.4	0.572	1.3	0.144	0.179	1.20
5.0	0.2	0.572	1.3	0.144	0.162	1.09
5.0	0.1	0.572	1.3	0.144	0.155	1.04
∞	-	0.373	1.3	N/A	0.178	1.00
2.5	0.4	0.373	1.3	0.276	0.236	1.33
5.0	0.4	0.373	1.3	0.144	0.209	1.18

6.2.2 Results

In this study extreme cases were investigated. Some of these fall within the trans-critical flow regime. It should be noted that results which correlate to the trans-critical flow regime have been omitted as these are neither practical for the investigation nor are they validated. The first part of this section compares the effect of varying *W/B* and h_m/T on squat. This is followed by results for effect of Fr_h and *h/T* in varying lateral restriction conditions. Finally, results for the effect of hull principal particulars in varying lateral restriction conditions are discussed. Analysis of these results will help determine the important factors to be considered in the development of the correction factor as well as appropriately quantify the effect of these factors where necessary.

Figure 54 compares the sinkage and trim results for cases with fixed h_m/T but varying *W/B* against cases of fixed *W/B* but varying h_m/T at *h/T* = 1.3 (refer to Table 28 for the test matrix). As anticipated, the midship sinkage increases when normalised m_{eq} increases but more importantly, it can be seen that the increase in midship sinkage is collinear for both cases of fixed h_m/T and cases of fixed *W/B*. In addition, the magnitude of trim predicted for both sets of cases are also comparable for a given value of normalised m_{eq}. However, the change in trim with normalised m_{eq} is within the uncertainty limits and deemed insignificant. The lateral restriction's considerable impact on midship sinkage but minimal impact on trim observed here in this study is similar to the findings by Tuck (1967). The key finding here is that the resulting midship sinkage and trim will be similar for two channels with completely different widths and bank heights as long as both conditions have the same value of normalised m_{eq}.

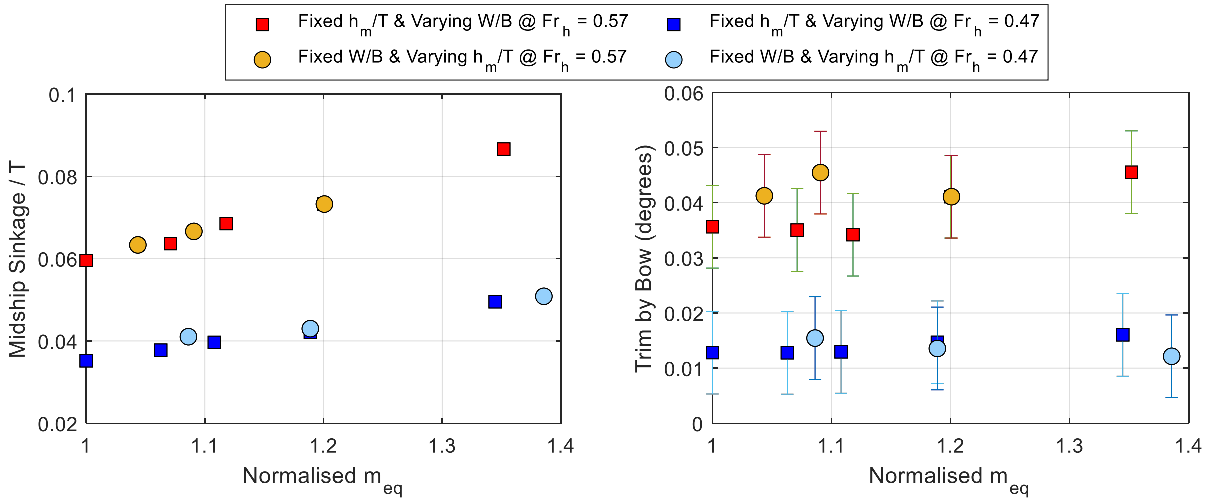

Figure 54: Comparison between cases with fixed h_m/T but varying W/B against cases of fixed W/B but varying h_m/T at h/T = 1.3. Midship sinkage results are shown on the left and trim on the right. For the same speed, sinkage increases collinearly for both fixed h_m and fixed W cases when normalised m_{eq} increases whereas there is no significant change in trim with respect to normalised m_{eq}.

Further comparison of cases at different speeds in Figure 55 illustrates that the gradient for sinkage increases when speed increases. The change in trim for each speed also varies but still relatively small variations that are within or near the uncertainty bounds. However, when comparing the effect of varying h/T (refer to Figure 56), the trendlines for sinkage results suggest that the gradient for sinkage also increases when h/T decreases. This observation implies that although the current method for blockage ratio calculation considers h/T, the magnitude of sinkage for a given normalised m_{eq} is still sensitive to h/T. Therefore, care must be taken to factor h/T as well as Fr_h in the modelling of lateral restriction effects. Trim only appears to increase with normalised m_{eq} for h/T = 1.1 but again, these differences are within the uncertainty bounds and are relatively negligible. Neglecting the change in trim due to blockage in these particular cases will result in maximum difference of only ±4% in AP/FP sinkage prediction.

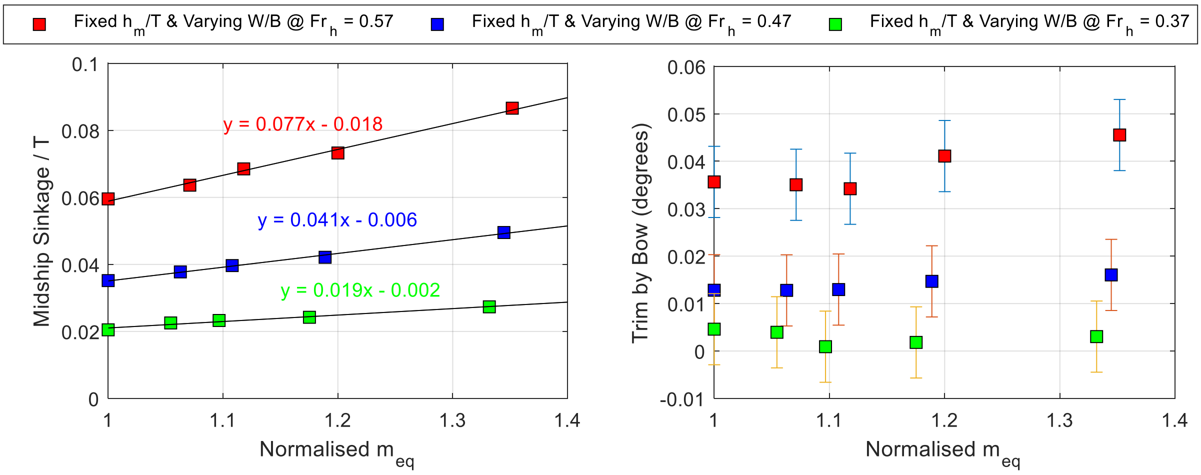

Figure 55: Comparison of the sinkage (left) and trim (right) results for fixed h_m/T cases at varying speeds for h/T = 1.3. The sinkage result trendlines show that the gradient increases with speed. The change in trim for each speed are relatively small when normalised m_{eq} increases.

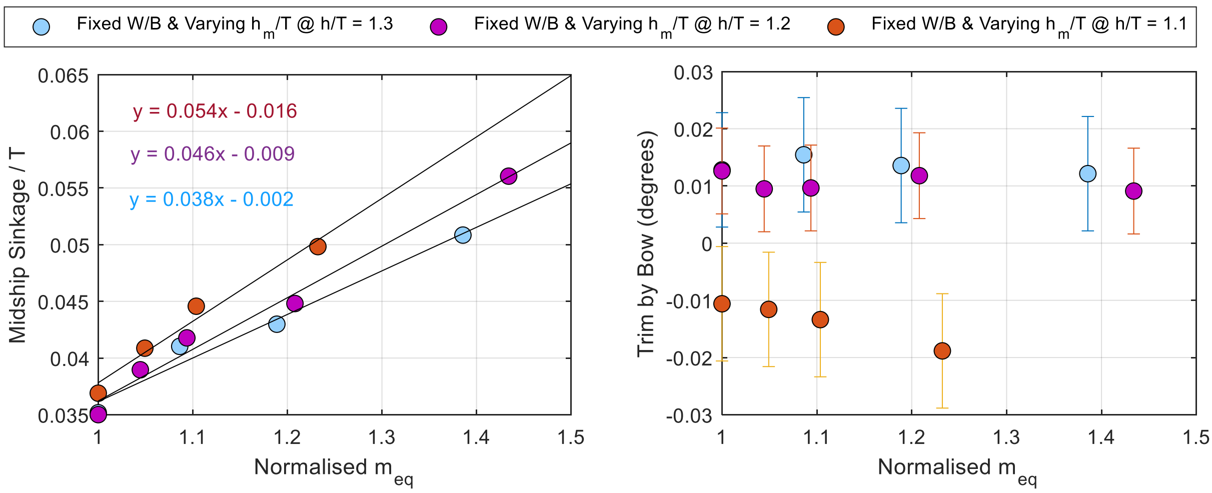

Figure 56: Comparison of the sinkage (left) and trim (right) results for fixed W cases at varying h/T for Fr_h = 0.47. The sinkage result trendlines show that the gradient increases with h/T. Trim only appears to increase with normalised m_{eq} for h/T = 1.1.

However, the observed trends above are all based on one hull form (the parent KCS). Hence, systematic variations of the KCS are also studied. The hull forms investigated are that of the extremities of the range of applicability of the empirical formulae i.e. L/B = 6.5, 8.6 & B/T = 2.5, 3.9. The results are as plotted in Figure 57. Trendlines for the sinkage suggest that the gradient is approximately similar regardless of the hull form. Thus, it is possible to estimate the resultant sinkage due to lateral restrictions with reasonable accuracy for other hull forms within the range of the cases tested by using the same gradient value and the estimated sinkage in laterally unrestricted conditions for those particular hulls. As for trim results, the changes in trim are unnoticeable for most of the hull forms except for one of the hulls (L/B = 6.5 & B/T = 2.5) which appears to exhibit increasing trim.

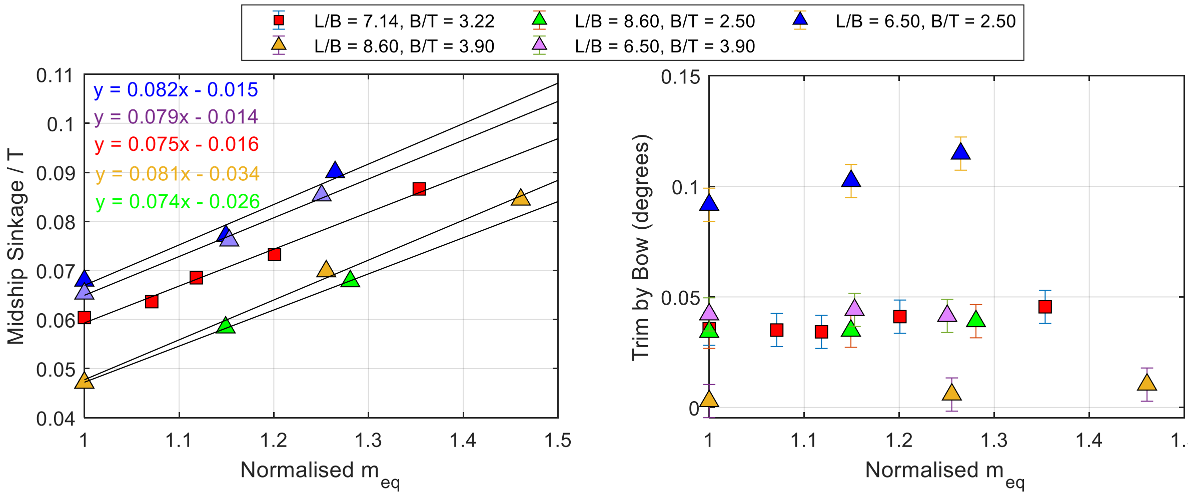

Figure 57: Comparison of the sinkage (left) and trim (right) results of various systematic hull form variations at Fr_h = 0.57 and h/T = 1.3. The gradient for sinkage is similar across all the different hull forms. Changes for trim is generally unnoticeable except for one of the hull forms.

The implications of the findings here are adequate and significant for the development of the correction factor. First of all, it is demonstrated that the current method for blockage ratio calculation (normalised m_{eq}) is a sufficiently accurate method to quantify a given laterally restricted condition. Laterally restricted waterways of different width and bank height yet similar normalised m_{eq} will result in similar changes to midship sinkage and the normalised m_{eq} can be used to predict the linear change in midship sinkage provided that the corresponding sinkage for the laterally unrestricted condition is known. Furthermore, it is found that the rate of change in midship sinkage with normalised m_{eq} is sensitive to Fr_h and h/T but not to hull form changes. On the contrary, the rate of change in trim with normalised m_{eq} is only sensitive to the hull form changes for the current range investigated.

Therefore, the correction factor for effects of lateral restriction based on the above mentioned observations can be developed. Here, the gradient (the rate of change) of midship sinkage with respect to normalised m_{eq} is denoted as ∇_S. The estimated value for ∇_S with respect to Fr_h and h/T as well as the resulting corrected midship sinkage for lateral restriction effects, $S_{\text{pred-LR}}$ are given in Equation 56. Note that the output $S_{\text{pred-LR}}$ is in terms of T of the hull.

$$\begin{aligned} \nabla_S &= -0.0800\frac{h}{T} + 0.2890 Fr_h + 0.0124 \\ S_{\text{pred-LR}} &= S_{\text{pred}} + \nabla_S \left(m_{\text{eq-norm}} - 1 \right) \end{aligned} \qquad 56.$$

Similarly, the rate of change of trim with respect to normalised m_{eq} is denoted as ∇_{Tr}. The estimated value for ∇_{Tr} with respect to L, B, and T as well as the resulting corrected trim for lateral restriction effects, $Tr_{\text{pred-LR}}$ are given in Equation 57. Note that the output $Tr_{\text{pred-LR}}$ is in degrees (positive by the bow).

$$\nabla_{Tr} = 1.153 - 0.1618\frac{L}{B} - 0.2676\frac{B}{T} + 0.004618\left(\frac{L}{B}\right)^2 + 0.02414\frac{L}{T} + 0.009901\left(\frac{B}{T}\right)^2 \quad 57.$$

$$Tr_{\text{pred-LR}} = Tr_{\text{pred-cor}} + \nabla_{Tr}\left(m_{\text{eq-norm}} - 1\right)$$

Since some of the cases in the initial test matrix are omitted due to reaching the trans-critical flow regime, the initial test matrix has been revised to develop the suggested limits of applicability for the lateral restriction correction factors. Generally, restrictions with resulting $m_{\text{eq-norm}}$ < 1.3~1.4 is recommended or alternatively, the ranges summarised in Table 30 is suggested. Note that the limits of applicability for the hull parameters in the laterally unrestricted formulae applies for the lateral restriction correction factors as well. The performance of the lateral restriction effect correction is discussed later in section 6.4 after consolidation of the current developments with the outcomes of the initial trim effect study.

Table 30: Suggested limits of applicability for the lateral restriction correction factors after consideration of trans-critical cases that were omitted from the derivation.

Min. W/B	Max h_m/T	Max Fr_h	Min. h/T
2.5	0.4	0.57	1.3
5.0	0.7	0.47	1.3
5.0	0.4	0.52	1.2
5.0	0.4	0.52	1.1

6.3 Initial Trim Effect

In practice, it is common for container ships to operate with a static initial trim either due to changes in loading condition or to optimise UKC in shallow water conditions (Harting & Reinking 2002) or to optimise energy efficiency to minimise emissions (Sherbaz & Duan 2014). Thus, a brief study is conducted to examine the effects of initial trim on squat and to then determine whether these effects are sufficiently significant to be considered in the formulae.

6.3.1 Cases Investigated

For this investigation, the parent KCS hull along with sister hulls no. 20 and 23 (refer to Appendix C) are used. Sister hulls no. 20 and 23 are chosen because these are variants with different C_B which in other words have unique L_{BF} values. Therefore, these hulls have significantly different running trim magnitudes and even direction according to previous findings. Five variations in initial trim were investigated for all three hull forms while the speed and water depth are kept constant (refer to Table 31). In each case, only the LCG of the hull is shifted to attain the desired initial trim without changing displacement. The domains for these cases are laterally unrestricted.

Table 31: Cases investigated for the study of initial trim effect.

Total Hulls	***Fr*$_h$**	***h/T***	***C*$_B$**	**Initial Trim (°)**
3	0.683	1.3	0.598, 0.648, 0.689	0.5, 0.2, 0, -0.2, -0.5

6.3.2 Results

A plot of the changes in midship sinkage and trim with respect to initial trim for the three hull forms are shown in Figure 58. Generally, it can be observed that the midship sinkage tends to increase when initial trim changes from stern down to bow down, but the rate of change is dependent on the hull form. The squat of the finer hull (C_B = 0.589) appears to be more sensitive to initial trim while the squat of the fuller hull (C_B = 0.689) is relatively indifferent to initial trim.

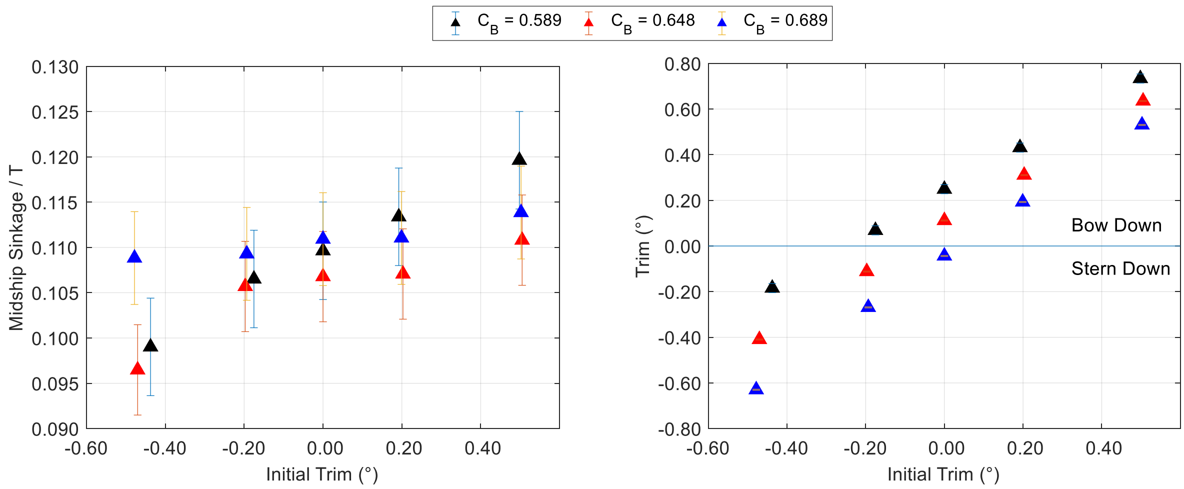

Figure 58: Plot of midship sinkage and running trim against initial trim for the three hull forms. The change in midship sinkage varies with hull form but are all still within uncertainty limits whereas changes in running trim are linear.

This behaviour is likely due to the differences in the fore and aft section of the hulls. Generally, the aft section has an increasingly larger volume from keel to deck and hence, when the hull is trimmed towards the stern, less sinkage is required to achieve dynamic equilibrium. In the case of the fuller hull however, the difference between the fore and aft sections are small which results in less sensitivity to the effects of initial trim. Nonetheless, it should be noted that these differences in midship sinkage inclusive of that of the finer hull are within the uncertainty limits. These differences are also only within 2% of T and can be deemed negligible from a practical perspective.

In regard to trim, linear trends are observed for all three hull forms. It can be seen that the different hull forms generally cause a vertical shift in magnitude with very minimal changes in terms of gradient. This signifies that the current hull form changes have a more pronounced effect on the magnitude of trim but minimal effect on the rate of change of trim with respect to initial trim. The greater bow trim exhibited by the finer hull for initial trim of +0.5° and the greater stern trim exhibited by the fuller hull for initial trim of -0.5° can be visually observed in the hydrodynamic pressure distribution plot in Figure 59.

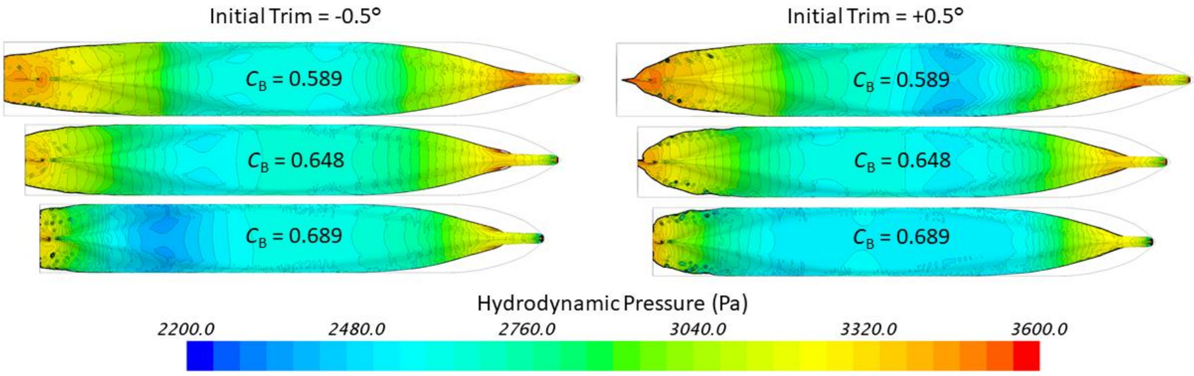

Figure 59: Hydrodynamic pressure distribution on the hulls for different initial trim conditions.

Further analysis is then undertaken to assess whether the overall changes in midship sinkage and trim with respect to initial trim observed earlier are significant. Therefore, a pair of comparison plots are depicted in Figure 60. Firstly, the net change in running trim is observed in Figure 60 (left). The net change in trim is simply the change in trim from the initially trimmed position when the hull is underway. A positive net change signifies the hull has a net bow down trim while negative net change signifies net stern down trim. For the case of the finer hull, the net change is similar for all initial trim cases but as C_B increases, deviations in net change in trim become observable and even the direction of net trim can differ such as for when C_B = 0.689 at initial trim of +0.5°.

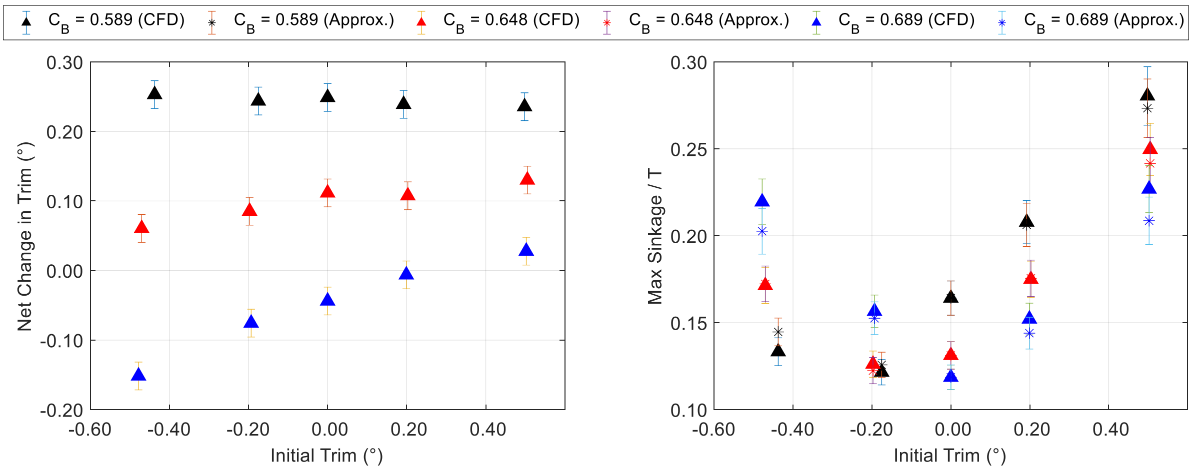

Figure 60: Plot of net changes in trim against initial trim (left) and comparison of the actual resultant maximum sinkage against the approximated resultant maximum sinkage (right). It is shown that the approximated maximum sinkage is a reasonable approximation to the actual results.

In order to better assess the overall significance of the impact of initial trim, a comparison is made between the actual CFD results and approximated results. The approximated results here are modified CFD results for even keel conditions where the net midship sinkage and running trim are assumed to be unaffected by initial trim. In other words, the approximated results assume that the change in midship sinkage and running trim at even keel condition applies to other initial trim conditions. Figure 60 (right) demonstrates that the difference between the actual results and approximated results are either unnoticeable or still relatively small. For all cases, the difference in maximum sinkage is within 2% of *T* and the location of the maximum sinkage (AP or FP) are also still correctly approximated even for the case where the direction of net change in trim is wrongly approximated. This observation implies that the effect of initial trim is generally negligible and the maximum sinkage due to the presence of an initial trim can be approximated based on the running trim at even keel conditions.

Therefore, the effects of initial trim that is within ±0.5° can be disregarded and no correction factor is necessary for the final form of the empirical formulae. The key equations for the complete empirical formulae up to this point are reiterated here:

$$S_{\text{pred}} = Fr_{\text{h}}\left[z_1 Fr_{\text{h}}^2 + z_2 Fr_{\text{h}}\, B/L + z_3 Fr_{\text{h}}\, T/h + z_4\, B^2\big/\left(L^2 Fr_{\text{h}}\right) + z_5 Fr_{\text{h}} + z_6\, B/L + z_7\right] + z_8 \qquad 58.$$

$$Tr_{\text{pred}} = -Fr_{\text{h}}\left[\begin{array}{l} k_1 Fr_{\text{h}}^3 + k_2\left(T/h\right)^3 + k_3 Fr_{\text{h}}^2\, T/B + k_4 Fr_{\text{h}}^2\, B/L + k_5 Fr_{\text{h}}\, T/L + \\ k_6 Fr_{\text{h}}\, TB\big/\left(hL\right) + k_7 Fr_{\text{h}}^2 + k_8\left(T/h\right)^2 + k_9 Fr_{\text{h}}\, T/B + k_{10} T/B + k_{11} T/h \end{array}\right] - k_{12} \qquad 59.$$

$$\begin{aligned} Tr_{\text{pred-cor}} &= \frac{(Tr_{\text{pred}} - c_1)}{3.485} \times L_{\text{BF}} + c_1 \\ c_1 &= 0.0055 - 0.3455 Fr_{\text{h}} \end{aligned} \qquad 60.$$

$$\begin{aligned} \nabla_S &= -0.0800\frac{h}{T} + 0.2890 Fr_{\text{h}} + 0.0124 \\ S_{\text{pred-LR}} &= S_{\text{pred}} + \nabla_S\left(m_{\text{eq-norm}} - 1\right) \end{aligned} \qquad 61.$$

$$\begin{aligned} \nabla_{Tr} &= 1.153 - 0.1618\frac{L}{B} - 0.2676\frac{B}{T} + 0.004618\left(\frac{L}{B}\right)^2 + 0.02414\frac{L}{T} + 0.009901\left(\frac{B}{T}\right)^2 \\ Tr_{\text{pred-LR}} &= Tr_{\text{pred-cor}} + \nabla_{Tr}\left(m_{\text{eq-norm}} - 1\right) \end{aligned} \qquad 62.$$

Alternatively, for the readers' convenience, a summary of all the required equations are repeated with important notes explaining the purpose and requirement of each equation in Appendix D. An implementation of the formulae in the form of a MATLAB script is also made available in Appendix D. The currently developed empirical formulae account for the effect of *L/B*, *B/T*, L_{BF}, *h/T*, Fr_{h} and varying bank configurations including changes in *W/B*, h_m/T and bank slope. The effects of a propeller operating at self-propulsion speed is inherently accounted for. No scale effect correction is provided but where a conservative estimate is preferred, a safety factor of 1.15 is suggested.

6.4 Evaluation of the New Formulae

In this section, various evaluations are conducted on the new empirical formulae developed. Firstly, the performance of the new formulae in predicting squat in laterally unrestricted conditions is examined. This is followed by comparisons of squat predictions between that of the new formulae against that of the existing empirical formulae to determine whether the new formulae satisfy the research objective of improving accuracy over currently existing empirical methods. Similarly, the performance of the new formulae for predictions in laterally restricted conditions are also assessed as well as the corresponding comparisons to the predictions of existing empirical methods. The cases investigated involve the parent and sister KCS hulls and also hull forms that are not used in the formulae development; the DTC and S175. The lateral restriction conditions investigated here also include conditions that are beyond the limits of applicability so that the performance of the formulae in these conditions can be assessed. The final set of performance review of the new formulae examines full scale squat prediction which is compared against full scale trials.

6.4.1 Evaluation for Laterally Unrestricted Cases

The results of the various cases compared for laterally unrestricted conditions are shown in Table 32. Overall, midship sinkage predictions are mostly within 5% of the CFD results. Trim predictions exhibit larger percentage differences as trim values are very small and sensitive but the differences for most cases are practically reasonable (in the order of ±0.01°**)**. Trim direction is also correctly predicted for all cases except for cases no. 2 and 9, which is understandable as the magnitude of trim for these cases is relatively small.

The resultant maximum sinkage predicted is also mostly within 6% of the CFD results. Effectively all the cases compared have difference of less than 1% of T with respect to CFD results. Good correlations are observed as well for cases involving the S175 and DTC hulls. The minimal trim of the S175 at high speeds is accurately predicted by the formulae (case no. 10). However, the trim direction of the S175 is wrongly predicted at a lower speed (case no. 9) but the magnitude of this trim is within 0.025° which is equivalent to 7 cm of sinkage difference in full scale. The more noticeable trim of the DTC hull particularly at high speeds (case no. 13) is predicted accurately by the formulae too. There are discrepancies noted for the maximum sinkage prediction for the DTC at very shallow conditions (case no. 14) but the difference is within 0.4% of T. Further tests for a near grounding condition is also undertaken (case no. 15) where CFD simulations are conducted at as high a speed possible while still being able to achieve convergence. The empirical predictions can be seen to have good correlation with the CFD results even though the speed is over the recommended limits of applicability.

In summary, the performance of the developed empirical formulae is encouraging and promising. Good correlations are observed for most cases even those at high speeds ($Fr_h > 0.5$) and discrepancies that are noted are all reasonable.

A few comparisons of squat predictions between that of the new formulae against existing empirical methods are shown in Figure 61. Throughout the cases examined, the new empirical formulae can be seen to have good correlation with the CFD results. On the contrary, as noted from previous investigations, currently available methods exhibit a large spread in predictions where the method of Millward (1992) tends to yield the largest predictions and that of Barrass II (1979) tends to yield the lowest predictions. It is interesting to note that the predictions of Hooft (1974) are reasonably accurate throughout these cases. However, the predictions of the new formulae are still the most accurate relative to the CFD results and thus, is an improvement over these existing methods for the cases investigated.

Table 32: Comparison of the empirical predictions against CFD results for various cases not used to develop the regression (no lateral restrictions). Fr_h values in orange signify it is beyond the recommended range of applicability.

Test No.	**Test Descript.**	***L/B***	***B/T***	***C*_B**	***L*_BF**	***Fr*_h**	***h/T***	**Results**	**Sinkage/*T***	**Trim (° by bow)**	**Max Sinkage/*T***
1	High Speed	6.50	3.90	0.648	3.49	0.576	1.3	CFD	0.064	-0.042	0.074
								Emp.	0.069	-0.043	0.078
								Diff %	1.601	3.112	4.283
2	High Speed + Very Shallow	7.52	2.90	0.648	3.49	0.570	1.1	CFD	0.058	-0.006	0.059
								Emp.	0.060	0.002	0.060
								Diff %	3.596	-128.986	2.338
3	Long L_{BF} + High Speed	7.14	3.22	0.589	4.79	0.683	1.3	CFD	0.110	0.249	0.165
								Emp.	0.108	0.233	0.160
								Diff %	-1.446	-6.318	-3.072
4	Long L_{BF} + High Speed	7.14	3.22	0.622	4.42	0.687	1.3	CFD	0.113	0.174	0.151
								Emp.	0.110	0.201	0.155
								Diff %	-2.161	15.577	2.350
5	Long L_{BF} + High Speed + Very Shallow	7.14	3.22	0.589	4.79	0.570	1.1	CFD	0.063	0.070	0.078
								Emp.	0.064	0.065	0.078
								Diff %	1.413	7.398	-0.330
6	Long L_{BF} + High Speed + Very Shallow	7.14	3.22	0.622	4.42	0.570	1.1	CFD	0.064	0.029	0.070
								Emp.	0.064	0.063	0.078
								Diff %	0.016	113.501	10.498
7	Short L_{BF} + High Speed	7.14	3.22	0.689	2.37	0.683	1.3	CFD	0.108	-0.044	0.116
								Emp.	0.108	-0.005	0.109
								Diff %	-0.287	-88.851	-6.191

8	Short L_{BF} + High Speed + Very Shallow	7.14	3.22	0.689	2.37	0.570	1.1	CFD	0.067	-0.077	0.080
								Emp.	0.064	-0.084	0.079
								Diff %	-4.406	8.797	-2.160
9	S175 Hull + High Speed	6.89	2.67	0.572	2.59	0.547	1.3	CFD	0.053	0.021	0.057
								Emp.	0.054	-0.025	0.058
								Diff %	1.207	-221.230	1.260
10	S175 Hull + High Speed	6.89	2.67	0.572	2.59	0.683	1.3	CFD	0.114	0.046	0.122
								Emp.	0.112	0.054	0.122
								Diff %	-1.399	16.806	-0.136
11	S175 Hull + Very Shallow	6.89	2.67	0.572	2.59	0.400	1.1	CFD	0.027	-0.006	0.028
								Emp.	0.025	-0.007	0.026
								Diff %	-6.630	13.918	-6.036
12	DTC Hull + High Speed	6.96	3.52	0.661	3.66	0.547	1.3	CFD	0.056	0.050	0.068
								Emp.	0.053	0.049	0.065
								Diff %	-5.418	-2.741	-4.957
13	DTC Hull + High Speed	6.96	3.52	0.661	3.66	0.683	1.3	CFD	0.114	0.109	0.139
								Emp.	0.111	0.117	0.138
								Diff %	-2.075	7.437	-0.338
14	DTC + Very Shallow	6.96	3.52	0.661	3.66	0.400	1.1	CFD	0.029	0.008	0.030
								Emp.	0.025	0.003	0.026
								Diff %	-12.217	-62.368	-15.233
15	Near Grounding	7.14	3.22	0.648	3.49	0.705	1.2	CFD	0.133	0.085	0.151
								Emp.	0.124	0.095	0.145
								Diff %	-6.689	12.873	-4.297

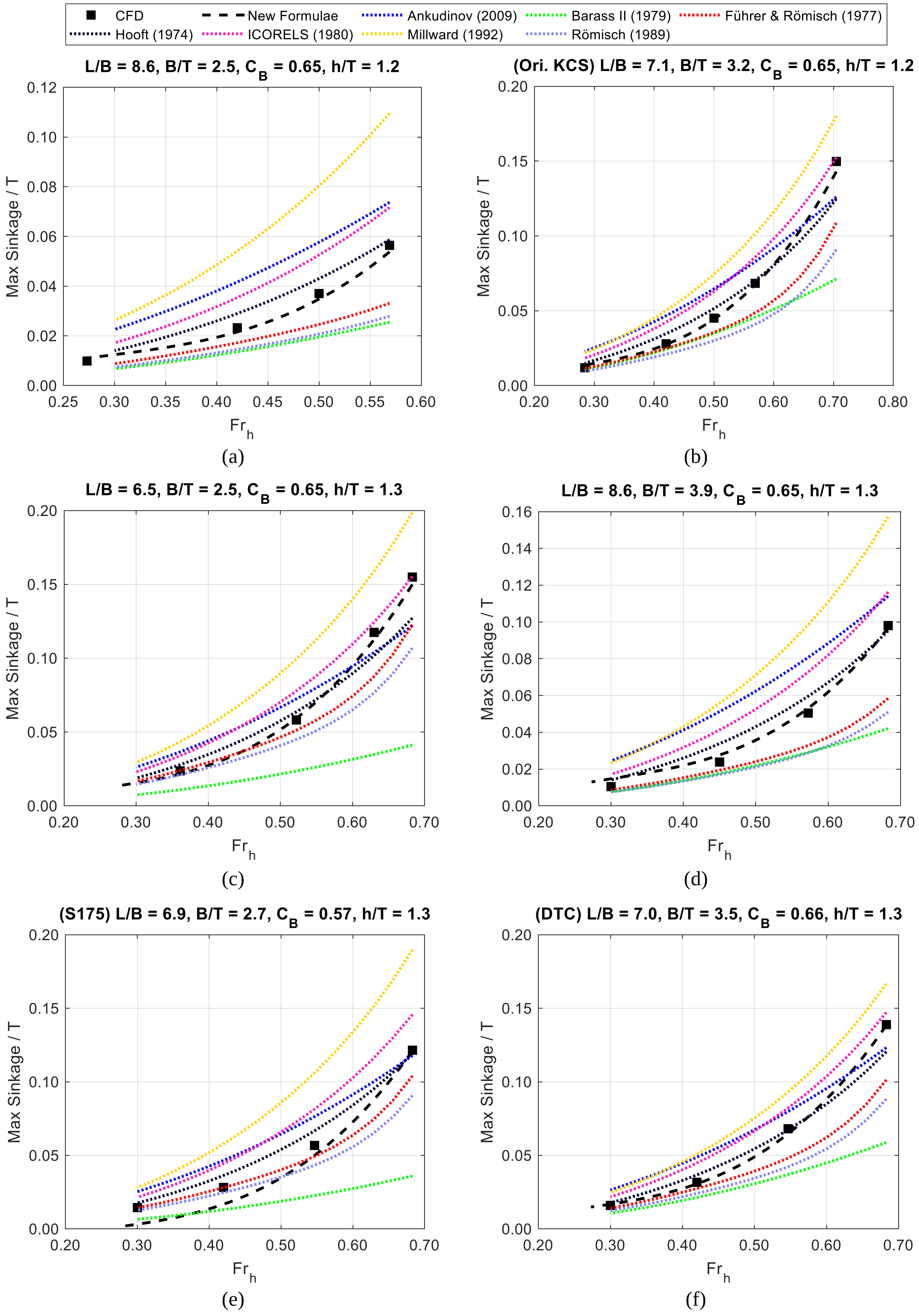

Figure 61: Comparison of the new empirical formulae predictions against CFD and existing empirical formulae for various laterally unrestricted cases. Cases (a) to (d) are used in the regression but cases (e) and (f) are not.

6.4.2 Evaluation for Laterally Restricted Cases

Predictions from the empirical formulae with correction factor for lateral restriction effects are compared against the original CFD or EFD results for a variety of cases that were not used for the derivation of the correction factor or the laterally unrestricted formulae. Some of these cases investigated include the use of the S175 and DTC hulls, lateral restrictions beyond the initially tested limits as well as fully confined shallow waterway configurations tested in a Towing Tank (confined cases were not included in the development of the correction factors). These cases are investigated to assess the versatility of the method and to assess the accuracy of the method on independent cases.

The results of the comparison are summarised in Table 33. Despite that most of the cases compared are at relatively high Fr_h and shallow h/T, strong correlations are still seen between the corrected predictions and original results. Most midship sinkage predictions are well within 10% difference to the original results (equivalent to difference of less than 1% of T) while trim predictions tend to be underestimated but are still reasonably similar. The resulting maximum sinkage predictions are also mostly within 10% difference to the original results.

Case no. 24 shows that good correlations can still be achieved for an entirely new hull form not used in the formulae derivation (S175) and more importantly the bank height for this case is significantly higher than those used for the formulae derivation. This signifies that the formulae could still be valid for conditions that are outside but near the range of applicability. Poor correlations only begin to manifest when the lateral restriction parameters are set to more extreme conditions such as in case no. 25. In case no. 25, a narrow canal is used and the resulting normalised m_{eq} is the largest tested in the study. This condition is well beyond the range of applicability. Consequently, the new empirical formulae overpredicts the maximum sinkage. This overprediction is likely due to non-linearities in the highly confined condition which the correction factors do not account for. However, when the lateral restrictions are less extreme such as in case no. 26 and 27 based on the DTC hull, more reasonable correlations are observable again. Nonetheless, it should be noted that the restrictions in case no. 26 and 27 are also still outside the range of applicability.

Table 33: Comparison of the empirical predictions against CFD/EFD results for various laterally restricted cases that were not used in the derivation of the laterally unrestricted formulae and the lateral restriction correction factor. Lateral restriction with orange values signifies it is beyond the limits of applicability by ±15% while red values are well beyond the limits of applicability (> ±15%).

Test No.	**Test Descript.**	***L/B***	***B/T***	C_B	L_{BF}	Fr_h	***h/T***	***Lateral Restrictions***			**Results**	**Sinkage/*T***	**Trim (° by bow)**	**Max Sinkage/*T***
								W/B	h_m/T	$m_{eq\text{-}norm}$				
16	High Speed + V. Shallow	7.14	3.22	0.648	3.49	0.520	1.1	5.00	0.40	1.239	CFD	0.066	-0.026	0.071
											Emp.	0.066	-0.002	0.067
											Diff %	-0.46	-90.69	-6.39
17	High Speed + V. Shallow	7.14	3.22	0.648	3.49	0.520	1.1	5.00	0.20	1.107	CFD	0.059	-0.021	0.063
											Emp.	0.056	-0.006	0.057
											Diff %	-4.73	-70.04	-8.69
18	Diff Hull + High Speed	6.46	2.50	0.648	3.49	0.500	1.2	5.26	0.33	1.157	CFD	0.054	0.050	0.062
											Emp.	0.056	0.049	0.064
											Diff %	3.54	-3.31	-2.69
19	Diff Hull + High Speed	6.49	3.90	0.648	3.49	0.500	1.2	4.55	0.44	1.266	CFD	0.060	0.011	0.063
											Emp.	0.063	0.014	0.066
											Diff %	4.13	-27.04	5.07
20	Diff Hull + High Speed	8.64	3.90	0.648	3.49	0.500	1.2	5.00	0.48	1.269	CFD	0.050	-0.010	0.053
											Emp.	0.049	0.017	0.054
											Diff %	-2.97	-280.436	-2.82
21	Diff Hull + High Speed + V. Shallow	6.46	2.50	0.648	3.49	0.500	1.1	5.26	0.33	1.174	CFD	0.058	-0.017	0.060
											Emp.	0.061	0.019	0.064
											Diff %	4.65	-213.81	5.78
22	Diff Hull + High Speed + V. Shallow	6.49	3.90	0.648	3.49	0.500	1.1	4.55	0.44	1.298	CFD	0.065	-0.051	0.075
											Emp.	0.069	-0.017	0.073
											Diff %	6.62	-67.30	-3.47

23	Diff Hull + High Speed + V. Shallow	8.64	3.90	0.648	3.49	0.500	1.1	5.00	0.48	1.302	CFD	0.054	-0.023	0.060
											Emp.	0.055	-0.002	0.056
											Diff %	2.63	-91.92	-7.25
24	S175 + High Speed	6.89	2.67	0.572	2.59	0.520	1.2	5.26	0.70	1.418	CFD	0.071	-0.001	0.071
											Emp.	0.076	0.003	0.077
											Diff %	7.16	-394.01	7.75
25	Canal + S175	6.89	2.67	0.572	2.59	0.400	1.2	4.00	Confined	2.621	EFD	0.067	-0.007	0.068
											Emp.	0.076	0.066	0.088
											Diff %	13.35	-1096.66	28.72
26	DTC + High Speed	6.96	3.52	0.661	3.66	0.520	1.2	6.00	0.69	1.3489	CFD	0.076	0.052	0.088
											Emp.	0.071	0.034	0.079
											Diff %	-6.46	-34.30	-10.92
27	Canal + DTC	6.96	3.52	0.661	3.66	0.400	1.3	7.69	Confined	2.032	CFD	0.039	0.021	0.044
											Emp.	0.034	0.024	0.039
											Diff %	-14.65	-18.40	-10.92

Overall, based on the investigated cases, the developed formulae with correction factor for lateral restrictions perform well for unique cases that are within the limits of applicability. Good correlation is also observed for some cases that are outside but near the limits of applicability by ±15% but for cases that are well outside the limits of applicability (> ±15%) especially highly confined cases, significant errors are observed. It is suggested that future work be conducted to examine more restricted cases to identify the point where non-linearities begin to manifest. This will help better understand the changes in squat in highly restricted conditions so that more accurate predictions in such conditions are possible. Regardless, the current correction factor and the method of quantification are adequate to output reliable predictions in the linear conditions.

Figure 62 compares squat predictions from the new formulae against that of the existing empirical methods for laterally restricted cases. All the cases here are not used in the derivation of the formulae and correction factors. The results show that existing methods tend to yield a large spread in predictions where the method of Barrass II (1979) and that of Millward (1992) tend to yield the largest predictions while the method of Führer and Römisch (1977) tends to yield the lowest predictions. In fact, certain methods are inapplicable (omitted) for some of these cases such as in the highly restricted case of Figure 62(b) where the method of Barrass II (1979) is not applicable.

When examining cases with gradually varying bank width (Figure 62(d)), most methods can be seen to predict similar trends where the sinkage increases when bank width decreases albeit at varying magnitudes. The method of Hooft (1974), ICORELS (1980) and Millward (1992) do not predict changes in sinkage with respect to bank width as these methods do not consider lateral restriction effects but the method of Führer and Römisch (1977) appears to predict a step change in sinkage due to the nature of the formulae. As for the case where bank height is manipulated (Figure 62(e)), the methods of Ankudinov (2009) and Römisch (1989) are the only existing methods which predicted increasing sinkage when bank height increases. The method of Huuska has no explicit limits of applicability and can be seen to yield unusual trends when bank height is varied. The methods of Ankudinov (2009) and ICORELS (1980) are the existing methods which produce the most reasonable predictions throughout.

Overall predictions from the new formulae are the most consistent. It should be noted that the cases in Figure 62(c) and (d) have bank heights which are significantly higher than that used for the formulae derivation yet reasonable correlations are still achieved. More importantly, the comparison in Figure 62(e) and (f) clearly demonstrates the superiority of the new formulae over existing methods in predicting the maximum squat with respect to changes in bank width and bank height respectively. The predictions from the new formulae are regarded as promising and satisfies the research objectives in developing a more accurate and robust, rapid squat prediction method for container ships. Nonetheless, expanding the current range of applicability and further investigation into the non-linearities arising from large blockage conditions are recommended in future work.

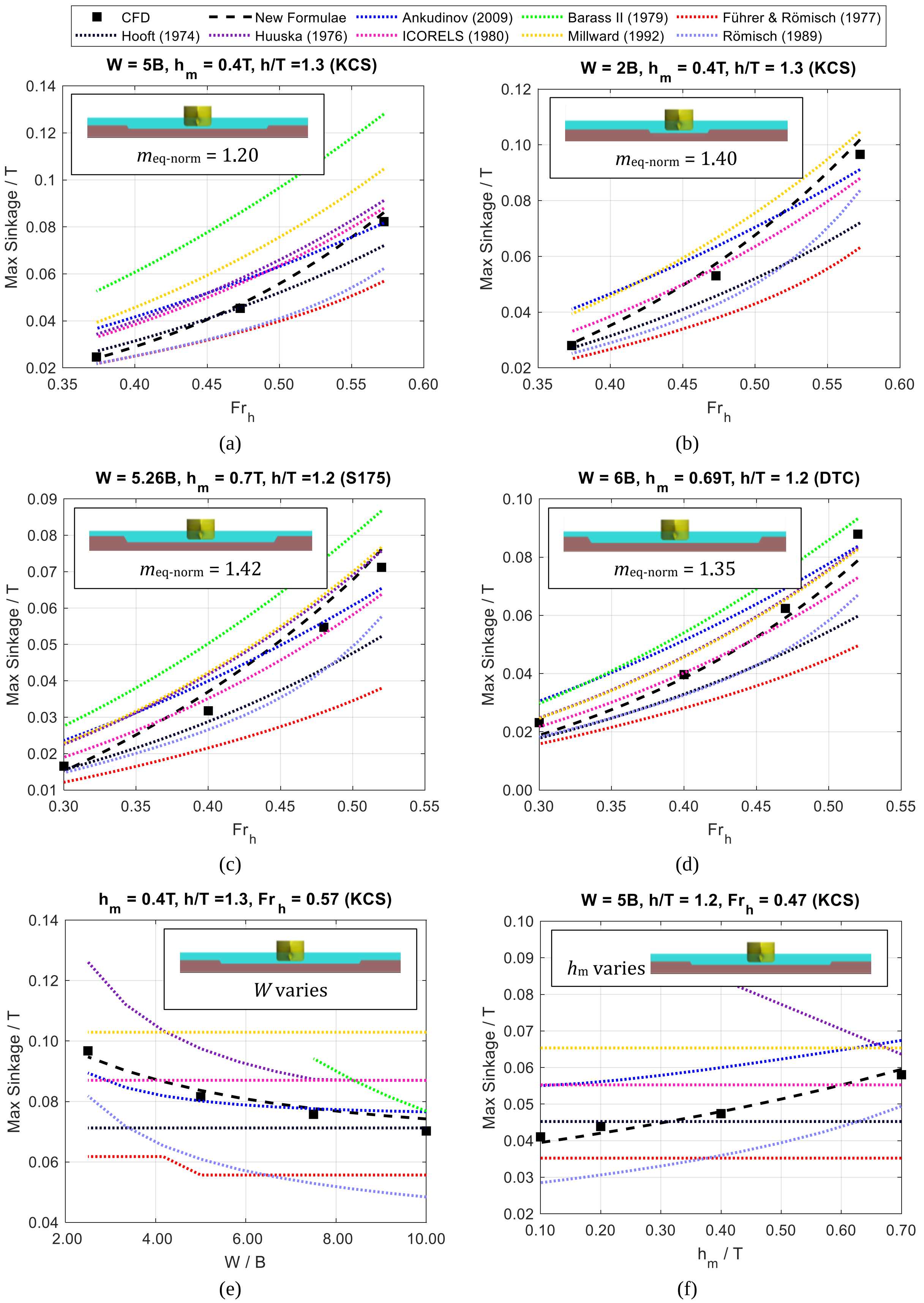

Figure 62: Comparison of the new empirical formulae predictions against CFD and existing empirical formulae for various laterally restricted cases. All cases shown are not used in the derivation of the correction factor.

6.4.3 Evaluation for Full Scale Trials

The performance of the new formulae in predicting full scale squat is also examined and compared against full scale trials data. It should be well noted that reliable full scale data is scarce due to the complexity and challenges present in an uncontrolled environment such as fluctuating current speed, drift angle due to heading changes, varying wind speed and direction, varying tide, varying bathymetry and seabed conditions. However, full scale measurements of reasonable quality for two cases are available to be investigated and every effort where possible has been undertaken to ensure accurate analysis for these cases. These full scale measurements are provided by OMC International and were obtained using three global navigation satellite system (GNSS) receivers; one on the starboard bridge wing, one on the port bridge wing and another by the bow. Tide gauge data along the transits, current logs with heading angle and depth soundings are also available and accounted for in the analysis. For confidentiality purposes, only partial details of the container ships are disclosed in Table 34.

Table 34: Principal particulars of the container ships in the full scale trials.

Ship	**Case FS1**	**Case FS2**
L/B	6.65	7.86
B/T	5.07	3.64
L/T	33.72	28.58
C_B	0.561	0.594

Predictions using the new formulae (direct extrapolation of model scale results without correction for scale effect) in comparison to the measurements for both cases are illustrated in Figure 63 and Figure 64. For Case FS1 (Figure 63), good correlation is observed between the predicted and measured AP and FP sinkages. The predictions of the new formulae can be seen to reproduce a similar trend to the measured squat when ship speed increases and when the water depth changes accordingly. Reasonable correlation is also observed for Case FS2 (Figure 64). The predictions of the formulae generally follow the trend of the measured sinkage as speed and water depth varies. There are some noticeable discrepancies observed between chainage of 85 – 90 km and 112 – 114 km. The discrepancy noted along chainage of 85 – 90 km could be considered to be anomalies since the water depth is relatively constant while there is a dip in speed within these points which theoretically should result in a reduction in sinkage as predicted by the new formulae but this is shown otherwise by the actual measurements. This may be due to issues which were not/could not be accounted for such as unsteady accelerations, dynamic effects or significant changes in the vicinity of the seabed that is not within the detectable range. However, the spike in squat predicted by the new formulae for chainage of 112 – 114 km, which does not correlate with the opposing trend of the actual measurements is very likely due to the dynamic effects caused by abrupt changes in the water depth. Investigations into the unsteady squat behaviour due to abrupt changes in water depth has been highlighted in the work of Duffy (2008) where it is noted that ships can “detect” abrupt changes ahead and cause instantaneous changes to the squat before the ship reaches the point of abrupt change in water depth. Therefore, it is very plausible that the dip in actual squat measured along this chainage is due to the abrupt reduction in water depth. Overall, the predictions throughout the transit are still reasonably accurate based on the available information. Therefore, the use of the new formulae for full scale predictions has been demonstrated to be viable with sufficiently accurate input for the limited cases assessed. The above findings also highlight the need in future work to include dynamic effects resulting from abrupt changes in water depth for better fidelity in real-time predictions and to compare the predictions against full scale trials for a wider range of vessels and channel cases.

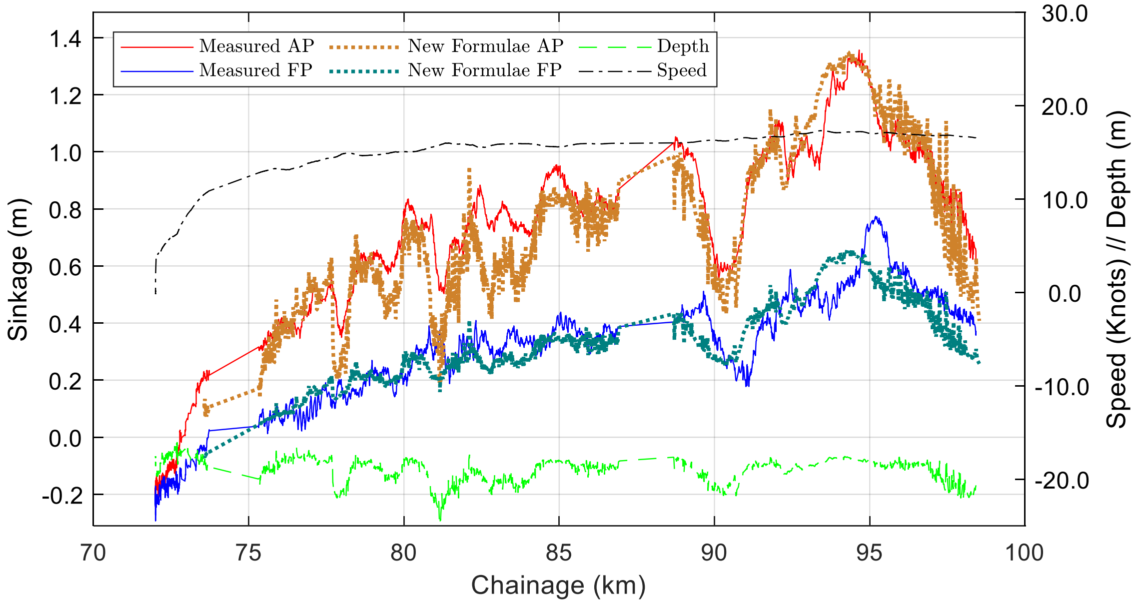

Figure 63: Comparison of Full scale squat predictions from the new formulae and actual measurements for Case FS1.

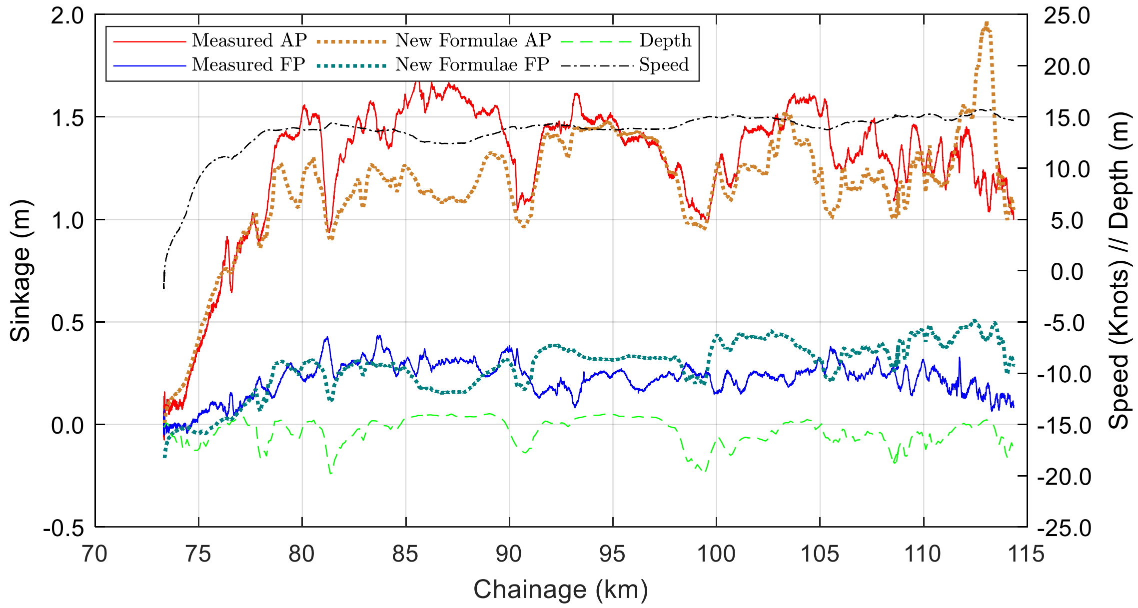

Figure 64: Full scale squat predictions from the new formulae in comparison to actual measurements for Case FS2.

6.5 Concluding Remarks

Further systematic computations have been conducted to extend the available squat data. A multiple linear regression method has been employed to derive a new set of empirical formulae. A correction factor for trim is also developed that accounts for the relative positions of the LCB and LCF. The performance of this set of formulae is then verified against the original data used to derive it. Strong correlations are observed between the formulae predictions and original data points for the cases tested.

Next, systematic computations are conducted to investigate and quantify the effect of lateral restrictions on squat. This is to derive a correction factor to account for the effect of lateral restrictions. Firstly, in order to quantify the degree of restriction accurately, the concept of "equivalent blockage" ratio, m_{eq}, introduced by Lataire and Vantorre (2008) is adapted to the current study and subsequently the normalised equivalent blockage ratio, $m_{eq\text{-}norm}$, is proposed to enable better comparison between different cases. Base on the cases investigated, it is shown that the midship sinkage increases linearly with normalised blockage ratio. Most importantly, the magnitude of sinkage is similar for cases with similar $m_{eq\text{-}norm}$ regardless of whether one case has wider bank widths or higher bank height than the other. Furthermore, the gradient of the linear trend is found to vary with speed and water depth but remains similar for different hull variations. Thus, a correction factor for midship sinkage is derived based on the quantified observations. On the contrary, the rate of change in trim in laterally restricted conditions is only found to be significantly affected by hull parameters *L/B* and *B/T* for the current range investigated. Hence, a correction factor for trim is derived with respect to the hull parameters.

Initial trim effect on squat is also briefly examined by using the sister hulls of the KCS which exhibit unique trim behaviours (one which trims by the stern when underway and another by the bow when underway). Changes in midship sinkage with respect to initial trim is noted where a more stern down initial trim would result in lower midship sinkage when underway. The rate of change of midship sinkage with respect to initial trim has been observed to vary with the hull volume distribution. The rate of net change in trim also varies with the hull volume distribution. Regardless, all these variations in midship sinkage and trim are practically insignificant. Approximated results where the change in midship sinkage and running trim at even keel are assumed to be similar to other initial trim conditions have been shown to yield practically similar results to CFD predictions which account for initial trim. Consequently, initial trim effect can be considered negligible for the cases tested and no correction factor is necessary for the new formulae.

The performance of the consolidated new formulae is then assessed based on new cases that are not used in the derivation of the formulae. For new laterally unrestricted cases, the comparisons show good correlation for most cases even those at high speeds ($Fr_h > 0.5$) and discrepancies that are noted are all reasonable. Similarly, for laterally restricted cases, good correlations are observed for most cases while reasonable correlations are still achievable when predicting cases with restrictions that are beyond those used in the formulae derivation (extrapolation). The new formulae overpredicts maximum squat when used for an extremely confined case well beyond the limits used in the derivation. When comparing the performance of the new formulae alongside existing methods, it can be seen that the new formulae correlates best with CFD results for all these cases while large spreads in predictions are observed for existing methods. The superiority of the new formulae over existing methods in predicting maximum sinkage with respect to bank width and bank height changes is clearly demonstrated. Therefore, the new formulae can be considered a successful improvement over existing methods for the cases tested. However, more work to widen the range of applicability particularly cases with higher blockage where non-linearities are present is suggested. Sample demonstration of the new formulae in predicting full scale cases are also undertaken which show reasonably promising correlations with the full scale measurements. Nonetheless, it is noted that future work should consider the dynamic effects arising from abrupt changes in water depth and to compare the predictions against full scale trials for a wider range of vessels and channel cases.

Chapter 7 – Conclusions and Future Work Recommendations

7.1 Conclusions

A series of investigations has been undertaken on the squat of modern container ship primarily using CFD simulations with supplementary model testing and full scale measurements. The gaps in literature which this study seeks to address are: developing a CFD model for squat prediction at relatively high speeds ($Fr_h > 0.5$) which includes self-propulsion effect, quantifying the scale effect in container ship squat, quantifying the effect of hull principal particulars on squat, improved quantification of lateral restriction effects, consideration of initial trim effects, and developing an improved rapid prediction technique in the form of empirical equations.

The first phase of the research explored various CFD modelling techniques which were benchmarked against model test data. Initially, a fully-discretised propeller model was simulated and validated against model test data. This validated propeller model and the body force propulsion virtual disc were then implemented in the many unique set-ups for squat simulation. Quasi-static and dynamic overset mesh set-ups were examined in the squat simulations. The results demonstrated that the effect of self-propulsion in squat is significant and the body force propulsion virtual disc was sufficiently accurate to capture the change in squat. It was also shown that the quasi-static set-up was viable for squat simulations. Experimental work was then conducted in the AMC to provide further benchmarking data. However, it was shown that the quasi-static method with virtual disc propeller approach was no longer accurate at higher speeds. The morphing mesh method with virtual disc propeller model was then introduced and found to correlate well with the new experimental results, even at high speeds. A third benchmarking study was conducted based on other published squat data and it was shown that the morphing mesh method performed well. Hence, the morphing mesh method is the preferred method for the present study. In addition, comparisons of squat predictions from various existing empirical methods were conducted. It was demonstrated that there were large deviations in predictions among the existing methods and these predictions were inconsistent with the benchmark data whereas the CFD methods tend to correlate better overall.

The next phase of the study investigated the influence of scale effect in squat. This required the modelling of a reliable full scale CFD set-up. However, there was no acceptable full scale experimental squat data for conventional validation purposes. Therefore, the credibility of the full scale CFD model was instead assessed against extrapolated deep water resistance data and empirically-derived confined water resistance data. Good correlations were seen between the full scale CFD predictions with benchmark/estimated resistance data for both deep water and confined water conditions. The predicted squat for both model scale and full scale conditions in confined water were then compared and found to exhibit differences that are within the numerical uncertainty limits. The wave elevation and pressure distribution on model scale and full scale hulls were also comparable. These observations led to the proposal that squat is highly dependent on the wave elevation around the hull for the cases tested. Since the wave elevation is governed by Froude scaling and the Froude scaling is conserved between model scale and full scale, there is minimal scale effect on squat for the cases investigated. Another set of simulations conducted at higher speeds ($Fr_h > 0.5$) also shows differences between model scale and full scale squat predictions are within the numerical uncertainty limits. It is acknowledged that the current findings contradict with some past literature. Nonetheless, a recent study by Shevchuk et al. (2019) revealed that the magnitude of scale effect is dependent on water depth, speed, hull surface roughness and different container ship hulls. The scale effect in their study varied anywhere from 5% to 15%. They also pointed out that no consistent trend could be identified from their results and concluded that the practicality of developing a correction factor for scale effect is questionable. Further investigations were undertaken in the current study where full scale squat cases were replicated in model scale CFD simulations. The extrapolated squat predictions from model scale simulations were found to match the full scale squat cases with reasonable accuracy. It was summarised that the development of a correction factor for scale effect in squat is not worthwhile for the given circumstances. However, a conservative safety factor of 1.15 is suggested should it be preferred.

The third phase of the research delved into quantifying the effect of parametric hull variations on squat. Results show that sinkage and trim are inversely related to length-to-beam ratio (L/B) while sinkage is independent of beam-to-draught ratio (B/T), but trim is inversely related to B/T. It was also identified that the block coefficient (C_B) may not be the most relevant or reliable parameter to consider for hull form influence on midship sinkage and trim respectively. Instead, the distance of the LCB relative to the LCF (termed as L_{BF}) should be considered. Trim magnitude was noted to become increasingly stern down when L_{BF} decreases and hence, it determines the direction of trim in this study. The L_{BF} is a sensitive variable where larger values result in trim by the bow whereas lower values result in trim by the stern. The quantified observation regarding L_{BF} in this study was also found to correlate with observations on past studies (Gourlay et al. 2015) and general observations that bulk carriers, which most likely have larger L_{BF}, tend to trim by the bow.

For the final phase of the research, additional CFD cases were conducted for the above study at varying water depths and speeds. A set of empirical formulae for sinkage and trim was derived using multiple linear regression analysis on the collected CFD data. The predictions from the new formulae have been shown to have excellent correlation with the original data used to derive it. The effect of lateral restriction was then investigated based on the concept of equivalent blockage (Lataire and Vantorre, 2008) to develop a correction factor for lateral restriction effects. The effect of initial trim on squat was also investigated for consideration as a correction factor but it was found to be negligible for the cases investigated. The final form of the formulae was demonstrated to be able to provide accurate predictions for various new cases that were neither used in the development of the regression formulae nor correction factors but are within the recommended range. The new formulae also tends to be more accurate than existing empirical methods for the cases investigated. When applied to actual full scale squat measurements, reasonable correlations are also observed. However, the need to account for unsteady dynamic effects due to uneven channel bottom was highlighted. Nonetheless, the new empirical prediction technique developed in this study is feasible for rapid assessment of modern container ship squat within the limits of applicability.

The objectives outline in this research has been achieved;

- A validated CFD model for container ship squat prediction at relatively high speeds ($Fr_h > 0.5$) which accounts for self-propulsion effects has been developed.
- Scale effect in squat has been investigated based on validated full scale simulations in comparison to validated model scale simulations where the difference is found to be within the uncertainties.
- The effect of hull principal particulars on squat has been examined where the effect of L/B and B/T on midship sinkage and trim is quantified. The change in trim direction has also been identified to be influenced by L_{BF}.
- A new set of empirical formulae has been developed and proven to improve prediction accuracies over existing methods. This provides a new tool to perform rapid assessment of container ship squat that is well suited to time domain mathematical models.

7.2 Future Work Recommendations

Based on the findings of the current study, the following future work is recommended:

- The current range of applicability is based on statistics of existing container ships operating in an Australian port where carrying capacities are below 10,000 TEU. More recent and/or upcoming designs may have parametric ratios that are far beyond the current range investigated and hence, cannot be predicted accurately using the current set of formulae. Extending the range of applicability in general can be useful by repeating the study for a wider range of new hull forms. In conjunction to this, it may also be worthwhile to investigate the effect of varying draft (or displacement) on squat for the same container ships since it is common for container ships to operate at various different loading conditions.
- The current dataset used to study the trim direction of container ships is considered small. Although the quantified findings from this small dataset correlate well with observations made in other published work and the subsequently derived correction factor also yields satisfactory predictions, it is still recommended to repeat the study for trim direction base on a different set

of parametrically transformed hull forms. This repeat study will provide further validation to the findings as well as data points for a more averaged quantification for the correction factor.

- A recent study by Shevchuk et al. (2019) demonstrated that the scale effect varies with ship speed, water depth, hull surface roughness and different container ship hulls. They also noted that a consistent trend for scale effect could not be identified from one container ship hull to another. A more comprehensive study using many more container ship models may need to be undertaken to gain further understanding about the variability of scale effect among different container ships.
- It is recommended to adopt the equivalent blockage concept (m_{eq} and $m_{eq\text{-}norm}$) to investigate and quantify the effect of asymmetrical banks or conditions where the ship is off-centre in the waterway since the current lateral restriction effect investigation is focused on symmetrical conditions only.
- Extending the lateral restriction effect studies by studying the squat in waterways which are much more restricted ($m_{eq\text{-}norm} > 1.4$) is important. This will help identify the point where non-linearities begin to manifest as well as help understand its behaviour so that better predictions are possible in such conditions. Systematic investigations on confined water conditions can also be insightful as the current cases conducted for the derivation of lateral restriction effect correction do not entail confined water conditions (i.e. canals, surface-piercing banks). Hydraulic effects are more prevalent in confined conditions and should be investigated.
- Unsteady squat due to abrupt changes in water depth should be investigated in detail. This will help provide more realistic real-time squat predictions in practice. In conjunction to this, it would be favourable to compare the predictions of the new formulae against full scale trials for a wider range of vessels and channel cases.
- The effect of manoeuvres in shallow water on sinkage and trim should be examined. Most of the manoeuvres that are executed by a ship are when approaching or departing a port. However, manoeuvring trials are often conducted in deep sea which does not reflect the actual performance in shallow water and the change in sinkage and trim is not known. There is a need to quantify the change in sinkage and trim during manoeuvres in shallow water to avoid grounding.
- An investigation into the effect of static heeling moment (due to wind or turning) on sinkage and trim when underway in shallow water could be worthwhile. When a ship is heeled to one side, the pressure distribution on the hull becomes transversely asymmetric. It would be useful to understand whether the transversely asymmetric pressure distribution will impact the overall sinkage and trim significantly.

References

Alderf, N., Lefrançois, E., Sergent, P. & Debaillon, P. 2011, "Dynamic Ship Response Integration for Numerical Prediction of Squat in Highly Restricted Waterways", *International Journal for Numerical Methods in Fluids*, 65(7): 743-763.

Balanin, V. & Bykov, L. 1965, "Selection of Leading Dimensions of Navigation Canal Sections and Modern Methods of Bank Protection", *Proceedings of the 21st International Navigation Congress*, Permanent International Association of Navigation Congresses (PIANC), Stockholm, Sweden.

Barnitsas, M.M., Ray, D, & Kinley, P. 1981, "KT, KQ and Efficiency Curves for the Wageningen B-Series Propellers", University of Michigan.

Barrass, C. 1979, "The Phenomena of Ship Squat", *International Shipbuilding Progress*, 26(294).

Bechthold, J. & Kastens, M. 2020, "Robustness and Quality of Squat Predictions in Extreme Shallow Water Conditions based on RANS-Calculations", *Ocean Engineering*, 197: 106780.

Blaauw, H. & Knaap, F. 1983, "Prediction of Squat of Ships Sailing in Restricted Water", *Proceedings of the 8th International Harbour Congress*, Antwerp, Belgium.

Bouwmeester, J. 1977, "Calculation of Return Flow and Water Level Depression; New Method", *Proceedings of the 24th International Navigation Congress*, Permanent International Association of Navigation Congresses (PIANC), Leningrad, USSR, 148-151.

Briggs, M.J. 2006, "Ship Squat Predictions for Ship/Tow Simulator", *Engineer Research and Development Center Vicksburg MS Coastal and Hydraulics Lab*.

Briggs, M.J. 2009, "Ankudinov Ship Squat Predictions-Part 1: Theory, Parameters, and FORTRAN Programs", *Engineer Research and Development Center Vicksburg MS Coastal and Hydraulics Lab*.

Castro, A.M., Carrica, P.M. & Stern, F. 2011, "Full Scale Self-Propulsion Computations using Discretized Propeller for the KRISO Container Ship KCS", *Computers & Fluids*, 51(1): 35-47.

Collinson, R. 1994, "A Review of Methods of Predicting the Squat of a Ship in Shallow Water", Masters Thesis, University of Liverpool.

Cong, L. & Hsiung, C. 1991, "Computing Wave Resistance, Wave Profile, Sinkage And Trim Of Transom Stern Ships", *Proceedings of the Third International Conference on Computer Aided Design, Maunfacture and Operation in the Marine and Offshore Industries (CADMO 91)*, Key Biscayne, US, pp. 99–112.

Constantine, T. 1960, "On the Movement of Ships in Restricted Waterways", *Journal of Fluid Mechanics*, 9(2): 247-256.

Dand, I. & Ferguson, A. 1973, "The Squat of Full Ships in Shallow Water", *National Physical Lab Teddington (England) Ship Div*.

Dawson, C. 1977, "A Practical Computer Method for Solving Ship-Wave Problems", *Proceedings of the 2nd International Conference on Numerical Ship Hydrodynamics*, Berkeley, US, pp. 30-38.

Delefortrie, G., Vantorre, M., Eloot, K., Verwilligen, J. & Lataire, E. 2010, "Squat Prediction in Muddy Navigation Areas", *Ocean Engineering*, 37(16): 1464-1476. doi:https://doi.org/10.1016/j.oceaneng.2010.08.003.

Deng, G., Guilmineau, E., Leroyer, A., Queutey, P., Visonneau, M. & Wackers, J. 2014, "Simulation of Container Ship in Shallow Water at Model Scale and Full Scale", *Proceedings of the 3rd National CFD Workshop for Ship and Offshore Engineering*, China.

Duffy, J. 2008, "Modelling of Ship-Bank Interaction and Ship Squat for Ship-Handling Simulation", PhD Thesis, University of Tasmania.

Duffy, J. & Renilson, M. 2000, "An Investigation into the Effect of Propulsion on Ship Squat", *Oceanic Engineering International*, 4(1): 1-12.

El Moctar, O., Shigunov, V. & Zorn, T. 2012, "Duisburg Test Case: Post-Panamax Container Ship for Benchmarking", *Ship Technology Research*, 59(3): 50-64.

Eloot, K., Verwilligen, J. & Vantorre, M. 2008, "An Overview of Squat Measurements for Container Ships in Restricted Water", *Proceedings of the International Conference on Safety and Operations in Canals and Waterways SOCW 2008*, Glasgow, UK, pp. 106-116.

Elsherbiny, K., Terziev, M., Tezdogan, T., Incecik, A. & Kotb, M. 2020, "Numerical and Experimental Study on Hydrodynamic Performance of Ships Advancing through Different Canals", *Ocean Engineering*, 195: 106696.

Eryuzlu, N., Cao, Y., & D'agnolo, F. 1994, "Underkeel Requirements for Large Vessels in Shallow Waterways", *Proceedings of the 28th International Congress*, Permanent International Association of Navigation Congresses (PIANC), Seville, Spain, S2-2, pp. 17-25.

Eryuzlu, N. & Hausser, R. 1978, "Experimental Investigation into Some Aspects of Large Vessel Navigation in Restricted Waterways", *Proceedings of the Symposium of Aspects of Navigability*, Delft, Netherlands, vol. 2, pp. 1-15.

Führer, M. & Römisch, K. 1977, "Effects of Modern Ship Traffic on Inland and Ocean Waterways and their Structures", *Proceedings of the 24th International Congress*, Permanent International Association of Navigation Congresses (PIANC), Leningrad, USSR, S1-3, pp. 79-93.

Garrison, C. 1978, "Hydrodynamic Loading of Large Offshore Structures: Three-dimensional Source Distribution Methods", *Numerical Methods in Offshore Engineering*, pp. 87-111.

Gates, E.T. & Herbich, J.B. 1977, "The Squat Phenomenon and Related Effects of Channel Geometry", *Proceedings of the 25th Annual Hydraulics Specialty Conference*, Texas, US, pp. 236-244.

Gilligan, L. 2015. "Investigation into Scale Effects when Extrapolating Model Scale Ship Squat Measurements", Undergraduate Thesis, University of Tasmania.

Gourlay, T. 2008a, "Sinkage and Trim of a Fast Displacement Catamaran in Shallow Water", *Journal of Ship Research*, 52(3): 175-183.

Gourlay, T. 2008b, "Slender-body Methods for Predicting Ship Squat", *Ocean Engineering*, 35(2): 191-200.

Gourlay, T., Ha, J.H., Mucha, P. & Uliczka, K. 2015, "Sinkage and Trim of Modern Container Ships in Shallow Water", *Australasian Coasts & Ports Conference 2015: 22nd Australasian Coastal and*

Ocean Engineering Conference and the 15th Australasian Port and Harbour Conference, Auckland, New Zealand.

Gourlay, T., Lataire, E. & Delefortrie, G. 2016, "Application of Potential Flow Methods to Ship Squat in Different Canal Widths", *Proceedings of the 4th International Conference on Ship Manoeuvring in Shallow and Confined Water (MASHCON 2016),* Hamburg, Germany, pp. 146-155.

Gourlay, T.P. 2011, "A Brief History of Mathematical Ship-Squat Prediction, Focussing on the Contributions of E.O. Tuck", *Journal of Engineering Mathematics,* 70(1-3): 5-16.

Gronarz, A., Broß, H., Müller-Sampaio, C., Jiang, T. & Thill, C. 2009, "SIMUBIN - Modellierung und Simulation der realitätsnahen Schiffsbewegungen auf Binnenwasserstraßen", *Report 1939 B*, Development Centre for Ship Technology and Transport Systems (DST).

Ha, J.H. & Gourlay, T. 2017, "Validation of Container Ship Squat Modeling using Full-Scale Trials at the Port of Fremantle", *Journal of Waterway, Port, Coastal, and Ocean Engineering,* 144(1): 04017037.

Han, S., Lee, Y.S. & Choi, Y.B. 2012, "Hydrodynamic Hull Form Optimization using Parametric Models", *Journal of Marine Science and Technology,* 17(1): 1-17.

Harting A. & Reinking, J. 2002, "SHIPS: A New Method for Efficient Full-Scale Ship Squat Determination", *Proceedings of the 30th International Congress*, Permanent International Association of Navigation Congresses (PIANC), Sydney, Australia, pp. 84-91.

Havelock, T.H. 1908, "The Propagation of Groups of Waves in Dispersive Media, with Application to Waves on Water Produced by a Travelling Disturbance", *Proceedings of the Royal Society of London. Series A,* 81(549): 398-430.

Hooft, J. 1974, "The Behaviour of a Ship in Head Waves at Restricted Water Depths", *International Shipbuilding Progress*, 21(244): 367-390.

Huuska, O. 1976, "On the Evaluation of Underkeel Clearances in Finnish Waterways", *Ship Hydrodynamics Laboratory Report No. 9*, Helsinki University of Technology.

ITTC. 2014, "ITTC Recommended Procedures and Guidelines - Open Water Test", *International Towing Tank Conference,* (7.5-02-03-02.1): 1-11.

Jachowski, J. 2008, "Assessment of Ship Squat in Shallow Water using CFD", *Archives of Civil and Mechanical Engineering,* 8(1): 27-36.

Jiang, T. 1998, "Investigation of Waves Generated by Ships in Shallow Water", *Proceedings of the 22nd Symposium on Naval Hydrodynamics*, Washington DC, US, pp. 601-612.

Jin, Y., Duffy, J., Chai, S. & Magee, A.R. 2019, "DTMB 5415M Dynamic Manoeuvres with URANS Computation using Body-Force and Discretised Propeller Models", *Ocean Engineering*, 182: 305-317.

Jones, W. & Launder, B.E. 1972, "The Prediction of Laminarization with a Two-Equation Model of Turbulence", *International Journal of Heat and Mass Transfer,* 15(2): 301-314.

Kaidi, S., Lefrançois, E. & Smaoui, H. 2020, "Numerical Modelling of the Muddy Layer Effect on Ship's Resistance and Squat", *Ocean Engineering*, 199: 106939. doi:https://doi.org/10.1016/j.oceaneng.2020.106939.

Kawamura, T., Ouchi, K. & Nojiri, T. 2012, "Model and Full Scale CFD Analysis of Propeller Boss Cap Fins (PBCF)", *Journal of Marine Science and Technology*, 17(4): 469-480.

Kok, Z., Duffy, J., Chai, S., Jin, Y. & Javanmardi, M. 2021, "Numerical Parametric Study of Medium Sized Container Ship Squat", *Applied Ocean Research*, 109, p.102563.

Kok Z., Duffy, J., Chai, S., Jin, Y. & Javanmardi M. 2020a. "Numerical Investigation of Scale Effect in Self-Propelled Container Ship Squat", *Applied Ocean Research*, 99, p. 102143.

Kok, Z., Duffy, J., Chai, S. & Jin, Y. 2020b, "Multiple Approaches to Numerical Modelling of Container Ship Squat in Confined Water", *Journal of Waterway, Port, Coastal, and Ocean Engineering*, 146(4), p.04020017.

Kok, Z., Duffy, J., Chai, S. & Jin, Y. 2020c, "Comparison of URANS Prediction of Self-Propelled Container Ship Squat against Empirical Methods and Benchmark Data", *International Journal of Maritime Engineering*, 162 (Part A), pp. 193-206.

Kok, Z., Duffy, J., Chai, S. & Jin, Y. 2020d, "Benchmark Case Study of Scale Effect in Self-propelled Container Ship Squat", *ASME 2020 39th International Conference on Ocean, Offshore and Arctic Engineering*. Virtual, Online.

Krasilnikov, V., Sun, J., & Halse, K.H. 2009, "CFD Investigation in Scale Effect on Propellers with Different Magnitude of Skew in Turbulent Flow", *Proceedings of the 1st International Symposium on Marine Propulsors*, Trondheim, Norway, pp. 25-40.

Landweber, L. 1939, "Tests of a Model in Restricted Channels", *EMB Report 460*, David Taylor Research Center.

Larsson, L. 1993, "Resistance and Flow Predictions Using SHIPFLOW Code", *19th WEGEMNT School*, Nantes, France.

Lataire, E., Delefortrie, G. & Vantorre, M. 2016, "Impact of Banks on Ship Squat", *Proceedings of the 4th International Conference on Ship Manoeuvring in Shallow and Confined Water (MASHCON 2016)*, Hamburg, Germany, pp. 115-121.

Lataire, E. & Vantorre, M. 2008, "Ship-Bank Interaction Induced by Irregular Bank Geometries", *Proceedings of the 27th Symposium on Naval Hydrodynamics*, Seoul, South Korea, pp. 5-10.

Lataire, E., Vantorre, M. & Delefortrie, G. 2012, "A Prediction Method for Squat in Restricted and Unrestricted Rectangular Fairways", *Ocean Engineering*, 55(Supplement C): 71-80. doi:https://doi.org/10.1016/j.oceaneng.2012.07.009.

Lee, C.Y., Lee, H.L. & Zhang, J. 2015, "The Impact of Slow Ocean Steaming on Delivery Reliability and Fuel Consumption", *Transportation Research Part E: Logistics and Transportation Review*, 76, pp.176-190.

Linde, F., Ouahsine, A., Huybrechts, N. & Sergent, P. 2015, "3D Numerical Simulation of Ship Resistance in Restricted Waterways Including Ship Squat Effects", *Proceedings of the Congrès Français de Mécanique*, Lyons, France.

Liu, F. 2016, "A Thorough Description of How Wall Functions are Implemented in OpenFOAM", *Proceedings of CFD with OpenSource Software*, pp. 1-33.

Longo, J. & Stern, F. 2005, "Uncertainty Assessment for Towing Tank Tests with Example for Surface Combatant DTMB Model 5415", *Journal of Ship Research*, 49(1): 55-68.

Macfarlane, G.J. 2012, "Marine Vessel Wave Wake: Focus on Vessel Operations within Sheltered Waterways", PhD Thesis, University of Tasmania.

McNown, J.S. 1976, "Sinkage and Resistance for Ships in Channels", *Journal of Waterways, Harbors & Coast Eng Div*, 102(3): 287-299.

McTaggart, K. 2018, "Ship Squat Prediction using a Potential Flow Rankine Source Method", *Ocean Engineering*, 148: 234-246. doi:https://doi.org/10.1016/j.oceaneng.2017.10.016.

Merk, O. 2018, "Container Ship Size and Port Relocation", *International Transport Forum*, Paris, France.

Millward, A. 1990, "A Preliminary Design Method for the Prediction of Squat in Shallow Water", *Marine Technology and SNAME News*, 27(01): 10-19.

Millward, A. 1992, "Comparison of the Theoretical and Empirical Prediction of Squat in Shallow Water", *International Shipbuilding Progress*, 39(417): 69-78.

Montgomery, D.C., Peck, E.A. & Vining, G.G. 2012, "Introduction to Linear Regression Analysis", John Wiley & Sons.

Mucha, P., El Moctar, O. & Böttner, C.U. 2014, "PreSquat–Workshop on Numerical Prediction of Ship Squat in Restricted Waters", *Ship Technology Research*, 61(3): 162-165.

Naghdi, P. & Rubin, M. 1984, "On the Squat of a Ship", *Journal of Ship Research*, 28(2): 107-117.

Norrbin, N.H. 1976, "Bank Effects on a Ship Moving Through a Short Dredged Channel", *10th ONR Symposium on Naval Hydrodynamics*, Cambridge, UK.

Pettersen, B. 1982, "Calculation of Potential Flow about Three-Dimensional Bodies in Shallow Water with Particular Application to Ship Maneuvering", *Journal of Ship Research*, 26(03): 149-165.

PIANC. 1997, "Approach Channels - a Guide for Design", Supplement to PIANC Bulletin 95.

Pompée, P.J. 2015, "About Modelling Inland Vessels Resistance and Propulsion and Interaction Vessel-Waterway Key Parameters Driving Restricted/Shallow Water Effects", *Proceeding of Smart Rivers 2015 (PIANC)*, Buenos Aires, Argentina.

Prakash, M. & Chandra, B. 2013, "Numerical Estimation of Shallow Water Resistance of a River-Sea Ship using CFD", *International Journal of Computer Applications*, 71(5): 33-40.

Raven, H.C. 2019, "Shallow-Water Effects in Ship Model Testing and at Full Scale", *Ocean Engineering*, 189, 106343.

Sánchez-Caja, A., González-Adalid, J., Pérez-Sobrino, M. & Sipilä, T. 2014, "Scale Effects on Tip Loaded Propeller Performance using a RANSE Solver", *Ocean Engineering*, 88: 607-617. doi:https://doi.org/10.1016/j.oceaneng.2014.04.029.

Schijf, J.B. 1949, "Protection of Embankments and Bed in Inland and Maritime Waters, and in Overflows or Weirs", *Proceedings of the PIANC 17th International Navigation Congress 1949*, Lisbon, Portugal, Section SI C2.

Serban, P.S. & Panaitescu, V.N. 2015, "Comparison Between Formulas of Maximum Ship Squat", *Mircea cel Batran Naval Academy Scientific Bulletin*, 19(1): 105-111.

Sharp, B. & Fenton, J.D. 1968, "Report of Investigation of a Proposed Dock at Yarraville", University of Melbourne.

Sherbaz, S. & Duan, W. 2014, "Ship Trim Optimization: Assessment of Influence of Trim on Resistance of MOERI Container Ship", *The Scientific World Journal*, pp. 1-6.

Shevchuk, I., Böttner, C.U. & Kornev, N. 2016, "Numerical Analysis of the Flow in the Gap Between the Ship Hull and the Fairway Bottom in Extremely Shallow Water", *Proceedings of the 4th International Conference on Ship Manoeuvring in Shallow and Confined Water (MASHCON 2016)*, Hamburg, Germany, pp. 37-42.

Shevchuk, I., Böttner, C.U. & Kornev, N. 2019, "Numerical Investigation of Scale Effects on Squat in Shallow Water. *Proceedings of the 5th International Conference on Ship Manoeuvring in Shallow and Confined Water (MASHCON 2019)*, 19–23 May 2019, Ostend, Belgium, pp. 390-402.

Stern, F., Wilson, R.V., Coleman, H.W. & Paterson, E.G. 2001, "Comprehensive Approach to Verification and Validation of CFD Simulations—Part 1: Methodology and Procedures", *Journal of Fluids Engineering*, 123(4): 793-802.

Stern, F., Yang, J., Wang, Z., Sadat-Hosseini, H., Mousaviraad, M., Bhushan, S. & Xing, T. 2013, "Computational Ship Hydrodynamics: Nowadays and Way Forward", *International Shipbuilding Progress*, 60(1-4): 3-105.

Terziev, M., Tezdogan, T., Oguz, E., Gourlay, T., Demirel, Y.K. & Incecik, A. 2018, "Numerical Investigation of the Behaviour and Performance of Ships Advancing through Restricted Shallow Waters", *Journal of Fluids and Structures*, 76: 185-215.

Tezdogan, T., Demirel, Y.K., Kellett, P., Khorasanchi, M., Incecik, A. & Turan, O. 2015, "Full-Scale Unsteady RANS CFD Simulations of Ship Behaviour and Performance in Head Seas due to Slow Steaming", *Ocean Engineering*, 97: 186-206.

Tezdogan, T., Incecik, A. & Turan, O. 2016, "A Numerical Investigation of the Squat and Resistance of Ships Advancing through a Canal using CFD", *Journal of Marine Science and Technology*, 21(1): 86-101.

Tothill, J. 1967, "Ships in Restricted Channels - A Correlation in Model Tests, Field Measurements and Theory", *Marine Technology*, pp. 111-128.

Tuck E.O. 1967, "Sinkage and Trim in Shallow Water of Finite Width", *Schiffstechnik*, 14: 92-94.

Tuck, E.O. 1966, "Shallow-Water Flows Past Slender Bodies", *Journal of Fluid Mechanics*, 26(1): 81-95.

Tuck, E.O. & Taylor, P. 1970, "Shallow Water Problems in Ship Hydrodynamics", *Proceedings of the 8th Symposium on Naval Hydrodynamics*, Washington DC, US, pp. 627-659.

Uliczka, K. & Wezel, M. 2005, "Dynamisches Fahrverhalten Grosser Containerschiffe bei Revierfahrt auf Unter-und außenelbe", *Proceedings of the HTG-Kongress*, Bremen, Germany.

Vermeer, H. 1977, "The Behaviour of a Ship in Restricted Waters", *International Shipbuilding Progress*, 24(280): 323-336.

Wilson, R.V., Stern, F., Coleman, H.W. & Paterson, E.G. 2001, "Comprehensive Approach to Verification and Validation of CFD Simulations—Part 2: Application for RANS Simulation of a Cargo/Container Ship", *Journal of Fluids Engineering*, 123(4): 803-810.

Yao, J.X. & Zou, Z.J. 2010, "Calculation of Ship Squat in Restricted Waterways by Using a 3D Panel Method", *Journal of Hydrodynamics*, Ser. B, 22(5): 489-494.

Yasukawa, H. 1993, "A Rankine Panel Method to Calculate Steady Wave-Making Resistance of a Ship Taking the Effect of Sinkage and Trim into account", *Transactions of the West-Japan Society of Naval Architects*, 86: 27-35.

Yuan, S., Xia, L., Zou, Z.J. & Zou, L. 2019, "CFD-Based Numerical Prediction of Vertical Motions and Resistance for DTC Container Carrier in Shallow Water Waves", *Proceedings of the 5th International Conference on Ship Manoeuvring in Shallow and Confined Water (MASHCON 2019)*, Ostend, Belgium, pp. 488-501.

Appendix A – Model Test Study (*Model Test Case 2*)

Test Description

Model tests were conducted as part of this research in the towing tank facility situated on the *Australian Maritime College* campus in Launceston, Tasmania, Australia. The towing tank has a length of 100m and width of 3.55m. The work conducted in these model tests serves to supplement the main research. The specific aims of the model tests are to:

- Produce additional benchmarking squat data for CFD simulations at higher speeds ($Fr_h > 0.5$).
- Study the significance of operating a propeller at model scale self-propulsion point (MSSPP) and full scale self-propulsion point (FSSPP) on squat.

For this study, the 1:70 scale S175 hull form was used along with a Wageningen B-series propeller where self-propulsion is required. The particulars of the hull and propeller are shown in Table 3 of Section 3.1.2. The hull was set-up such that it was allowed to heave and pitch freely. The forward post was connected to the hull via a ball joint whilst the aft post was connected to a ball joint coupled with a linear slider. Both tow posts were counter balanced to avoid affecting the hull displacement and the post connection points were positioned along the thrust line to avoid artificial trim. Linear variable differential transducers (LVDTs) are equipped on both forward and aft posts to measure the change in sinkage in these positions. The midship sinkage and running trim can then be derived from the measurements of the LVDTs. A MARIN Type 421 force transducer is also equipped between the forward tow posts and the forward ball joint to measure surge for self-propulsion purposes. A Leadshire ES-M Series 3Nn stepper motor with variable RPM was used to power the propeller. Hama strips were used for turbulence stimulation. A schematic of the set-up is shown in Figure A1. The test matrix is shown in Table A1.

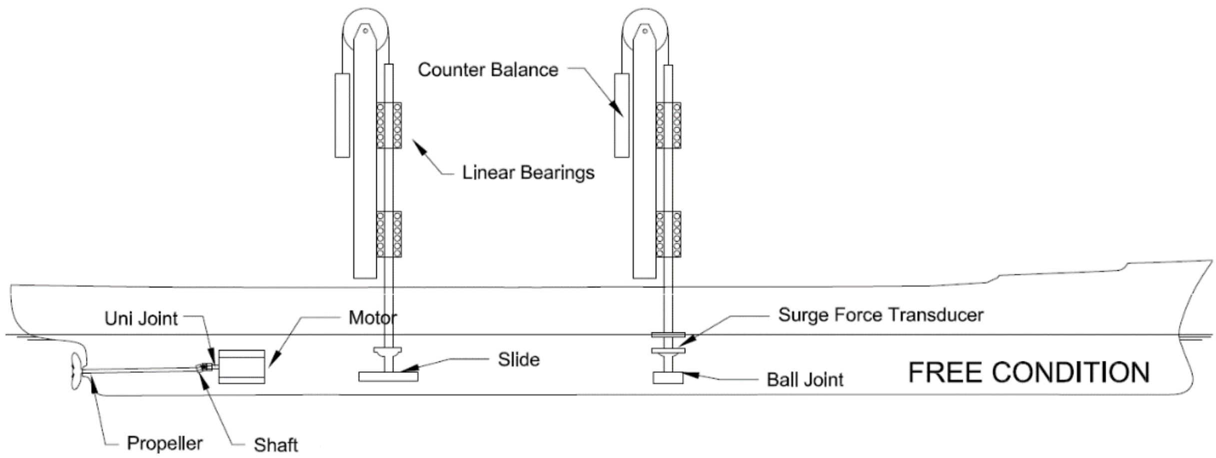

Figure A1: Schematic of the model set-up.

Table A1: Model test matrix.

Condition no.	*h/T*	Full-Scale Speed (knots)	Model Scale Speed (m/s)	Propeller Operation
1	1.5	8-20	0.49-1.23	No Prop
2	1.3	8-15	0.49-0.92	No Prop
3	1.3	8-13	0.49-0.80	MSSPP
4	1.3	8-13	0.43-0.80	FSSPP
5	1.2	7-13.5	0.43-0.83	No Prop
6	1.2	8-13	0.49-0.80	MSSPP
7	1.1	7-11	0.43-0.67	No Prop
8	1.1	7-11	0.43-0.67	MSSPP

Test Results

Firstly, results for varying speed and water depth are discussed. This is then followed by comparisons between towed condition, MSSPP condition and FSSPP condition. All results presented are within the sub-critical regime which is more practical for the study. Figure A2 depicts the results for varying speed and water depth for towed condition. It can be observed that the trend and magnitude of non-dimensionalised midship sinkage with respect to Fr_h is relatively similarly for each *h/T*. The midship sinkage results also extend further than 0.5 Fr_h which satisfies one of the objectives of the experiment. Changes in trim however are more obscure. This is because the magnitude of trim is very small and difficult to measure accurately at this scale. Nonetheless, it can be roughly observed that the trim tends to become stern down as *h/T* decreases.

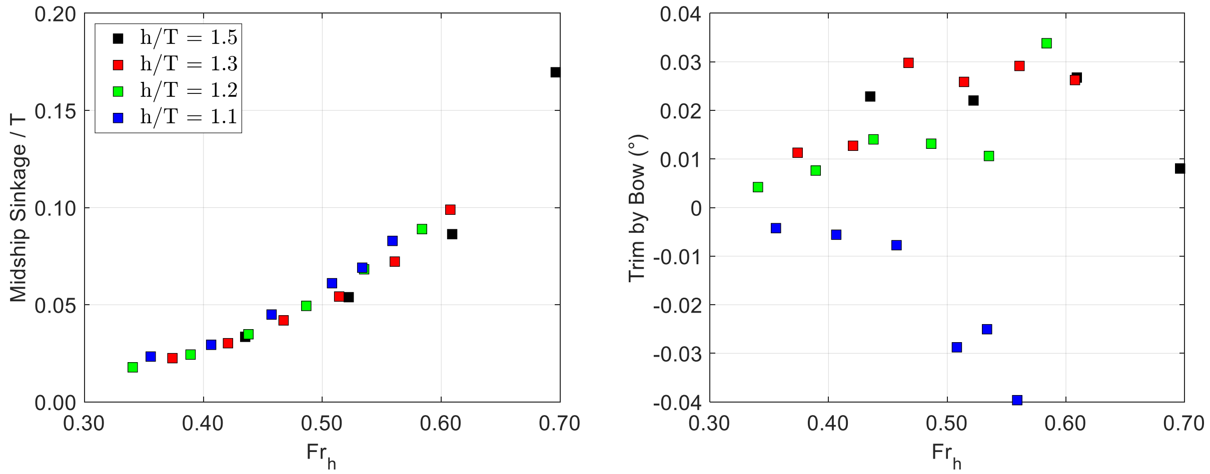

Figure A2: Plot of midship sinkage (right) and trim (left) results for varying Fr_h and *h/T* for towed condition.

Figure A3 shows the comparisons between results for towed condition, MSSPP condition and FSSPP condition. The midship sinkage results for towed condition can be seen to be consistently smaller than that of the MSSPP and FSSPP conditions by approximately 10%. However, there are no significant differences between the midship sinkage of MSSPP and FSSPP conditions. As for trim, the towed condition tends to yield bow down trim whereas both MSSPP and FSSPP conditions tend to yield stern down trim. Therefore, midship sinkage and trim are dependent on whether the hull is towed or self-propelled but the operation of the propeller at either MSSPP or FSSPP does not result in significant differences. Thus, more squat data were collected for MSSPP condition as shown in Figure A4 for CFD benchmarking purposes.

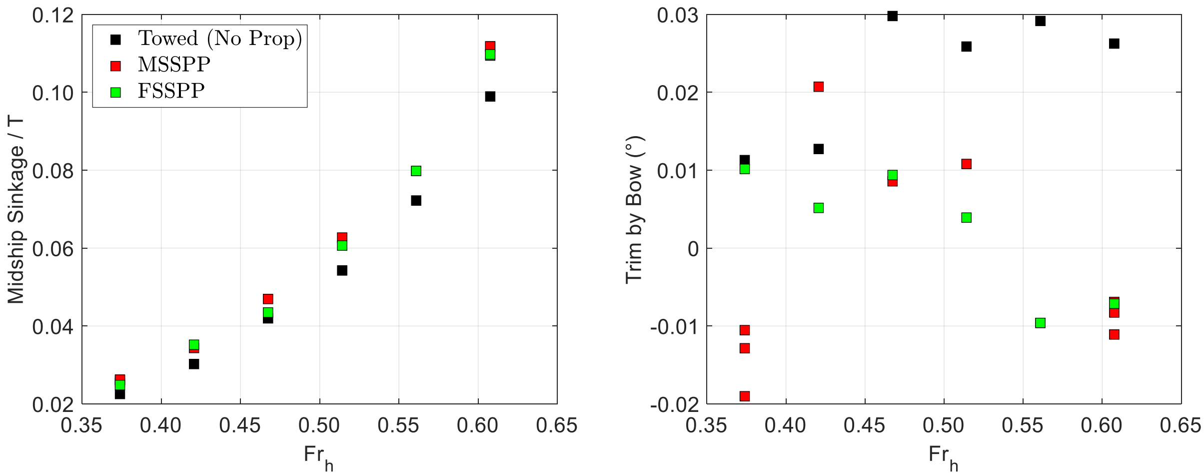

Figure A3: Comparison of midship sinkage (left) and trim (right) results between towed condition, MSSPP condition and FSSPP condition.

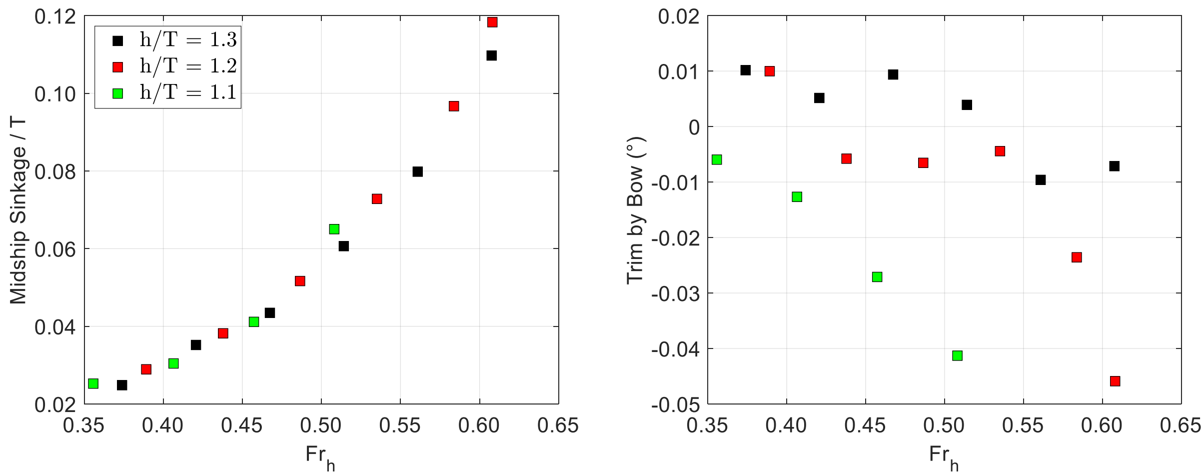

Figure A4: Plot of midship sinkage (right) and trim (left) results for varying Fr_h and *h/T* for MSSPP condition.

Conclusions

Model testing has been conducted to obtain additional benchmarking squat data for CFD simulations at higher speeds ($Fr_h > 0.5$). The model test was successful in producing benchmarking data for both towed and self-propelled conditions. It was also shown that the midship sinkage and trim were affected by whether the hull was towed or self-propelled. However, operation of the propeller at either MSSPP or FSSPP does not significantly affect the midship sinkage and trim.

Appendix B – List of Currently Available Empirical Formulae Investigated.

Formulae Name	Formulae
Ankudinov (2009)	$S_{\max} = L\left(S_{mid} \pm 0.5 Trim\right)$ *where – is for bow squat, + is for stern squat* $S_{mid} = \left(1 + K_P^S\right) P_{Hu} P_{Frh} P_{+h/T} P_{Ch1}$ $K_P^S = 0.15$ *for single propeller* $K_P^S = 0.13$ *for twin propellers* $P_{Hu} = 1.7 C_B \left(\frac{BT}{L^2}\right) + 0.004 C_B{}^2$ $P_{Frh} = Fr_h{}^{(1.8+0.4 Fr_h)}$ $P_{+h/T} = 1 + \frac{0.35}{(h/T)^2}$ $P_{Ch1} = 1$ *for unrestricted channel* $P_{Ch1} = 1 + 10 S_h - 1.5(1 + S_h)\sqrt{S_h}$ *for restricted/canal* $S_h = C_B \left(\frac{A_S / A_C}{h/T}\right)\left(\frac{h_T}{h}\right)$ $Trim = 1.7 P_{Hu} P_{Frh} P_{h/T} K_{Tr} P_{Ch2}$ $P_{h/T} = 1 - e^{\left[\frac{2.5(1-h/T)}{Fr_h}\right]}$ $K_{Tr} = C_B^{nTr} - \left(0.15 K_P^S + K_P^T\right) - \left(K_B^T - K_{Tr}^T - K_{T1}^T\right)$ $nTr = 2 + 0.8 \frac{P_{Ch1}}{C_B}$ $K_P^T = 0.15$ *for single propeller* $K_P^T = 0.20$ *for twin propellers* $K_B^T = 0.1$ *for bulbous bow* $K_B^T = 0$ *for no bulbous bow* $K_{Tr}^T = 0.04$ *for stern transom* $K_{Tr}^T = 0$ *for no stern transom* $K_{T1}^T = \frac{T_{ap} - T_{fp}}{T_{ap} + T_{fp}}$ *where T_{ap} is aft perp. static draft* *where T_{fp} is fwd perp. static draft* $P_{Ch2} = 1$ *for unrestricted channel* $P_{Ch2} = 1 - 5 S_h$ *for restricted/canal*
Barrass II (1979)	$S_{\max} = \frac{C_B (A_S / A_W)^{2/3} V_k^{2.08}}{30}$ *where A_W is net cross section area of waterway* *V_k is ship speed in knots*
Führer & Römisch (1977)	$S_{\max} = 8\left[\frac{V}{V_{Crit,p}}\right]^2 \left[\left(\frac{V}{V_{Crit,p}} - 0.5\right)^4 + 0.0625\right] S_{Crit}$ *$V_{Crit,p}$ is critical speed with self-propulsion effect:*

	$V_{Crit,p} = 0.92V_{Crit} \quad for\ \frac{A_m}{A_c} \geq \frac{1}{6}$ $V_{Crit,p} = 0.95V_{Crit} \quad for\ \frac{1}{15} < \frac{A_m}{A_c} < \frac{1}{6}$ $V_{Crit,p} = 1.00V_{Crit} \quad for\ \frac{A_m}{A_c} \leq \frac{1}{15}$ If $L \leqslant 3b$ & $A_m/A_c < 1/6$ $V_{Crit} = \left[\frac{hL}{80TB}\right]^{\beta}\sqrt{gh}$ $\beta = 0.24\left[\frac{L}{b}\right]^{0.55} \quad where\ b\ is\ channel\ waterline\ width$ If $L > 3b$ $V_{Crit} = \left[\frac{hL}{80TB}\right]^{0.125}\sqrt{gh}$ $S_{Crit} = 0.2\left[\frac{10C_B B}{L}\right]^2 T \quad for\ bow\ squat$ $S_{Crit} = 0.2T \quad for\ stern\ squat$
Hooft (1974)	$S_{bow} = \left(C_Z + \frac{1}{2}C_\theta\right)\frac{\nabla}{L^2}\frac{Fr_h^{\ 2}}{\sqrt{1-Fr_h^{\ 2}}}$ $C_Z = 1.46$ $C_\theta = 1.0$
Huuska (1976)	$S_{bow} = 2.4\frac{\nabla}{L^2}\frac{Fr_h^{\ 2}}{\sqrt{1-Fr_h^{\ 2}}}K_s$ $K_s = 7.45s_1 + 0.76 \quad for\ s_1 > 0.03$ $K_s = 1 \quad for\ s_1 \leq 0.03$ $s_1 = \left(A_{S1}/A_C\right) + 0.76$ $K_1 = refer\ to\ Figure\ A1$ $A_{S1} = midship\ section\ area\ - 0.98BT$ 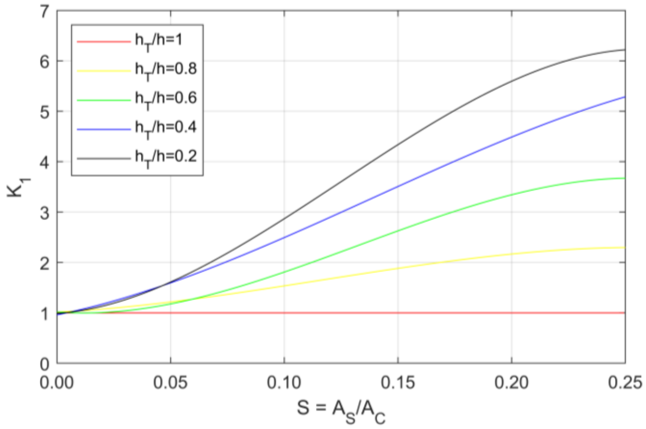 Figure B1: Plot of correction factor, K_1 (Huuska, 1976)
ICORELS (1980)	$S_{bow} = 2.4\frac{\nabla}{L^2}\frac{Fr_h^{\ 2}}{\sqrt{1-Fr_h^{\ 2}}}$

Millward (1992)	$S_{mid} = \frac{38.0 C_B T Fr_h^2}{100\sqrt{1-Fr_h^2}\, L}$ $S_{bow} = \left(\frac{61.7 C_B T}{L} - 0.6\right)\frac{Fr_h^2}{\sqrt{1-Fr_h^2}}\frac{L}{100}$
Römisch (1989)	$S_{\max} = C_V C_F K_{\Delta T} T$ $C_V = 8\left(\frac{V}{V_{Cr}}\right)^2\left[\left(\frac{V}{V_{Cr}} - 0.5\right)^4 + 0.0625\right]$ $C_F = \left(\frac{10 C_B B}{L_{PP}}\right)^2$ *for bow squat* $C_F = 1$ *for stern squat* $K_{\Delta T} = 0.155\sqrt{h/T}$ *Unrestricted shallow water:* $V_{Cr} = 0.58\left(\frac{h}{T}\frac{L}{B}\right)^{0.125}\sqrt{gh}$ *Restricted channel:* $V_{Cr} = \left[K_{ch}\left(1 - \frac{h_T}{h}\right) + K_C \frac{h_T}{h}\right]\sqrt{gh_{mT}}$ $K_{ch} = 0.58\left(\frac{h}{T}\frac{L}{B}\right)^{0.125}$ $h_{mT} = h - h_T\left(1 - h_m/h\right)$ *where h_m is mean water depth* *h_T is trench height* *Canal:* $V_{Cr} = K_C\sqrt{gh}$ $K_C = 0.2306\log\left(\frac{A_C}{A_S}\right) + 0.044$

Appendix C – Particulars of the Sister KCS Hulls Developed from Parametric Transformations.

* LCB & LCF given as % of *L* forward of aft perpendicular.

No.	***L/B***	***B/T***	C_B	***L*** (m)	***B*** (m)	***T*** (m)	**LCB** (%*L*)	**LCF** (%*L*)	A_W (m^2)	A_W **Coeff.**	GM_L (m)	***S*** (m^2)
FIXED BLOCK COEFFICENT												
1	6.50	2.50	0.648	6.28	0.97	0.387	48.28	44.79	4.90	0.809	6.56	8.30
2	6.50	2.90	0.648	6.60	1.02	0.350	48.28	44.79	5.42	0.809	8.29	8.54
3	6.50	3.39	0.648	6.95	1.07	0.316	48.28	44.79	6.00	0.809	10.41	8.85
4	6.50	3.90	0.648	7.29	1.12	0.287	48.28	44.79	6.60	0.809	12.97	9.23
5	6.80	3.06	0.648	6.92	1.02	0.333	48.28	44.79	5.70	0.809	9.76	8.77
6	6.80	3.55	0.648	7.28	1.07	0.301	48.28	44.79	6.30	0.809	12.26	9.12
7	7.14	3.22	0.648	7.28	1.02	0.316	48.28	44.79	6.00	0.809	11.52	9.02
8	7.20	2.50	0.648	6.73	0.93	0.374	48.28	44.79	5.08	0.809	8.05	8.59
9	7.52	3.39	0.648	7.66	1.02	0.301	48.28	44.79	6.30	0.809	13.76	9.30
10	7.52	2.90	0.648	7.28	0.97	0.333	48.28	44.79	5.70	0.809	10.89	8.96
11	7.52	3.90	0.648	8.03	1.07	0.274	48.28	44.79	6.93	0.809	16.69	9.67
12	7.87	3.07	0.648	7.64	0.97	0.316	48.28	44.79	6.00	0.809	12.87	9.21
13	7.87	3.54	0.648	8.01	1.02	0.288	48.28	44.79	6.60	0.809	15.81	9.55
14	8.00	2.50	0.648	7.21	0.90	0.361	48.28	44.79	5.26	0.809	9.74	8.89
15	8.23	3.23	0.648	8.01	0.97	0.301	48.28	44.79	6.30	0.809	14.93	9.45
16	8.60	2.50	0.648	7.59	0.88	0.352	48.28	44.79	5.40	0.809	13.83	9.11
17	8.60	2.90	0.648	8.01	0.93	0.316	48.28	44.79	6.00	0.809	14.22	9.39
18	8.60	3.54	0.648	8.53	0.99	0.279	48.28	44.79	6.81	0.809	18.79	9.92
19	8.60	3.90	0.648	8.81	1.02	0.261	48.28	44.79	7.26	0.809	21.23	10.13
VARYING BLOCK COEFFICENT												
20	7.14	3.22	0.589	7.54	1.06	0.33	49.79	45.00	6.11	0.769	11.79	9.35
21	7.14	3.22	0.622	7.40	1.04	0.32	49.34	44.93	6.12	0.798	11.65	9.22
22	7.14	3.22	0.648	7.28	1.02	0.32	48.28	44.79	6.00	0.809	11.52	9.02
23	7.14	3.22	0.689	7.05	0.99	0.31	47.06	44.69	5.79	0.832	11.22	8.60

Appendix D – Equations of the New Empirical Formulae

<table>
<tr><th>Description</th><th>Equations</th><th>Recommended Range of Applicability</th></tr>
<tr><td>These are the base formulae for prediction of midship sinkage and trim in laterally unrestricted shallow water.
S_{pred} is the predicted midship sinkage and is in terms of T of the queried hull.
T_{pred} is the default predicted trim in degrees (+ by bow). If LCB and LCF are known, it is highly recommended to apply the corrected trim prediction, $T_{\mathrm{pred\text{-}cor}}$</td>
<td>

$$S_{\mathrm{pred}} = Fr_{\mathrm{h}}\left[z_1 Fr_{\mathrm{h}}^2 + z_2 Fr_{\mathrm{h}}\, B/L + z_3 Fr_{\mathrm{h}}\, T/h + z_4\, B^2\big/\left(L^2 Fr_{\mathrm{h}}\right) + z_5 Fr_{\mathrm{h}} + z_6\, B/L + z_7\right] + z_8$$

$$Tr_{\mathrm{pred}} = -Fr_{\mathrm{h}}\begin{bmatrix} k_1 Fr_{\mathrm{h}}^3 + k_2\left(T/h\right)^3 + k_3 Fr_{\mathrm{h}}^2\, T/B + k_4 Fr_{\mathrm{h}}^2\, B/L + k_5 Fr_{\mathrm{h}}\, T/L + \\ k_6 Fr_{\mathrm{h}}\, TB\big/\left(hL\right) + k_7 Fr_{\mathrm{h}}^2 + k_8\left(T/h\right)^2 + k_9 Fr_{\mathrm{h}}\, T/B + k_{10} T/B + k_{11} T/h \end{bmatrix} - k_{12}$$

$$c_1 = 0.0055 - 0.3455 Fr_{\mathrm{h}}$$

$$Tr_{\mathrm{pred\text{-}cor}} = \frac{(Tr_{\mathrm{pred}} - c_1)}{3.485} \times L_{\mathrm{BF}} + c_1 \qquad L_{\mathrm{BF}} = \frac{(\mathrm{LCB} - \mathrm{LCF})}{L} \times 100\%$$

<table>
<tr><th colspan="4">S_{pred}</th><th colspan="4">T_{pred}</th></tr>
<tr><th>Coeff.</th><th>Value</th><th>Coeff.</th><th>Value</th><th>Coeff.</th><th>Value</th><th>Coeff.</th><th>Value</th></tr>
<tr><td>z_1</td><td>0.7771</td><td>z_7</td><td>0.3826</td><td>k_1</td><td>1.4597</td><td>k_7</td><td>0.1865</td></tr>
<tr><td>z_2</td><td>3.4937</td><td>z_8</td><td>-0.0314</td><td>k_2</td><td>3.7578</td><td>k_8</td><td>-6.0074</td></tr>
<tr><td>z_3</td><td>0.1093</td><td>-</td><td>N/A</td><td>k_3</td><td>-6.9341</td><td>k_9</td><td>6.9351</td></tr>
<tr><td>z_4</td><td>1.0202</td><td>-</td><td>N/A</td><td>k_4</td><td>-15.5692</td><td>k_{10}</td><td>-0.7477</td></tr>
<tr><td>z_5</td><td>-1.0904</td><td>-</td><td>N/A</td><td>k_5</td><td>-17.4567</td><td>k_{11}</td><td>1.5585</td></tr>
<tr><td>z_6</td><td>-1.5493</td><td>-</td><td>N/A</td><td>k_6</td><td>15.0199</td><td>k_{12}</td><td>0.0892</td></tr>
</table>
</td>
<td>$6.50 \le L/B \le 8.60$

$2.50 \le B/T \le 3.90$

$0.589 \le C_{\mathrm{B}} \le 0.648$

$2.37 \le L_{\mathrm{BF}} \le 3.49$

For $h/T = 1.3$:
$0.273 \le Fr_{\mathrm{h}} \le 0.683$

For $h/T = 1.1$:
$0.273 \le Fr_{\mathrm{h}} \le 0.570$

Initial Trim within ±0.5°</td></tr>
</table>

<table>
<tr>
<td>These are the corrections for the effect of lateral restriction (LR) on midship sinkage, $S_{\text{pred-LR}}$ which is in terms of T and that for trim, $Tr_{\text{pred-LR}}$ in degrees (+ by bow).</td>
<td>$\nabla_S = -0.0800\frac{h}{T} + 0.2890 Fr_{\text{h}} + 0.0124$
$S_{\text{pred-LR}} = \nabla_f \cdot m_{\text{eq-norm}} + S_{\text{pred}} - \nabla_S$

$\nabla_{Tr} = 1.153 - 0.1618\frac{L}{B} - 0.2676\frac{B}{T} + 0.004618\left(\frac{L}{B}\right)^2 ...$
$+0.02414\frac{L}{T} + 0.009901\left(\frac{B}{T}\right)^2$
$Tr_{\text{pred-LR}} = Tr_{\text{pred-cor}} + \nabla_{Tr}\left(m_{\text{eq-norm}} - 1\right)$</td>
<td>Hull Particulars Same as Above</td>
</tr>
<tr>
<td>These are the required equations to compute the normalised equivalent blockage ratio, $m_{\text{eq-norm}}$ needed for the correction for LR effect. Most of these equations are adapted from the work of Lataire and Vantorre (2008).
Here, χ, is the “weight” of a body of water or hull. Sample calculations of χ are shown; for a rectangular body of water, χ_{rect}, an infinitely deep and wide body of water, χ_{ocean}, a hull, χ_{ship}, and a shallow but laterally unrestricted body of water, $\chi_{\text{unrestricted}}$. χ_{p} and χ_{s} denotes the “weight” of the fairway at port side and starboard side of the hull respectively (excluding χ_{ship}). Thus, the limits of integration for χ_{p} and χ_{s} depends on the case and both will be identical in a symmetrical waterway.</td>
<td>$y_{\text{infl}} = 5B(Fr_{\text{h}} + 1)$

$a = \frac{3}{y_{\text{infl}}}$ $b = \frac{1}{3T}$

$\chi = \iint e^{-(ay+bz)} dy\ dz$

$\chi_{\text{rect}} = \int_{z_1}^{z_2}\int_{y_1}^{y_2} e^{-(ay+bz)} dy\ dz$
$= \frac{1}{ab}\left(e^{-ay_1} - e^{-ay_2}\right)\left(e^{-bz_1} - e^{-bz_2}\right)$

$\chi_{\text{ocean}} = 2\int_0^{\infty}\int_0^{\infty} e^{-(ay+bz)} dy\ dz$
$= \frac{2}{ab} = 2y_{\text{infl}}T$

$\chi_{\text{ship}} = 2\int_0^{T}\int_0^{B/2} e^{-(ay+bz)} dy\ dz$
$= \frac{2}{ab}\left(1 - e^{-aB/2}\right)\left(1 - e^{-bT}\right)$

$\chi_{unrestricted} = 2\int_0^{h}\int_0^{\infty} e^{-(ay+bz)} dy\ dz$
$= \frac{2\left(1 - e^{-hb}\right)}{ab} = 2y_{\text{infl}}T\left(1 - e^{-\frac{h}{3T}}\right)$

$m_{\text{eq}} = \frac{\chi_{\text{ship}}}{\chi_{\text{p}} + \chi_{\text{s}}} - \frac{\chi_{\text{ship}}}{\chi_{\text{ocean}} - \chi_{\text{ship}}}$

$m_{\text{eq-unrestricted}} = \frac{\chi_{\text{ship}}}{\chi_{\text{unrestricted}} + \chi_{\text{ship}}} - \frac{\chi_{\text{ship}}}{\chi_{\text{ocean}} - \chi_{\text{ship}}}$

$m_{\text{eq-norm}} = m_{\text{eq}} / m_{\text{eq-unrestricted}}$</td>
<td>Estimated limits vary from case to case:

<table>
<tr><th>Min. W/B</th><th>Max. h_{m}/T</th><th>Max. Fr_{h}</th><th>Min. h/T</th></tr>
<tr><td>2.5</td><td>0.4</td><td>0.57</td><td>1.3</td></tr>
<tr><td>5</td><td>0.7</td><td>0.47</td><td>1.3</td></tr>
<tr><td>5</td><td>0.4</td><td>0.52</td><td>1.2</td></tr>
<tr><td>2.5</td><td>0.4</td><td>0.45</td><td>1.1</td></tr>
<tr><td>5</td><td>0.4</td><td>0.52</td><td>1.1</td></tr>
</table>
</td>
</tr>
</table>

MATLAB Script for the Implementation of the New Formulae

```
% Authored by: Zhen Kok
% Created: 04/08/2020
% Updated: 25/03/2021
% Description: This script predicts the midship sinkage and trim for
container ships
% based on the L,B,T,LCB & LCF of the vessel. Lateral restriction effects
% are also included with account of channel width, bank height & bank
% slope. This edition is only meant to showcase single case predictions
i.e.
% output a pair of sinkage and trim predictions for only one speed at one
water depth for the given hull and
% channel parameters. Modify as necessary for a range of outputs.
%
% Contact: zhen.kok@utas.edu.au

%% Clear workspace, close all figures, clear command window
clear all
close all
clc

%% General Input
prompt = {'Vessel Length, L (m):','Vessel Beam, B (m):','Vessel Draft, T
(m):','Froude Depth No., Frh:','Water Depth-to-Draft Ratio, h/T:',...
    'Vessel LCB (%L}:','Vessel LCF (%L):','Bottom Width of Channel, W
(m):','Bank Height, hm (m):','Bank Slope, ? (degrees):'};
dlgtitle = 'Input';
dims = [1 40];
definput = {'2.5','0.363','0.1357','0.52','1.2','2.59','0','inf','0','0'};
input = inputdlg(prompt,dlgtitle,dims,definput);

L = str2double(input{1});
B = str2double(input{2});
T = str2double(input{3});
Frh = str2double(input{4});
hT = str2double(input{5});
LCB = str2double(input{6});
LCF = str2double(input{7});
w = str2double(input{8})/2; %half width of bottom of channel
hm = str2double(input{9});
theta = str2double(input{10});

%% Squat Calc. (No Lateral Restriction Effect Considered)
Th = 1/hT;         % pre-process data
BL = B/L;
TB = T/B;
LBF = LCB-LCF;
h = hT*T;
W = w*2;

Spowers = [0    0    0        %define power matrix for sinkage predictor
variables
1    0    0
1    0    1
2    0    0
0    0    2
2    1    0
2    0    1
3    0    0];
```

```
S = ones(1,length(Spowers));

for j = 1:length(Spowers)          %create the matrix of sinkage predictor
variable
    S(j) = Frh^Spowers(j,1)* Th^Spowers(j,2)*BL^Spowers(j,3);
end

coeffSinkage = [-0.03142998       %define coefficients for sinkage
predictor variables
0.382623893
-1.549271878
-1.090442307
1.020221284
0.10925937
3.493726693
0.777096377];

Spred = S*coeffSinkage;         %compute the sinkage

 Trpowers = [0   0    0    0          %define power matrix for trim predictor
variables
1    1    0    0
1    0    0    1
2    0    0    1
1    2    0    0
3    0    0    0
2    1    1    0
2    0    1    1
3    0    1    0
3    0    0    1
1    3    0    0
4    0    0    0];

Tr = ones(1,length(Trpowers));

for j = 1:length(Trpowers)         %create the matrix of trim predictor
variables
    Tr(j) = Frh^Trpowers(j,1)*
Th^Trpowers(j,2)*BL^Trpowers(j,3)*TB^Trpowers(j,4);
end


coeffTrim = [0.089190661          %define coefficients for trim predictor
variables
1.558544348
-0.747708337
6.935083881
-6.007404185
0.186466709
15.01990904
-17.45666605
-15.56918047
-6.934129206
3.757806624
1.459704757];

Tpred = Tr*-coeffTrim;              %compute the trim
c = -0.3455*Frh+0.0055;               %compute the trim correction factor
```

```
TpredCor = (Tpred-c)/3.485*LBF+c;     %compute the corrected trim

%% Calculation of Correction for Lateral Restriction Effect
As = T*B*0.98;                        %compute the max cross-sectional area
of the ship, section area coefficient assumed to be 0.98!
Yinfl = 5*B*(Frh+1);                  %compute the influence width, Yinfl
a = 3/Yinfl;                        %compute variables required for the
calculation of "weight" and equivalent blockage ratio
b = 1/(3*T);

func = @(x,y) exp(-(a.*x)-(b.*y));          %compute weight of different
segments of the unoccupied channel area
ymax = @(x) -x.*tand(theta)+h+w.*tand(theta);
if theta == 90                              %compute weight of triangular
area above the sloped bank
    TriW=0;
else
    TriW=integral2(func,w,(w+hm./tand(theta)),h-hm,ymax);
end
botRec = integral2(func,0,w,h-hm,h);              %compute weight of
rectangular area bounded by the channel bottom and bank
unRec = integral2(func,0,inf,0,h-hm);             %compute weight of the
unrestricted area above the bank
latUnrec = integral2(func,0,inf,0,h);             %compute weight of
similar but laterally unrestricted condition (for normalising purposes)
W_channel = (TriW+botRec+unRec)*2;                %compute total weight for
the channel
W_urchannel = latUnrec*2;                         %compute weight of
similar but laterally unrestricted channel
W_ocean = 2*Yinfl*T;                              %compute weight of deep,
open water condition
meq = As/(W_channel-As)-As/(W_ocean-As);            %compute total
equivalent blockage ratio for the channel
meq_unrec = As/(W_urchannel-As)-As/(W_ocean-As);    %compute total
equivalent blocakge ratio for similar but laterally unrestricted channel
n_meq = meq/meq_unrec;                            %compute the normalised
equivalent blockage ratio

grads = -
0.08*hT+0.289*Frh+0.01238;
%compute the sinkage correction factor for lat. res. effect
gradtr = 1.153-0.1618*L/B-
0.2676*B/T+0.004618*(L/B)^2+0.02414*L/T+0.009901*(B/T)^2;     %compute the
trim correction factor for lat. res. effect

Slr = grads*n_meq+(Spred-grads);         %compute the corrected sinkage for
lat. res. effect
Tlr = TpredCor+gradtr*(n_meq-1);           %compute the corrected trim for
lat. res. effect

%% Check Input Against Recommended Range
warn = 0;
if (hT < 1.3) && (Frh > 0.57)
    msgbox('WARNING: Frh exceeds recommended range!!')
    warn=1;
end

if (hT == 1.3) && (Frh > 0.683)
    msgbox('WARNING: Frh exceeds recommended range!!')
    warn=1;
```

```
end

if (hT < 1.1) || (hT > 1.3)
    msgbox('WARNING: h/T exceeds recommended range!!')
    warn=1;
end

if (LBF < 2.37) || (LBF > 3.49)
    msgbox('WARNING: LBF exceeds recommended range!!')
    warn=1;
end

if (hT == 1.3)
    if (W/B < 2.5)
        msgbox('WARNING: Channel width, W, is smaller than recommended
range!!')
        warn=1;
    elseif (W/B < 5) && (hm/T > 0.4)
        msgbox('WARNING: bank height, hm, is larger than recommended
range!!')
        warn=1;
    elseif (W/B >= 5) && (hm/T > 0.7)
        msgbox('WARNING: bank height, hm, is larger than recommended
range!!')
        warn=1;
    elseif (Frh > 0.57)
        msgbox('WARNING: Frh exceeds recommended range!!')
        warn=1;
    end
elseif (hT < 1.3) && (hT >= 1.2)
    if (W/B < 5)
        msgbox('WARNING: Channel width, W, is smaller than recommended
range!!')
        warn=1;
    elseif (hm/T > 0.4)
        msgbox('WARNING: bank height, hm, is larger than recommended
range!!')
        warn=1;
    elseif (Frh > 0.52)
        msgbox('WARNING: Frh exceeds recommended range!!')
        warn=1;
    end
elseif (hT < 1.2) && (hT >= 1.1)
    if (W/B < 2.5)
        msgbox('WARNING: Channel width, W, is smaller than recommended
range!!')
        warn=1;
    elseif (W/B < 5) && (Frh > 0.45)
        msgbox('WARNING: Frh exceeds recommended range!!')
        warn=1;
    elseif (Frh > 0.52)
        msgbox('WARNING: Frh exceeds recommended range!!')
        warn=1;
    end
end

if (n_meq > 1.3) && (n_meq < 1.4)
    msgbox('CAUTION: normalised equivalent blockage ratio value is slightly
large')
elseif (n_meq > 1.4)
```

```
    msgbox('WARNING: normalised equivalent blockage ratio value is
large!!')
    warn=1;
end

%% Display Results
lryn = isnan(Slr);                              %determine whether lat. res.
effects are in play/valid & sort relevant outputs to be displayed
if lryn == 1
    disp('CAUTION: Lateral restriction effect not considered or is
invalid')
    disp(['Midship sinkage = ',num2str(Spred),' T']);
    disp(['Trim = ',num2str(Tpred),' degrees']);
else
    disp('Lateral restriction effect taken into account')
    disp(['Midship sinkage = ',num2str(Slr),' T']);
    disp(['Trim = ',num2str(Tlr),' degrees']);
end

if warn==1
    disp('Certain parameter(s) exceeded recommended range, predictions may
be inaccurate!!')
end
```

Appendix E – Publications

List of Peer-Reviewed Publications

Paper 1 (Journal Article): Kok, Z., Duffy, J., Chai, S. & Jin, Y. 2020c, "Comparison of Unsteady Reynolds-Averaged Navier-Stokes Prediction of Self-Propelled Container Ship Squat against Empirical Methods and Benchmark Data", *Transactions of the Royal Institution of Naval Architects, Part A: International Journal of Maritime Engineering*, 162 (Part A), pp. 193-206. Removed from thesis for copyright reasons

Paper 2 (Journal Article): Kok, Z., Duffy, J., Chai, S. & Jin, Y. 2020b, "Multiple Approaches to Numerical Modelling of Container Ship Squat in Confined Water", *Journal of Waterway, Port, Coastal, and Ocean Engineering*, 146 (4), p.04020017. Removed from thesis for copyright reasons

Paper 3 (Conference Paper): Kok, Z., Duffy, J., Chai, S. & Jin, Y. 2020d, "Benchmark Case Study of Scale Effect in Self-propelled Container Ship Squat", *ASME 2020 39th International Conference on Ocean, Offshore and Arctic Engineering*. Virtual, Online. Removed from thesis for copyright reasons

Paper 4 (Journal Article): Kok, Z., Duffy, J., Chai, S., Jin, Y. & Javanmardi, M. 2020a, "Numerical Investigation of Scale Effect in Self-propelled Container Ship Squat", *Applied Ocean Research*, 99, p.102143.

Paper 5 (Journal Article): Kok, Z., Duffy, J., Chai, S., Jin, Y. & Javanmardi, M. 2021, "Numerical Parametric Study of Medium Sized Container Ship Squat", *Applied Ocean Research*, 109, p.102563.

Applied Ocean Research 99 (2020) 102143

Contents lists available at ScienceDirect

Applied Ocean Research

journal homepage: www.elsevier.com/locate/apor

Numerical investigation of scale effect in self-propelled container ship squat

Zhen Kok[a,*], Jonathan Duffy[a], Shuhong Chai[a], Yuting Jin[b], Mohammadreza Javanmardi[c]

[a] National Centre for Maritime Engineering and Hydrodynamics, Australian Maritime College, University of Tasmania, Locked Bag 1395, Launceston, Tasmania 7250, Australia

[b] Technology Centre for Offshore and Marine Singapore, 12 Prince George's Park, 118411, Singapore

[c] OMC International, 126 Trenery Crescent, Abbotsford, Victoria 3067, Australia

ARTICLE INFO

Keywords:
Ship squat
Reynolds averaged Navier–Stokes equations
Body-force propulsion
Scale effect
Resistance extrapolation
Confined water

ABSTRACT

A URANS CFD-based study has been undertaken to investigate scale effect in container ship squat. Initially, CFD studies were carried out for the model scale benchmarking squat cases of a self-propelled DTC container ship. Propulsion of the vessel was modelled by the body-force actuator disc method. Full scale investigations were then undertaken. Validation of the full scale set-up was demonstrated by computing the full scale bare hull resistance in deep, laterally unrestricted water and comparing against the extrapolated resistance of model scale benchmark resistance data. Upon validating the setup, it was used to predict full scale ship squat in confined waters. The credibility of the full scale confined water model was checked by comparing vessel resistance in confined water against the Landweber (1933) empirical prediction. To quantify scale effect in ship squat predicitons, the benchmarking squat cases were computed by adopting the validated full scale CFD model with body-force propulsion. Comparison between the full scale CFD, model scale CFD and model scale benchmark EFD squat results demonstrates that scale effect is negligible. In addition, model scale predicted ship squat results were compared with physical full scale squat measurements of similar hulls. The two series of results are in good agreement which also demonstrate that the scale effect is insignificant.

1. Introduction

The highly competitive nature of the shipping industry has driven the need for shipping operators to employ ever larger ships for more favourable economic return. Nonetheless, the size growth rate of next generation ships will inevitably outpace costly dredging and harbour expansion projects [14]. Hence, the low under keel clearance in undersized ports and the subsequent ship squat phenomena will continue to be a severe threat to port operation safety.

Ship squat has been studied extensively where pioneering investigations were conducted by Constantine [5] regarding the different squat behaviour in open water for subcritical ($Fr_h < 1$), critical ($Fr_h = 1$) and supercritical ($Fr_h > 1$) vessel speeds. Tuck [38] formulated a slender-body theory that was valid for squat estimation in laterally unrestricted shallow water and eventually presented a new method to account for finite channel widths [39]. The slender body theory presented by Tuck [38] became the foundation for the development of many other prediction methods such as the work of Beck et al. [2], Naghdi and Rubin [31], and Cong and Hsiung [4]. Various empirical-based modifications of the slender body theory were also introduced such as those of Hooft [17], Huuska [18], ICORELS (1980) and Millward [28].

Model scale experiments were heavily implemented in the study of ship squat. Dand and Ferguson [6] developed a semi-empirical formula for full form ships based on their model scale squat measurements. Fuehrer and Römisch [11] presented an empirical formula derived from their model tests which account for varying cross section parameters of the canal. Similarly, Barrass [1] conducted model scale experiments to develop a prediction formula accounting for ship speed, block coefficient and blockage factor. Duffy and Renilson [9] conducted model scale experiments to derive empirical corrections for the propulsion effect for bulk carriers. Delefortrie et al. [7] developed a mathematical model with empirical data for the effects of muddy bottom and propeller action.

The advancement of computation power has enabled the implementation of numerical methods in the study of ship squat. For instance, a potential flow method which has been used by Yao and Zou [41] and Zhang et al. [42] to investigate the shallow water hydrodynamics was satisfactory accurate for subcritical and supercritical flow but not for trans-critical flow due to neglection of non-linear effects. Computational Fluid Dynamics (CFD) method has also been adopted in the study of ship squat where non-linear and viscous effects can be

* Corresponding author.
E-mail address: zhen.kok@utas.edu.au (Z. Kok).

https://doi.org/10.1016/j.apor.2020.102143
Received 7 November 2019; Received in revised form 8 February 2020; Accepted 24 March 2020

Nomenclature

Symbol Description

A_E	Propeller expanded area (m^2)
A_O	Propeller disc area (m^2)
AP	Aft perpendicular (m)
B	Ship beam (m)
$c_{0.7}$	Propeller chord length at 0.7 radius (m)
C_B	Block coefficient
D	Propeller diameter (m)
FP	Forward perpendicular (m)
Fr_h	Froude depth number ($Fr_h = V/\sqrt{gh}$)
FS	Full scale
g	Gravitational constant (m/s^2)
h	Water depth (m)
L_{PP}	Length between perpendiculars of ship (m)
M_{TC}	Moment to change trim by 1 cm (tonne m/cm)
MS	Model scale
m	Blockage ratio (Midship section area / Waterway cross-section area)
S	Wetted surface area (m^2)
T	Ship draft (m)
T_{PC}	Tonnes per centimetre immersion (tonne/cm)
$P_{0.7}$	Propeller blade pitch at 0.7 radius (m)
V	Ship speed (m/s)
Δ	Displacement (tonne)
λ	Scale
ρ	Fluid density (kg/m^3)
∇	Volumetric displacement of ship (m^3)

accounted for. Jachowski [19] showed that the squat predictions in laterally unrestricted shallow water using a commercial RANS solver have a good correlation with experimental observations and wave theory. Similarly, Tezdogan et al. [37] were able to obtain accurate midship sinkage prediction for a container ship with fixed propeller using a commercial RANS solver while trim was deemed to be negligible and not considered in the analysis.

Nonetheless, the above mentioned work is all based on model scale experiments or model scale computations. There is limited literature available regarding full scale investigations and scale effect in ship squat. Harting and Reinking [16] have conducted full scale ship squat measurements using the SHore Independent Precise Squat observation (SHIP) method. Gourlay and Klaka [13] used high-accuracy GPS receivers and a fixed base station to measure container ship sinkage, trim and roll. Ha and Gourlay [15] demonstrated that the slender-body theory can predict squat with reasonable accuracy for container ships at full scale in open dredged channels. However, scale effect in ship squat was investigated by Eryuzlu et al. [10] where it was noted that the boundary layer thickness and viscous effects on the model scale ship hull cannot be extrapolated linearly as the model scale experiments are conducted at a smaller Reynolds number than the full scale scenario. Furthermore, model and full scale CFD simulation comparisons conducted by Deng et al. [8] and Gilligan [12] have shown for isolated simplified cases that scale effect is indeed significant. Nevertheless, these analyses based on full scale CFD simulations do not include self-propulsion effect which has been highlighted by Lataire et al. [26] and Kok et al. [[23]ess] to have noticeable effect on squat, particularly trim.

Therefore, further investigation is required to study the significance of scale effect in self-propelled container ship squat. The present study investigates scale effect in self-propelled container ship squat via numerical simulation of the Duisburg Test Case (DTC) hull appended with a Wageningen B-series propeller traversing in an asymmetric canal in both model scale and full scale conditions. Verification and validation are conducted for the benchmark model scale simulation for which the full scale simulation set-up methodology is based upon. The credibility of the full scale simulation is then investigated by computing and comparing the bare hull deep water resistance and confined water resistance against the ITTC (1987) extrapolated resistance and Landweber [25] confined water resistance estimation respectively. In addition, the feasibility of extrapolating model scale simulations of measured full scale cases are also investigated.

2. Hull form and tank geometry

In this investigation, the hull and domain studied are based on an asymmetric confined water canal benchmark case conducted in the Federal Waterways Engineering and Research Institute (BAW) [30]. In this study, confined water is defined as a waterway with finite depth and restricted laterally. The hull used is the 1:40 scale Duisburg Test Case (DTC) hull, a typical 14,000 TEU container ship developed by the Institute of Ship Technology, Ocean Engineering and Transport Systems (ISMT) of the University of Duisburg-Essen for benchmarking purposes. The DTC hull represents a typical hull form for modern post-panamax container vessels. Fig. 1 depicts the profile view of the DTC hull and the cross section of the asymmetrical canal investigated. The propeller implemented in the benchmark case is the Wageningen B-series 4 bladed propeller which was operated at model scale self-propulsion point for the given water depth [30]. Details of the hull and propeller principal particulars are summarised in Table 1.

3. Computational methods

The STAR-CCM+ URANS solver was used to conduct the computations where the incompressible RANS equation is resolved in integral form using the finite volume method of discretisation. In this study, a quasi-static approach is adopted where the hull was fixed from sinking and trimming while the hydrodynamic forces and moments on the hull are computed. The heave displacement and the pitch angle comprising the squat are then estimated using the hydrostatic data of the hull (refer to Section 3.2 for further details). The reason for the use of the quasi-static method instead of dynamic meshes that enable direct motion such as the overset mesh is that the quasi-static method has been found to be

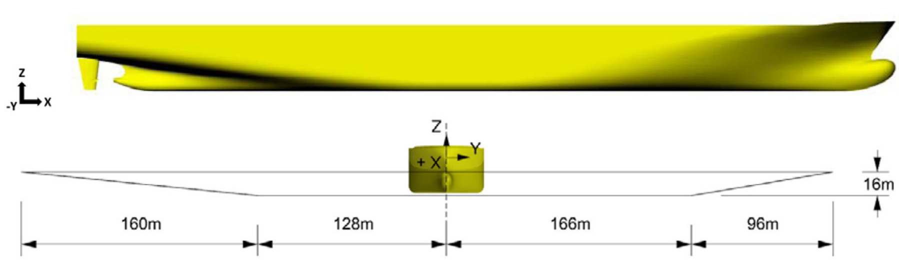

Fig. 1. Profile view of the DTC hull (top) and the Cross section view of the asymmetric canal geometry (bottom).

Table. 1
Principal particulars of the DTC hull and the Wageningen B-series propeller.

Principal particulars Ship particulars	Model scale (1:40)	Full scale (1:1)
L_{PP} (m)	8.875	355
B (m)	1.275	51.0
T (m)	0.325	13.0
Δ (tonnes)	2.618	163.5
C_B	0.661	0.661
Propeller particulars		
D (m)	0.223	8.92
Blades	4	4
$P_{0.7}/D$	1.275	1.275
A_E/A_O	0.55	0.55
$c_{0.7}$ (m)	0.066	2.635

significantly more computationally efficient, stable and accurate in previous similar studies even without multiple iterations of the force/moment and motion balance Kok et al. [[23]ess].

3.1. RANS equations

In turbulent flow the velocity and pressure fields can be resolved by expressing them as the sum of mean and fluctuating parts. The Reynolds-averaged Navier–Stokes equations are effectively derived by applying the mean and fluctuating parts into the incompressible form of Navier–Stokes equations [3]:

$$\frac{\partial U_i}{\partial x_i} = 0 \tag{1}$$

$$\rho\frac{\partial U_i}{\partial t} + \rho\frac{\partial}{\partial x_j}(U_iU_j) = -\frac{\partial P}{\partial x_i} + \frac{\partial}{\partial x_j}(2\mu S_{ij} - \rho\overline{u_i'u_j'}) \tag{2}$$

$$S_{ij} = \frac{1}{2}\left(\frac{\partial U_i}{\partial x_j} + \frac{\partial U_j}{\partial x_i}\right) \tag{3}$$

In the equations above, i and j are the spatial indexes, whereas $U_{i(j)}$ and P are the time-averaged velocity and pressure fields respectively. ρ is the density of the effective flow, μ the viscosity, S_{ij} the mean strain-rate tensor and $\overline{u_i'u_j'}$ the Reynolds stress tensor which is sometimes expressed as τ_{ij}. The Reynolds stress tensor is symmetric and possesses six components but remains unknown since three more unknown quantities are introduced into the equations when the instantaneous properties are decomposed into mean and fluctuating components. Therefore, additional equations known as turbulence models are required to close the system. The closure of the equation for this particular investigation is discussed in the following section.

3.2. Physics modelling

The standard k–ε turbulence model was implemented to close the RANS equations in this study on the basis that the k–ε model is also more computationally economical compared against k–ω model [37] and that the sinkage prediction is not influenced greatly when using different turbulence model [8].

As a hull advances through water, the squat experienced is affected by the free surface position [8]. Thus, modelling of the free surface has been accounted for by applying the volume of fluid (VOF) method. The VOF model is numerically efficient in simulating flows where the overall contact area between the different phases is low.

The dynamic fluid body interaction (DFBI) module was used to enable free movement of the hull in surge only. The hydrodynamic heave force and trim moment experienced by the hull are predicted by the RANS solver and then the sinkage and trim component of the squat are estimated manually using the Eqs. 4 and 5 respectively where F_z is the hydrodynamic force acting in the z-axis and M_y is the hydrodynamic moment acting about the y-axis. It should be noted that such an approach is a simplification of the actual phenomenon and is different from reality where the change in free surface will result in squat motion to the hull which consequently increases the blockage factor.

$$\text{Sinkage [m]} = \frac{F_Z\,[\text{N}] \times 0.01\,[\text{m/cm}]}{T_{PC}\,[\text{tonne/cm}] \times 9.81\,[\text{m/s}^2] \times 1000\,[\text{kg/tonne}]} \tag{4}$$

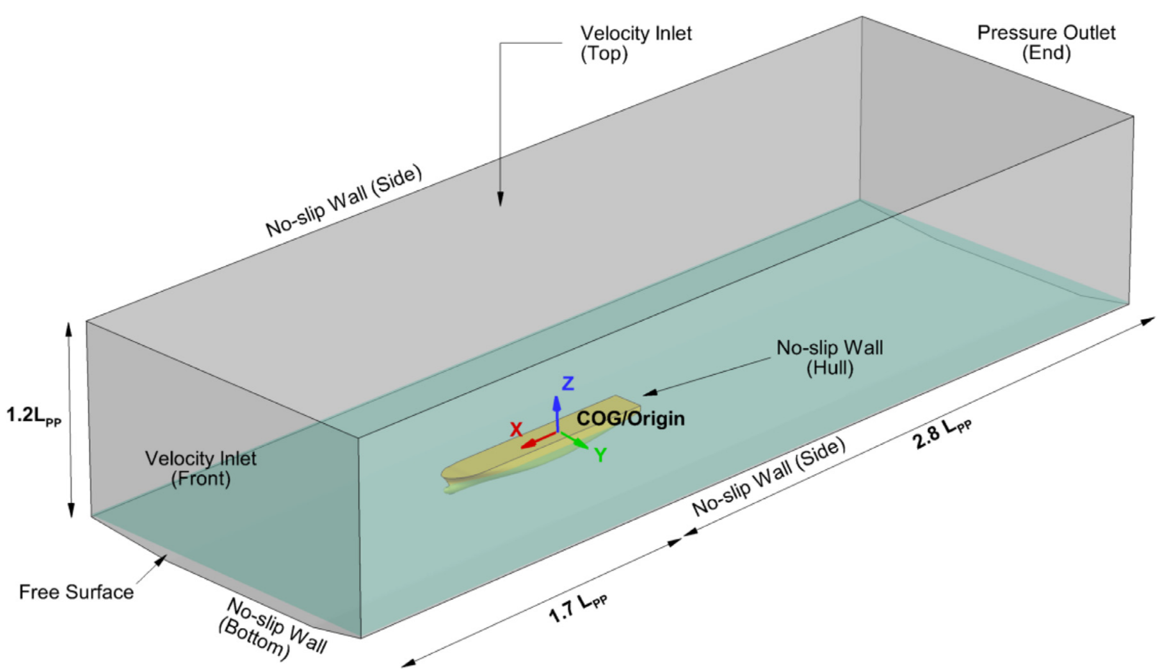

Fig. 2. The canal domain dimensions and boundary conditions.

$$\text{Trim}[°] = \tan^{-1}\left(\frac{M_Y\,[\text{Nm}] \times 0.01\,[\text{m/cm}]}{M_{TC}\,[\text{tonne}\cdot\text{m/cm}] \times 9.81\,[\text{m/s}^2] \times 1000\,[\text{kg/tonne}]} / L_{PP}\,[\text{m}]\right) \tag{5}$$

Self-propulsion effect is also considered in this study as Kok et al. [[23]ess] demonstrated that propeller action influence container ship squat in confined water, particularly when $Fr_{\mathrm{h}} > 0.5$. The body force propulsion actuator disc method was implemented in the solver to account for the self-propulsion effect. The method is a computationally economical yet sufficiently accurate for squat prediction in comparison to fully discretised propellers [3]. The open water performance curve data for the same Wageningen B-series propeller was supplemented to the virtual disc model to compute the propeller thrust.

3.3. Computational domain, boundary conditions and mesh development

Fig. 2 depicts the computation domain designed for this investigation based on the benchmark model test set-up discussed in Section 2. The longitudinal length of the domain was designed in accordance to CD-Adapco (2014) recommendations where the inlet is at least 1 L_{PP} away from the hull and the outlet is at least 2 L_{PP} downstream. The velocity inlet at the forward end of the domain was assigned to generate zero velocity flat waves while the pressure outlet at the aft end of the domain prevented backflow. In addition, VOF wave damping of length 1.13 L_{PP} was applied at both inlet and outlet to avoid unrealistic wave reflections from these boundaries. Boundary layer growth on the hull during forward movement was accounted for by applying no-slip wall condition on the hull surfaces.

However, it should be noted that the simulation designed in this study is such that the ship and domain move forward together in a stationary body of water. Therefore, the bottom and side walls of the domain were modelled as no-slip walls with constant tangential velocity equal to zero relative to the global axis. This setting ensures that the velocity profile development on the bottom and side walls are due to the wake of the ship instead of the movement of the domain.

The STAR-CCM+ built-in hexahedral trimmed cell mesher, surface remesher and prism layer meshers were implemented with reference to CD-Adapco [3] recommendations for virtual towing tank simulations to generate the computational grids. Additional mesh refinements were applied to the hull surfaces, the free surface region and the small underkeel clearance to accurately capture the flow physics in these regions. Smooth mesh size transition between regions of highly refined mesh and coarser regions was maintained by applying slow cell growth rate. A $y+$ value of above 30 was achieved by using the prism layer mesher. Fig. 3 depicts the mesh generated for the computation domain.

4. Verification and validation

The triplets method of verification and validation discussed by Wilson et al. [40] and Stern et al. [35] was implemented in this study. The verification and validation study was conducted for the benchmark EFD case [30] where $h/T = 1.23$ and $Fr_{\mathrm{h}} = 0.553$ (the crtitical Froude depth number, $Fr_{\mathrm{h,Crit}}$ for this case is 0.628 base on Eq. 6 presented by Schijf [34]). The following section briefly discusses the key calculation methodology only. The process is based on the verification and validation study presented by Jin et al. [21].

$$Fr_{\mathbf{h,Crit}} = \frac{V_{\mathbf{Cr}}}{\sqrt{gh}} = \left(\mathbf{2sin}\left(\frac{\mathbf{Arcsin(1}-m)}{\mathbf{3}}\right)\right)^{3/2} \tag{6}$$

4.1. Verification and numerical uncertainty analysis

The numerical uncertainty U_{SN} was approximated as the combination of iterative convergence uncertainty U_{I}, grid spacing uncertainty U_{G} and time step uncertainty U_{T} as shown in Eq. 7. However, according to Tezdogan et al. [36], the iterative uncertainty for ship motion response simulations in Star-CCM+ URANS solver is less than 0.2% for seakeeping applications and hence, U_I was neglected in this study.

$$U_{SN}^2 = U_I^2 + U_G^2 + U_T^2 \tag{7}$$

Triple solutions were obtained for both the grid and time step uncertainty convergence study where the grid spacing uncertainty analysis was conducted with the smallest time-step while the time-step uncertainty study was conducted with the finest mesh setting. Table 2 presents the details of the mesh count and time-step employed in the uncertainty study. A refinement ratio $r_G = \sqrt{2}$ was applied for the grid

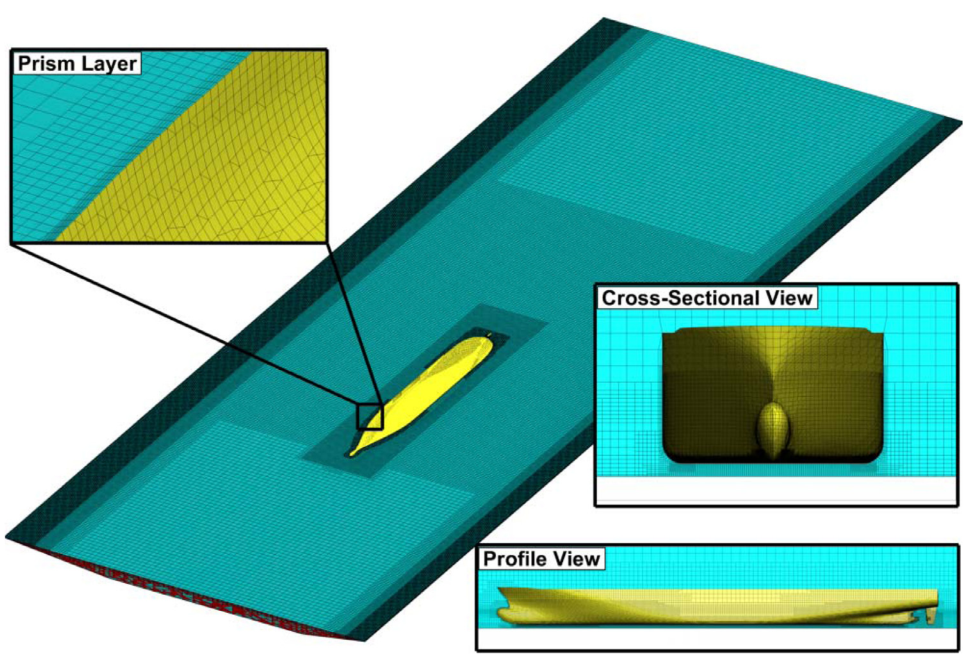

Fig. 3. Perspective view of the computation domain mesh sliced at the free surface in addition to the mesh view of the prism layer, cross-section and profile of the hull.

Table. 2
Mesh count and time-step details applied in the verification study.

Configuration	Total mesh	Time-step
Coarse (3)	1,355,800	0.02
Medium (2)	2,304,861	0.01
Fine (1)	3,388,145	0.005

spacing uncertainty study. For the time-step uncertainty study, the time-step was determined using the Courant number (CFL) (Eq. 8) where Δl is the mesh dimension, V is the ship speed and CFL was set to value of 1. The refinement ratio for time-step r_T was 2.

$$\Delta t = \frac{\mathrm{CFL}\times\Delta l}{V} \tag{8}$$

The changes in solution ε, between the three consecutive grids and three time steps were calculated where S represents the solution obtained for that particular grid or time step:

$$\varepsilon_{32} = S_3 - S_2$$
$$\varepsilon_{21} = S_2 - S_1 \tag{9}$$

The convergence ratio R_i was then determined based on the changes in solution using the following relation:

$$R_i = \frac{\varepsilon_{21}}{\varepsilon_{32}} \tag{10}$$

When assessing the convergence ratio R_{i} the possible outcomes are as follows:

1) $0 < R_{\mathrm{i}} < 1$, where monotonic convergence has been achieved (MC)
2) $R_{\mathrm{i}} < 0$; $|R_{\mathrm{i}}| < 1$, where oscillatory convergence has been achieved (OC)
3) $1 < R_{\mathrm{i}}$, where monotonic divergence has been achieved (MD)
4) $R_{\mathrm{i}} < 0$; $|R_{\mathrm{i}}| > 1$, oscillatory divergence has been achieved (OD)

No uncertainty estimates can be made for divergent cases (outcomes 3 and 4) whereas further calculations of the uncertainty for convergent cases (outcomes 1 and 2) can be referred from similar work presented by Jin et al. [21]. Tables 3 and 4 presents the outcome of the grid spacing and time-step uncertainty analysis, respectively. Three parameters were monitored in the verification study, which were the AP sinkage, FP sinkage and ship speed. Monitoring both AP and FP sinkage allows for assessment of the predicted sinkage and trim while ship speed was monitored because it directly impacts the predicted squat and is also dependent on the virtual disc rotation speed, mesh size and time-step. Observations on the change of ship speed, AP and FP sinkage solutions among the three grid spacings show monotonic convergence where the corresponding uncertainties are less than 7%. For the time-step uncertainty study, oscillatory convergence was achieved for all three parameters but the uncertainties are less than 6%. Therefore, the verification study conducted suggests that the computational model yields acceptable numerical uncertainties.

4.2. Validation against model test data

Validation for the numerical method was conducted against experimental data by computing and comparing the comparison error, E, with the validation uncertainty, U_{V}, which is the combination of numerical uncertainty, U_{SN} and experimental uncertainty, U_{D}, as given below:

$$U_V = \sqrt{U_{SN}^2 + U_D^2} \tag{11}$$

The comparison error E, is given as the difference between the experimental data, D, and simulation data, S. The numerical results are considered to be validated if E is less significant than U_{V}:

$$E = D - S \tag{12}$$

The U_{D} is not provided in literature and consequently, a compromise was made to approximate the value of U_{D} to be 5%. U_{V} was then computed and then compared with E as depicted in Table 5. The estimated E for AP sinkage is evidently smaller than U_{V} and therefore validated. However, the estimated E for FP sinkage appears to be slightly greater than U_{V}. Regardless, considering that the value of U_{D} is assumed and that the magnitude of AP and FP sinkage are relatively small values where small differences will result in large percentage differences, it is reasonable to deem that the current numerical method is sufficiently feasible for further simulations. In addition, further comparison of the CFD AP and FP sinkage predictions at different speeds with respect to that of the benchmark EFD AP and FP sinkage in Fig. 4 demonstrates strong correlation between the CFD predictions and the EFD data. Resistance measurements are unavailable from the benchmark EFD for comparison.

5. Full scale simulation investigation

Having verified and validated the CFD physics setup, the model was adapted for full scale investigations. Nonetheless, prior to conducting the full scale squat investigation, it is necessary to check the credibility of the full scale simulation set-up. Hence, this section of the paper will firstly discuss the credibility of the full scale simulation methodology applied by computing and examining the predicted full-scale deep water resistance and full-scale confined water resistance. Finally, this is followed by full scale squat simulation in the same canal domain shown in Fig. 1 to compare against the model scale condition to investigate if the difference in scale influences squat.

5.1. Full scale deep water resistance validation

In the absence of resistance data for the PreSquat workshop benchmark case [30], an alternative method to assess the credibility of full scale simulations is to compute and compare bare hull deep water resistance predictions against full scale extrapolated resistance of benchmark data as demonstrated by Jin et al. [20]. The full scale deep water resistance validation study was conducted based on a deep water resistance benchmarking EFD conducted by Moctar et al. [29]. The said benchmark resistance test was conducted in the SVA Potsdam using the same DTC hull at a scale factor of 1:59.4. A new computation domain for deep water resistance was modelled based on the previously verified and validated CFD modelling technique. Fig. 5 depicts the computation domain designed for the deep water resistance benchmarking where the bottom and side wall of the domain were set as slip walls and only half of the domain was modelled to reduce computation time since the

Table. 3
Grid spacing uncertainty analysis summary.

Variable	r_G	Solutions			R_G	Convergence	U_G (%S_{G1})
		S_{G3}	S_{G2}	S_{G1}			
Ship speed (Fr_h)	$\sqrt{2}$	0.5672	0.5545	0.5528	0.333	MC	1.02
AP sinkage (m)	$\sqrt{2}$	4.75×10^{-2}	4.49×10^{-2}	4.39×10^{-2}	0.226	MC	6.80
FP sinkage (m)	$\sqrt{2}$	2.51×10^{-2}	2.37×10^{-2}	2.33×10^{-2}	0.242	MC	3.23

Table. 4
Time-step uncertainty analysis summary.

Variable	r_G	Solutions S_{T3}	S_{T2}	S_{T1}	R_G	Convergence	U_G (%S_{T1})
Ship speed (Fr_h)	2	0.5631	0.5503	0.5528	−0.20	OC	1.16
AP sinkage (m)	2	4.67×10^{-2}	4.21×10^{-2}	4.39×10^{-2}	−0.41	OC	5.17
FP sinkage (m)	2	2.43×10^{-2}	2.21×10^{-2}	2.33×10^{-2}	−0.54	OC	4.66

Table. 5
Validation results.

Sinkage	U_{SN} (%)	U_D (%)	U_V (%)	E (%)
AP	8.54	5.00	9.90	5.93
FP	5.67	5.00	7.60	9.00

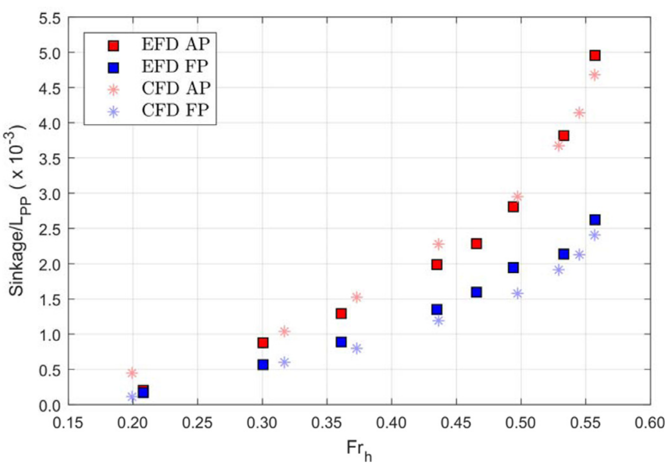

Fig. 4. Plot of CFD AP and FP sinkage predictions against the benchmark EFD AP and FP sinkage [30].

domain is laterally symmetrical. Justification for the full scale self-propulsion modelling is discussed in section 0. Two variations of the new computation domain were made where one was modelled at a scale of 1:59.4 and the other was modelled at full scale. In both cases, the physics settings were kept similar, except that the full scale mesh was scaled up by 59.4 times and have additional prism layers to maintain reasonable $y+ > 30$ value. The mesh generated for the model scale domain and full scale domain have 1,048,748 cells and 1,677,894 cells respectively and are also visually identical as shown in Fig. 6.

The deep water resistance test was conducted for ship speed corresponding to full scale speed of 25 knots. Fig. 7 compares the free surface elevation between the full scale and model scale CFD predictions. The wake pattern is identical for both scales but the divergent waves from the bow and stern of the full scale condition appear to be larger in magnitude compared to that of the model scale. This is due to the higher viscous effect at model scale causing a greater loss of the kinetic energy of the flow in model scale conditions, which results in lower pressure recovery and subsequently smaller wake magnitude [10].

The ITTC 1978 formulae were used to calculate the total resistance coefficient, C_T, the frictional resistance coefficient, C_F, and residuary resistance coefficient, C_R, as shown below where the form factor, k for the model scale hull is 0.094 and that of the full scale hull is 0.145 as computed by Moctar et al. [29]:

$$C_T = R_T/(0.5\rho SV^2) \tag{13}$$

$$C_F = 0.075/(\log_{10}\mathrm{Re}-2)^2 \tag{14}$$

$$C_R = C_T - (1+k)C_F \tag{15}$$

As stated in the ITTC 1978 procedure, the model scale EFD resistance was extrapolated to full scale using the above equations and assuming that C_R is identical in both model scale and full scale conditions. Table 6 summarises the resistance results from the CFD predictions to the benchmark EFD for both model scale and full scale conditions. Overall, the C_T difference between CFD and EFD in model scale condition is approximately 6.35%, whereas for the full scale condition is 5.96%. Therefore, the full scale simulation has been successfully validated against the benchmark EFD extrapolation. This observation demonstrates the feasibility of URANS CFD in full scale computations and that the current full scale CFD model is viable for further investigations.

5.2. Full scale confined water resistance validation

It may be argued that validation of the full scale set-up in deep water may not necessarily reflect validated flow physics in confined water conditions, such as that in the canal benchmark investigation presented by Mucha et al. [30]. Thus, validation of full scale resistance in a confined water condition was undertaken by computing the full scale resistance in the same canal domain shown in Fig. 1 with $h/T = 1.23$. The analysis was undertaken at $Fr_h = 0.557$. However, in order to ensure accurate resistance prediction in confined water, the steady-state sinkage and trim of the moving hull must be accounted for [27]. Hence, in the resistance simulations conducted, the hull is repositioned to the steady-state squat predicted in Fig. 4. The deep water resistance data presented by Moctar et al. [29] was extrapolated to full scale and the Landweber [25] method was used to adjust the data to represent a confined water case for the purpose of comparing against the CFD predictions.

According to Pompée [32], Landweber's method is an extension of Schlichting's formula which assumes that the wave length in shallow water of depth h at a speed of V_I (Schlichting's intermediate speed) is the same as the wave length in deep water at speed of V_∞ and hence the residuary resistance at the speed V_I will be equal to the residuary resistance at the speed of V_∞ in deep water, yielding the below equation:

$$\frac{V_I}{V_\infty} = \sqrt{\tanh\left(\frac{gh}{V_\infty^2}\right)} \tag{16}$$

R_{Th}, the total resistance at shallow water of depth h at speed of V_h (the actual shallow water speed of interest) is then the sum of R_{FI}, the frictional resistance at speed of V_I and $R_{R\infty}$, the residuary resistance at speed of V_∞:

$$R_{Th} = R_{FI} + R_{R\infty} \tag{17}$$

The ratio of V_h/V_I with respect to the hull and canal geometry has been determined experimentally by Landweber [25] as shown in Fig. 10.

In Fig. 8, A_X is the maximum immersed section area of the ship and R_h is the hydraulic radius calculated as shown below, where b is the breadth of the canal and p is the perimeter of the maximum immersed section of the ship.

$$R_h = \frac{bh - A_X}{b + 2h + p} \tag{18}$$

The outcome of the full scale confined water resistance estimation

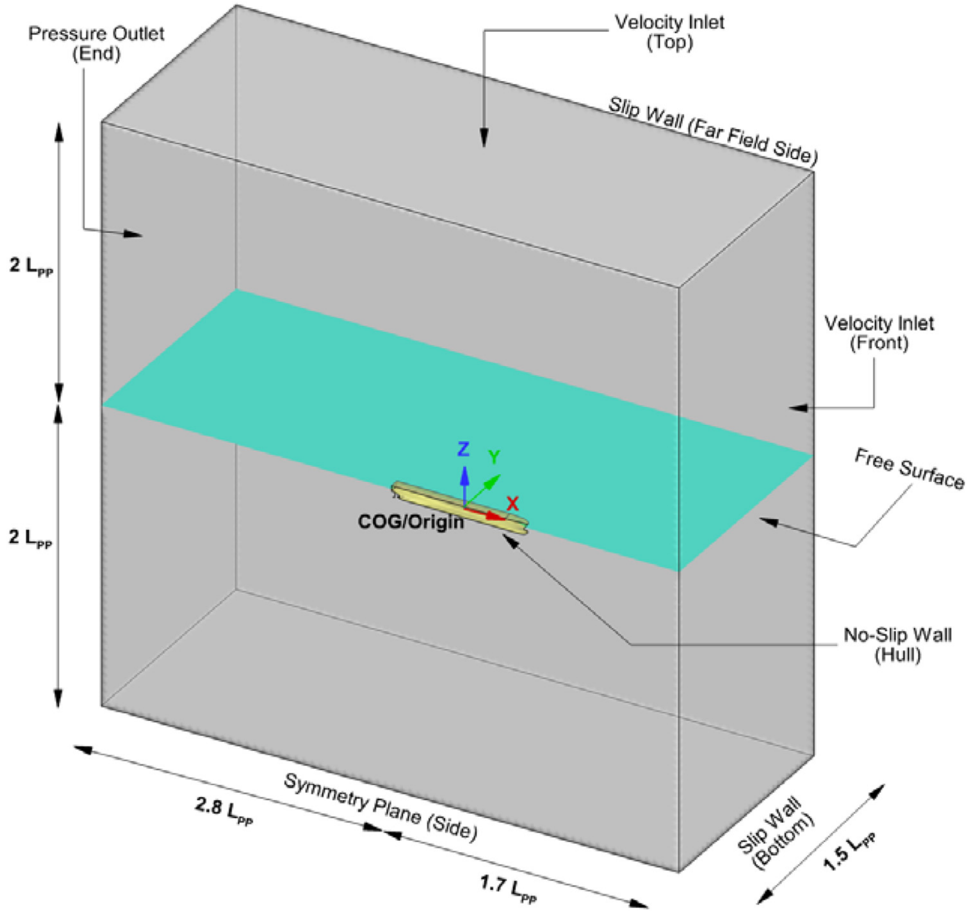

Fig. 5. The computation domain for deep water resistance prediction (similar for both model scale and full scale cases).

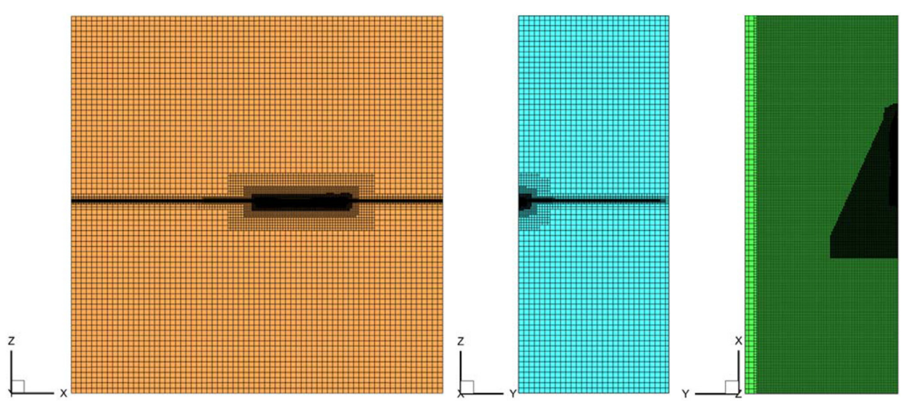

Fig. 6. The mesh generated for the computation domain viewing from (left to right) the symmetry plane, the front end and the free surface plane.

using the Landweber [25] method in comparison with the CFD prediction is shown in Fig. 9. The relative differences in confined water total resistance between Landweber's estimations and the CFD predictions are approximately 13–3%. The said differences are considerably reasonable considering that the Landweber [25] method is an engineering approximation and that the full scale deep water resistance inputted in the method was extrapolated from model scale. Thus, it can be said that the full scale confined water CFD squat model presented in this study is sufficiently accurate for the intended prupose.

5.3. Scale effect in squat results

Based on the validated full scale CFD squat model in confined water, CFD simulations are performed at model scale and full scale in confined water. The results are compared to establish if the non-dimensional squat is different for the two cases. The same full scale CFD model implemented in the confined water resistance study was modified such that the ship is self-propelled by means of a body force propulsion technique similar to that applied in the model scale squat verification and validation study. In this investigation, scale effect of propeller action was assumed to be negligible based on multiple findings suggesting that the scale effect of thrust for propellers without skew is approximately 6% or lower [22,24,33]. Figs. 10 and 11 depicts the results of the full scale squat in comparison to that of the model scale condition for $h/T = 1.23$ and $h/T = 1.10$ respectively.

It can be seen that the difference in non-dimensional squat between

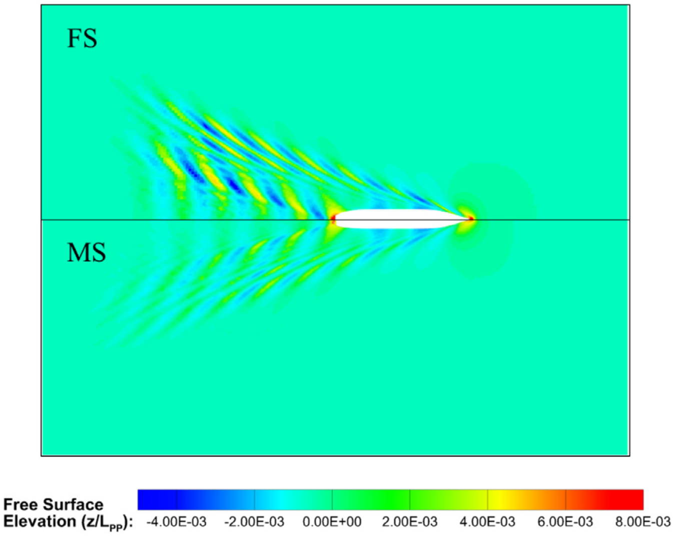

Fig. 7. Free surface elevation comparison between full scale and model scale deep water CFD computations.

Table. 6
Comparison of resistance results from CFD and benchmark EFD.

Case Model scale	R_T (N)	C_T (x10^{-3})	Relative difference (%)
EFD MS	31.83	3.670	6.35
CFD MS	33.85	3.909	
Full scale			
EFD FS extrapolation	3.299×10^6	1.814	5.96
CFD FS	3.490×10^6	1.922	

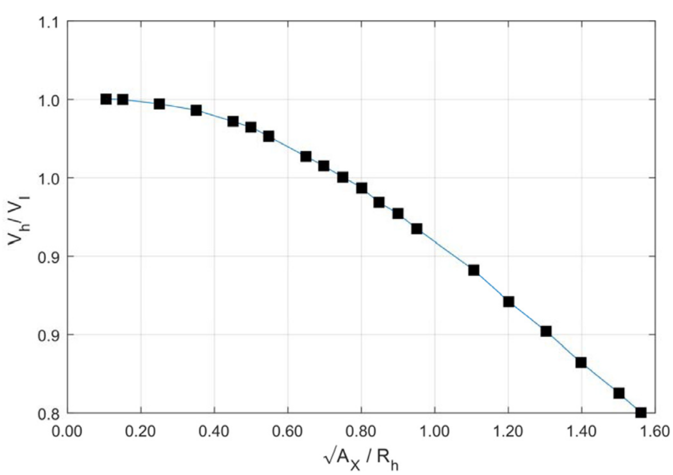

Fig. 8. Experimental data depicting the relationship between V_h/V_I and $\sqrt{A_X}/R_h$ presented by Landweber [25].

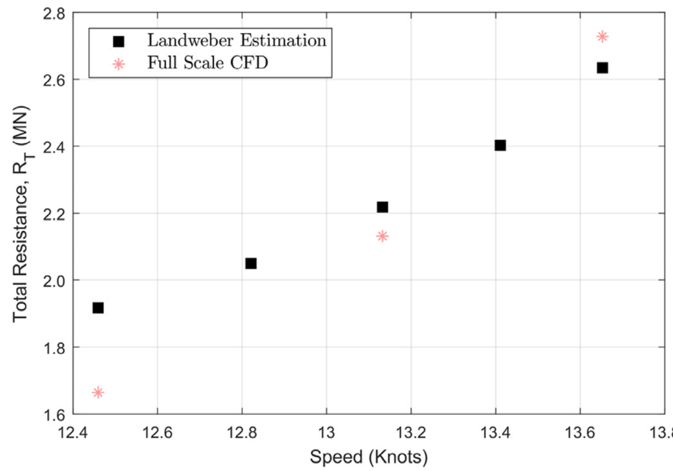

Fig. 9. Confined water resistance comparison between Landweber [25] estimation of the extrapolated benchmark resistance data against full scale CFD prediction.

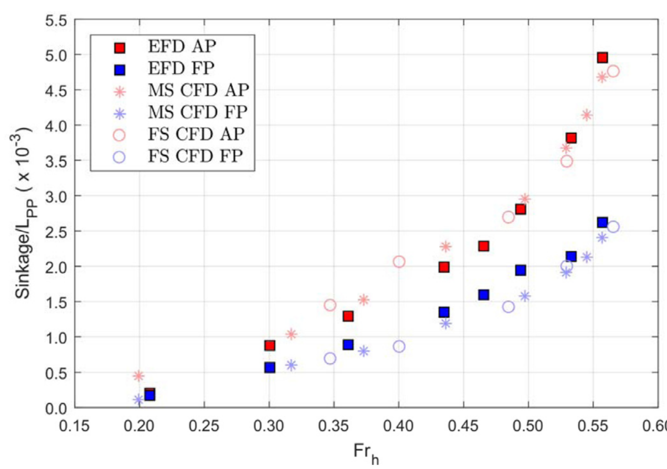

Fig. 10. Comparison of model scale and full scale CFD AP and FP sinkage against that of the benchmark EFD at h/T = 1.23 [30].

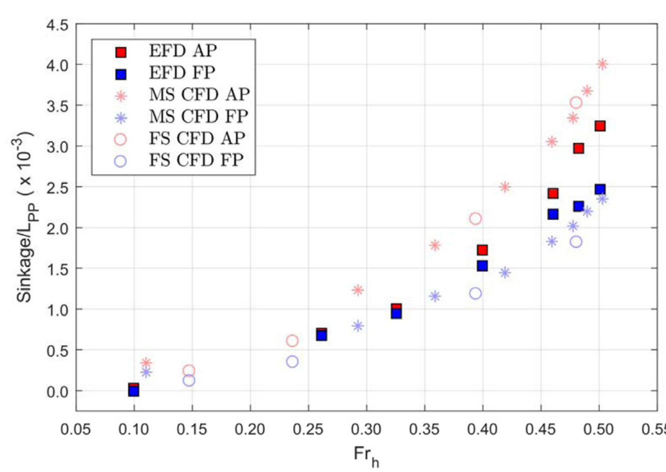

Fig. 11. Comparison of model scale and full scale CFD AP and FP sinkage against that of the benchmark EFD at h/T = 1.10 [30].

full scale and model scale condition is negligible for both h/T = 1.23 and h/T = 1.10. For instance, at h/T = 1.23 and Fr_h = 0.53, the difference between full scale and model scale non-dimensional squat is only 5.32%. Fig. 12 shows that the wake pattern for h/T = 1.23 at Fr_h = 0.53 between full scale and model scale are nearly identical but the midship trough directly adjacent to the model scale hull sides is slightly greater in magnitude than the full scale condition. The low dynamic pressure acting on the bottom of both the full scale and model scale hulls are also relatively similar (refer to Fig. 13). For h/T = 1.10, despite the fact that both model scale and full scale CFD predictions are overestimated relative to the benchmark data, the difference in squat between the two CFD scales are still insignificant. The minimal scale effect in squat noticed is likely due to the fact that the Bernoulli wave around the hull is a more dominant factor which obeys the Froude

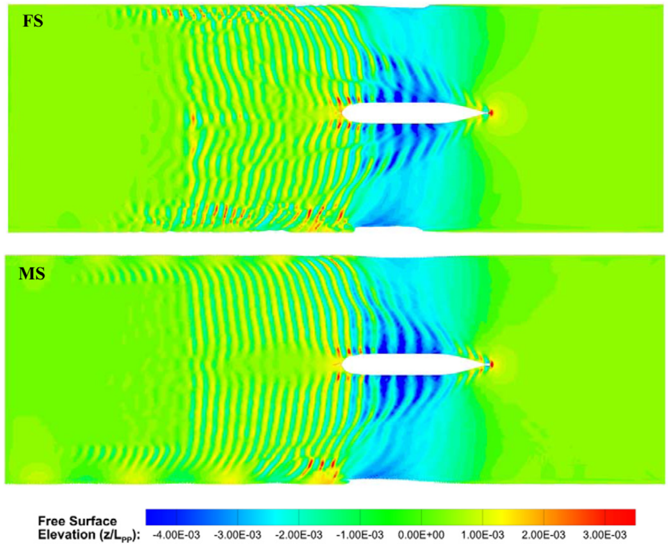

Fig. 12. Plan view of free surface elevation comparison between full scale and model scale conditions in confined water for $h/T = 1.23$ at $Fr_h = 0.53$.

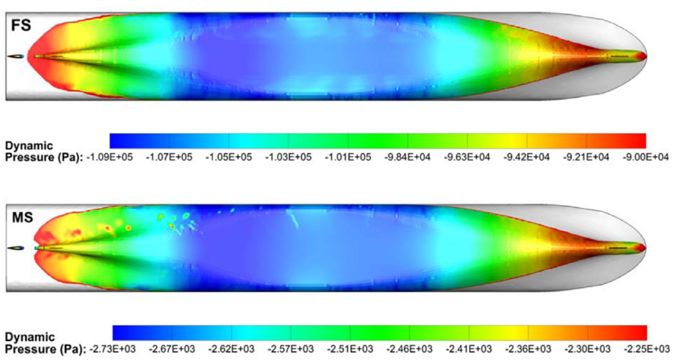

Fig. 13. The dynamic pressure distribution on the bottom of the full scale and model scale hulls in confined water for $h/T = 1.23$ at $Fr_h = 0.53$.

Table. 7
The representative hull for CFD computation for each transit case base on the measured dynamic trim.

Ship	DTC	Case A	Case B
L_{PP}/B	6.96	8.72	7.86
B/T	3.64	2.76	3.64
L_{PP}/T	25.36	24.07	28.58
C_B	0.661	0.671	0.594
Dynamic trim	By Stern	By Stern	By Stern

scaling law and it is conserved in both model and full scale conditions.

6. Full scale case studies

Since having established that non-dimensional squat it similar for full scale and model scale simulations, the self-propelled URANS CFD approach will be compared to full scale squat measurements to assess the accuracy and capability of the method. The CFD simulations will be conducted at model scale as they are less computationally intensive then full scale simulations. CFD predictions are compared to full scale squat measurements for 2 container ships. The full scale measurements are provided by OMC International and were obtained using three global navigation satellite system (GNSS) receivers; one on the starboard bridge wing, one on the port bridge wing and another by the bow.

The hull form geometry of each case was unavailable and due to the lack of different modern benchmark container ship hull forms available, the two transit case hulls were approximately represented in the simulations using the same DTC hull (see Table 7). The chosen representative hulls were then scaled to match the length (L_{PP}), beam and draft of the actual ship in model scale (1:40). The bathymetries in the two transit cases were simplified as restricted channels of varying depth and width with respect to the respective bathymetry soundings.

Using the model scale simulations, sinkage and trim predicted for various water depth to draught ratios and speeds were collected to obtain an empirical trend specific to that particular transit case. This CFD-derived empirical trend is then used to produce a continuous prediction of AP and FP sinkages over the course of the transit. The results of the CFD-derived empirical prediction in comparison to the actual transit measurements are illustrated in Figs. 14 and 15. It can be observed that there is good correlation between the model scale CFD predicted squat and the measured squat albeit that the CFD models have modified and approximated hull forms of the actual hull, simplified bathymetry, neglection of current and neglection of dynamic motion effects. Hence, the implementation of model scale CFD for full scale container ship squat prediction is a viable option.

7. Concluding remarks

The study of scale effect in confined water self-propelled container ship squat has been undertaken in this investigation using commercial URANS solver STAR-CCM+. The cases investigated were based on an asymmetric canal benchmark case [30]. Firstly, model scale simulations with body-force actuator disc self-propulsion for the said case at $h/T = 1.23$ were conducted, verified and validated against the benchmark EFD data. Full scale simulations were then undertaken. The credibility of the full scale simulation set-up was investigated by computing and comparing the full scale CFD deep water bare hull resistance against the full scale extrapolation of benchmark model scale bare hull resistance presented by Moctar et al. [29]. Further examination of the full scale simulation's credibility in confined water was undertaken by computing the resistance of the bare hull in the aforementioned asymmetric canal and comparing against the approximated confined water resistance calculated using the Landweber [25] method.

Having successfully proven the reliability of the full scale simulation, the full scale CFD model was modified with body-force actuator disc to account for self-propulsion effects during squat computations. Comparison of non-dimensional full scale squat predictions against non-dimensional model scale predictions for $h/T = 1.23$ and $h/T = 1.10$ shows negligible differences (approximately 5.32%). This demonstrates that scale effect is negligible for the cases tested in this study and thus, further model scale simulations of actual full scale container ship squat measurements were conducted. Two transit cases were investigated and the CFD-predicted squat can be seen to have good correlation with the measurements. Therefore, scale effect in container ship squat has been shown to be negligible in this study and the implementation of model scale CFD simulations to predict full scale container ship squat is encouraging.

CRediT authorship contribution statement

Zhen Kok: Formal analysis, Investigation, Writing - original draft. **Jonathan Duffy:** Supervision, Conceptualization, Writing - review & editing. **Shuhong Chai:** Supervision, Writing - review & editing. **Yuting Jin:** Methodology, Visualization, Writing - review & editing. **Mohammadreza Javanmardi:** Resources, Writing - review & editing.

Declaration of Competing Interest

The authors declare that they have no known competing financial

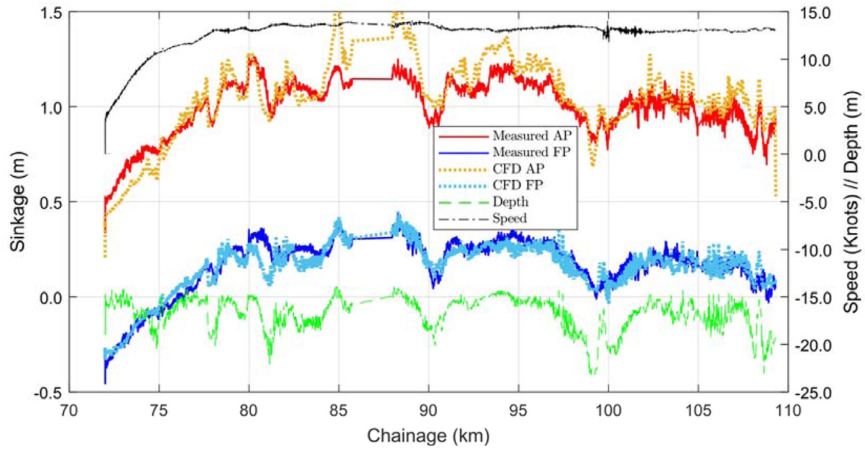

Fig. 14. Plot of Case A squat measurement (OMC International, 2003) in comparison to the CFD prediction.

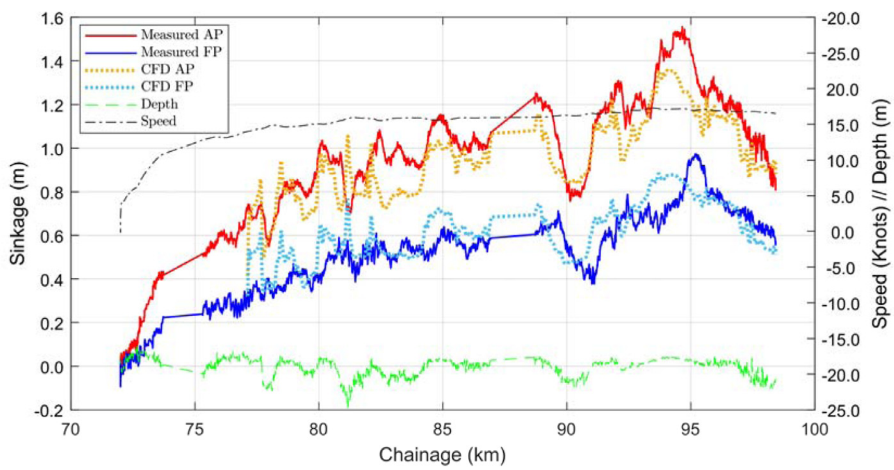

Fig. 15. Plot of Case B squat measurement (OMC International, 2003) in comparison to the CFD prediction.

interests or personal relationships that could have appeared to influence the work reported in this paper.

Acknowledgements

The authors acknowledge the resources provided by NCMEH Australian Maritime College, University of Tasmania and the Tasmanian Partnership for Advanced Computing for the HPC for performing the computations. The authors would also like to acknowledge OMC International for sharing full scale squat measurement data for the benefit of this research.

Supplementary materials

Supplementary material associated with this article can be found, in the online version, at doi:10.1016/j.apor.2020.102143.

References

[1] C. Barrass, "The phenomena of ship squat, Int. Shipbuild. Progress 26 (294) (1979).
[2] R.F. Beck, J.N. Newman, E.O. Tuck, "Hydrodynamic forces on ships in dredged channels, J. Ship Res. 19 (03) (1974) 166–171.
[3] CD-Adapco. 2014. User guide STAR-CCM+ Version 9.0.6.
[4] L. Cong, C. Hsiung, "Computing wave resistance, wave profile, sinkage and trim of transom stern ships, Proceedings of the Third International Conference on Computer Aided Design, Maunfacture and Operation in the Marine and Offshore Industries (CADMO 91), Key Biscayne, 1991, pp. 99–112.
[5] T. Constantine, "On the movement of ships in restricted waterways, J. Fluid Mech. 9 (1960) 247–256.
[6] I. Dand, A. Ferguson, "The Squat of Full Ships in Shallow Water.", National Physical Lab Teddington, England, 1973 Ship Div.
[7] G. Delefortrie, M. Vantorre, K. Eloot, J. Verwilligen, E. Lataire, "Squat prediction in muddy navigation areas, Ocean Eng. 37 (2010) 1464–1476, https://doi.org/10.1016/j.oceaneng.2010.08.003.
[8] G. Deng, E. Guilmineau, A. Leroyer, P. Queutey, M. Visonneau, J. Wackers, "Simulation of container ship in shallow water at model scale and full scale, Proceedings of the 3rd National CFD Workshop for Ship and Offshore Engineering. Dalian, China, 2014.
[9] J. Duffy, M. Renilson, "An investigation into the effect of propulsion on ship squat, Ocean. Eng. Int. 4 (2000) 1–12.
[10] N. Eryuzlu, Y. Cao, F. D'agnolo, "Underkeel requirements for large vessels in shallow waterways, Proceedings of the PIANC Proceedings 28th International Congress, Section II, Seville, Spain, 1994.
[11] M. Fuehrer, K. Römisch, "Effects of modern ship traffic on islands and ocean waterways and their structures, 24th International Navigation Congress, PIANC, Leningrad, USSR, 1977, pp. 236–244.
[12] L. Gilligan, Investigation into scale effects when extrapolating model scale ship squat measurements, University of Tasmania, Tasmania, Australia, 2015 Bachelor of Engineering (Hons) Thesis.
[13] T. Gourlay, K. Klaka, "Full-scale measurements of containership sinkage, trim and roll, Aust. Nav. Archit. 11 (2) (2007) 30–36.
[14] T.P. Gourlay, J.H. Ha, P. Mucha, K. Uliczka, "Sinkage and trim of modern container ships in shallow water, Proceedings of the Australasian Coasts & Ports Conference 2015, Auckland, New Zealand, 2015.
[15] J.H. Ha, T. Gourlay, Validation of container ship squat modeling using full-scale trials at the Port of Fremantle, J. Waterway Port Coast. Ocean Eng. 144 (1) (2017) 04017037.
[16] A. Harting, J. Reinking, "SHIPS: a new method for efficient full-scale ship squat determination, Proceedings of the 30th PIANC-AIPCN Congress 2002, (2002) Sydney, N.S.W. Australia.
[17] J. Hooft, "The behaviour of a ship in head waves at restricted water depths, Int. Shipbuild. Prog. 21 (244) (1974) 367–390.
[18] O. Huuska, "On the evaluation of underkeel clearances in Finnish waterways", University of Technology, Ship Hydrodynamics Laboratory, HelsinkiOtaniemi, 1976 Report, 9.
[19] J. Jachowski, Assessment of ship squat in shallow water using CFD, Arch. Civ.

Mech. Eng. 8 (1) (2008) 27–36.
[20] Y. Jin, J. Duffy, S. Chai, C. Chin, N. Bose, URANS study of scale effects on hydrodynamic manoeuvring coefficients of KVLCC2, Ocean Eng. 118 (2016) 93–106.
[21] Y. Jin, J. Duffy, S. Chai, A.R. Magee, DTMB 5415M dynamic manoeuvres with URANS computation using body-force and discretised propeller models, Ocean Eng. 182 (2019) 305–317.
[22] T. Kawamura, K. Ouchi, T. Nojiri, Model and full scale CFD analysis of propeller boss cap fins (PBCF), J. Mar. Sci. Technol. 17 (4) (2012) 469–480.
[23] Kok Z., Duffy J., Chai S., & Jin Y. (in press). "Multiple approaches to numerical modelling of container ship squat in confined water". J. Waterway, Port, Coastal Ocean Eng. doi: 10.1061/(ASCE)WW.1943-5460.0000580.
[24] V. Krasilnikov, J. Sun, K.H. Halse, "CFD investigation in scale effect on propellers with different magnitude of skew in turbulent flow, Proceedings of the The First International Symposium on Marine Propulsors, Trondheim, 2009.
[25] L. Landweber, "Tests of a Model in Restricted Channels", David Taylor Model Basin, Washington DC, 1939.
[26] E. Lataire, M. Vantorre, G. Delefortrie, "A prediction method for squat in restricted and unrestricted rectangular fairways, Ocean Eng. 55 (Supplement C) (2012) 71–80, https://doi.org/10.1016/j.oceaneng.2012.07.009.
[27] F. Linde, A. Ouahsine, N. Huybrechts, P. Sergent, "3D numerical simulation of ship resistance in restricted waterways including ship squat effects, Proceedings of the Congrès français de mécanique, Lyon, France, 2015.
[28] A. Millward, "Comparison of the theoretical and empirical prediction of squat in shallow water, Int. Shipbuild. Prog. 39 (417) (1992) 69–78.
[29] Oe. Moctar, V. Shigunov, T. Zorn, "Duisburg test case: post-panamax container ship for benchmarking, Ship Technol. Res. 59 (3) (2012) 50–64.
[30] P. Mucha, O. el Moctar, C.-U. Böttner, "PreSquat–workshop on numerical prediction of ship squat in restricted waters, Ship Technol. Res. 61 (3) (2014) 162–165.
[31] P. Naghdi, M. Rubin, "On the squat of a ship, J. Ship Res. 28 (2) (1984) 107–117.
[32] P.-J. Pompée, "About modelling inland vessels resistance and propulsion and interaction vessel-waterway key parameters driving restricted/shallow water effects, Proceeding of Smart Rivers 2015, (2015) Buenos Aires, Argentina.
[33] A. Sánchez-Caja, J. González-Adalid, M. Pérez-Sobrino, T. Sipilä, "Scale effects on tip loaded propeller performance using a RANSE solver, Ocean Eng. 88 (2014) 607–617, https://doi.org/10.1016/j.oceaneng.2014.04.029.
[34] J.B. Schijf, "Protection of embankments and bed in inland and maritime waters, and in overflows or weirs, Proceedings of the PIANC 17th International Navigation Congress 1949, Lisbon, 1949 Section SI C2.
[35] F. Stern, R.V. Wilson, H.W. Coleman, E.G. Paterson, "Comprehensive approach to verification and validation of CFD simulations—part 1: methodology and procedures, J. Fluids Eng. 123 (4) (2001) 793–802.
[36] T. Tezdogan, Y.K. Demirel, P. Kellett, M. Khorasanchi, A. Incecik, O. Turan, "Full-scale unsteady RANS CFD simulations of ship behaviour and performance in head seas due to slow steaming, Ocean Eng. 97 (2015) 186–206.
[37] T. Tezdogan, A. Incecik, O. Turan, "A numerical investigation of the squat and resistance of ships advancing through a canal using CFD, J. Mar. Sci. Technol. 21 (1) (2016) 86–101.
[38] E. Tuck, Shallow-water flows past slender bodies, J. Fluid Mech. 26 (1) (1966) 81–95.
[39] E. Tuck, "Sinkage and trim in shallow water of finite width, Schiffstechnik (1973) 14.
[40] R.V. Wilson, F. Stern, H.W. Coleman, E.G. Paterson, "Comprehensive approach to verification and validation of CFD simulations—Part 2: Application for RANS simulation of a cargo/container ship, J. Fluids Eng. 123 (4) (2001) 803–810.
[41] J.X. Yao, Z.J. Zou, "Calculation of ship squat in restricted waterways by using a 3D panel method, J. Hydrodyn. Ser. B (English Ed.) 22 (5) (2010) 489–494 Ser. B.
[42] Z.H. Zhang, H. Deng, C. Wang, "Analytical models of hydrodynamic pressure field causing by a moving ship in restricted waterways, Ocean Eng. 108 (2015) 563–570.

Applied Ocean Research 109 (2021) 102563

Contents lists available at ScienceDirect

Applied Ocean Research

journal homepage: www.elsevier.com/locate/apor

Numerical parametric study of medium sized container ship squat

Zhen Kok [a,*], Jonathan Duffy [a], Shuhong Chai [a], Yuting Jin [b], Mohammadreza Javanmardi [c]

[a] National Centre for Maritime Engineering and Hydrodynamics, Australian Maritime College, University of Tasmania, Launceston, Tasmania, 7250, Australia
[b] Technology Centre for Offshore and Marine Singapore, 12 Prince George's Park, Singapore, 118411, Singapore
[c] OMC International, 126 Trenery Crescent, Abbotsford, Victoria 3067, Australia

ARTICLE INFO

Keywords:
Ship squat
Principal particulars
URANS
Self propulsion
Shallow water

ABSTRACT

A numerical investigation has been undertaken to study the impact of varying a container ship's principal particulars on squat in shallow water. Initially, a statistical review of the principal particulars of commonly operating container ships is discussed and used to determine the range for length-to-beam ratio (L/B), beam-to-draft ratio (B/T) and block coefficient (C_B) to be analysed systematically. Unsteady RANS CFD simulations are adopted to predict the squat of a self-propelled S175 container ship where the approach is successfully verifed and validated against benchmark experimental data. The same methodology is adapted to a KCS hull as a representation of modern container ships and systematic parametric transformations are conducted to study the effect of varying L/B, B/T and C_B on squat. The results show that sinkage and trim are inversely related to L/B while sinkage is independent of B/T, but trim is inversely related to B/T. Sinkage is also found to be independent of C_B whereas trim magnitude becomes increasingly stern down when C_B increases due to the nature of the parametric transformations in this study. It is identified in this study that the relative position of the LCB to the LCF is responsible for the change in trim direction. Most empirical predictions show similar trends for varying L/B and B/T but contradicting trends are observed for varying C_B.

1. Introduction

In the competitive nature of the container shipping industry, economies of scale is a fundamental tactic which can help reap substantial cost savings by introducing larger container ships that have lower unit costs. The substantial cost savings contribute to considerable decrease in maritime transport cost which in turn facilitates trade (Merk, 2018). Consequently, the increase in container ship size has accelerated and this growth can be seen in Fig. 1. This trend has continuously brought challenges to operate larger container ships in relatively shallow approach channels and ports due to the accentuated squat phenomenon in such conditions. Apart from increasing in size, container ship hullform have changed noticeably over the years, including more pronounced bulbous bows, stern bulbs and transom sterns(Gourlay et al., 2015). Even container ships designed within the same generation can have markedly different parameters which are dictated by different priorities and compromises made for many conflicting requirements in the design spiral (Papanikolaou, 2014). Some past studies suggest that subtle changes in hullform can alter squat behaviour (Uliczka and Wezel, 2005). Therefore, it is beneficial to understand the influence of hull principal particulars on squat in shallow water. A reliable CFD numerical investigation can play a vital role to predict squat and avoid grounding accidents, while larger container ships are maneourving into approach channels at different tidal conditions.

Ship squat has been investigated extensively where pioneering investiations were presented by Constantine (1960) regarding the different squat behaviour in open water for subcritical ($Fr_h < 1$), critical ($Fr_h = 1$) and supercritical ($Fr_h > 1$) vessel speeds. A slender-body theory for squat estimation in laterally unrestricted shallow water was developed by Tuck (1966). The work of Tuck (1966) then became the foundation for the development of various other prediction methods such as the work of Beck et al. (1974); Naghdi and Rubin (1984); Cong and Hsiung (1991).

Furthermore, model scale experiments were widely used to aid the study of ship squat, most of which were then used to develop semi-empirical formulae. For example, a semi-empirical prediction technique for full form ships was developed by Dand and Ferguson (1973), whereas Fuehrer and Römisch (1977) presented an empirical formula which accounted for varying cross section parameters of the canal. Empirical corrections for the propulsion effect on bulk carriers were derived by Duffy and Renilson (2000). Similarly, Delefortrie et al.

* Corresponding author at: National Centre for Maritime Engineering and Hydrodynamics, Australian Maritime College, University of Tasmania, Locked Bag 1395, Launceston, Tasmania, 7250, Australia
E-mail address: zhen.kok@utas.edu.au (Z. Kok).

https://doi.org/10.1016/j.apor.2021.102563
Received 13 October 2020; Received in revised form 25 January 2021; Accepted 1 February 2021
Available online 13 February 2021
0141-1187/

Nomenclature

A_E	Propeller expanded area (m^2)
A_O	Propeller disc area (m^2)
A_W	Waterplane area (m^2)
AP	Aft perpendicular (m)
B	Ship beam (m)
C_B	Block coefficient
C_P	Pressure Coefficient $(p - p_0)/(0.5\rho V^2)$
CSA	Cross-sectional Area
D	Propeller diameter (m)
FP	Forward perpendicular (m)
Fr_h	Froude depth number ($Fr_h = V/\sqrt{gh}$)
$\overline{GM_L}$	Longitudinal metacentric height (m)
g	Gravitational constant (m/s^2)
h	Water depth (m)
L	Length between perpendiculars of ship (m)
p	Pressure at the point of interest (N/m^2)
p_0	Ambient pressure in undisturbed flow (N/m^2)
S	Wetted surface area (m^2)
T	Ship draft (m)
$P_{0.7}$	Propeller blade pitch at 0.7 radius (m)
V	Ship speed (m/s)
Δ	Displacement (tonne)
λ	Scale
ρ	Fluid density (kg/m^3)
∇	Volumetric displacement of ship (m^3)

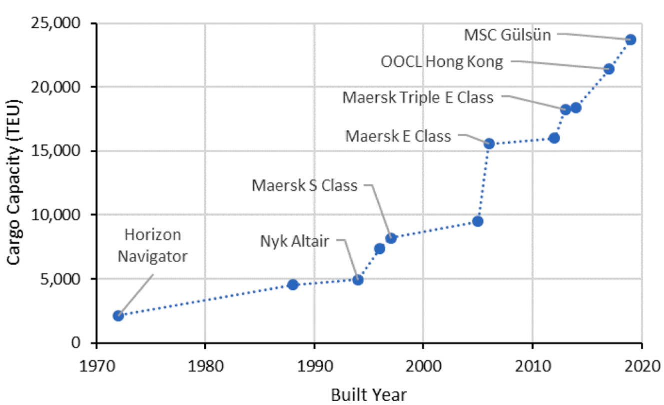

Fig. 1. Flagship container ship cargo capacity trend over a span of 5 decades.

(2010) empirically developed a mathematical model for the effects of muddy bottom and propeller action.

In addition, numerical methods have quickly become favoured in ship squat studies as computation power improves. Potential flow methods have been applied by Yao and Zou (2010); Zhang et al. (2015) to investigate the shallow water hydrodynamics where promising results were obtained for subcritical and supercritical flow but not for trans-critical flow due to neglection of non-linear effects. Jachowski (2008) demonstrated early use of Computational Fluid Dynamics (CFD) for squat prediction where non-linear and viscous effects can be accounted for in laterally unrestricted shallow water. Various other CFD studies have been conducted recently such as investigation of container ships advancing through different canals (Elsherbiny et al., 2020), the study of muddy layer effect on ship resistance and squat (Kaidi et al., 2020) as well as scale effect in squat (Kok et al., 2020c).

Throughout the studies, it is well agreed that bulk carriers tend to trim by the bow when squatting. However, the squat behaviour of container ships is not as well understood as different container ship hull forms may trim either by the bow or stern (Gourlay et al., 2015). Initial suggestions that the block coefficient determines the trim (Barrass, 1979) proved otherwise as Uliczka and Wezel (2005) pointed out that the trim depends on hull form details and, vessels with the same block coefficient but a subtly different hull form may exhibit different trim direction.

Given that subtle changes to hullform can cause substantial difference in squat and that the container ship hull design parameters can vary significantly, it is beneficial to understand the effect of manipulating certain design variables on squat. Currently, there are no literature discussing the sensitivity of squat to ship design parameters particularly that of a modern container ship hullform. Thus, this paper aims to investigate the influence of modern container ship principal particulars on squat by means of unsteady Reynolds Averaged Navier-Stokes (URANS) simulations.

Table 1
Statistics of different ships visiting/departing an Australian port (OMC International, 2018). The non-dimensional parameters here are used as the range to be investigated.

Data	Δ (Tonnes)	L (m)	B (m)	T (m)	L/B	B/T	C_B
Average	74,619	268	38.0	11.8	7.11	3.23	0.607
Std. Dev.	9,093	16.7	3.47	0.487	0.690	0.332	0.0421
Max	100,757	293	42.8	13.1	8.80	3.92	0.773
Min	55,708	225	32.2	10.7	6.04	2.47	0.544

The ensuing section presents the deviation in parameters for a sample of medium sized, currently operating container ships (to be used as a reference for the range for each principal particulars) followed by discussion regarding the hull forms and set-ups used in the study. The structure of this paper is such that discussions of the numerical modelling method as well as the verification and validation process are based on a model test of a self-propelled S175 container ship. Upon successful verification and validation, the same method is adapted to the KRISO Container Ship (KCS) hull form which serves as a representation of modern container ships. A systematic parametric investigation of the KCS hull is then conducted to investigate the main objective of this study; the effects of each principal particular on squat. The cause for change in trim direction is discussed. Comparisons with empirical predictions are also presented.

2. Statistics of container ship principal particulars

Sample data of 85 different container ships visiting/departing an Australian port courtesy of OMC International (2018) is used to study the range of parameters of currently operating container ships. Statistics of these ships are provided in Table 1. These container ships are considered medium sized (no ultra large crude carriers involved) and have an average length of 268m with displacement of approximately 75,000 tonnes. A plot of the parametric ratios of these ships are shown in Fig. 2. The statistical study results explicitly indicate that the range of ship parameters, L/B, B/T and C_B of currently operating container ships, are disparate. Thus, this range of parameters is adopted as a basis for the numerical investigation into the influence of hull form on container ship squat.

3. Hull form and set-up

As mentioned, two hullforms are used in the present study; the S175

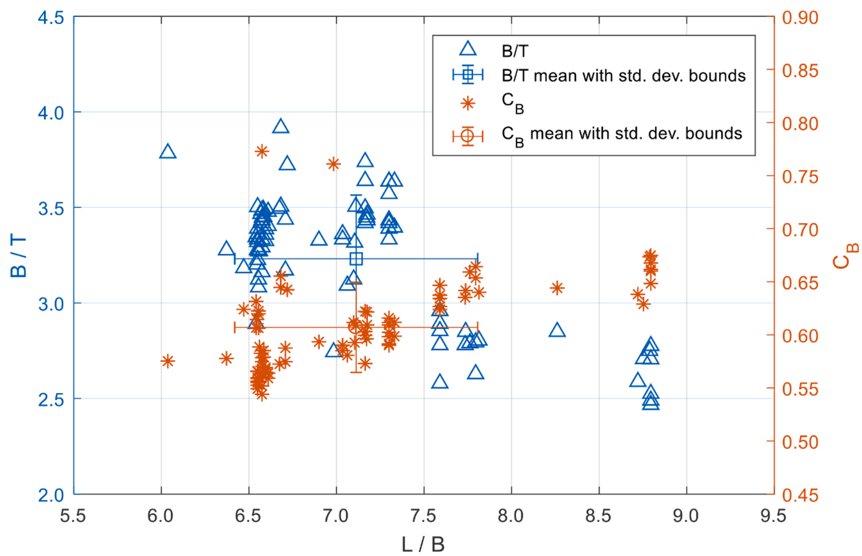

Fig. 2. Parametric variation of 85 container ships visiting/departing an Australian port (OMC International, 2018). The mean of each parameter is shown with standard deviation bounds (B/T or C_B for vertical bound and L/B for horizontal bound).

Fig. 3. Profile view of S175 hull (top) and KCS hull appended with rudder (bottom, not to scale).

Table 2
Principal particulars of the hulls and propellers investigated.

Hull Model Scale	S175 Model Scale (1:70)	S175 Full Scale (1:1)	KCS Model Scale (1:31.6)	KCS Full Scale (1:1)
L (m)	2.50	175	7.28	230
B (m)	0.363	25.4	1.02	32.2
T (m)	0.136	9.50	0.316	10.0
Δ (tonnes)	0.702×10^{-1}	24,070	1.615	50,950
L/B	6.89	6.89	7.14	7.14
B/T	2.67	2.67	3.23	3.23
C_B	0.570	0.570	0.648	0.648
Propeller	Wageningen B-series		SVA - VP1193	
D (m)	0.223	8.92	0.25	7.9
Blades	4	4	5	5
$P_{0.7}/D$	1.275	1.275	1.3	1.3
A_E/A_O	0.55	0.55	0.7	0.7

for verification and validation purposes followed by the KCS as the parent hullform for the ensuing systematic parametric study. The S175 is a well-documented benchmark hullform used in various studies but it is a relatively dated design as discussed by Gourlay et al. (2015). On the contrary, the KCS is one of the very few publicly available benchmark hull form that is considered modern. Although it should still be acknowledged that the KCS design is more than a decade old, the pronounced bow bulb, stern bulb and transom stern features of the KCS are still representative of recent designs (refer to Fig. 3). Therefore, the systematic studies conducted based on the KCS would still be valid for recent designs.

In this study, the S175 is appended with a 4-bladed Wageningen B-series propeller whereas the KCS is appended with a Schiffbau-Versuchsanstalt Potsdam (SVA)-developed VP1193 stock propeller and rudder. The principal particulars of the hull forms and their respective propellers are given in Table 2.

The S175 model test was conducted in the *Australian Maritime College (AMC) 100m x 3.55m Towing Tank*. In the conduct of the experiment, the hull was allowed to sink and trim freely where the sinkage and trim motions were captured using variable differential transducers (LVDTs) on both forward and aft counter-balanced tow posts. The forward post was connected to the vessel using a ball joint whilst the aft post was connected to a ball joint coupled with a linear slide. The forward and aft post connections were positioned along the thrust line to avoid artificial trim. Hama strips were installed near the bow of the model for turbulence stimulation. The model was operated at model scale self-propulsion point in water depth to draft ratio (h/T) of 1.10 and 1.20 at even trim conditions. Part of the results of this model test are used for validation purposes in this study.

Hence, the design of the S175 computation domain is similar to the geometry of the *AMC Towing Tank*. For the KCS simulations, the computation domain is a simple shallow waterway without lateral restrictions so that the effect of hull parametric transformations can be emphasised.

4. Computational method

4.1. Governing equations

In this investigation, the commercial CFD software STAR-CCM+ is used to conduct the computations where the incompressible RANS equation is resolved using the finite volume method of discretisation.

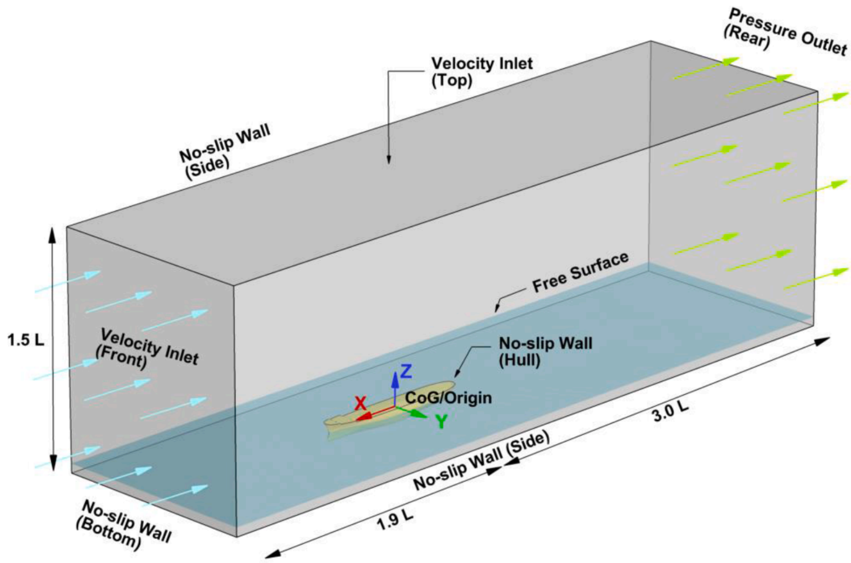

Fig. 4. The computation domain dimensions and boundary conditions.

The free surface effect (air and water phases) is accounted for by implementation of the Volume of Fluid (VOF) method. According to Rusche (2002), the governing equations for two phase incompressible flow are given as:

$$\nabla \cdot \mathbf{u} = 0 \tag{1}$$

$$\frac{\partial \rho \mathbf{u}}{\partial t} + \nabla \cdot [\rho \mathbf{u}\mathbf{u}] = -\nabla p^* - \mathbf{g} \cdot \mathbf{x} \nabla \rho + \nabla \cdot [\mu \nabla \mathbf{u} + \rho \boldsymbol{\tau}] + \sigma_T \kappa_\gamma \nabla_\gamma \tag{2}$$

$$\boldsymbol{\tau} = \frac{2}{\rho} \mu_t \mathbf{S} - \frac{2}{3} k \mathbf{I} \tag{3}$$

In the above equations, $\mathbf{u} = (u,v,w)$ i.e. the velocity field in cartesian coordinates. ∇ is the gradient operator ($\partial/\partial x$, $\partial/\partial y$, $\partial/\partial z$), p^* is the pressure including hydrostatic pressure, ρ is the fluid density which varies with the content of air/water in the computational cells, $\mathbf{g}$ is the gravitational acceleration, μ is the dynamic molecular viscosity, σ_T is the surface tension coefficient and κ_γ is the surface curvature. The term $\boldsymbol{\tau}$ is known as the Reynolds stress tensor where μ_t is the effective dynamic eddy viscosity, $\mathbf{S} = (1/2\,(\nabla \mathbf{u} + (\nabla \mathbf{u})^T))$ is the fluid strain rate tensor, k is the turbulent kinetic energy per unit mass and $\mathbf{I}$ is the identity matrix.

The air and water phases are tracked using the volume of fraction, γ. γ indicates the relative proportion of fluid in each cell and its value is 0 for air, 1 for water or any intermediate value for a mixture of the two fluids. The following advection equation models the distribution of γ:

$$\frac{\partial \gamma}{\partial t} + \nabla \cdot [\mathbf{u}\gamma] + \nabla \cdot [\mathbf{u_r}\gamma(1-\gamma)] = 0 \tag{4}$$

where $\mathbf{u_r} = \mathbf{u_{water}} - \mathbf{u_{air}}$ is the relative velocity. With the implementation of γ, the spatial variation in ρ and μ in the governing equations are defined as:

$$\rho = \gamma \rho_{water} + (1-\gamma)\rho_{air} \tag{5}$$

$$\mu = \gamma \mu_{water} + (1-\gamma)\mu_{air} \tag{6}$$

Closure of the RANS equations is achieved with implementation of the k-ε model with wall function i.e. y+ of above 30 is maintained. The k-ε model is chosen as it is more computationally economical compared against k-ω model (Tezdogan et al., 2016). Furthermore, it is known that the squat prediction is not influenced greatly by different turbulence models nor is it sensitive to different near wall treatments (Deng et al., 2014). Various past studies have also demonstrated good correlations with benchmark data when using k-ε model with wall function (Bechthold and Kastens, 2020; Deng et al., 2014; Kok et al., 2020c; Tezdogan et al., 2016).

4.2. Ship motion and propeller modelling

In this study, ship motion in sinkage and trim are made possible through the use of the Dynamic Fluid Body Interaction (DFBI) module in conjunction with morphing mesh technique. In summary, the resultant forces and moments acting on the hull (rigid body) are computed by the 6-DOF (degrees of freedom) solver and the 6-DOF motion solver then solves the governing equation of rigid body motion but only for sinkage and trim in this case to compute the new position of the hull. The morphing motion variant of the DFBI module is implemented since the squat motion is a relatively small motion which can be efficiently captured by the morphing mesh as proven by Yuan et al. (2019).

In addition, it has been demonstrated in previous studies that propeller action influence container ship squat in confined waters ("confined" is the combination of "shallow" (vertical restriction) and "restricted" (horizontal restriction)). This is particularly observable when $Fr_h > 0.5$ and it is also shown that the body-force propulsion virtual disc module is sufficiently accurate to model the self-propulsion effect (Kok et al., 2020b). Thus, propeller modelling is taken into account in this investigation using the same body-force propulsion virtual disc model. The open water performance curve data for the 4-bladed Wageningen B-series propeller is used for the virtual disc modelling.

4.3. Computational domain, boundary conditions and mesh development

The computation domain is designed in accordance to CD-Adapco (2014) recommendations where the inlet is at least 1 *L* away from the hull and the outlet is at least 2 *L* downstream while maintaining the cross-sectional geometry of the *AMC Towing Tank*. Two variations of the computation domain are produced where one has a depth of $h/T = 1.10$ and another with $h/T = 1.20$ accordingly to the model test.

For both domains, the forward end is assigned as velocity inlet generating flat waves moving at the desired ship velocity while the aft end of the domains are assigned as a pressure outlet to prevent backflow. VOF wave damping of length 1.2 *L* is applied at both inlet and outlet to avoid unrealistic wave reflections. The top wall is set as a velocity inlet to avoid development of velocity gradient. In contrast, the side and bottom walls are set as no-slip walls to capture the development of velocity gradient but with tangential velocity equal to the intended ship

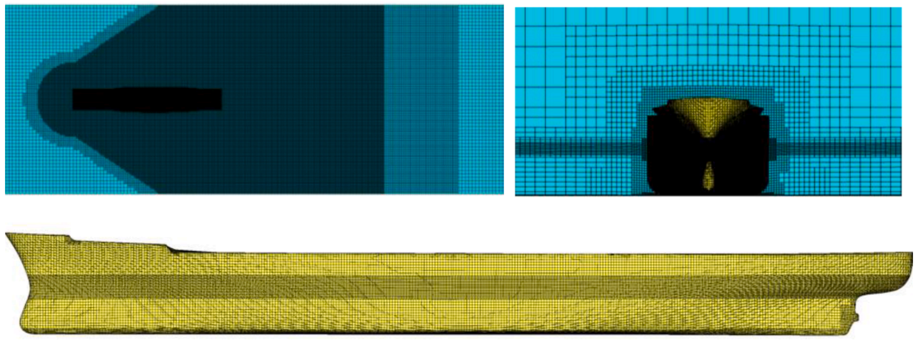

Fig. 5. Top view of the Kelvin wake pattern mesh refinement at the free surface (top left), cross-sectional view of the mesh (top right) and profile view of the hull mesh (bottom).

velocity so that any velocity gradient developed on these boundaries is due to the relative motion of the ship instead of the initial velocity inlet flow. Similarly, no-slip wall condition is applied to the hull surfaces but the tangential velocity is zero relative to the hull itself to mimic forward motion of the hull relative to the body of water. In addition, morphing motion condition is applied on the hull whereas all the remaining domain boundaries are fixed. Fig. 4 depicts the computation domain designed.

The computation grids are developed using the STAR-CCM+ built-in hexahedral trimmed cell mesher, surface remesher and prism layer meshers with reference to CD-Adapco (2014) recommendations for virtual towing tank simulations. Care is taken to refine the hull surfaces, the free surface and the small underkeel clearance to accurately capture the flow physics in these regions. Slow cell growth rate is used to ensure smooth mesh size transition between regions of highly refined mesh and coarser regions. The prism layer mesher is used to maintain a $y+$ value of above 30. The mesh generated for the computation domain is depicted in Fig. 5.

5. Verification and validation

In this study, the verification and validation procedure was conducted based on the triplets method presented by Wilson et al. (2001); Stern et al. (2001). However, only the grid spacing uncertainty (U_G), and time step uncertainty (U_T), were considered whereas iterative uncertainty (U_I), was neglected as the iterative uncertainty for ship motion response simulations in Star-CCM+ URANS solver is less than 0.2% for seakeeping applications (Tezdogan et al., 2015). Hence, the total numerical uncertainty (U_{SN}), was approximated as:

$$U_{SN}^2 = U_G^2 + U_T^2 \tag{7}$$

The convergence study was conducted with triple solutions using systematically refined grid spacing and time step, respectively. For the grid spacing uncertainty study, a refinement ratio of $r_G = \sqrt{2}$ was applied with the shortest time step whereas the time-step uncertainty study was conducted with refinement ratio $r_T = 2$ with the smallest grid spacing. The Courant number (CFL) equation below was used to determine the time-step where Δl is the grid spacing, V is the ship speed and CFL was set to value of 1:

$$\Delta t = \frac{\text{CFL} \times \Delta l}{V} \tag{8}$$

The convergence ratio (R_i), is defined by the solutions of the three grids or time step where S_i ($i = 1,2,3$) are the solutions for smallest, medium and largest grid spacing or time step respectively:

$$R_i = \frac{S_2 - S_1}{S_3 - S_2} \tag{9}$$

The possible outcomes when assessing the convergence ratio (R_i), are as follows:

1) $0 < R_i < 1$, where monotonic convergence has been achieved (MC)
2) $R_i < 0$; $|R_i| < 1$, where oscillatory convergence has been achieved (OC)
3) $1 < R_i$, where divergence has been achieved (D)

No uncertainty estimates can be made for divergent cases (outcome 3) while further calculations of the uncertainty for convergent cases (outcomes 1 and 2) can be referred from similar work presented by Jin et al. (2019).

In the current uncertainty study, the mesh count and time step configurations are as shown in Table 3 while the outcome of the uncertainty study is summarised in Table 4 in which the parameters of interest are the AP and FP sinkage. The condition investigated is where $h/T = 1.10$ and $Fr_h = 0.508$ since very shallow water conditions are more difficult to simulate and it is in the authors' intended future study to conduct the current systematic study in very shallow conditions ($h/T = 1.10$). The successful verification and validation for very shallow conditions will also ensure the reliability of the method in deeper water conditions.

Observations on the change of AP and FP sinkage solutions among the three grid spacings show changes in the order of 0.1mm and the resulting uncertainty is less than 1% and 7% for the AP and FP sinkage, respectively. Similarly, the solutions from the three time steps within the order of 0.1mm and the uncertainties are approximately 1% for both AP

Table 3
Mesh count and time step applied in the verification study.

Configuration	Total Mesh	Time step
Coarse (3)	1,341,079	0.020
Medium (2)	3,021,664	0.014
Fine (1)	7,536,130	0.010

Table 4
Results of the grid spacing and time step uncertainty study.

Variable	r_i	Solutions S_3	S_2	S_1	R_i	Convergence	U_i (% S_1)
Grid Spacing							
AP Sinkage (mm)	$\sqrt{2}$	9.431	9.519	9.448	-0.807	OC	0.46
FP Sinkage (mm)	$\sqrt{2}$	7.863	7.648	7.468	0.834	MC	6.31
Time Step							
AP Sinkage (mm)	2	9.479	9.288	9.448	-0.839	OC	1.01
FP Sinkage (mm)	2	7.535	7.380	7.468	-0.568	OC	1.04

Table 5
Validation results. Experimental uncertainty (U_D) is derived based on the method presented by Duffy (2008).

Sinkage	U_{SN} (%)	U_D (%)	U_V (%)	E (%)
AP	1.11	4.31	4.45	2.91
FP	6.40	1.29	6.52	6.06

and FP sinkage. Thus, the results of the verification study suggests that the current model yields acceptable numerical uncertainties.

In order to validate the numerical model against the experimental data, the following variables were computed; the comparison error (E), the validation uncertainty (U_V) which is the combination of numerical uncertainty (U_{SN}), and experimental uncertainty (U_D) as given below:

$$U_V = \sqrt{U_{SN}^2 + U_D^2} \tag{10}$$

The comparison error (E) is defined as the difference between the experimental data (D) and simulation data (S). Validation of the numerical model is deemed successful if E is less significant than U_V:

$$E = D - S \tag{11}$$

Table 5 shows that the calculated E for both AP and FP sinkage is slightly smaller than U_V. Therefore, validation is successful. Further comparison of the CFD model predictions against the experimental results at different speeds for h/T =1.1 and h/T =1.2 in Fig. 6 also demonstrates good correlation. Having shown that the current method is sufficient for such shallow conditions, it suffices to say that the current method will also be sufficient for the main study which is in slightly deeper waters (h/T =1.3). Further successful benchmarking exercises based on the model test conducted by Gronarz et. al. (2009) which involves the bare hull KCS in h/T of up to 1.3 and Fr_h up to 0.683 are also available in Appendix B.

6. Parametric study

Upon verified and validated the numerical method, further systematic studies of the effect of parametric variations can be conducted. The computation domain for this study is similar to the previous set-up with the exception that the KCS hullform is used instead and the waterway is laterally unrestricted. In order to ensure that the lateral boundaries are sufficiently far away from the vessel, the distance of the side walls are placed greater than the influence width (y_{infl}), as derived by Lataire (2014) in Eq. (12) and slip-wall conditions are applied to these side walls (refer to Fig. 7). It should be noted that all cases are conducted in model scale as scale effects have been shown to be negligible while also being more computationally economical (Kok et al., 2020c).

$$y_{infl} = 5B(Fr_h + 1) \tag{12}$$

The parametric ratios to be investigated are the length-to-beam ratio

Table 6
Range of cases investigated.

Total Cases	L/B	B/T	C_B	h/T	Fr_h
19	6.50–8.60	2.50–3.90	0.648	1.3	0.683
4	7.14	3.22	0.589–0.689	1.3	0.683

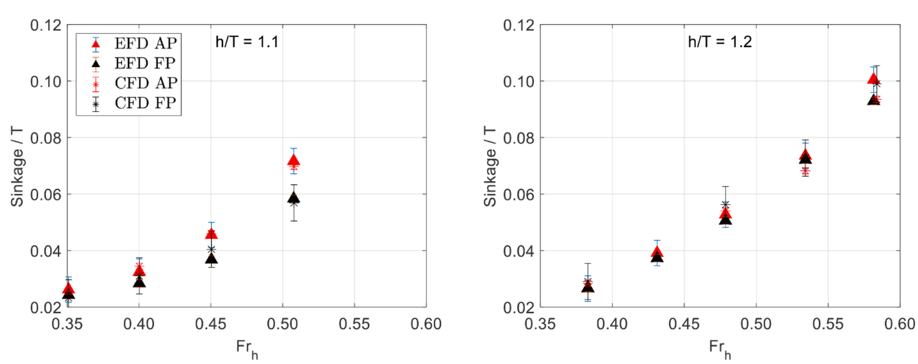

Fig. 6. Comparison of CFD predictions for AP and FP sinkage against EFD results for h/T = 1.1 (left) and h/T = 1.2 (right).

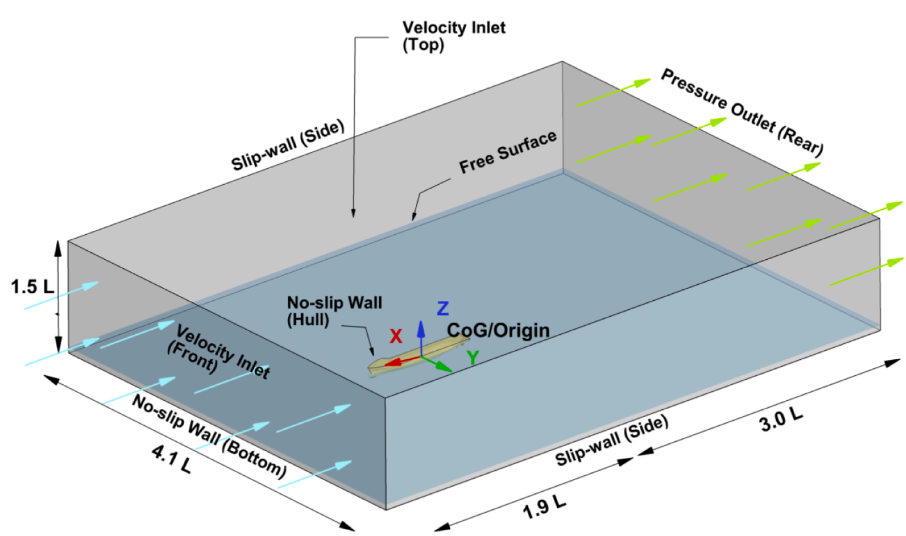

Fig. 7. Computation domain for the systematic study of effect of KCS hull parametric variations on squat.

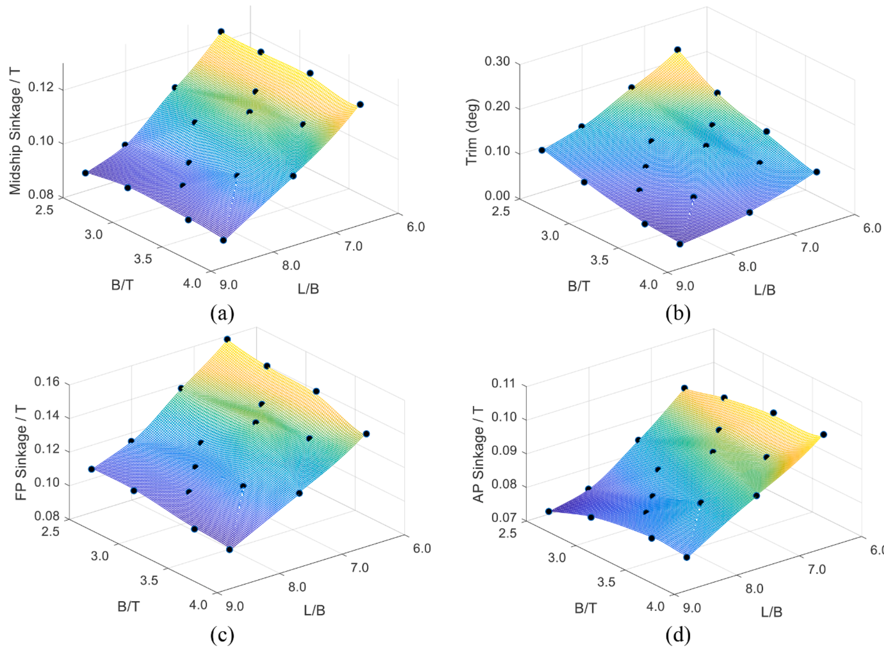

Fig. 8. Surface plot of the changes in (a) midship sinkage/T, (b) trim (positive by the bow), (c) FP sinkage/T, and (d) AP sinkage/T with respect to B/T and L/B for h/T =1.3 at 0.683 Fr_h and fixed C_B of 0.648.

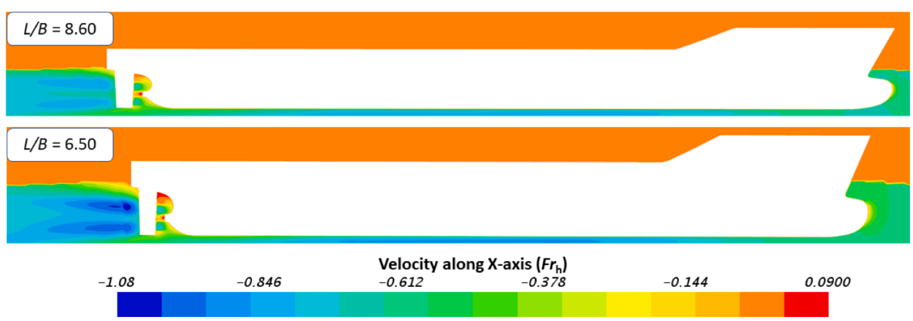

Fig. 9. Comparison of the velocity profile between hulls of varying L/B but equal B/T of 2.50 at 0.683 Fr_h in 1.3 h/T. The slender hull of L/B = 8.60 (top) has relatively lower flow velocity magnitude in the underkeel and wake region in comparison to the stubby hull of L/B = 6.50 (bottom).

(L/B), beam-to-draft ratio (B/T), and block coefficient (C_B), where the range of each ratio is based on the statistics presented previously in section 2. The range of values to be tested are summarised in Table 6. Two sets of systematic investigations are to be investigated; cases with fixed C_B and cases with varying C_B. The cases with fixed C_B includes variations in L/B and B/T while the cases with varying C_B has fixed L/B and B/T . All parametric transformations are completed using the Maxsurf Modeler Advanced version 20 software and conducted such that the displacement is constant for all hulls. Further details of the hulls produced from the parametric transformations are tabulated in

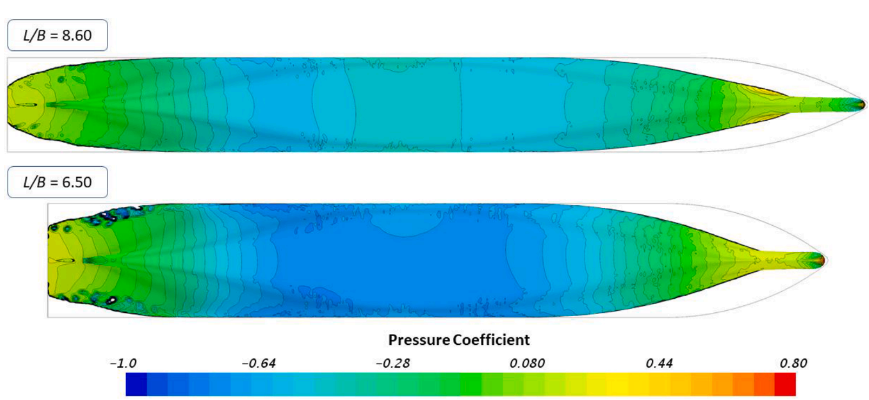

Fig. 10. Comparison of the pressure coefficient contours between the hull of L/B = 8.60 (top) against hull of L/B = 6.50 (bottom) at 0.683 Fr_h in 1.3 h/T. The pressure distribution on the keel of the hull L/B = 6.50 is significantly lower which results in greater sinkage and trim.

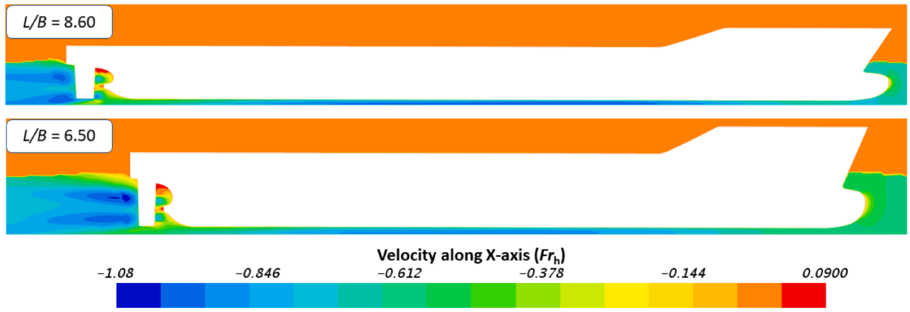

Fig. 11. Comparison of the velocity profile between hulls of varying B/T but equal L/B of 6.50 at 0.683 Fr_h in 1.3 h/T. The wider hull of B/T = 3.90 (top) has relatively similar underkeel flow velocity magnitude in comparison to the deeper hull of L/B = 2.50 (bottom).

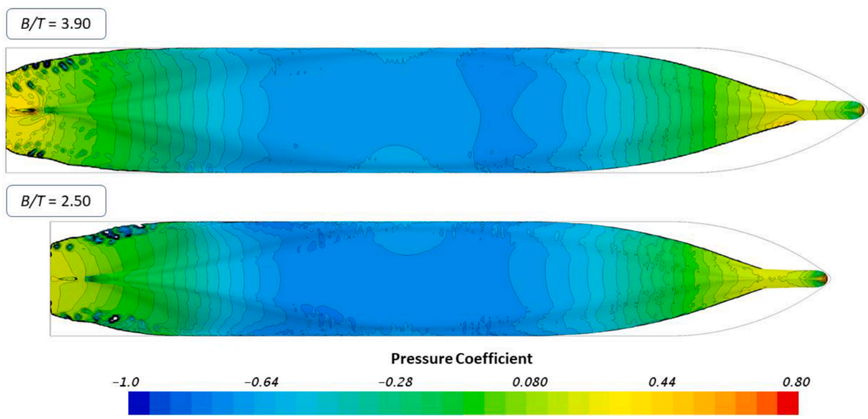

Fig. 12. Comparison of the pressure coefficient contours between the hull of B/T = 3.90 (top) against hull of B/T = 2.50 (bottom) at 0.683 Fr_h in 1.3 h/T. The pressure distribution on the keel of both hulls are fairly similar which effectively yields comparable proportion of sinkage.

Appendix A Table A1.

7. Results

The following section will firstly discuss the results in terms of the effect of varying L/B ad B/T. This is followed by the effect of varying C_B and a discussion regarding the factors affecting trim direction in this study. Finally, a brief comparison between various empirical predictions against the CFD results are examined.

7.1. Effect of L/B & B/T

Fig. 8 depicts the surface plots of the results for fixed C_B cases at h/T =1.3 and Fr_h of 0.683. When the midship sinkage is expressed as a fraction of T, it can be clearly observed in Fig. 8(a) that the midship sinkage/T has an inverse relationship with L/B but is independent from the variation of B/T. On the contrary, trim (by the bow) has an inverse relationship with both L/B and B/T (Fig. 8(b)). Consequently, the maximum sinkage occurs by the FP and Fig. 8(c) demonstrates that the FP sinkage/T increases as L/B and B/T decreases albeit the effect of B/T

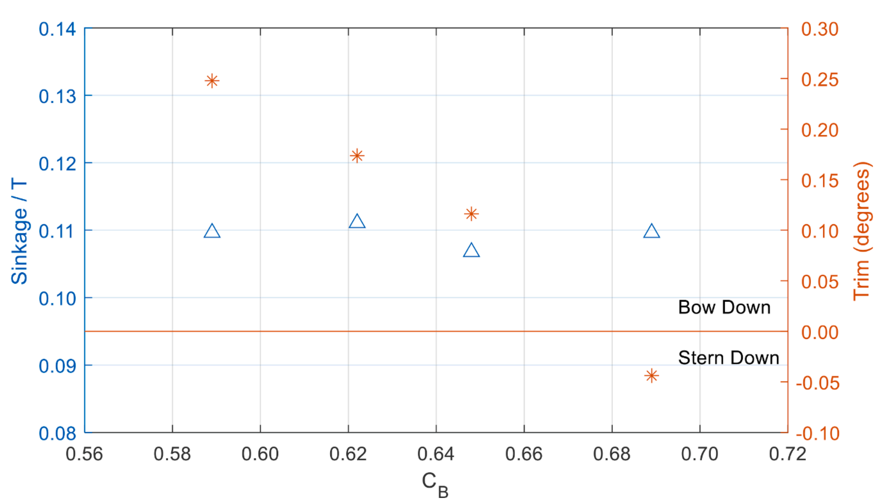

Fig. 13. Plot of midship sinkage/T and trim (positive by the bow) as a function of C_B. The change in sinkage/T is negligible while trim varies linearly with C_B and eventually changes direction.

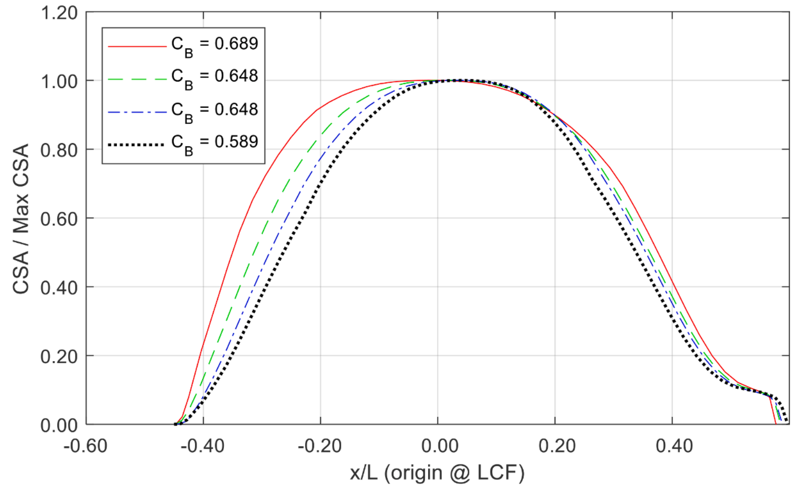

Fig. 14. Comparison of the curve of areas about the LCF among the hulls of varying C_B. The increase in aft section area is greater than that of the fore section for this hullform using the Maxsurf Modeler Advanced parametric transformation tool.

is less dominant. Conversely, Fig. 8(d) shows that the AP sinkage/T increase when L/B decreases but increases slightly with B/T. It is of interest to note that the trim direction never changed which implies that the principal dimensions of the hull only affects the magnitude but not the direction of the trim in this set of results.

In order to understand the observed trends relating to the effect of L/B, velocity profile plots for two cases of similar B/T but varying L/B are compared as shown in Fig. 9. The hull with the more slender profile (L/B = 8.60) can be seen to have lower flow velocity magnitude in the underkeel and wake region in comparison to that of the stubbier hull (L/B = 6.50). The relatively lower flow velocity in the underkeel region for the slender hull implies that the suction pressure and therefore sinkage, is less significant for the slender hull as presented in Fig. 10. This is in agreement with the findings of Han et al. (2012) where a "longer" hullform has lower Froude number and lower wavemaking resistance which results in smaller magnitude of the pressure distribution. Similarly, since there is less pressure acting on a more slender hull, then the net trimming moment, will be less for a more slender hull as well. Furthermore, trim is also expected to reduce for a relatively longer hull as longitudinal length contributes to a greater longitudinal metacentric height (refer to Table A1). A larger moment is required to trim a hull with larger longitudinal metacentric height.

A similar comparison between two hullforms of similar L/B but varying B/T is made to observe the effect of varying B/T on the velocity profile (Fig. 11Figure 11). The underkeel and wake region for both cases appear to be comparable in magnitude. Consequently, comparison of the pressure distribution on the hull (Fig. 12) demonstrates that the magnitude of the pressure distribution on both hulls are similar. Effectively, the proportion of sinkage experienced by both hulls are similar. In regards to trim, the wider hull has a longer length for the same L/B ratio which implies greater longitudinal metacentric height and hence reduced trim relative to the deeper hull.

7.2. *Effect of block coefficient*

The plot of midship sinkage as a function of C_B in Fig. 13 shows that there are no significant changes (the differences in sinkage/T among the datapoints are in the order of 1-4%) whereas a linear relationship is identified between trim and C_B. The independence of midship sinkage with respect to C_B is likely due to the fact that the sinkage component of squat is greatly influenced by the geometry of the midship region where the suction pressure acts. The parametric transformations for altering the C_B of hulls only alters the shape of the fore and aft section of the hull while the parallel midbody is either elongated or shortened. Effectively,

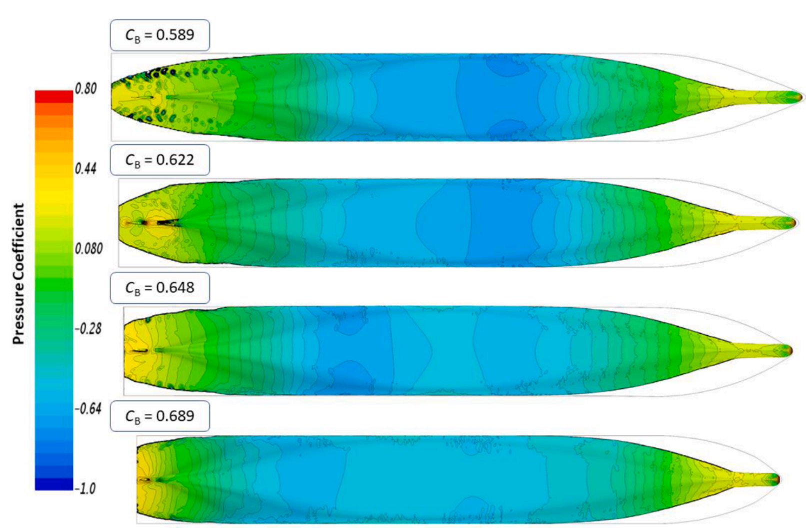

Fig. 15. Comparison of the pressure coefficient contours among the hulls of varying C_B at 0.683 Fr_h in 1.3 h/T. The maximum suction pressure gradually shifts aftward as the C_B increases for this particular hullform using the Maxsurf Modeler Advanced parametric transformation tool.

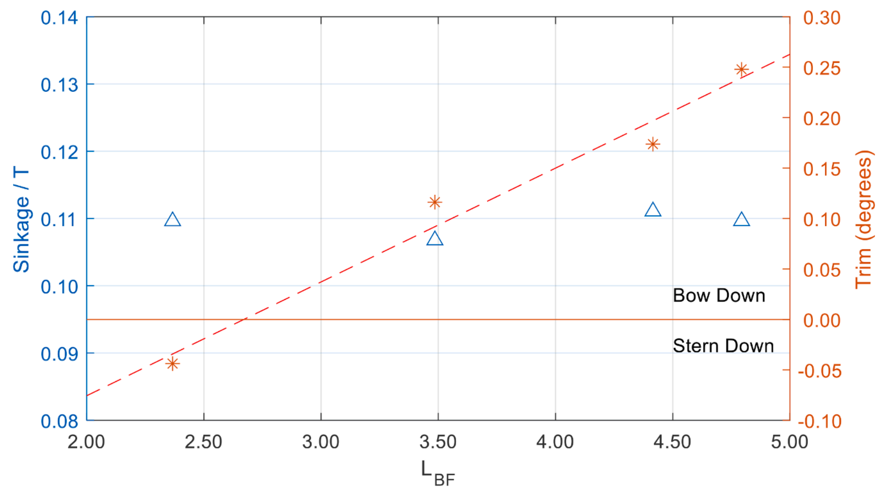

Fig. 16. Plot of midship sinkage/T and trim with respect to L_{BF}. The change in sinkage/T is negligible while trim varies linearly with C_B and eventually changes direction.

the midship region where the suction pressure acts is left unaltered and hence, the proportion of midship sinkage is similar between hulls of different C_B. Conversely, since the parametric transformations alter the fore and aft sections of the hull, the flow fore and aft is expected to differ accordingly and thus, the trimming moment and subsequent trim changes as well. It can be clearly seen from the curve of areas in Fig. 14 that the parametric transformation undertaken in this study has inevitably expanded the aft section more than the fore section when increasing value of C_B. Consequently, there is a larger area on the aft section for the suction force to act which results in progressively more stern-down trim as C_B is increased for this hullform. This is evident in Fig. 15 where the maximum suction pressure gradually shifts aftward as the C_B is increased because of the disproportionately larger aft area growth relative to the fore area. The observations here imply that it is the hull volume distribution which affects the trim direction instead of C_B. Thus, as proven in Figs. 13 and 15, a larger C_B does not necessarily result in a greater likelihood of bow down trim.

7.3. Changes in trim direction

In the previous section, changes in C_B are known to inevitably result in changes to the hull volume distribution which in turn causes change in trim direction. This change in hull volume distribution is manifested in the relative change of LCB and LCF position (refer to Appendix A Table A1). Incidentally, changes to L/B and B/T which maintains the position of the LCB relative to the LCF do not result in changes to trim direction. Thus, it is evident that the hull volume distribution of a container ship can be described as the relative position of the LCB to the LCF (this will now be expressed as L_{BF} and given in Eq. (13)). Therefore, the changes in trim should be analysed with respect to L_{BF} as illustrated in Fig. 16.

$$L_{BF} = \frac{(\mathrm{LCB} - \mathrm{LCF})}{L} \times 100\% \tag{13}$$

From this study it is identified that the change in trim is still linear when analysed with respect to L_{BF} and midship sinkage remains unaffected by changes in L_{BF}. Generally, the shorter the L_{BF}, the more stern down the trim is. It is also noted that the change in trim is very sensitive to L_{BF} considering that there are significant changes in trim between L_{BF} of 2-5%. The point of direction change for this particular case is approximately $L_{BF} = 2.7\%$. This is in agreement with observations made in the work of Gourlay et al. (2015) where the JUMBO hull that has L_{BF}

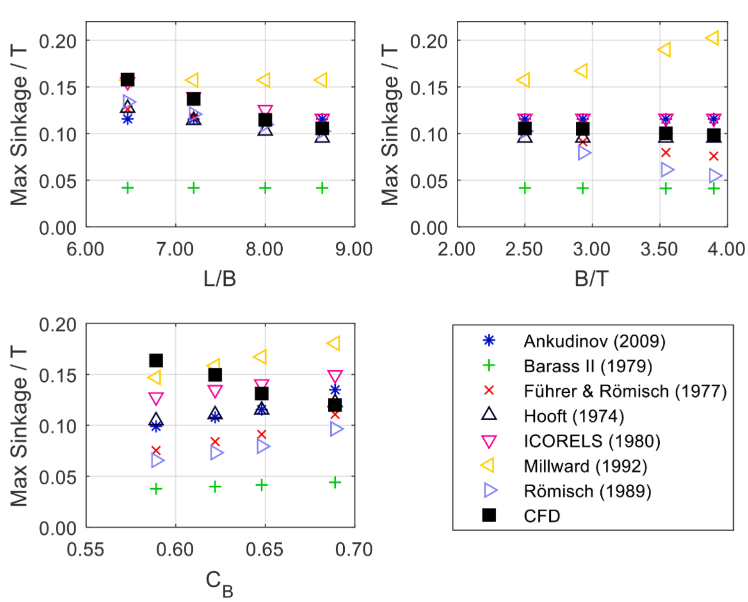

Fig. 17. Sample case comparison between empirical predictions against CFD results for varying L/B, B/T and C_B for the KCS hull.

of 3.46% was seen to trim by the bow whereas the MEGA-JUMBO hull that has L_{BF} of 0.85% trims by the stern. Hence, it is proposed that the L_{BF} should considered as one of the factor(s) in determining the direction of trim of a container ship.

7.4. Comparison against empirical predictions

Having observed the CFD predictions for the effect of *L/B, B/T* and C_B on squat, it is of interest to observe whether existing empirical formulae are able to produce similar findings for this laterally unrestricted case study. Thus, the following empirical formulae are investigated; Ankudinov (2009), Barrass II (1979), Führer & Römisch (1977), Hooft (1974), ICORELS (1980), Millward (1992) and Römisch (1989) where the formulae of each method are available in the appendix of Kok et al. (2020a). It should be noted that all of these formulae investigated are not necessarily derived from container ship models but these are the only few that are applicable for the given scenario. A few sample cases from the CFD results are compared against the corresponding empirical formulae predictions as shown in Fig. 17.

For the case of varying *L/B*, most empirical formulae can be seen to demonstrate a similar trend to the CFD results where maximum sinkage (trim is accounted for) has an inverse relation to *L/B* albeit having slight differences in slope and magnitude. However, the methods of Barrass II (1979) and Millward (1992) are indifferent to *L/B*. For the case of varying *B/T*, most empirical predictions demonstrate minimal changes in maximum sinkage, which is similar to the CFD results. Nonetheless, there are more conflicting trends observed such as increasing and decreasing maximum sinkage with respect to *B/T* are both predicted by Millward (1992) and Römisch (1989) respectively. ICORELS (1980) have shown the best correlation to the CFD results in terms of trend and magnitude for varying *L/B* and *B/T* followed by that of Hooft (1974).

However, conflicting trends are observed when comparing predictions for varying C_B. All empirical predictions suggest that maximum sinkage increases with C_B whereas the CFD results suggest the opposite. It is postulated that the empirical predictions behave as such to compromise for bulk carrier squat predictions. Bulk carriers are at the larger end of the C_B spectrum ($C_B > 0.7$) and generally trim by the bow due to their signature fuller bow. Therefore, the empirical methods tend to predict increasing maximum sinkage when C_B increases. In contrast, the parametrically transformed hulls in this particular study inevitably altered L_{BF} where there is increasingly greater aft volume which results in more sternwards trim for increasing C_B. Effectively, the CFD predictions for maximum sinkage reduces when C_B increases since the trim direction is gradually changing from bow down to stern down and this is not anticipated by the empirical methods studied. This highlights that caution should be exercised when using the presented empirical methods to predict squat for particular changes in hull design. A more accurate empirical method to determine the squat of a container ship may have to consider the hull volume distribution i.e. L_{BF}.

8. Conclusions

A systematic numerical investigation has been undertaken to study the effect of parametric hull variations on container ship squat. In this study, the statistics of the principal particulars of currently operating container ships surveyed by OMC International (2018) were studied and used as the range to be investigated.

Prior to the main investigation, a URANS simulation is modelled based on a self-propelled model scale S175 squat experiment in the *AMC Towing Tank* for verification and validation purposes. Upon successful verification and validation, the modelling method is adapted to the KCS hull as a representation of currently operating modern container ships. Systematic computations are then conducted with the variations of the KCS hull where the lateral bounds of the computation domain are placed sufficiently far away to avoid lateral restriction effects. The findings of the study follow for the range of specific cases investigated in this study:

- Sinkage and trim increases as *L/B* decreases. Sinkage increases due to increase in midship suction pressure as a result of increasing wave-making resistance and thus, worsening pressure distribution when *L/B* decreases. Trim increases when the suction pressure increases as well. Trim also increases because the hull length and hence, longtiduinal metacentric height decreases when *L/B* decreases for the same *B/T* ratio.
- Sinkage is not affected by *B/T* whereas trim increases when *B/T* decreases. The pressure distribution on the hull of varying *B/T* is relatively similar which results in comparable proportion of sinkage. Trim increases because again, the hull length and thus, longitudinal metacentric height decreases when *B/T* decreases for the same *L/B* ratio.
- Sinkage is not affected by C_B whereas trim becomes increasingly stern-down when C_B increases in this study. When C_B increases, the midship region where the majority of the suction pressure acts upon is unchanged which results in similar sinkage. However, the parametric transformations conducted in this study for varying C_B increases the area of the aft section more than the fore section. Thus, the maximum suction pressure gradually shifts aftward and results in relatively more stern-down trim.
- Change in trim direction is shown to be governed by the position of the LCB relative to LCF (L_{BF}) in this study. The shorter the L_{BF}, the more stern down the trim is.The change in trim is very sensitive to L_{BF} where changes in the range of 2-5% in L_{BF} can result in changes to direction of trim.
- Comparison between empirical predictions against the CFD results show that most empirical methods are able to reproduce similar trends for the effect of varying *L/B* and *B/T* with only a few contradicting predictions particularly for varying *B/T* cases. On the contrary, all empirical predictions tested are found to have opposite trends to that of the CFD results for cases of varying C_B. This is thought to be due to the compromise of empirical methods to account for bulk carrier predictions instead of evaluating the hull's actual volume distribution (L_{BF}). A more accurate empirical method may have to consider the said factor.

CRediT authorship contribution statement

Zhen Kok: Formal analysis, Investigation, Writing - original draft. **Jonathan Duffy:** Supervision, Conceptualization, Writing - review & editing. **Shuhong Chai:** Supervision, Writing - review & editing. **Yuting Jin:** Methodology, Visualization, Writing - review & editing. **Mohammadreza Javanmardi:** Resources, Writing - review & editing.

Declaration of Competing Interest

The authors declare that they have no known competing financial interests or personal relationships that could have appeared to influence the work reported in this paper.

Acknowledgements

The authors acknowledge the funding and resources provided by NCMEH Australian Maritime College, University of Tasmania and the Tasmanian Partnership for Advanced Computing for the HPC for performing the computations. The geometry model of the S175 used for the URANS simulation is derived from 3D scanning of the existing 1:70 scale model in AMC towing tank courtesy of the *Defence Science and Technology Organisation* and the *AMC Underwater Collision Research Facility*. The authors would also like to acknowledge the Port of Melbourne container ship visits log supplemented by *OMC International*.

Appendix A. Sister hull particulars

Table A1.

Table A1
Particulars of the hulls developed from parametric transformations (LCB & LCF given as % of L forward of aft perpendicular).

No.	L/B	B/T	C_B	L (m)	B (m)	T (m)	LCB (%L)	LCF (%L)	A_W (m^2)	A_W Coeff.	$\overline{GM_L}$ (m)	S (m^2)
FIXED BLOCK COEFFICENT												
1	6.50	2.50	0.648	6.28	0.97	0.387	48.28	44.79	4.90	0.809	6.56	8.30
2	6.50	2.90	0.648	6.60	1.02	0.350	48.28	44.79	5.42	0.809	8.29	8.54
3	6.50	3.39	0.648	6.95	1.07	0.316	48.28	44.79	6.00	0.809	10.41	8.85
4	6.50	3.90	0.648	7.29	1.12	0.287	48.28	44.79	6.60	0.809	12.97	9.23
5	6.80	3.06	0.648	6.92	1.02	0.333	48.28	44.79	5.70	0.809	9.76	8.77
6	6.80	3.55	0.648	7.28	1.07	0.301	48.28	44.79	6.30	0.809	12.26	9.12
7	7.14	3.22	0.648	7.28	1.02	0.316	48.28	44.79	6.00	0.809	11.52	9.02
8	7.20	2.50	0.648	6.73	0.93	0.374	48.28	44.79	5.08	0.809	8.05	8.59
9	7.52	3.39	0.648	7.66	1.02	0.301	48.28	44.79	6.30	0.809	13.76	9.30
10	7.52	2.90	0.648	7.28	0.97	0.333	48.28	44.79	5.70	0.809	10.89	8.96
11	7.52	3.90	0.648	8.03	1.07	0.274	48.28	44.79	6.93	0.809	16.69	9.67
12	7.87	3.07	0.648	7.64	0.97	0.316	48.28	44.79	6.00	0.809	12.87	9.21
13	7.87	3.54	0.648	8.01	1.02	0.288	48.28	44.79	6.60	0.809	15.81	9.55
14	8.00	2.50	0.648	7.21	0.90	0.361	48.28	44.79	5.26	0.809	9.74	8.89
15	8.23	3.23	0.648	8.01	0.97	0.301	48.28	44.79	6.30	0.809	14.93	9.45
16	8.64	2.50	0.648	7.59	0.88	0.352	48.28	44.79	5.40	0.809	13.83	9.11
17	8.64	2.93	0.648	8.01	0.93	0.316	48.28	44.79	6.00	0.809	14.22	9.39
18	8.64	3.54	0.648	8.53	0.99	0.279	48.28	44.79	6.81	0.809	18.79	9.92
19	8.64	3.90	0.648	8.81	1.02	0.261	48.28	44.79	7.26	0.809	21.23	10.13
VARYING BLOCK COEFFICENT												
20	7.14	3.22	0.589	7.54	1.06	0.33	49.79	45.00	6.11	0.769	11.79	9.35
21	7.14	3.22	0.622	7.40	1.04	0.32	49.34	44.93	6.12	0.798	11.65	9.22
22	7.14	3.22	0.648	7.28	1.02	0.32	48.28	44.79	6.00	0.81	11.52	9.02
23	7.14	3.22	0.689	7.05	0.99	0.31	47.06	44.69	5.79	0.832	11.22	8.60

Appendix B. Further benchmarking exercise

Further benchmarking exercises were conducted based on past experiments on the KCS in a *200m x 10m* rectangular canal in DST in Duisburg (Gronarz et al., 2009). This validation exercise was conducted to examine the accuracy of the current CFD set-up in predicting squat in h/T of up to 1.3 where higher speeds of up to $Fr_h = 0.683$ are possible. The test was conducted at a scale of 1:40 and for bare hull conditions. Test conditions are given in Table A2.

Table A2
Test conditions investigated in the model test by Gronarz et al. (2009).

h/T	Ship Speed Full Scale (knots)	Model Scale (m/s)	Fr_h	m
1.3	6.03–15.00	0.49–1.22	0.274–0.683	0.061
1.2	6.01– 12.04	0.49–0.98	0.285–0.571	0.066

The same CFD set-up described in section 3 was applied in this exercise except that the body-force propulsion virtual disc was removed from the model to conform with the bare hull conditions of this model test. The comparisons between the morphing mesh method predictions against the experimental data for $h/T = 1.30$ and $h/T = 1.20$ are shown in Fig. A1 and Fig. A2 respectively. For both h/T conditions, good correlations can be observed for midship sinkage predictions throughout the speed range investigated but the trim predicted by CFD tends to be significantly greater than the experimental data at higher speeds. Nonetheless, this overestimation of trim is reasonable and does not result in a significant deviation in the overall squat between the CFD and experimental results. For instance, when the resulting squat is expressed in terms of AP and FP sinkage, it can be seen that there is still good correlation for both h/T conditions even at high speeds. Based on the authors' experience, the presence of self-propulsion will increase the sinkage at higher speeds in the experiment but the current CFD body

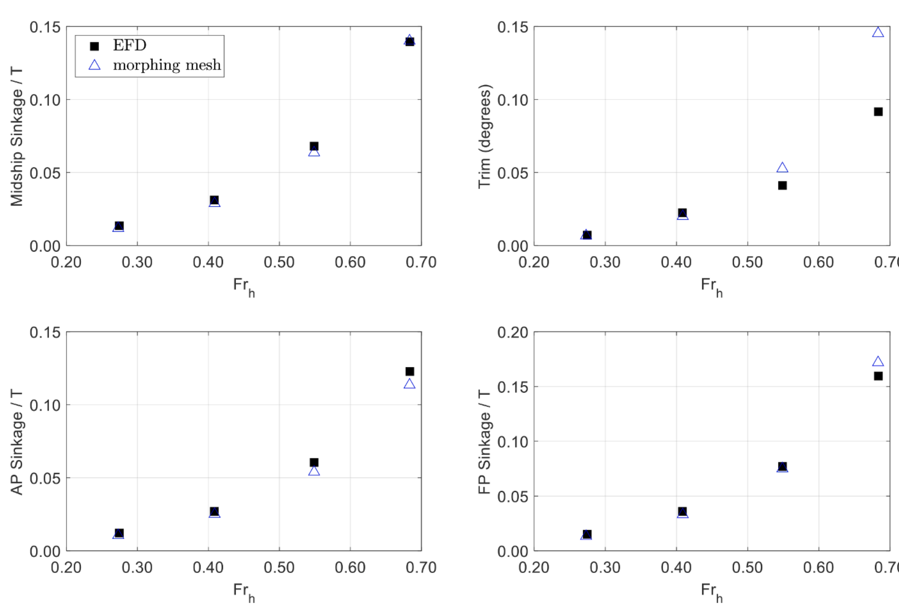

Fig. A1. Comparison of CFD (morphing mesh) predictions against model test results by Gronarz et. al. (2009) at $h/T = 1.30$.

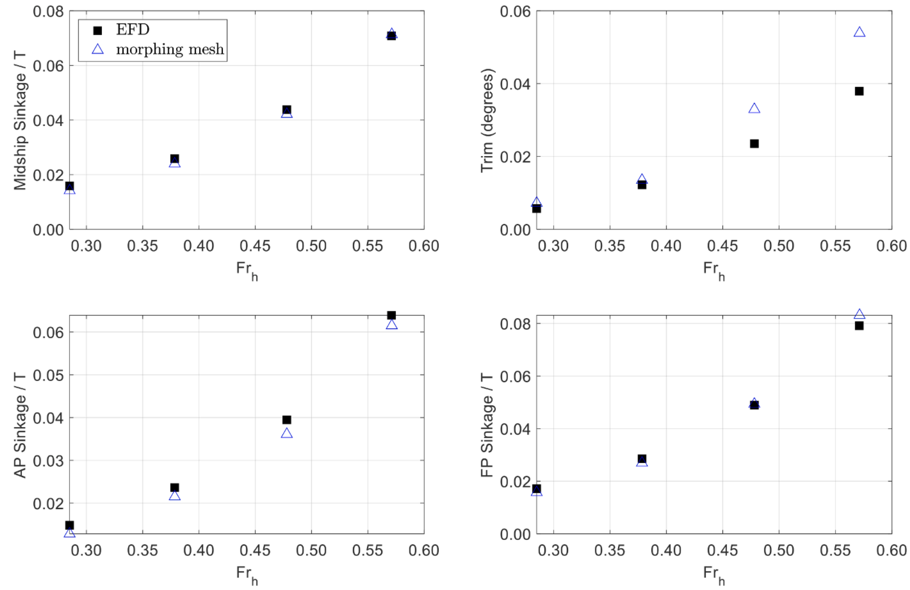

Fig. A2. Comparison of CFD (morphing mesh) predictions against model test results by Gronarz et. al. (2009) at $h/T = 1.20$.

force virtual disc has been tested to be able to capture this increase in sinkage well (refer to findings in Kok et. al. (2020b)). Therefore, this benchmarking exercise has demonstrated that the current morphing mesh method is reliable for squat predictions in h/T of up to 1.3 and at Fr_h up to 0.683.

References

Barrass, C., 1979. The phenomena of ship squat. Int. Shipbuild. Prog. 26.
Bechthold, J., Kastens, M., 2020. Robustness and quality of squat predictions in extreme shallow water conditions based on RANS-calculations. Ocean Eng. 197, 106780.
Beck, R.F., NewmAN, J.N., TUCK, E.O., 1974. Hydrodynamic forces on ships in dredged channels. J. Ship Res. 19 (03), 166–171.
CD-Adapco 2014. User guide STAR-CCM+ Version 9.0.6.
Cong, L., Hsiung, C., 1991. Computing wave resistance, wave profile, sinkage and trim of transom stern ships. In: Proceedings of the Third International Conference on Computer Aided Design, Maunfacture and Operation in the Marine and Offshore Industries (CADMO 91. Key Biscayne, pp. 99–112.
Dand, I., Ferguson, A., 1973. The Squat of Full Ships in Shallow Water. National Physical Lab Teddington (England) Ship Div.
Delefortrie, G., Vantorre, M., Eloot, K., Verwilligen, J., Lataire, E., 2010. Squat prediction in muddy navigation areas. Ocean Eng. 37, 1464–1476. https://doi.org/10.1016/j.oceaneng.2010.08.003.
Deng, G., Guilmineau, E., Leroyer, A., Queutey, P., Visonneau, M., Wackers, J., 2014. Simulation of container ship in shallow water at model scale and full scale. In: Proceedings of the 3rd National CFD Workshop for Ship and Offshore Engineering. Dalian, China.
Duffy, J., 2008. Modelling of Ship-Bank Interaction and Ship Squat for Ship-Handling Simulation. University of Tasmania.
Duffy, J., Renilson, M., 2000. An investigation into the effect of propulsion on ship squat. Ocean. Eng. Int. 4, 1–12.
Elsherbiny, K., Terziev, M., Tezdogan, T., Incecik, A., Kotb, M., 2020. Numerical and experimental study on hydrodynamic performance of ships advancing through different canals. Ocean Eng. 195, 106696.
Fuehrer, M, Römisch, K., 1977. Effects of modern ship traffic on islands and ocean waterways and their structures. In: 24th International Navigation Congress, PIANC. Leningrad, USSR, pp. 236–244.
Gourlay, T.P., Ha, J.H., Mucha, P., Uliczka, K., 2015. Sinkage and trim of modern container ships in shallow water. In: Proceedings of the Australasian Coasts & Ports Conference 2015. Auckland, New Zealand.
Gronarz, A.; Broß, H.; Mueller-Sampaio C., Jiang, T., Thill, C. 2009. "SIMUBIN - modellierung und simulation der realitaetsnahen schiffsbewegungen auf binnenwasserstraßen (in German)". Report 1939 B. *Development Centre for Ship Technology and Transport Systems (DST)*.
Han, S., Lee, Y.-S., Choi, Y.B., 2012. Hydrodynamic hull form optimization using parametric models. J. Mar. Sci. Technol. 17, 1–17.
Jachowski, J., 2008. Assessment of ship squat in shallow water using CFD. Arch. Civ. Mech. Eng. 8 (1), 27–36.
Jin, Y., Duffy, J., Chai, S., Magee, A.R., 2019. DTMB 5415M dynamic manoeuvres with URANS computation using body-force and discretised propeller models. Ocean Eng. 182, 305–317.
Kaidi, S., Lefrançois, E., SmaoUI, H., 2020. Numerical modelling of the muddy layer effect on Ship's resistance and squat. Ocean Eng. 199, 106939.
Kok, Z., Duffy, J., Chai, S., Jin, Y., 2020a. Comparison of of URANS prediction of self-propelled container ship squat against empirical methods and benchmark data. Int. J. Maritime Eng.
Kok, Z., Duffy, J., Chai, S., JiN, Y., 2020b. Multiple approaches to numerical modelling of container ship squat in confined water. J. Waterway, Port, Coast. Ocean Eng.
Kok, Z., Duffy, J., Chai, S., Jin, Y., Javanmardi, M., 2020c. Numerical investigation of scale effect in self-propelled container ship squat. Appl. Ocean Res. 99, 102143.
Lataire, E., 2014. Experiment Based Mathematical Modelling of Ship-Bank Interaction. Ghent University.
Merk, O., 2018. Container ship size and port relocation. Int. Transp. Forum Discuss. Pap.
Naghdi, P, Rubin, M., 1984. On the squat of a ship. J. Ship Res. 28 (2), 107–117.
Papanikolaou, A., 2014. Ship Design: Methodologies of Preliminary Design. Springer.
Rusche, H., 2002. Computational Fluid Dynamics of Dispersed Two-Phase Flows at High Phase Fractions. University of London.
Stern, F., Wilson, R.V., Coleman, H.W., Paterson, E.G., 2001. Comprehensive approach to verification and validation of CFD simulations—part 1: methodology and procedures". J. Fluids Eng. 123 (4), 793–802.
Tezdogan, T, Demirel, YK, Kellett, P, Khorasanchi, M, Incecik, A, Turan, O., 2015. Full-scale unsteady RANS CFD simulations of ship behaviour and performance in head seas due to slow steaming. Ocean Eng. 97, 186–206.
Tezdogan, T., Incecik, A., Turan, O., 2016. A numerical investigation of the squat and resistance of ships advancing through a canal using CFD. J. Mar. Sci. Technol. 21 (1), 86–101.
Tuck, E., 1966. Shallow-water flows past slender bodies. J. Fluid Mech. 26 (1), 81–95.
Uliczka, K., Wezel, M., 2005. Dynamisches Fahrverhalten Grosser Containerschiffe bei Revierfahrt Auf unter-und außenelbe. HTG-Kongress, Bremen, Germany.
Wilson, R.V., Stern, F., Coleman, H.W., Paterson, E.G., 2001. Comprehensive approach to verification and validation of CFD simulations—Part 2: application for RANS simulation of a cargo/container ship". J. Fluids Eng. 123 (4), 803–810.
Yao, J.-X., Zou, Z.-J., 2010. Calculation of ship squat in restricted waterways by using a 3D panel method. *J. Hydrodynam.* Ser. B 22 (5), 489–494.
Yuan, S., Xia, L., Zou, Z.-J., Zou, L., 2019. CFD-based numerical prediction of vertical motions and resistance for DTC container carrier in shallow water waves. In: 5th MASHCON. Ostend, Belgium, pp. 488–501.
Zhang, Z-h, Deng, H, Wang, C., 2015. Analytical models of hydrodynamic pressure field causing by a moving ship in restricted waterways. Ocean Eng. 108, 563–570.